

# THE OPTIMUM PARTICLE-SIZE DISTRIBUTION OF COAL FOR COAL-WATER SLURRIES

C.B. Henderson and R.S. Scheffee

Atlantic Research Corporation  
5390 Cherokee Avenue  
Alexandria, Virginia 22314

## ABSTRACT

The development of coal-water slurries as a boiler fuel is rapidly approaching commercialization. As distinguished from dilute pipeline slurries, fuel slurries are stable, highly-loaded (e.g. 70% dry coal by weight) liquids which can be transported, stored, pumped, and burned like residual fuel oil. One of the key technologies required to obtain highly-loaded, low-viscosity mixtures is the particle size distribution of the coal. Two derivations of the optimum particle-size distribution for minimum slurry viscosity are compared and shown to result in equivalent forms. The theory of grinding is reviewed, and calculated distributions are presented. Experimentally-determined particle-size distributions obtained by both wet and dry grinding in ball mills are given and compared with the theoretical grinding results. It is shown that near-optimum distributions can be obtained by blending.

## I. INTRODUCTION

For several years, the Atlantic Research Corporation has been developing coal-water slurries as a low-cost liquid boiler fuel. As distinguished from dilute pipeline slurries, fuel slurries are stable, highly-loaded (e.g. 70% dry coal by weight) liquids which can be transported, stored, pumped, and burned like residual fuel oil. To achieve the required rheological properties in highly-loaded suspensions, requires a very carefully selected distribution of particle sizes and the incorporation of surface-active additives. The subject of particle-size distribution, its optimization and control, is the subject of this paper.

## II. OPTIMUM PARTICLE-SIZE DISTRIBUTION

The rheology of a suspension of particles within a liquid is influenced by a number of factors which include the size and the distribution of sizes of the particles, particle concentration, particle shape, and surface charge. The effects of surface properties, although often very important, do not fall within the scope of this paper.

The sizing of particles to obtain minimum viscosity of a suspension is closely related to the sizing of particles for maximum packing density of powder beds. If we ignore liquid-particle and particle-particle surface effects, the particle-size distribution resulting in maximum bed density will also result in minimum viscosity for a specified particle concentration. Consequently, the large body of literature addressing both suspensions and powder beds can be utilized. A review of the extensive literature will not be addressed here; only the work of three authors will be discussed. All of the work will be limited to either ideal powder beds consisting of spherical particles with only mechanical interactions or ideal suspensions containing spherical particles and within which all surface interactions are absent.

In 1928, Furnas (1) derived a theory for the maximum packing density of bimodal mixtures, i.e. a bed containing particles of two discrete particle diameters. Assuming that the fractional void volumes,  $\nu$ , of the individual monomodal beds are identical and that the ratio of the two particle diameters is large, the composition of maximum density

is obtained if the small particles fill the interstices of the large particles such that the total bed volume does not increase. In a unit cell, the absolute volume of large particles is  $V_l = 1 - \nu$ . Filling the void volume  $\nu$  with small particles, the absolute volume of small particles is  $V_s = \nu(1 - \nu)$ . The volume ratio of large particles to small particles is  $1/\nu$  and the void volume of the mixed bed is  $\nu^2$ . When the ratio of the two particle diameters is greater than about 50, the theory is in good agreement with experimental data. For ratios, less than 50, Furnas employed experimental data to obtain generalized relationships between voids in the bimodal bed, concentration of large particles, void fraction in the monomodal beds, and the particle diameter ratio. These relationships have been greatly utilized in many industries for discrete particle mixtures. Both theory and experiment have subsequently been extended to multimodal mixtures of discrete particles.

Andreasen and Andersen in 1930 (2) and Furnas in 1931 (3) extended the theory to continuously varying particle diameters. Andreasen and Andersen start by approximating the continuous distribution with a series of particle size fractions in which the particle diameters form a geometrical progression. Starting with the fine fraction they successively add the coarser fractions in such a way that the amount of each fraction added is proportional to the amount of undersize already present:

$$\delta v_j \sim \sum_{i=1}^{j-1} v_i \quad (1)$$

where  $i = 1$  designates the smallest size fraction

Reducing the constant ratio between size fractions to a differential amount, results in a differential equation:

$$\frac{d \ln V}{d \ln D} = n = \text{constant}, \quad (2)$$

which upon solution leads to a continuous particle size distribution:

$$F_p = cD^n \quad (3)$$

where  $F_p$  = cumulative volume of particles smaller than  $D$   
 $c = \text{constant}$

The somewhat arbitrary method by which this result is obtained is justified by comparison with experimental data which indicate that the exponent  $n$  should be in the range of  $1/3 - 1/2$ .

Apparently independently, Furnas in 1931 arrived at a similar but somewhat more general result. He also approximates the continuous distribution as a geometrical series of discrete particle diameters. Designating the diameter of the largest particles as  $D_l$ , the smallest as  $D_s$ , and the size ratio of successive size fractions as  $q$  (Furnas used  $\sqrt{2}$ , but his derivation is applicable to any constant value), the size of each individual fraction is (starting from the finest fraction):

$$D_1 = D_s, D_2 = qD_s, \dots, D_i = q^{i-1} D_s, \dots, D_l = q^{N-1} D_s \quad (4)$$

where  $N$  = number of component particle sizes

If  $q$  is very large (e.g. 50), the extension of bimodal theory to multimodal mixtures requires that the volume ratio of each size fraction to the next smallest size fraction,  $R$ , be a constant. Furnas makes the assumption\* that this theorem also holds for any  $q$ , however small, with the provision that the volume ratio of consecutive size fractions is

\* This can be shown to be equivalent to the basic assumption employed by Andreasen and Andersen

no longer the same as for the optimum mixture at large values of  $q$ . Based on this assumption, Furnas obtains his equation for the optimum particle size distribution which he writes as follows:

$$F_p)_i = \frac{R \log D_i - R \log D_s}{R \log D_l - R \log D_s} \quad (5)$$

Furnas did not specify the base of his logarithm. By following his derivation, it is readily shown that the base is equal to  $q$ . Rewriting the preceding equation and defining the log's as the natural logarithms:

$$F_p)_i = \frac{R \ln D_i / \ln q - R \ln D_s / \ln q}{R \ln D_l / \ln q - R \ln D_s / \ln q} \quad (6)$$

Since  $a^{\ln b} = b^{\ln a}$  for any values of  $a$ ,  $b$ , and  $c$ , the preceding equation can also be written

$$F_p)_i = \frac{D_i^n - D_s^n}{D_l^n - D_s^n} \quad (7)$$

$$n = \ln r / \ln q \quad (8)$$

Furnas' Equation 7 is a more general form of the Andreasen equation, the latter being equivalent to the former for  $D_s = 0$ . The similarity in form between the two equations is to be expected considering the equivalence in the basic assumptions.

$R$  is equal to  $1/\nu$  for particle fractions separated by large values of  $q$ , but as  $q$  becomes smaller,  $R$  must decrease. Furnas presents a method for obtaining this relationship. First, he considers the optimum discrete particle-size distribution in a particle-size range specified by upper and lower limits,  $D_l$ , and  $D_s$ , respectively. He maintains that there is an optimum number of size fractions within the specified range for maximum loading since the volume decrease on mixing particles of different sizes becomes less efficient as the particle diameters become closer together. He next assumes that the experimentally determined relationship between the volume decrease and the size ratio in a binary system is the same as the relationship between the overall volume decrease and the ratio between consecutive sizes in an  $N$ -component system. The optimum number of size fractions is obtained by minimizing the overall volume decrease on mixing the size fractions in the multicomponent system. Furnas is now ready to obtain his expression for  $R$ . He assumes that the volumetric ratio of the largest particles to the smallest particles should be the same for any  $N$  and therefore  $R^{N-1}$  should be a constant independent of  $q$ , or equivalently of  $N$ . He obtains this constant from his optimum number of size fractions obtained for a specified size range. Combining results, the exponent  $n$  in Equation 8, is found to be a complex function of  $\nu$  and the ratio  $D_l/D_s$ . The first, and most important conclusion, is that  $n$  is independent of  $q$ . This means that the derivation is as valid for continuous distributions, as claimed by Furnas, as for discrete distributions. The validity is of course dependent upon the assumptions employed. For  $\nu = 0.4$  and  $D_l/D_s = 500$ , the optimum value of  $n$  according to the Furnas analysis is calculated to be 0.256.

Farris (4) presents his analysis in terms of the viscosity behavior of multimodal suspensions in a liquid instead of the maximum packing of a particle bed. He optimizes the particle size distribution to obtain the minimum viscosity for a given volumetric concentration of particles. He also makes an assumption which is equivalent to that made by Andreasen and Andersen as represented in Equation 1 and to that made by Furnas in deriving Equation 5. Farris, however, presents his arguments more logically and with an improved basis of experimental data.

Farris noted that there were several references in the experimental literature to the fact that the finer particles in a bimodal suspension behave essentially as a fluid toward the coarser particles. To be more specific, if the ratio of particle sizes is large (e.g.

10 or greater), the resistance to motion encountered by a large sphere is the same when passing through a suspension of smaller spheres as when it passes through a pure liquid of the same viscosity and density as the suspension.

Farris first starts with the relative viscosity (ratio of suspension viscosity to liquid viscosity) of a monomodal system, which for non-interacting spherical particles has been shown experimentally to be a unique function of the volume fraction of solids. He next adds coarser particles of much larger diameter (i.e.  $q$  is large) to the suspension. Based on the assumption that the fines act like the liquid, he calculates the relative viscosity of the bimodal mixture using the same form as for the monomodal system. By successively adding coarser fractions, each larger by a large factor than the next smaller fraction, he extends his analysis to multicomponent distributions.

Farris obtains the optimum particle size distribution by differentiating the viscosity of the suspension with respect to composition, equating to zero, and solving for the compositional variables. The optimum composition of a multicomponent system is expressed as follows:

$$\phi_1 = \phi_2 = \phi_3 \dots = \phi_N \quad (9)$$

$$\text{where: } \phi_i = V_i / \sum_{k=0}^i V_k \quad (10)$$

$V_i$  = volume of  $i^{\text{th}}$  component

$V_0$  = volume of liquid

The form of this series of  $N-1$  equations is perfectly satisfactory to define the optimum composition. As it stands, however, it is difficult to compare with other equations. If, however, the  $N-1$  equations are used to solve for  $N-1$  values of  $V_i$  in terms of an  $N^{\text{th}}$  variable, a particle-size distribution can be constructed. It is convenient to select the particle-loading,  $g$ , defined as the volume of particles divided by the total volume, as the  $N^{\text{th}}$  variable. After considerable algebra, the final equation is as follows:

$$\left( \frac{F}{P} \right)_i = \frac{\theta^{i-1} - 1}{\theta^N - 1} \quad (11)$$

$$\text{where } \theta = (1-g)^{-1/N} \quad (12)$$

This distribution is independent of the size of the individual fractions. If we specify size fractions with a geometrical progression of particle diameters and minimum and maximum particle diameters  $D_s$  and  $D_\ell$ , respectively, the preceding equation is transformed to:

$$\left( \frac{F}{P} \right)_i = \frac{D^n - D_s^n}{D_\ell^n - D_s^n} \quad (13)$$

$$\text{where } n = \frac{\ln \left( \frac{1}{1-g} \right)}{\ln \left( \frac{D_\ell}{D_s} \right)} \quad (14)$$

We note that the form of the distribution equation, Eq (14), is exactly the same as that given by Furnas, Eq. (7). The exponent differs, however. For  $g = 0.65$  and  $D_\ell/D_s = 500$ , a value of 0.17 is calculated for  $n$ .

The derivation just described is based on particle-size fractions separated by large factors, that is by large values of  $q$ . Farris claims that his results, i.e. Eqns. (9) and (10) are also applicable in systems in which there is an equal interaction between

particles of a different size. For interacting particles, Farris defines a crowding factor  $f$  as the fraction of one size that behaves as if it were the next largest size. For spherical particles that interact only mechanically: similarity should apply,  $f$  should be equal for all particle sizes, and Equation 9 will be applicable. Applying a definition of  $f$  and proceeding through considerable algebra, it can be shown that Equations 13 and 14 are still pertinent and independent of the value of  $f$ .

Equations 13 and 14 were derived starting with a discontinuous particle-size distribution. In arriving at the final form, the factor  $q$ , denoting the separation in size between successive fractions, does not appear. Consequently, it can be concluded that the results are equally applicable to continuous distributions.

### III. EFFECT OF PARTICLE-SIZE DISTRIBUTION ON VISCOSITY

In the preceding section, the concept that fine particles in a suspension behave as a fluid toward coarser particles was used to obtain an optimum particle-size distribution. This same concept was also used by Farris to calculate the viscosity of multimodal suspensions provided the particle size fractions are separated by large factors. These calculations can be extended to suspensions of mechanically interacting particles (i.e., the individual size fractions are separated by small factors), provided the crowding factors are known - presumably obtained experimentally.

The viscosity of coal-water suspensions is greatly influenced by surface chemistry, which is outside the scope of this paper. Consequently, the viscosities calculated ignoring these effects are of limited value, and the principal value of these calculations is to illustrate qualitatively the effect of particle-size distribution on viscosity. The viscosity of a monomodal system is shown as a function of volume fraction of solids in Figure 1. This relationship has been obtained experimentally for non-interacting rigid spheres and is valid for particles as small as  $4\mu\text{m}$  and as large as  $250\mu\text{m}$ . As the volume fraction of solids approaches 0.605, the relative viscosity (the ratio of the viscosity of the suspension, to that of the carrier) tends to very high numbers. This volume fraction corresponds approximately to a slurry consisting of 65% by weight of coal in water. Also shown are the relative viscosities of an optimal bimodal suspension. The reduction in viscosity by using a bimodal suspension is apparent. Additional reductions are obtained by increasing modality even further; for a volume fraction of 0.66 (corresponding to a 70% slurry of coal in water), relative viscosities of infinity, 51, 30, and 23 are calculated for monomodal, bimodal, trimodal, and tetramodal mixtures, respectively.

### IV. PARTICLE-SIZE DISTRIBUTIONS OBTAINED IN BALL MILLS

Coal as ordered from the mine may have a top size of 5 cm or larger. The top size of the coal to be employed in a fuel slurry is typically  $250\mu\text{m}$  or smaller. The particle size must be reduced, therefore, by a factor of at least 200; the final particle-size distribution must meet stringent requirements as noted in prior sections; and the comminution must be accomplished in an economical manner.

The process employed in the laboratory by the Atlantic Research Corporation starts with a hammer crusher with a cylindrical grating placed beneath the rotor, followed by a ball mill operated in the batch mode. The crushed product is introduced into the ball mill in either dry or slurry form.

The ball mill is one of only a number of different comminution devices which can be used to prepare pulverized coal. It has been selected for a number of reasons. First, it can achieve the desired results economically. Second, it is available in a range of sizes from laboratory mills to production mills with capacities of hundreds of tons per hour. Third, there exists a wealth of experimental data which enable one to predict performance, production costs, wear and machine life, and maintenance. Finally, grinding theories have been developed and compared with experimental ball mill results. These theories can be a useful aid in obtaining specific particle size distributions and will be discussed next.

## Grinding Theory

A large body of literature exists on the theory of grinding, much of it emanating from Pennsylvania State University (5-7) and from the University of Utah (8). Most theories agree on a basic equation for batch grinding which can be written in a number of different ways. The form used in this work is most useful in obtaining results with a digital computer. It is convenient to treat the particle size distribution as a series of discrete sizes as would be obtained if ascertained by a series of screens. Consider a set of  $m$  screens, the coarsest screen being designated by 1 and the finest by  $m$ . The size of the  $i^{\text{th}}$  screen is designated by its aperture  $x_i$ . A constant screen ratio,  $q$ , is used so that  $x_{i-1}/x_i = q$ . Material which is retained on screen  $i$  after passing through screen  $i-1$  has a size range from  $x_i$  to  $x_{i-1}$  and has a weight  $W_i(t)$  at time  $t$ . This material will be referred to as being of size  $x_i$ . The breakage equations representing weights in fractional form are:

$$\frac{dW_i(t)}{dt} = \sum_{j=1}^{i-1} b_{ij} k_j W_j(t) - k_i W_i(t) \quad (15)$$

$$W_R(t) + \sum_{i=1}^m W_i(t) = 1 \quad (16)$$

where  $W_R(t)$  = fractional weight passing finest screen

$k_i$  = rate constant =  $\ln W_i/dt$

$b_{ij}$  = breakage function = fraction of material obtained by primary breakage of size  $j$  retained on screen  $i$ .

In the general case,  $k_i$  is a function of both time and size  $x_i$ . The  $m^2$  values of  $b_{ij}$  are functions of the two sizes,  $x_i$  and  $x_j$ . In certain cases (which must be ascertained by comparison with experiment),  $k_i$  is independent of time and proportional to  $x_i$ , and  $b_{ij}$  is a normalized function which can be fit by the following equation:

$$b_{ij} = \left( \frac{x_{i-1}}{x_j} \right)^\gamma - \left( \frac{x_i}{x_j} \right)^\gamma, \quad (17)$$

where  $\gamma$  is an empirically determined constant

Combining the restricted equations for  $k_i$  and  $b_{ij}$  with the differential equation, permits one to solve for particle size and particle size distribution as a function of time. Converting to finite difference form, and employing a fourth-order Runge-Kutta numerical solver, the equations have been programmed for a digital computer. Input values are the number of sieves, the screen ratio,  $q$ , the fractional weights initially on each screen, and the constant  $\gamma$ . The output consists of the fractional weights on each screen at generalized times,  $a \cdot t$ , where  $a$  is equal to the ratio  $k_i x_i / x_i$ .

Particle-size distributions obtained from ball mills often fit a Rosin-Rammler-Bennett (RRB) equation:

$$F_p)_D = 1 - \exp \left[ -0.693 \left( \frac{D}{D_{50}} \right)^\lambda \right] \quad (18)$$

where  $D$  = diameter  
 $\lambda, D_{50}$  = constants  
 $D_{50}$  = 50% by volume of particles are smaller than this diameter

This distribution of particle diameters extends from zero to infinity, and, for practical purposes, must be truncated. In obtaining RRB fits of either computer results or experimental data, only points falling within the range  $0.05 < F_p < .97$  are used.

Typical results of particle-size distributions as predicted by the theoretical model are given in Figure 2. An empirical correlation of  $D_{50}$  values is shown in Figure 3. Predicted reciprocal  $D_{50}$  values are linear with time, based on the breakage function selected.

### Experimental Results

Coal-water slurries can be made from a wide range of coals. Although coals of lower ranks can be employed, bituminous coals have received the greatest attention. Typical coals have volatile contents between 25 and 40% and Hardgrove indices between 40 and 80. Approximately 30 such coals have been investigated thus far. Only a single coal will be discussed here; one with 35% volatile matter, 6% ash, and a Hardgrove index of 41. It can be considered a typical coal except for the grindability index. Considerable savings are obtained by using coals with larger Hardgrove indices.

Particle-size distribution curves are determined by wet sieving and by Fraunhofer plane diffraction for sub-sieve sizes. A Malvern Model 2200 particle sizer and Model 8T1800 analyzer is used for particles in the range of  $1.2 - 118 \mu m$ .

Prior to ball milling, the coal is crushed in a Holmes Bros. Model 201 crusher with grates containing 1.6 mm diameter holes. A size distribution curve for the product is shown in Figure 4 and 5. The curve fits the RRB equation with a  $D_{50}$  of  $204 \mu m$  and a value of 0.96 for  $\lambda$ . Values of  $\lambda$  are more meaningful when expressed as a ratio of  $D_{80}/D_{50}$ , the conversion equation being:

$$\frac{D_{80}}{D_{50}} = e^{.8424/\lambda} \quad (19)$$

For the crushed coal, the ratio  $D_{80}/D_{50}$  is equal to 2.4 and the  $D_{80}$  is  $491 \mu m$ .

A jar mill without lifters, 21.3 cm in diameter, and 16.5 cm long is rotated at 60 rpm (70% of critical speed) with grinding media consisting of steel balls 1.59 cm in diameter. The empty volume of the jar is  $5800 \text{ cm}^3$ , the ball charge has a bulk volume of  $2900 \text{ cm}^3$  (50% loading), and the void volume within the ball bed is  $1150 \text{ cm}^3$ . The volume of dry coal or slurry introduced as a charge to the mill is equal to the void volume,  $1150 \text{ cm}^3$ .

The change in particle-size distribution with dry milling is shown in Figure 4. Figure 5 shows the results for wet milling in a slurry consisting of equal parts of coal and water and containing two parts of a petroleum-based surfactant per thousand parts of coal. These results were statistically fitted to the RRB equation; the resulting RRB curves are also shown in Figures 4 and 5. Using the RRB equations which best represent the data, the  $D_{50}$  values were calculated; reciprocal values are plotted against time in Figure 6. The  $D_{50}$  values as well as the distributions are well represented by the

theoretical milling equations with  $\gamma = 2$  for both wet and dry milling and with  $a = 4.0 \text{ s}^{-1}$  for dry milling and  $a = 9.3 \text{ s}^{-1}$  for wet milling. A comparison of the rate constants for wet and dry milling show that the former is the larger by a factor of more than two.

Although the milling results shown here are well-represented by simple breakage functions, such is not always the case. More complicated functions are required for different coals and different ball mill conditions.

#### Obtaining The Optimum Distribution

One method of processing coal-water slurries is to blend dry milled coal with a slurry of wet milled coal. For example, combining two parts of dry milled coal with three parts of a 50% slurry results in a slurry containing 70% coal. A blend carried out in this ratio using the 50% slurry milled for 60 minutes and dry coal milled for 20 minutes has the particle-size distribution shown in Figure 7. A comparison is made with an optimum distribution calculated according to Equation 13 with  $D_f = 140$ ,  $D_s = 2.5$ , and  $n = 0.24$ . The blend of the coarse dry milled coal ( $D_{50} = 56 \mu\text{m}$ ) and the finer wet-milled coal ( $D_{50} = 11 \mu\text{m}$ ) results in a near-optimum blend with a  $D_{50} = 19 \mu\text{m}$ . This blend of a coarse and a fine grind to obtain an optimum distribution is sometimes called a bimodal blend even though that designation is more appropriately limited to distributions with two maxima.

#### V. CONCLUSIONS

The optimum particle-size distributions for minimum viscosity or maximum packing density as derived by Furnas and by Farris have been shown to be equivalent in form, namely Equation 7. Furnas' equation for the exponent,  $n$ , differs somewhat from Farris' equation, the latter being preferred. These equations have been found to be very valuable in the formulation of coal-water slurries. It is not possible to predict the viscosity of these slurries from knowledge only of particle sizes because of the importance of surface chemistry and the influence on the chemistry of certain additives which which have been found useful in slurry development.

Near-optimum distributions of particle size can be obtained by blending products obtained by ball mills even though the individual distributions obtained from these mills are not optimum. Comminution in ball mills can be described theoretically; these techniques, derived from the literature, are useful in interpolating and extrapolating results.

#### VI. REFERENCES

1. Furnas, C.C., Bur Mines, Rept. Investigations 2894, 7 (1928); Bur. Mines Bull. 307, 74-83 (1929).
2. Andreasen, A.H.M. and J. Andersen, Kolloid-Z 50, 217-228 (1930).
3. Furnas, C.C., Industrial and Engineering Chemistry 23:7, 1052 - 1058 (1931).
4. Farris, R.J., Transactions of the Society of Rheology 12:2, 281-301 (1968).
5. Klimpel, R.R. and L.G. Austin, Ind. Eng. Chem. Fundam. 9:2, 230-237, (1970).
6. Austin, L.G., Powder Technol. 5, 1-17 (1971)
7. Austin, L.G., P.T. Luckie, and R.R. Klimpel, Trans. Soc. Mining Engineers 252, 87-94 (1972).



8. Herbst, J.A., and D.W. Fuerstenau, International Journal of Mineral Processing, 7, 1-31 (1980).

VII. NOMENCLATURE

Particle-Size Distribution

$D$  = particle diameter  
 $f$  = crowding factor defined by Farris  
 $g$  = volume fraction of solids in a slurry  
 $F_p(D)$  = cumulative volume of particles smaller than  $D$   
 $N_p$  = number of component particle sizes  
 $R$  = ratio of absolute volume of particles present in consecutive size fractions.  
 $q$  = diameter ratio between consecutive size fractions  
 $V$  = volume  
 $\nu$  = void volume  
 $\phi$  = volume ratio defined by Farris, Equation 10

Subscripts

$i$  = designates size fractions;  $1$  is the smallest fraction  
 $l$  = designates largest diameter present  
 $s$  = designates smallest diameter present  
50,80 = designate the volume percentage of particles smaller than specified diameter.

Grinding

$b_{ij}$  = breakage function  
 $k$  = breakage rate constant  
 $m$  = number of sieves  
 $t$  = time  
 $W_i$  = weight of material retained on the  $i^{\text{th}}$  sieve  
 $x_i$  = aperture of the  $i^{\text{th}}$  sieve size  
 $\gamma$  = constant in Equation 17  
 $\lambda$  = constant in RRB distribution function, Equation 18

Subscripts

$i$  = designates sieves of different sizes, 1 being the largest sieve

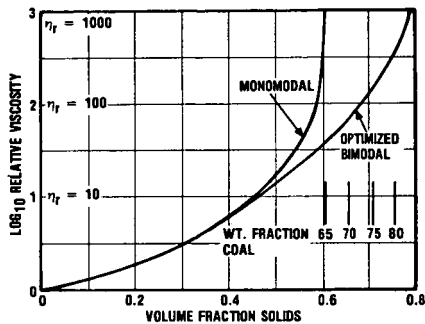


Figure 1. Effect of Bimodal Distribution on the Relative Viscosity of Suspensions of Non-interacting Spheres.

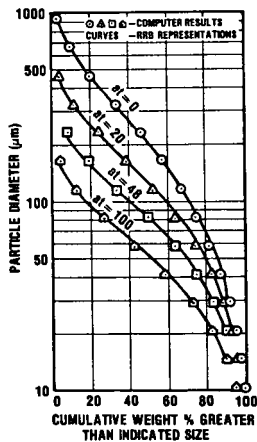


Figure 2. Particle Size Reduction in a Ball-Mill as Predicted by Theoretical Model  $\gamma=2$ .

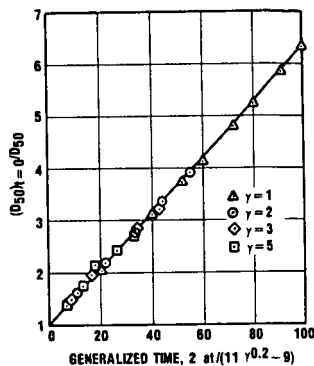


Figure 3. Empirical Correlation of  $D_{50}$  Values of Ball-Milled Coal as Predicted by Theoretical Model.

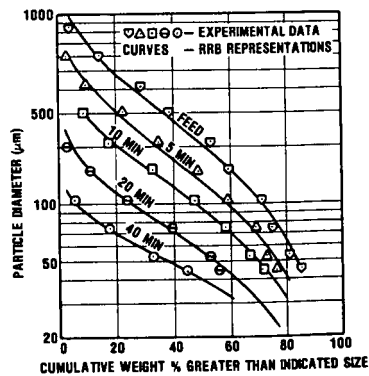


Figure 4. Experimental Particle Size Distributions Obtained in Dry Milling.

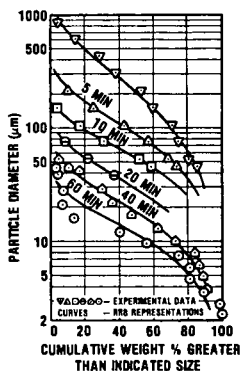


Figure 5. Experimental Particle Size Distributions Obtained in Wet Milling.

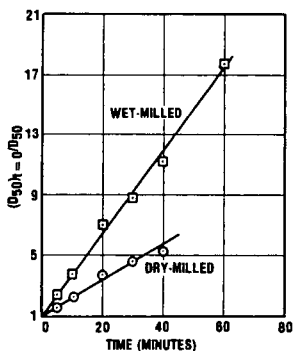


Figure 6. Correlation of Experimental  $D_{50}$  Values ~ Batch Grinding in Laboratory Ball Mill.

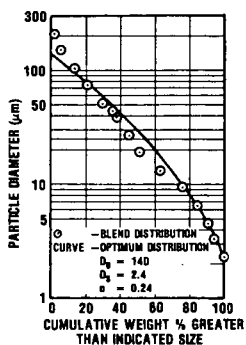


Figure 7. Comparison of Particle-Size Distribution of Blended Coal with Optimum Distribution.

## CWS Rheology: The Role of the Coal Particle

Dean C. Marvin & Theodore C. Frankiewicz

Occidental Research Corporation  
2100 S.E. Main Street  
Irvine, California 92713

### Introduction

The rheological properties of concentrated suspensions are important in a number of industries, particularly paints and coatings. The work of Chang et al (1) mentions some of the early experimental work in this area, but theoretical work on concentrated systems is quite limited(1-5). The reason for this is clear--the assumption of independent particles interacting only with fluid surroundings is not valid under these conditions, and the coupled motions of particles can be treated only empirically. The current research activity in coal slurry fuels has caused a renewed interest in this problem because the rheological properties of these fuels are of primary importance. Typically, one desires a liquid fuel with 65-70 weight percent solids, viscosity on the order of  $10^3$  centipoise, and resistance to sedimentation and shear degradation. These properties can be manipulated by the use of different particle size distributions of the powdered coal, surfactants or wetting agents, and water soluble polymers which act as stabilizers.

However, the wide variety of choices for these three compounding variables makes the task of finding the optimal formulation quite tedious and unsure. For this reason the work described below was undertaken. It represents an attempt to isolate the effect of particle size distribution (PSD) on the resulting slurry viscosity given that all other variables, i.e., the additive package, remain fixed. Comparison of theoretical predictions of relative viscosities of slurries with different PSD with experimental results show that the theory can be useful in optimizing the PSD.

### Theory

There are two steps in the development of a model for predicting relative viscosity for particle size distribution. The first is to compute the maximum packing efficiency (volume fraction)  $\phi_p$  possible for a given PSD. At this loading the viscosity of a slurry at realistic shear rates is assumed to be infinite, since it represents a random dense packing. Another way of viewing this limit is to consider the flow of a slurry as motion of the larger particles over one another as being "lubricated" by the motion of the smaller particles in the interstices. At  $\phi_p$  no motion of these smaller particles is possible and hence the viscosity becomes very high. Thus it is expected that the viscosity of a slurry will increase rapidly as the actual particle loading  $\phi$  approaches the value  $\phi_p$ . The second step of the model is to quantify this behavior.

In order to calculate  $\phi_p$  for a given PSD the method of Lee (7) has been used. A brief description of this procedure will be given here, but for a detailed discussion the reader is referred to the original work. Consider a binary PSD, that is one which consists of only two sizes of spherical particles, and ask how the maximum packing fraction can be determined. One procedure is to fill a volume with the dense random packed larger spheres giving a packing fraction  $\phi_{max,L}$  and then filling the remaining volume with the smaller spheres. The final packing fraction is

$$\phi_{\max} = \phi_{\max,L} + (1 - \phi_{\max,L}) \cdot \phi_{\max,S}$$

It is assumed that  $\phi_{\max,L} = \phi_{\max,S}$ , that is that monodisperse spheres all pack with the same efficiency in dense random packings. The value assigned is determined by experiment to be .639. The composition of this mixture is  $x_{\max,L} = \phi_{\max,L} / \phi_{\max} = .735$ . An assumption which is implicit in the above is that the large and small particles are sufficiently different in diameter ( $D_L/D_S > 100$ ) that the interstitial volumes between the large spheres can be summed and treated as a bulk void for purposes of packing the smaller spheres. The experimental work of McGeary (8) is used to determine the  $\phi_{\max}$  for diameter ratios  $1 < D_L/D_S < 20$ . Thus far this process gives the  $\phi_{\max}$  for binary mixtures of arbitrary sized spheres. The next extension is to compute the packing fraction  $\phi_p$  for binary mixtures with a specified composition. Lee has given an analytical procedure for doing this under the assumption that the  $x_{\max,L}$  is independent of the diameter ratio of the spheres. This reasonable assumption is based on the premise that any optimal packing will contain a dense, random packing of the largest spheres in the system, which is then filled in with any available smaller spheres. Clearly the replacement of a large sphere in such a packing arrangement with the maximum number of inscribed smaller spheres will produce a less efficient packing. Finally, Lee has given an algorithm for computing the packing fraction  $\phi_p$  for mixtures which contain an arbitrary distribution of spherical particles. The algorithm, which is based on a geometrical construction, is given below.

$$(\phi_p)_i = \sum_{j=1}^N \phi_{ij} x_j \quad 1 = \sum_{j=1}^N x_j$$

where  $\phi_{ii} = .639$

$$\phi_{ij} = .639 + (\phi_{\max}(D_i/D_j) - .639) / .265$$

$$\phi_{ji} = .639 + (\phi_{\max}(D_i/D_j) - .639) / .735$$

$$D_i/D_j > 1 \text{ or } i > j$$

$$x_j = \text{volume fraction of particles of diameter } D_j$$

$$N = \text{number of discrete diameters present in mixture}$$

$$\phi_{\max}(D_i/D_j) = \text{maximum packing fraction of binary mixture consisting of spheres of diameter } D_i \text{ and } D_j.$$

The set of  $(\phi_p)$  values has N members and the smallest one is chosen as the packing fraction  $\phi_p$ . The algorithm is not easily understood by inspection because it is graphical in nature, but is developed in a straightforward way in Reference 7. In order to use this technique to predict  $\phi_p$  for a coal grind, one simply performs a particle size analysis, discretizes the distribution into N bins, and then computes  $\phi_p$ .

There are several equations available for obtaining the relative viscosity of concentrated slurries from a knowledge of the packing fraction  $\phi_p$  and the actual volume fraction solids  $\phi$ . The Mooney equation (9)

$$\eta = \eta_0 \exp[2.5\phi / (1 - \phi/\phi_p)] \quad (1)$$

expresses the hydrodynamic viscosity of the suspension in the limit of high shear rate, relative to the viscosity of the pure suspending medium  $\eta_0$ . This expression is valid in the range where  $\phi \approx \phi_p$ , and where the double layer thickness surrounding particles in aqueous solution is small compared to the particle diameter. Both of these criteria are satisfied by the coal slurries described here.

However, the justification for this form is clear only for monodisperse or slightly polydisperse systems. An alternative is the empirical equation (1,10)

$$\eta = \eta_0 \left[ 1 + .75 \frac{\phi/\phi_p}{1-\phi/\phi_p} \right]^2 \quad (2)$$

which has been successful in describing results obtained with suspensions of glass beads in polyisobutylene.

### Experiments

The theory presented above has been used in two different ways to predict the viscosity of coal water slurries. One application involved mixing a fine grind of coal with a coarse grind in varying proportions to produce bimodal particle size distributions. It was found by experiment that there always existed an optimum blending proportion which produced a slurry of minimum viscosity (with the additive package remaining fixed). The theory was tested to see if it could successfully predict this optimum blend given the PSD for the two starting grinds and the total weight fraction of coal to be used. The procedure was simply to compute the packing fraction  $\phi_p$  using the above algorithm, convert the weight fraction coal to a volume fraction  $\phi$  in the slurry, and use equation (1) or (2) to evaluate the relative viscosity  $\eta/\eta_0$ . The value of  $\eta_0$  was then selected to scale the data at one point (usually the minimum viscosity). The results of this procedure are shown in Figures 1 and 2. The data in the former utilized two different grinds of the same coal which had median diameters of  $5\mu$  and  $35\mu$ . Although the viscosities are not predicted quantitatively, the shapes of the curves are similar and the location of the minimum is given correctly. In Figure 2 the data was obtained from mixtures of two different coals with median sizes  $15\mu$  and  $40\mu$ . Again the blend composition giving the minimum viscosity is given correctly. Both of these coal slurries were 65% coal by weight. Also equation (2) was used to compute the theory points in both cases but equation (1) was equally suitable, the difference being in the width of the curves rather than in the location of the minima.

A second application was to predict the change in viscosity with coal loading in coal water slurries. Figures 3 shows viscosity data for a coal subjected to different grinding conditions which resulted in different size distributions, A and B. The volume median (or equivalently, weight) sizes were  $50\mu$  and  $25\mu$ , respectively. The  $\phi_p$  corresponding to each of these PSD's were computed, and theoretical curves drawn using equation (2) with  $\phi$  being the independent variable. Note that the x axis in the figure is the more familiar weight percent coal while the  $\phi_p$  in equation (2) is the volume fraction coal (conversion was made assuming a coal density of  $1.34 \text{ g/cm}^3$ ). The theory is quite successful in fitting these results, but substantially less so when equation (1) is used.

### Conclusion

The effect of coal particle size distribution on the viscosity of coal water slurries has been analyzed using a particle packing model due to Lee in conjunction with an empirical relationship between packing efficiency and viscosity. The technique is able to predict the optimum PSD when one degree of freedom is present, such as the blending ratio between a coarse and a fine grind of coal. The results presented here illustrate this for the cases where the two grinds are the same coal and where they are different coals. In addition data has been presented which shows that one can predict the behavior of viscosity vs. coal loading curves as the PSD of the coal is varied. Both of these achievements are quite useful in the development of coal water slurry formulations in that they allow the value of specific coal

grinds to be assessed without extensive slurry preparation and measurement. The method can also be used to assess the relative merits of unimodal and bimodal size distributions.

#### Acknowledgement

The authors wish to acknowledge discussions held with Dr. Richard G. Donnelly and Dr. Hilmar von Schonfeldt in the course of preparing this paper.

## References

1. J.S.Chong, E.B. Christiansen and A.D.Baer, J. Appl. Polymer Sci. 15, 2007(1971)
2. H. De Bruijn, Rec. Trav. Chim. 61, 863(1942).
3. E. Guth and R. Simha, Kolloid-Z 74, 266(1936).
4. V. Vand, J. Phys. and Colloid Chem. 52, 277 (1948).
5. R. Simha, J. Research NBS 72, 409(1949).
6. H. Filers, Kolloid-Z 97, 313(1941).
7. D.I. Lee, J. Paint Tech. 42, 579(1970).
8. R.K. McGeary, J. Am. Ceram. Soc. 44, 513(1961).
9. M. Mooney, J. Colloid Sci. 6, 162(1951).
10. H. Eilers, Kolloid-Z. Z. Polym 97, 313(1941).

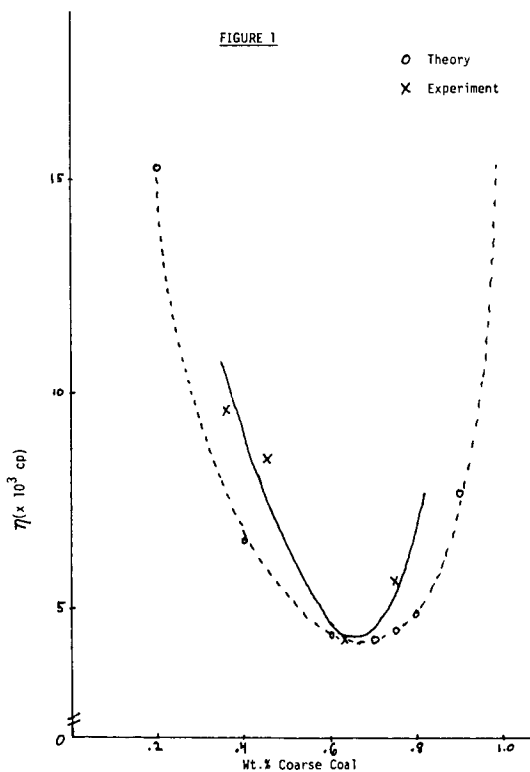




FIGURE 2

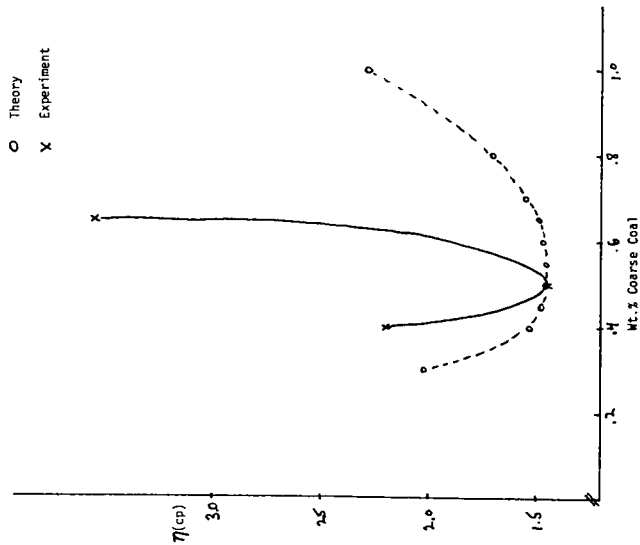
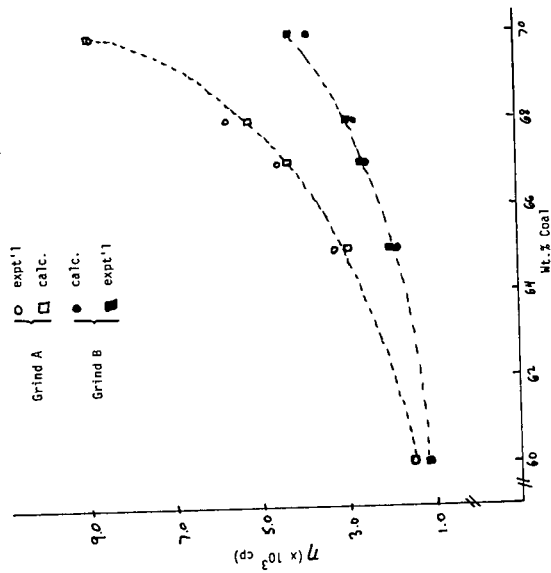


FIGURE 3



## BENEFITS OF COAL CLEANING UPON THE PERFORMANCE OF COAL-WATER SLURRIES

R. A. Wolfe & D. S. Walia

United Coal Company, Bristol, Virginia 24203

### Introduction

Coal preparation as described in "days gone-by" functioned around the one word - "TIPPLE". This word, tipple, is rapidly losing its identification within the coal industry except for those we admire so much who have devoted their entire industrial life to this coal industry. Now, through the modern coal industry, we hear such terms as coal washing, coal preparation, coal cleaning, coal beneficiation, which also in themselves create confusion about what is meant.

As you drive along the Appalachian roads today, remnants of the tipples of "days gone-by" can be seen. Long chutes can be seen coming down the mountainside to the loading truck ramps. These wooden structures remind us of the technology of that day and they are now left only to the imagination of the artist to describe those days.

Today's coal preparation facility looks more like a massive industrial complex with long belt lines coming in and out of a preparation facility and ancillary facilities such as dewatering and refuse handling systems. An aerial view of one of our preparation plants is shown in Figure 1. This plant, located at one of our operations near Grundy, Virginia, processes in excess of 700 TPH of feed coal in both coarse and fine coal cleaning circuits. It is true that the coal industry is now directed more by the characteristics and quality of coal than if it were just a black versus gray color used years ago. Even in a few years from now, this preparation plant will be obsolete. One will see a complex which looks similar to an oil refinery. Various grades of coal products will be produced and tank cars will be used to carry the liquid coal product away from the plant. The coal industry is becoming more concerned with the needs of the customer than ever before. Oil has replaced coal in many markets because it is a liquid that can be pumped, stored and burned much easier and cleaner than coal. With the development of new technology to convert coal into a liquid fuel form through coal-oil mixing, coal-water mixing and even with some new technology still on the horizon, coal can be placed into a converted liquid form similar to oil. However, one major technology gap remains and that is the need to remove the non-carbon products of ash and sulfur from the coal to a level equivalent to that required for burning oil. Now I did not say the same ash and sulfur levels must be achieved. No, one must look at the burning, off-gas systems, and regulations and then decide what the ash and sulfur levels of any liquid coal product must be.

### Coal Preparation & Impact on Utilization

The steel industry has generally benefitted from coal preparation from production of metallurgical grade coal with desirable coking coal through optimum blending of seams of coals and reduced ash, sulfur, and moisture of coal. Today, almost 100% of metallurgical coal is processed in preparation plants. Whereas, less than 25% of the coal burned by industry for utility generation is cleaned before combustion.

What coal preparation can do.

- Reduce ash - and sulfur oxide - forming components from coal before combustion.
- Produce consistent quality fuel.
- Upgrade the heat value of fuel.
- Optimize the size consist of fuel.
- Produce multigrade fuel with varied levels of ash, sulfur, and heat content.

The coal producer benefits from the coal preparation through production of improved and premium fuel with broad market acceptability. With our recent emphasis to utilize the low ash and low sulfur coal, the premium quality coal in the ground is depleting. Coal preparation is the only technology available to producers to increase the utilization of low-grade coals. The continuous mining operations are producing more fine size and higher ash coal which can only be upgraded through proper coal preparation. However, dewatering of the fine size coal is still problematic which not only affects the fuel value but also is a major problem in handling and transportation due to freezing in winter months.

Coal users for industrial applications have been motivated in the past primarily by the lowest price coal. Not until the last decade have many of the more modern utility companies started to appreciate that just because coal is black does not mean it is all the same. To date, compliance of air quality standards has been the prime incentive for using beneficiated coal. However, a number of recent studies by the utilities, Electric Power Research Institute and the U. S. Department of Energy have shown the benefits of coal preparation on overall systems and significant reduction on the cost of electricity production. (1,2,3,4,5)

These benefits include:

- Reduced transportation cost through more Btu per ton.
- Improved boiler efficiency and boiler availability due to consistent and high quality fuel.
- Reduced operating costs of pulverization, ash-handling systems, flue-gas clean-up, and ash-disposal systems.
- Reduced capital cost of boiler and flue gas clean-up equipment.

The American Electric Power Company has been one of the prime advocates of benefits of coal preparation of utility application. Mr. Gerald Blackmore, the Vice President of AEP, has spent almost his entire life in the coal industry and advocating the benefits of coal preparation. He has been referred to many times as the "Patron Saint of Coal Washing". To prove his point, he points out that AEP's

average price to all its customers in 1979 was 2.86 cents against an estimated national average of 3.94 cents.(6)

#### Benefits of Coal Cleaning Upon Performance of Coal-Water Mixtures

One of the major problems that has hampered coal utilization for industrial use is the materials handling problems associated with bulky coal. With the advent of new technologies associated with coal-oil, coal-water, and coal-methanol mixtures, it is becoming possible to put coal into a liquid form where it can be stored in tankers, shipped by pipeline and fed into boilers without the manual labor associated with coal handling as it is today.

This type of developing market encourages coal preparation of fine size coal and mixing of the coal into a stabilized solution even at the preparation plant and shipped directly to boilers through pipeline and fed into boilers without even being touched.

If this market does develop, as it is expected to do, the utilities then will be able to replace oil with liquid coal as well as develop new boilers designed specifically for this liquid coal form. However, much of the development depends upon cleaning the coal to very low ash and sulfur levels. United Coal has been pursuing this development for the past several years. In fact, UCC has now developed and optimized a commercial coal preparation plant to produce up to 300 TPH of 2% ash coal. Currently, no customers are beating our door down for this super-clean coal primarily because the market for replacing oil with a liquid coal has not developed. The prime purpose of developing this super-clean coal is to optimize the coal feed to make a premium coal-water mixture fuel for testing purposes.

To date, United Coal Company has produced 300 tons of this super-clean coal in our commercial plant to optimize our processing conditions, establish economics of the process and prepare test samples for combustion tests by various organizations. A preliminary report on the Department of Energy's tests on our coals is given below. A comprehensive detailed report on these tests is currently under preparation at DOE.

#### Coal-Water Combustion Tests on Beneficiated Coal

The Department of Energy has conducted several combustion tests on coal-water mixture fuel prepared with beneficiated coals. These tests were conducted at DOE's Pittsburgh Energy Technology Center 700 HP combustion test facility. United Coal Company supplied the beneficiated coals from their commercial process and advanced beneficiation process.

The primary purpose of the tests was to evaluate the particulate emissions and furnace ash deposits as a function of ash content in the coal. The Department of Energy's combustion test conditions were set at excess air of 15 weight %, combustion air temperature of 500°C, with a steam output of about 24,000 lbs/hr. Significant test results are listed in Table I.

TABLE I. TEST RESULTS OF DOE COMBUSTION TESTS  
ON COAL-WATER MIXTURE WITH BENEFICIATED COALS

<u>Coal Type</u>	<u>Ash%</u>	<u>Particulate Emission, lb/hr</u>	<u>Furnace Ash Deposit, lb/hr</u>	<u>Carbon Conversion Efficiency</u>
UCC Commercial Coal	~ 8	120	8.9	97.5
UCC Super-Clean Coal	~ 2	79	2.3	97.4

These test results show that even though the carbon conversion efficiency remains about the same, there is significant decrease in particulate emissions and furnace ash deposits. The composition of furnace ash deposits from the low-ash coal was primarily aluminum silicate and is highly friable and non-sticky and thus can be blown off with blower action.

These results indicate that by cleaning the coals to low levels of ash, the most serious problem of furnace ash deposits can be solved thus making coal-water mixture fuel compatible with boilers designed for firing low-ash fuel oil.

### References

1. Yeager, K. E. "More Coal Per Ton." Combustion (April 1980).
2. Buder, M. K., K. L. Clifford, H. Hueltenhain, and C. R. McGowin. "The Effects of Coal Cleaning on Power Generation Economics." Combustion (April 1980).
3. Phillips, P. J. and R. M. Cole. "Economic Penalties Attributable to Ash Content of Steam Coals." Mining Engineering (March 1980).
4. Thode, E. F., J. M. Williams, E. M. Wewerka, and P. Wagner. "Costs of Coal and Electric Power Production - The Impact of Environmental Control Technologies for Coal-Cleaning Plants." Los Alamos Scientific Laboratory Informal Report No. LA-803-MS (October 1979).
5. Holt, E. C. Jr. "Effect of Coal Quality on Maintenance Costs at Utility Plants." U. S. Department of Energy DOE/ET/12512-1 (June 1980).
6. Smith, G. "Blackmore Backs Doctrine of Washed Coal with Fact." Coal Industry News (November 30, 1981).

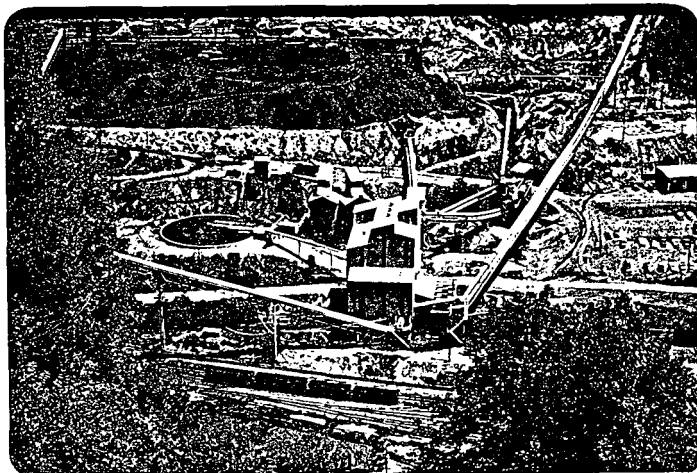


FIG. 1: COAL PREPARATION PLANT (WELLMORE NO. 7)  
OF UNITED COAL COMPANY AT  
GRUNDY, VIRGINIA

## COAL AQUEOUS MIXTURES

SEYMOUR MARK

### ADVANCED FUELS TECHNOLOGY

A Gulf+Western Company  
Zerbe Research Center  
Bethlehem, PA 18017

Coal aqueous mixtures can be prepared by simply mixing pulverized coal with water. Table 1 shows the formulation for such a slurry and compares it to one for a modern slurry.

#### Simple Slurry Versus Modern Slurry

A visual inspection of slurries made with these formulations would show them to be quite similar. Both would appear to be black fluids with comparable viscosities. A closer examination would reveal that the simple slurry had a considerable degree of settling while the modern slurry was uniform. Another difference between the two slurries is their concentration of coal.

Table 1 shows that the simple slurry contains 518.5 pounds of coal per hundred gallons and that the modern slurry has 725.9 pounds. Expressed another way, simple slurry contains 53% coal and modern slurry 70% coal. A comparison of the volume relationships of the ingredients in these slurries shows that simple slurry contains about 45% coal and 55% water. In the modern slurry formulation we see that the volume of coal is considerably greater than that of the water; 62.6% coal, 36.9% water. This higher ratio of coal to water is achieved in part with the use of additives. These additives, which can total only 0.5% of the weight of the slurry in some cases, not only allows a greater concentration of coal to be incorporated into the mixture; but they also disperse the particles, keep them apart and

suspended in the medium, and provide the type of flow properties necessary to pump and atomize this fuel.

What are these additives, and how did they come to be used in preparing coal aqueous mixtures? The additives are primarily surface active compounds. The technology is guided by the sciences of colloid and surface chemistry, and of rheology.

### Preparing Coal Aqueous Mixtures

The first challenge in preparing coal aqueous slurry is to disperse the coal particles into the medium. When coal has been ground into a powder, the coal particles can adhere to each other in aggregates. A dispersion of the particles must be accomplished. The process involves separating the particles in an aggregate until they are dispersed. Figure 1 shows different aspects of wetting and dispersion, as now viewed. The cluster of coal particles shown as "aggregated" has various degrees of air and moisture on the surface of the particles and in the spaces between them. Work and surfactants are used to break up these aggregates, by replacing the air with water. The separated particles are shown as "wetted." They are covered with a layer of water, that has displaced the air. They also contain adsorbed surface active agents and protective colloids on their surface. Coal will occupy less space when it is wetted by a liquid, than when it is mixed with air and moisture. The volume of air displaced is considerable, it demonstrated by weighing the amount of powdered coal that can fit into a gallon container. This is generally about 4 pounds. Yet we know from our examination of a modern slurry formulation that it contains over 7.25 pounds of coal per gallon, and still has room in the



container for over 3 pounds of water.

It is believed that after the coal particles are wetted-out, they disperse uniformly throughout the medium into individual pieces shown as "dispersed." The dispersed state is achieved if the particles in the suspension are separated sufficiently for the repulsive force to exceed the attractive force<sup>(1)</sup>. If the attractive force is stronger, the particles are believed to re-combine as flocculates. The cluster shown as "Flocculated" differs from the aggregated cluster in that the surface of the particles and the space between them contain water rather than air. As a result they are easier to redisperse. Nevertheless, they act as if they are single large particles, and tend to settle more rapidly.

#### The Interaction Forces Between Particles

There are three major types of interaction forces between colloidal particles: 1. London - van der Waals, 2. Coulombic forces (DLVO), 3. Solvation, adsorbed layers<sup>(2)</sup>. The effect of these forces is shown graphically in Table 2.

London - van der Waals forces are due to the influence of the dipoles within the particles acting on each other. They are attractive forces which are electromagnetic in nature. It is conventional to assign a negative value to an attraction potential and a positive value to a repulsion potential.

Coulombic forces may be either attractive or repulsive, but are almost always repulsive when dealing with coal particles dispersed

in water. They are electrostatic in nature and arise from the unequal distribution of ions in solution around the particle and at its surface. This unequal distribution causes one side of the interface to acquire a net charge of a particular sign and the other side to acquire a net charge of the opposite sign, giving rise to a potential across the interface and the so-called electrical double layer<sup>(3)</sup>. The stability of a dispersion can depend upon the degree of electrostatic repulsion. The degree of which is related to the thickness of the electrical double layer.

The interplay of the electromagnetic and electrostatic forces forms the substance of the DLVO theory, which deals in a fundamental manner with the kinetics of flocculation and the stabilization of particle dispersions. Although the DLVO theory is very useful in predicting the effect of ionic surfactants as electrical barriers to flocculation, other factors must be considered to explain the effect of surfactants on dispersion stability.

Surfactants that are polymers or that have long polyoxyethylene chains may form non-electrical barriers to flocculation in aqueous media. An adsorbed layer of non-ionic surfactant on the surface of a particle can provide a steric hindrance to close particle approach by interposing a mechanical barrier. When particles collide, the distance between the surfaces is increased by twice the thickness of the adsorbed layer. When the attractive force at this distance is still sufficiently large that interaction of the adsorbed layers occurs, there is a decrease in the entropy of the system. The term "entropic repulsion" was introduced by Mackor and van der Waals in reference to the loss of movement in the tails of the adsorbed molecules when two adsorbed layers interpenetrate<sup>(4)</sup>.

## Properties of Coal

The water requirement of coal aqueous mixtures is a function of the properties of the constituents in the slurry. These are the coal, the water, and the additives. The chemical and physical properties of the coal have a major influence on the amount of water needed to achieve a slurry with desired flow characteristics. Coal is a heterogeneous substance that is a mixture of combustible metamorphosed plant remains that vary in physical and chemical composition<sup>(5)</sup>.

Coal may be classified by rank according to fixed carbon content and heating values. Higher carbon content generally correlate with higher BTU values that designate the coals that usually make better fuels. Coals with higher volatile matter improve the combustion properties of aqueous slurries.

Coals also differ considerably in physical structure. The structure of coal can be so intricate and extensive as to make them something like a solid sponge<sup>(6)</sup>.

The mineral matter and sulfur content of coal show large variations. Of course, coals that are low in these materials produce slurries that are lower in pollutants and cause less ash deposits in furnace. Another way to make slurries that are low in pollutants and less prone to furnace fouling, is to beneficiate the coal prior to its incorporation into slurry. Beneficiation processes have been developed that remove a substantial part of the ash content of a coal and lower its sulfur concentration. This can now be accomplished at very high rates of recovery and excellent slurries are being prepared with this beneficiated coal.

### Coal Size Consist

Another property of coal to be studied that may influence its water requirement in aqueous mixtures is size consist. Coal with a coarse size consist has a relatively small surface area per unit weight and requires less water to coat the coal particles. Consequently, a lower amount of water is needed to fluidize the particles, and slurry of higher solids content can be produced. Coal with a fine size consist has a relatively large surface area per unit weight which requires more water to coat the coal particles. However, the finer particles may fit into the interstices between the larger particles thereby reducing the void volume.

Predictions of the packing patterns of coal particles are complicated by many factors among which are size, size distribution, and particle shape. The Rosin-Rammler relationship was developed for representing the size distribution of powdered coal<sup>(7)</sup>. This formula, as well as empirical methods, have been employed to determine coal size consists that have the lowest water requirement. However, the type of particle size distribution likely to give the lowest water requirement would include sizes that might be too large for good combustion and suspension properties, and the procedures needed to produce this type of size distribution would be expensive. Certainly, economic considerations as well as fuel properties are influential in determining the size consist of coal to be used in aqueous slurry.

### Slurry Formulation

Coal aqueous mixtures have been prepared containing coal, water, a nonionic surfactant, and also defoaming agents, gums and salts. Nonionic surfactants containing polyoxyethylene can be used. It is believed that they lower the surface tension of the water, keep the coal particle from flocculating, promote suspension, and provide good flow properties. While playing a major role in producing coal aqueous mixtures, nonionics can be employed at concentrations of less than 0.4%.

Anti-foam agents can be used to lower the amount of foam in the slurry. Also, gums such as water soluble resins can be used to increase the viscosity of the medium. The quality of the water can also influence the stability of the slurry and its solid concentration. Water can contain soluble minerals which become electrolytes in the slurry, that can have an effect on the electrical balance of the system. Slurries stabilized with non-ionic surfactants are less susceptible to their influence.

### NonIonic Surfactants

Some nonionic surfactants that contain long chains of polyoxyethylene are shown in Figure 2. Figure 2a shows a surfactant having an ethylene diamine backbone, which is a block polymer containing chains of propylene oxide and ethylene oxide of various lengths. Another compound of this type containing chains of propylene oxide and ethylene oxide is shown in Figure 2b. This surfactant has a propylene glycol base. The formula shown in Figure 2c contains a single chain of ethylene oxide attached to a nonylphenoxy group. It has no propylene oxide.

Each of the formulas shown in Figure 2 represent a different series. The individual surfactants in each series differ from each other primarily by the length of the ethylene oxide chain. The moles of ethylene oxide on these molecules range from 4 to over 300.

The nonionic compounds are polar and have hydrophobic and hydrophilic portions. In coal aqueous mixtures, the hydrophobic end of the surfactant is believed oriented toward the coal particle and the hydrophilic end toward the aqueous medium. In Figure 2a, the hydrophobic portion encompasses the ethylene diamine and propylene oxide part of the molecule. For the molecule shown in Figure 2b, it is the propylene glycol portion together with the propylene oxide chain that comprises the hydrophobic segment of the surfactant, and in Figure 2c, the nonyl hydrocarbon chain and benzene ring are the hydrophobic end of the compound. For all these molecules, it is the ethylene oxide portion that is hydrophilic. For each of the compounds, those with the highest molecular weight in the series have the longest polyoxyethylene chains. The longer the chain of ethylene oxide, the further they extend into the solution.

### Experiments

Experimental work done with these surfactants in coal aqueous slurry was revealing. A comparison of the compounds that were effective in producing a 70% solids slurry, with those that were not, showed that between the primary difference between them was in the ethylene oxide content. The surfactants that were found effective contained 100 or more moles of ethylene oxide, while all

that were not, contained less. Molecular weight did not appear to be as influential because two of the compounds deemed not effective had higher molecular weights than the one that was.

### Slurry Properties

Coal aqueous mixtures are designed to conform to two major categories of properties: fuel and rheological. Fuel properties relate to the BTU content of the slurry, its level of ash, sulfur, and volatile matter, and sieve analysis. Rheological properties are concerned with the flow and handling characteristics of the slurry, and its stability to settling and shear.

A viscosity profile of a coal aqueous slurry is shown in Figure 3. This slurry exhibits desired rheological properties; its viscosity is well above 10,000 centipoise at low shear rates of  $0.3 \text{ sec}^{-1}$  and below, and it is lower than 2000 cP at shear rates above  $100 \text{ sec}^{-1}$ . The high viscosity at low shear rates indicates that this slurry will resist settling when it is at rest. The lower viscosity at  $100 \text{ sec}^{-1}$  indicates that it will pump readily. Shear rates during atomization are estimated to be at least  $10,000 \text{ sec}^{-1}$ . The curve in Figure 3 suggests that the viscosity of this slurry at that shear rate will be low, and that it will atomize well.

Slurries that decrease in viscosity with increased shear stress are described as pseudoplastic, and the curve in Figure 3 shows a material with this property. If this slurry was measured at even lower shear rates, and the data showed that flow did not begin until a certain minimum shear stress was exceeded, then the slurry could be described as a Bingham plastic. The point at which flow starts in such a system

is called yield value, which is often manifested in materials with high concentrations of powder dispersed in liquids.

### Summary

Coal aqueous mixtures can be prepared that have high coal content, are stable to settling, and can be pumped and atomized. The concentration of coal in a slurry depends upon the water requirement of the system. This requirement is effected by the grade of coal used, its size consist, and upon the additives in the formulation. Of particular importance is the type of surfactant used. Surfactants lower the surface tension of water and adsorb at the solid/solution interface to hinder close particle approach, ionic surfactants do so primarily by electrostatic repulsion. Nonionic surfactants do so primarily by steric hindrance.

Coal aqueous slurry can be made at a cost that is lower than that of No. 6 fuel oil by over \$1.00 per million BTU. This differential has provided the economic incentive to develop aqueous slurry as a replacement fuel. The findings presented in this study, and in work done by others in the industry, indicate that the research in this field has succeeded in developing a new fuel.



## REFERENCES

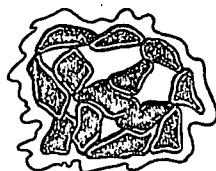
1. Parfitt, G. D., Dispersion of Powders in Liquids, Elsevier, Amsterdam, 1969.
2. Patton, T. C., Paint Flow and Pigment Dispersion, Wiley, New York, 1979.
3. Rosen, M. J., Surfactants and Interfacial Phenomena, Wiley, New York, 1979.
4. Matijevic, E., Surface and Colloid Science, Volume 8, Wiley, New York, 1976.
5. Leonard, J. W., Mitchell, D. R., Coal Preparation, The American Institute of Mining, Metallurgical, and Petroleum Engineers Inc., New York, 1966.
6. Berkowitz, N., An Introduction to Coal Technology, Academic Press, New York, 1979.
7. Cadle, R. D., Particle Size, Reinhold Publishing Corp., New York, 1965.

Figure 1

### ASPECTS OF WETTING AND DISPERSION



AGGREGATED



FLOCCULATED

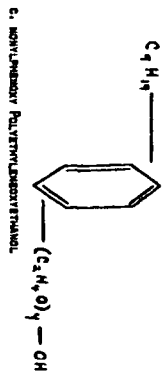
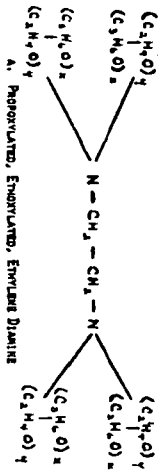


DISPERSED



WETTED

## MONOMERIC SURFACTANTS



**Figure 3**

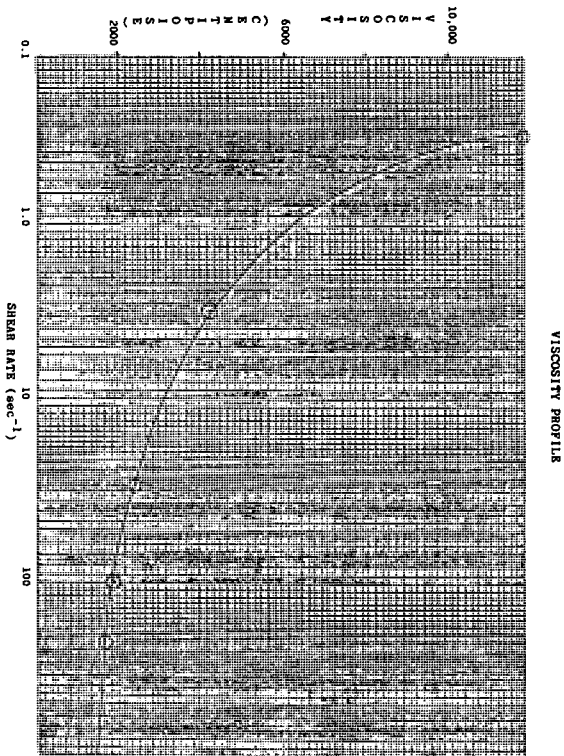


Table 1

Coal Aqueous Mixture Formulations  
(per 100 gallons slurry)

	<u>Simple Slurry</u>		<u>Modern Slurry</u>	
	<u>Weight</u>	<u>Volume</u>	<u>Weight</u>	<u>Volume</u>
	<u>Lb.</u>	<u>% (Gal.)</u>	<u>Lb.</u>	<u>% (Gal.)</u>
Coal (MF)	518.5	(53.0)	725.9	(70.0)
Water	460.1	(47.0)	306.6	(29.5)
Additives			5.0	(0.5)
	978.6	100.0	1037.5	100.0

Table 2

Interaction Forces Between Particles

	<u>Forces</u>		<u>Nature</u>
	<u>+   -</u>		
DLVO THEORY	1. London	Attraction	Electromagnetic
	2. Coulombic	Primarily Repulsion	Electrostatic (Electrical Double Layer)
STERIC HINDRANCE THEORY	3. Solvation	Repulsion	Adsorbed Layers Entropic

CURRENT PROGRESS IN  
COAL-WATER SLURRY BURNER DEVELOPMENT

R. K. Manfred - EPRI  
R. W. Borio  
D. A. Smith  
M. J. Rini  
R. C. LaFlesh  
J. L. Marion

Combustion Engineering, Inc.  
Under EPRI Sponsorship

To be presented at  
AMERICAN CHEMICAL SOCIETY SYMPOSIUM  
Division of Fuel Chemistry  
March 20-25, 1983  
Seattle, Washington

"LEGAL NOTICE"

"This paper was prepared by Combustion Engineering as an account of work sponsored by the Electric Power Research Institute, Inc. (EPRI). Neither EPRI, members of EPRI, Combustion Engineering, nor any person acting on their behalf: (a) makes any warranty, express or implied, with respect to the accuracy, completeness, or usefulness of the information contained in this paper, or that the use of any information, apparatus, method, or process disclosed in this paper may not infringe privately owned rights; or (b) assumes any liabilities with respect to the use of, or for damages resulting from the use of, any information, apparatus, method, or process disclosed in this paper."

## CURRENT PROGRESS IN COAL-WATER SLURRY BURNER DEVELOPMENT

### INTRODUCTION

There has been significant interest in recent years in development of domestic fuels which could displace those presently imported by U.S. industry. Because of the large quantity of fuel consumed by the electric power generation industry, much of this interest has been focused on fuels to replace oil and gas combusted in existing utility boilers. Many of these efforts have focused on the use of coal as the replacement fuel since it is the United States' most abundant fossil fuel.

Unlike oil, coal cannot be easily nor inexpensively refined into a consistent definable fuel. Every coal type is different in combustible properties as well as mineral matter content and composition. Unfortunately, these are two key parameters which significantly influence the determination of a particular coal's successful application as a replacement fuel in an existing utility boiler. Successful application also depends on several other key economic factors as well; boiler derating, differential fuel savings between the presently used fuel and the candidate alternate fuel, and lastly, the resulting payback period over which the utility must amortize the cost of converting to the new fuel.

Figure 1 shows the relationship of these economic parameters. If one considers seven (7) years a reasonable payback period, Figure 1 illustrates that, with realistic unit deratings of up to 25%, a differential fuel cost of between \$1.00 and \$2.00 per million BTU's must be achieved to make conversion economic. This delicate economic balance is the very reason utilities have been slow to accept coal/oil slurries as a viable alternative to oil alone. With the nominal cost of oil at approximately \$6.00/MMBTU and the nominal coal price at \$2.00/MMBTU, and the practical amount of coal that can be mixed with oil limited to about 50% on a mass basis, the raw products alone are about \$4.00/MMBTU without any allowance for slurry preparation. With this narrow differential in cost, many utilities are unwilling to risk conversion of operating units to this new fuel.

Because of the marginal economic incentive of coal/oil slurries, interest has shifted to a relatively new potential conversion fuel-coal/water slurry (CWS). Coal/water slurries have the distinct advantage of requiring no oil and therefore the potential differential in fuel cost over operation on oil alone can be much greater than that with coal/oil slurries. Coal/water slurries have several possible technical limitations, however, which must be reconciled before they can be considered as a viable replacement for oil or gas in utility boilers.

One of the concerns which must be addressed is the development of an atomizer that will properly atomize this new fuel. A problem that the atomizer development engineer faces is that most CWS fuels under development today have been designed to maximize coal content and fuel stability (i.e., minimization of settling). From an economics and transportation standpoint this approach makes sense but results in a fuel which maybe viscous, and therefore difficult to effectively atomize. If a slurry cannot be economically atomized it will not be a viable commercial fuel. Therefore, the successful CWS fuels will have to have both acceptable storage stability and rheological properties to permit good atomization with realistic levels of atomizing assist fluid.

Other concerns, in addition to rheological fuel properties, are fuel ignition and warm-up requirements, burner stability and turn-down, and carbon conversion and thermal efficiencies. Most CWS testing to date has been in small laboratory facilities of 1 to 4 MMBTU/hr and, in general, results have been poor, compared to that which must be achieved if CWS fuels are to be accepted as a viable replacement fuel by utilities. Test furnaces have required extensive preheat, burner turn-down has been extremely limited and carbon conversion efficiencies have, at best, been in the high 80% to mid 90% range(1,2,3).

In addition to these potential problems with CWS combustion, Figure 1 indicates that unit derating can play a significant role in dictating the success of a fuel conversion. For this reason coals to be used for CWS's must either be carefully selected on the basis of their original ash characteristics or they must be beneficiated (i.e., cleaned of mineral matter) to minimize furnace slagging/fouling and erosion such that significant boiler deratings will not be encountered.

#### CWS BURNER DEVELOPMENT

This paper is a progress report on a joint program between Combustion Engineering (C-E) and the Electric Power Research Institute (EPRI) to develop and demonstrate a commercial scale CWS burner which meets reasonable commercial success criteria. As such, a burner is presently being developed which meets the following constraints:

1. Permits ignition in a cold furnace with conventional ignition equipment.
2. Operates stably over a 4 to 1 turndown range without supplemental ignition fuel.
3. Employs fuel and atomizing media pressures that are obtainable with commercially available equipment.
4. Requires atomizing media to fuel mass flow ratios similar to those used for oil.
5. Produces carbon conversion efficiencies comparable with oil (i.e., high 90% range) at acceptable excess air levels (i.e., 20-30%) and reasonable air preheat temperatures (i.e., 250 to 400°F) over the full load range of the burner.

To achieve these goals C-E is using a proven three step firing system development approach.

1. Development of a CWS atomizer using C-E's Atomization Test Facility.
2. Development of an aerodynamically sound burner register using C-E's Burner Modeling Facility.
3. Integration of the developed atomizer and burner register, and optimization of the CWS firing system's combustion performance at a commercial firing scale of 80/MMBTU/hr in C-E's Full Scale Burner Test Facility.

This paper does not contain all combustion data which was still being analyzed at the time this paper was prepared; the combustion data is, therefore, preliminary.

#### FUEL PREPARATION AND CHARACTERIZATION

The fuel required for this development program was donated by Advanced Fuels Technology (AFT), a Gulf and Western Company. The coal used was a Clearfield County, Pennsylvania bituminous, selected by EPRI. The required coal was cleaned, prior to testing and slurry preparation, at EPRI's Coal Cleaning Test Facility in Homer City, Pennsylvania. A simplified flow schematic of the cleaning process used is shown in Figure 2, and the analysis of the cleaned coal is shown in Table 1.

Coal to be cleaned by EPRI's test facility is initially crushed to a nominal 3/4" x 0 size and then processed through a multistage "desliming screen". The first screening stage removes oversized material (+3/4") from the process stream. The second stage removes coal which is of a 3/4" x 28 mesh size. This is the main process stream. Separated material (+3/4" and -28 mesh) is collected in a refuse pile for future independent treatment. The main coal stream is then processed through two stages of "heavy media cyclones" followed by a "sieve bend & screen" to separate the clean coal from the refuse portion. The separation principle is based on the mass density differences between the coal (which is relatively light) and the high mineral matter

fractions (which are relatively heavy). After passing through these steps the coal is passed through a "basket centrifuge" to be partially dewatered. At this point the coal is considered "cleaned". It is metered by a weigh belt and is passed to a storage pile.

The high ash refuse obtained from the separation processes is collected in a refuse pile for disposal and/or future reprocessing. Process fluids are separated from the refuse and cleaned coal streams, and collected for reuse. For the special purpose of generating a very low ash coal for this testing program, refuse material was not reprocessed and combined with the initially cleaned main coal stream as would be the normal procedure.

In all, approximately 150 tons of cleaned coal were prepared for this program. Approximately 40 tons of the cleaned coal was reserved for base coal testing to establish a meaningful reference base for comparison to CWS combustion performance. The balance of the coal (approximately 110 tons) was processed, by AFT, into a nominal 70% solids CWS of predetermined specifications. These specifications were developed jointly by C-E and AFT to assure the maximum probability for combustion success through careful attention to oversized particles and minimization of fuel viscosity. The developed fuel specifications are presented in Table 2 with an analysis of the produced CWS. A schematic of AFT's CWS preparation system is shown in Figure 3.

Figure 4 shows a typical viscosity profile of the CWS which was obtained using a Haake Rotovisco viscometer. As can be seen in Figure 4, the CWS exhibited Newtonian to slightly pseudoplastic behavior (i.e., viscosity remains constant or decreases slightly with increasing shear rate). From an atomization standpoint, pseudoplasticity is desirable since the viscosity decreases at the high shear rates encountered within the atomizer. A Newtonian behavior is also acceptable since the viscosity remains constant with increasing shear rate. Dilatent behavior is not acceptable since the viscosity increases with increasing shear rate and would lead to poor atomization.

It is important to note that in order for CWS to attain commercial acceptance, a balance must be achieved between the high static viscosity required for transport and storage stability and the rheological properties required for atomization and combustion. Also, rigid control of particle top size and stringent quality control by the slurry manufacturers is necessary to insure a consistent supply of usable CWS.

#### FUEL SHIPPING, STORAGE AND HANDLING

The CWS prepared by AFT was shipped to C-E's Kreisinger Development Laboratory (KDL) at Windsor, Connecticut in conventional pressurizable tanker trucks. Although the tankers used had volumetric capacities of approximately 6500 gallons, five tankers were needed to transport the required 21,000 gallons of slurry because each was limited to a capacity of only about 4,200 gallons due to the legal over-the-road weight limit of 45,000 lbs. Photographs 1 and 2 show a tanker truck arriving at C-E and being unloaded, respectively.

C-E's Alternate Fuels Handling Facility (AFHF) is shown schematically in Figure 5. This facility is comprised of a 15,000 gallon storage tank, a 2500 gallon day tank, an homogenizer and several pumps, filters and heaters configured to handle slurry-type fuels. Figure 6 shows the arrangement of those components of the AFHF specifically utilized for the CWS testing program.

Preliminary testing indicated that the tanker trucks could be effectively unloaded two ways. One manner was by pumping the CWS from the tanker in an unpressurized state. A Tuthill model 120A pump was used and permitted unloading to the AFHF 15,000 gallon storage tank at a rate of 12-15 gpm. The second procedure, which was used for the balance of the required unloading, was to by-pass the pump and unload the fuel by pressurizing the tanker to 30 psig. At this pressure, the tankers were unloaded at an average rate of 50-70 gpm, or 1-1½ hours per 4,200 gallon tanker load.

As was previously mentioned, a total of five tanker truck loads of CWS were received for the test program. The initial two tankers received contained CWS of proper specification (see Table 2) and appeared to maintain storage stability and slurry uniformity over a period of several weeks with only occasional recirculation using the Tuthill pump. A portion of the fuel from these initial two tankers was used for the atomizer development phase which will be discussed later.

These were some off-spec. changes in the third tanker shipment of fuel which affected rheological properties of previously shipped fuel as well as the fourth tanker load of CWS fuel. On-site adjustments by G&W personnel combined with increased fuel circulation at C-E permitted testing to continue. The last tanker of fuel was significantly higher in viscosity than the previous fuel batches; this required higher fuel supply pressures to achieve the same mass flow rates as the previous fuel shipments.

### CWS ATOMIZER DEVELOPMENT

The development of an atomizer for CWS was essential to the developmental success of the C-E/EPRI CWS burner. The purpose of the atomizer is to fragment the CWS fuel stream into readily combustible droplets. The size, velocity and trajectory of these fuel droplets is a function of both the atomizer's design and the burner's near-stream aerodynamics, and directly affects burner performance in terms of flame length, stability and carbon burnout.

In the course of development, careful consideration was given to both the CWS atomizer's generic design as well as its specific geometric dimensions. Of generic atomizer designs reviewed by C-E, the "Y" jet configuration (Figure 7) appeared to have the greatest potential for success with CWS. Two properties of CWS were identified as potentially problematic to effective atomization. These were its erosive nature and high viscosity (Figure 4). "Y" jet type atomizers utilize pressurized atomizing media (superheated steam or compressed air) to initiate fuel stream breakup through high shear turbulent mixing of the atomizing media and fuel streams. This "Y" jet atomization principle has been shown(4) to be effective for the atomization of viscous fuels and thus would be potentially successful with CWS. Secondly, because of the atomizer design's simple geometry, with no tortuous paths, it permits fabrication with erosion resistant materials (Figure 8).

Combustion Engineering has extensive experience in "Y" jet atomizer design and has developed a computer design code and a full scale Atomization Test Facility (ATF) to assist in "Y" jet atomizer design development. These were utilized in a three step approach which resulted in the successful development of a CWS atomizer. These steps were:

1. Theoretical identification of critical atomizer geometric dimensions based on fuel properties and atomizing media considerations.
2. Preliminary ATF testing and performance optimization of the theoretical atomizer design.
3. Detailed ATF performance characterization of an optimum atomizer design over a matrix of operation.

### ATOMIZER TEST FACILITY

C-E's Atomizer Test Facility (ATF) is designed to quantitatively characterize the atomization quality of full scale (10 gpm) burner atomizers. The facility is uniquely configured to obtain droplet size distribution and droplet ballistics (velocity and trajectory) information from fuel sprays.

The facility operates in a cold flow (non-combustion) mode and has provisions for studying both conventional liquid and slurry fuels. Provisions for slurry fuels include



a 700 gallon transportable fuel tank for storing and heating fuels prior to ATF testing. The tank is equipped with a mixer and recirculation system to minimize potential slurry solids stratification.

A schematic of the Atomization Test Facility is shown in Figure 9. The actual facility is presented in Photo 3.

Test atomizers are centrally located in the spray chamber and spray vertically down, thus minimizing the effect of gravity in atomization droplet ballistics measurements. Also, a constant velocity profile (10 ft/sec) airflow passes by the atomizer during testing to prevent potential droplet recirculation which would otherwise bias droplet trajectory information. Large windows in the spray chamber permit optical access across the atomized sprays. Optical spray diagnostic equipment is located on the two benches as shown. Once data is obtained from the spray, the fuel droplet-laden air flow is demisted and exhausted from the facility. The collected fuel is then removed for reuse or disposal.

#### OPTICAL DIAGNOSTIC TECHNIQUES

Two optically-based techniques are utilized by C-E in the ATF to quantify spray quality. A laser diffraction technique is used to determine the spray droplet size distribution and a high speed double spark photographic technique is utilized to define droplet velocity and trajectory.

The laser diffraction technique is based on the Fraunhofer diffraction of a parallel beam of mono-chromatic light by moving of stationary droplets or particles(5). A Fourier Transform lens yields a stationary light pattern from the light diffracted by the particles. A multi-element photo-electric detector located at the focal plane of the Fourier Transform lens produces an electrical signal analogous to the diffracted light. A mini-computer compares this signal with the derived signal based on a Rosin-Rammler model which continuously modifies the mean diameter and exponent parameters until a best fit is obtained(5). Percentage weight fraction and normalized percentage number density are then calculated from the best fit model.

Figure 10 shows a schematic of the laser diffraction apparatus. The laser is the monochromatic light transmission source and the diffracted light is received and analyzed by a Fourier Transform lens, a photoelectric detector, and a mini-computer. Note, the optical probe included in the schematic is used to alleviate measurement errors in dense fuel sprays.

The optical arrangement for the high speed double spark photographic technique is depicted schematically in Figure 11. Two spark-gap light sources are located on one side of the facility. Each source produces one intense, short duration (1 microsecond) flash of light. These flashes of light are directed through the atomizer spray by a lens system and into a camera lens located on the opposite side of the facility. The camera lens is focused on a specified plane within the spray field (object plane). Silhouette images of the droplets located in the camera's object plane and field of view are recorded on film.

The two flashes produce a double exposure silhouette photograph of the droplets. Accurate droplet velocity information is then obtained by measuring the distance traveled by an individual droplet between exposures with knowledge of the time interval between flashes. Similarly, droplet trajectory is determined by observing the direction of travel for individual droplets.

#### INITIAL CWS ATOMIZER DESIGN

The CWS atomizer was designed in part by the application of a computer code previously developed by C-E to predict "Y" jet atomizer atomization quality (in terms of spray droplet mass median diameter) with heavy fuel oils. This program code estimates atomizer performance as a function of critical fuel properties and atomizing media

constraints. These include, fuel viscosity, atomizing media density, and atomizing media to fuel mass flow. C-E utilized this code to predict CWS atomization quality. The predictions, in conjunction with pressure drop calculations, fluid momentum considerations, and geometric correlations obtained in previous atomizer development efforts, resulted in the identification of specific atomizer dimensions; these are shown in Figure 7. The target CWS atomization quality was that which is typical for firing residual fuel oil using a "Y" jet atomizer. Based on previous tests conducted in the ATF(6), a spray mass median diameter of 120 microns or less is characteristic of effective residual oil atomization. Note, that this droplet diameter is significantly larger than that of the individual coal particles of conventionally ground coal for P.C. firing.

This phase of CWS atomizer design actually yielded two distinctly different "Y" jet atomizer geometries with similar performance, given identical fuel and atomizing media conditions.

#### PRELIMINARY ATF TESTING

Preliminary ATF testing involved a comparative performance evaluation of the two "Y" jet atomizer geometries identified during initial CWS atomizer development. The laser diffraction system was utilized for this effort. Each atomizer nozzle design was tested at 100%, 50%, and 25% of maximum firing rate over a wide range of atomizing media to fuel mass flow ratios ( $.06 < A/F < 1.1$ ). Compressed air was used as the atomizing media. For these tests, CWS and atomization air were maintained at ambient temperature. Data obtained from these comparative tests is presented in Figures 12, 13, and 14.

At 100% load, nozzle design 5A produced finer sprays than nozzle 5B at A/F ratios greater than 0.17. Operation with such high atomizing media consumption is undesirable, however, because it is a parasitic energy loss, and thus negatively impacts boiler economics. Nozzle design 5B consistently produced a finer spray than design 5A at more favorable A/F ratios of 0.17 and below.

At both 50% and 25% load, nozzle design 5B produced equivalent or finer CWS sprays than nozzle design 5A at given A/F ratio settings. Based on these tests, nozzle design 5B was chosen for further detailed atomization quality optimization and characterization.

#### DETAILED CWS ATOMIZER TESTING

Detailed parametric testing of the optimum atomizer (design 5B) provided insight into the key operating parameters which influence atomizer performance. Parameters studied included:

- Atomizing media to fuel mass flow ratio
- Fuel mass flow rate
- Fuel temperature
- Atomizing media temperature

#### Atomizing Media to Fuel (A/F) Mass Flow Ratio

The ratio of atomizing media to fuel mass flow was found to have a significant effect on the performance of the CWS atomizer. Data depicted in Figure 15, taken at 100% load, indicates that above an A/F ratio of 0.17, the spray mass median diameter remains constant. A gradual degradation in atomizer performance occurred between A/F ratios of 0.17 and 0.06, and rapidly degraded below an A/F ratio of 0.06. Similar trends were noted at 50% and 25% load.

The spray droplet size distribution obtained on CWS at full load was similar to that obtained through previous testing of "Y" jet atomizers spraying fuel oil. The optimum range of A/F ratios for the CWS atomizer appeared to be between .08 and .14, which are also typical of those required for fuel oil atomization.

### Effect of Slurry Temperature

The effect of CWS temperature on atomization quality is presented in Figure 16. Atomizing air temperature was held constant at 95°F during these tests. CWS was tested at 95°F (ambient temperature) and at 150°F over a range of atomizing media to fuel mass flow ratios.

The data indicates that a slight decrease in spray mass median diameter (MMD) of approximately 10% occurred when the particular CWS tested was preheated prior to atomization. The reduction in MMD could possibly be attributed to a reduction in fuel viscosity at elevated temperature.

The slight decrease in MMD did not appear to provide sufficient justification for preheating the fuel in the combustion phase of the testing.

### Effect of Atomizing Air Temperature

The effect of atomizing air temperature on atomization quality is presented in Figure 17. CWS temperature was held constant at 95°F during this series of tests.

The data indicates that a reduction in MMD, of approximately 10%, can occur by preheating the atomizing air. Again, however, this reduction would not appear to be significant enough to warrant preheating the atomizing air.

### Effect of Slurry and Air Temperature

The combined effect of both elevated CWS and air temperature on atomization quality is shown in Figure 18. It was concluded from ATF testing that heating both slurry and air produced a finer spray yet than either fluid heated individually.

This information would be useful should a particular burner/atomizer combination prove to perform marginally on a specific CWS. Preheating both fuel and air may shift the droplet size distribution down to within a range capable of improving combustion performance. The improvement in performance would have to be evaluated against the increased capital equipment costs and energy costs incurred when preheating these fluids.

Overall, the performance of the developed CWS atomizer, with ambient CWS and air temperature, was quite similar to conventional C-E "Y" jet atomizer performance and fuel oil. For this reason, for the combustion evaluation of CWS, fuel was supplied at ambient temperature and atomization air was not heated beyond the compressor's nominal delivery temperature of 160°F.

### Droplet Ballistics

Droplet velocity and trajectory information, obtained through the use of the high speed double spark photographic technique, indicated that CWS droplet velocities were similar to those obtained for conventional fuel oils. Velocities ranged between 2 and 24 meters/second, at an axial downstream distance from the atomizer of 140 nozzle diameters. Droplet trajectories tended to follow predictable streamlines of a freely expanding jet.

Droplet velocity is a strong dependent function of droplet diameter for both oil and CWS.

Since the velocities obtained for both oil and CWS were similar, no droplet ballistics related changes in burner aerodynamic design appeared necessary.

## BURNER REGISTER DEVELOPMENT - COLD FLOW MODELING

A full-scale model of the proposed burner register was fabricated and flow model tested under isothermal conditions. The purpose of this work was to confirm that the register design exhibited satisfactory aerodynamic characteristics over the full range of air flows expected to be used during combustion operation. An important and necessary aerodynamic characteristic for good flame stability is the existence of a strong well developed recirculation zone at the burner throat. In the C-E CWS burner, the recirculation zone is established through combustion air swirl and a divergent burner throat. These are well known methods of inducing a recirculating flow and have been used commercially for some time(8,9).

Flow visualization techniques were employed by C-E and confirmed the CWS register design's satisfactory aerodynamics over a range of simulated operation. Figure 19 shows, schematically, the model used and the observed recirculation zone boundary.

## BURNER DESCRIPTION

The C-E coal-water slurry burner is a swirl stabilized unit configured for tangential firing and is shown schematically in Figure 20. The basic burner design is adaptable to wall firing with suitable modifications. The principle elements of the burner system are: a refractory-lined divergent throat, a combustion air swirler through which a portion of the combustion air is passed, auxiliary air nozzles, above and below the burner, through which the balance of the combustion air is ducted (unswirled), and a slurry gun with an atomizer.

The purpose of the refractory-lined divergent throat is to increase the mass recirculation ratio and therefore to stabilize the flame both aerodynamically and thermally. The swirled combustion air stabilizes the flame and contributes to high combustion efficiency. The atomizer's production of relatively fine CWS droplets combined with the overall burner aerodynamics has yielded acceptable stability, over a to 1 load turndown range. Acceptable combustion efficiencies have also been demonstrated with this burner/atomizer combination. Preliminary data documenting this performance will be covered in the following section.

## COMBUSTION TESTING

The combustion performance of the CWS burner was optimized and extensively evaluated at a commercial load which ranged from 20 to 80 MMBTU/hr. These tests were conducted in C-E's Full Scale Burner Facility (FSBF). The burner's combustion performance was parametrically investigated on both CWS and parent coal so that a meaningful combustion evaluation of CWS could be made via comparison to a known reference fuel. Test condition matrices for each fuel (shown in Tables 3 and 4) were designed to parallel one another so that direct test-by-test comparisons could be made. Test variables were; firing rate, excess air level, combustion air preheat temperatures, and also, for CWS, atomization air/fuel mass ratio. Data were obtained, depending on specific test conditions, of numerous independent parameters. These were gaseous emissions ( $\text{CO}$ ,  $\text{CO}_2$ ,  $\text{NO}_x$ ,  $\text{SO}_2$ , and  $\text{O}_2$ ), heat flux profile, calculated combustion efficiency, flame quality, fuel flowrate/temperature/pressure, combustion air flowrates/temperatures/pressures, atomization media flowrate/temperature/pressure, and at selected test points in-stack fly-ash sampling, which included dust loading, carbon content, particle size distribution and in-situ resistivity.

Prior to conducting these detailed combustion tests, prematrix and shakedown tests were performed to qualitatively define burner performance and to establish the probable ranges of operability. During these tests burner performance was optimized through combustion airflow distribution adjustments. Detailed parametric performance testing was then initiated once these preliminary tests indicated acceptable burner performance on CWS.

As stated previously, this paper is a progress report on C-E's CWS burner development program with EPRI. As of the date of writing (November 1982) combustion testing is complete, but detailed data analysis is still in progress. The data presented must be considered preliminary.

### CWS Combustion Testing

Observed CWS flame stability and appearance was acceptable over the range of burner operation tested. In general the flame was "attached" or nearly "attached" to the burner. No major burner operability problems were noted during testing, although several items warrant mention. Because of the CWS storage tank settling problems previously discussed, fuel quality varied appreciably from test to test. Solids content varied from 67.1 to 70.0%. Some degree of combustion data scatter may be attributable to this, although data presented here was well within measurement confidence limits.

Secondly, the CWS was ignited satisfactorily in a cold, unheated test furnace using the facility's standard 5 MMBTU/hr natural gas side pilot ignitor. There was only one unusual requirement identified for ignition. This was the necessity of "prewetting" (with water) the atomizer and slurry gun prior to CWS introduction to prevent the absorption of a small but apparently critical amount of the slurry's water component. This was accomplished by inclusion of a water supply line to the fuel piping at the slurry gun. Failure to follow this procedure significantly increased the potential for nozzle pluggage during ignition.

The ignition procedure was as follows. First, a 5 MMBTU/hr natural gas side pilot ignitor was turned-on. Second, a small amount of water was passed through the slurry gun and atomizer. Next, the water was turned-off and simultaneously the CWS and compressed atomization air were turned-on, resulting in satisfactory CWS ignition. The side pilot was normally shut-off after about fifteen minutes of operation. Nominal burner firing rate for light-off was 25 MMBTU/hr and combustion air preheat of 250°F was utilized. Note, ignition was consistently achieved in the test furnace while in a cold and unpreheated state. However, because the furnace was lined with a thin layer of refractory blanket to simulate normal furnace heat losses and hence actual furnace outlet temperature, the furnace wall temperature may have risen at a somewhat higher rate than would be seen in an actual clean cold boiler. Thus the time that the ignitor is required to be on for a field application may be somewhat longer than the period discussed here.

Lastly, all tests were conducted with the 70° spray angle, tungsten carbide sleeved, "Y"-jet atomizer described under atomizer development. Approximately 20 hours and 100,000 lbs of slurry throughput were logged on this atomizer. The atomizer port diameters were precision measured before and after testing and indicated no measurable wear in the critical zones protected by the tungsten carbide sleeve. By comparison a carbon steel atomizer was used for prematrix testing, and while no meaningful erosion rate data could be obtained because of the intermittent and variable operation, significantly greater wear was noted in this atomizer over a much shorter period (i.e. 4 hours and 25,000 lbs. of slurry).

### Parent Coal Combustion Tests

Parent coal combustion tests were conducted to provide baseline data to which the CWS combustion data could be compared. The parent coal was ground, for combustion testing, to a nominal size distribution of 70%-200 mesh which is standard for use as a boiler fuel firing pulverized coal.

Parent coal fuel injection modeled that of CWS so that meaningful fuel performance comparisons could be made. Coal was supplied in "dense phase" through a 1" ID fuel admission port to the center of a 70° diffuser cone. In this way the parent coal was "sprayed" into the furnace at the same 70° angle as that of atomized CWS. Note that the same combustion air register was used for both the parent coal and CWS tests.

Coal was supplied in dense phase with a C-E developed coal pumping, storage and supply system(10). This system permitted dense phase pulverized, parent coal, transport with transport air to fuel mass flow ratios in the range of 9 to 26. The parent coal was pneumatically conveyed from a 30 ton storage silo through an 1½" ID hose to the FSBF firing front. Pressure drop across the transport line varied from 6 to 26 psig.

Qualitatively, the combustion performance of the parent coal was excellent. Observed flame stability and appearance was similar, but slightly better than that noted previously for CWS over the same range of operation. The parent coal burned with a bright flame which was always "attached" to the burner.

Parent coal was readily ignitable in a cold, unpreheated test furnace using the facility's 5 MMBTU/hr natural gas side pilot ignitor. Once the parent coal was ignited in a cold furnace, the side pilot could be turned-off between one and five minutes with maintained flame quality and burner stability. For CWS ignition, 15 to 20 minutes were required before the side pilot could be turned-off. C-E has previously demonstrated that a similar type of dense-phase coal burner could be dependably ignited with an electric arc discharge within 30 seconds with no supplementary ignition or stabilization source, such as the side pilot.

A discussion of the comparative combustion performances of CWS and parent coal follows.

#### Combustion Performance Comparison of CWS to Parent Coal

To reiterate, both CWS and parent coal burned with bright, stable, "attached" or nearly "attached" flames over the burner load range tested. It was observed that as burner load was increased, from 20 to 80 MMBTU/hr, the axial flame length increased, but stability and attachment to the burner were maintained.

Figure 21 compares the carbon conversion efficiency of parent coal and CWS, as a function of excess air level at full load (80 MMBTU/hr). It can be seen that, at this load, parent coal combusted with 99+% carbon conversion efficiencies, and the CWS combusted with efficiencies about 1% less.

While the trends indicated in this figure are typical of those encountered at the other loads tested, preliminary data analysis indicates differences in carbon conversion efficiency of as much as 4% between parent coal and CWS existed at some test conditions. For most test conditions, however, carbon conversion efficiencies for CWS were diminished no more than 1 to 2 percent below that of the parent coal.

A comparison of carbon conversion efficiency as a function of burner load, between CWS and parent coal, at a constant 30% excess air level is shown in Figure 22. This figure reiterates the efficiencies noted in Figure 21. Parent coal was combusted with 99+% carbon conversion efficiency and again the CWS burned with approximately 1% lower efficiency over the load range presented. Note also that for each fuel, carbon conversion efficiency did not significantly vary as a function of load (40 to 80 MMBTU/hr) at 30 percent excess air.

Figure 23 illustrates the importance of good CWS atomization with regard to carbon conversion efficiency. All other conditions remaining the same, atomizer air to fuel mass ratio (A/F) was varied about an optimum value of 0.11 (identified during cold flow atomization development). Figure 23 indicates that below this optimum value carbon conversion efficiency drops off rapidly, while operation at higher A/F ratios yields no apparent efficiency change. This phenomena is in agreement with cold flow atomization results (Figure 15) which indicated rapid increase in mean atomized droplet size (diminished atomization quality) as A/F decreases from optimum and no improvement in atomization quality as A/F increased from optimum.

The resistivity values of the CWS and parent coal fly ashes, measured in-situ, are given in Table 5. These measurements indicate the fly ashes apparent collectability by electrostatic precipitation. What is important to note from Table 5 data is the lack of

significant difference between the CWS and the parent coal fly ashes. This implies that, at least for this specific case, the slurrying process had no significant effect upon fly ash resistivity (i.e., collectability). Fly ash collectability by ESP is also a function of particle size. Fly ash particle size distribution results have not yet been analyzed, however, and are necessary before any final statements can be made with regard to the comparative collectabilities of the CWS and parent coal fly ashes.

In conclusion, although the data obtained indicates satisfactory carbon conversion efficiencies for CWS, other factors influencing overall plant efficiency must be considered in dictating the viability of conversion to CWS. For instance, a latent energy penalty is incurred due to the water component in the CWS. For the CWS tested (30% water by weight) a latent loss of 2.44 percent thermal efficiency would result with stack gas exit temperatures of 212°F; higher stack gas exit temperatures, required above sulfur-related dewpoints, would result in proportionally higher latent thermal losses. Furthermore, based on C-E's experience in handling fuels on a large laboratory scale, coal/water slurries are less efficient than oil from a parasitic power consumption standpoint for storage, transport and atomization (see Table 6). These factors and others must be evaluated in determining the applicability of a given CWS conversion.

#### SUMMARY

A burner/atomizer combination has been developed by Combustion Engineering which will burn CWS with satisfactory combustion efficiency over a wide load range. This firing system was developed using a three step approach to the problem. These steps included: 1) Atomizer development and optimization using an advanced C-E developed computer program and state-of-the-art spray measurement techniques, 2) Cold flow burner modeling to optimize the burner register's aerodynamic flow field, and 3) Full scale combustion matrix testing firing coal water slurry and its parent coal to characterize combustor performance and gather emissions data.

The preliminary results of this project show that the developed atomizer effectively atomizes high viscosity CWS (up to 2800 CPS). Measured atomization qualities and atomizing media consumption rates were similar to those measured for heavy fuel oil. Spray droplet size distributors were equivalent to those of a pulverized coal grind (with 30% inherent moisture) ranging between 115 and 150 mesh. Measured droplets were still significantly larger than the individual coal particles in the slurry.

Atomizer geometry was found to significantly influence atomization quality. However, preheating CWS prior to atomization (to reduce viscosity) did not have a great influence and yielded little improvement. Preheating the atomizing air also proved to be of limited value. However, because atomization did improve slightly with increased atomizing air temperature, the elimination of air compressor intercoolers would benefit atomization at no additional cost. The combined effects of preheating both slurry and air prior to atomization was found to be greater than either influence alone, however the improvement in atomization quality did not seem significant enough to meret the additional energy penalty. For combustion testing, CWS was not heated and atomizer air was not heated beyond the compressor's delivery temperature.

The preliminary combustion testing results indicate that, with the proper combination of burner and atomizer design, coal-water slurry can be successfully burned with carbon conversion efficiencies in the range of 96 to 99%. This compares with a constant 99+% carbon conversion efficiency for the base coal fired under similar conditions. Additional improvements in CWS combustion efficiency may be possible through further firing system development and refinement.

This project has also successfully demonstrated that coal-water slurry could be reliably ignited in a cold furnace using conventional ignitors and low air preheat temperatures (250°F).

Although preliminary results have demonstrated satisfactory CWS combustion performance on a large laboratory scale, there are several other boiler-related areas which must be

addressed before CWS can become commercially viable. Furnace slagging, fouling and boiler derating, as well as, differential fuel costs and conversion costs must balance out favorably when compared to continuing operation on heavy oil. Detailed discussion of these factors is beyond the scope of this paper, but will dictate the ultimate viability of CWS as a boiler fuel.

#### REFERENCES

1. Farthing et al., Combustion Tests of Coal-Water Slurry, prepared by B&W, final report, March 1982 for EPRI Research Project #1895-2, Report No. EPRI CS-2286.
2. Mchale, Scheffee and Rossmeissel, "Combustion of Coal/Water Slurry", Combustion and Flame, 45:121-135 (1982).
3. Sommer, T. M., and Funk, J. E., "Development of a High-Solids, Coal-Water Mixture for Application as a Boiler Fuel", ASME paper 81-JP6C-Fu-4.
4. Marshall, W. R., Jr., Atomization and Spray Drying, American Institute of Chemical Engineers, Chem. Eng. Progress Monograph Series, No. 2, Vol. 50, 1954.
5. Swithenbank, J. et. al., "A Laser Diagnostic Technique for the Measurement of Droplet and Particle Size Distribution", University of Sheffield, Sheffield, England, Report # HIC 245.
6. Smith, D. A. and LaFlesh, R. C., Improved Atomization of Residual Fuels for Marine Boilers, Volume II, Dept. of Transportation Maritime Administration Report MA-RD-920-78074, August 1981.
7. Borio, R. W., and Hargrove, M. J., "The Effects of Coal Slurry Fuels on Steam Generators", ASME paper #82-JP6C-Pwr-42.
8. Beer, J. M. and Chigie, N. A., Combustion Aerodynamics, Halsted Press, New York (1972), pg. 100-145.
9. Singer, J. G. editor, Combustion, Combustion Engineering, Windsor, CT (1981) pg. 13-2, 13-3, 13-14.
10. Smith, D. A. and Lexa, G. F., "Dense Phase Pneumatic Transport: An Alternative for Conveying Pulverized Coal", paper presented at International Symposium on Conversion to Solid Fuels, sponsored by AFRC, Newport Beach, CA, October 26-28, 1982.



Figure 1

PAYBACK PERIOD vs FUEL COST AND DERATING  
REFERENCE 7

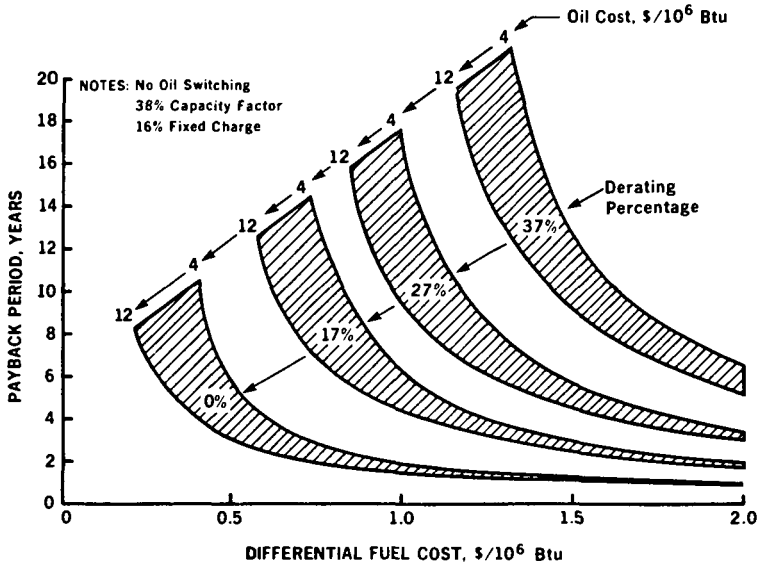


Figure 2

EPRI's HOMER CITY COAL CLEANING TEST FACILITY  
SIMPLIFIED SCHEMATIC OF EQUIPMENT CONFIGURATION USED FOR PRODUCING LOW ASH COAL

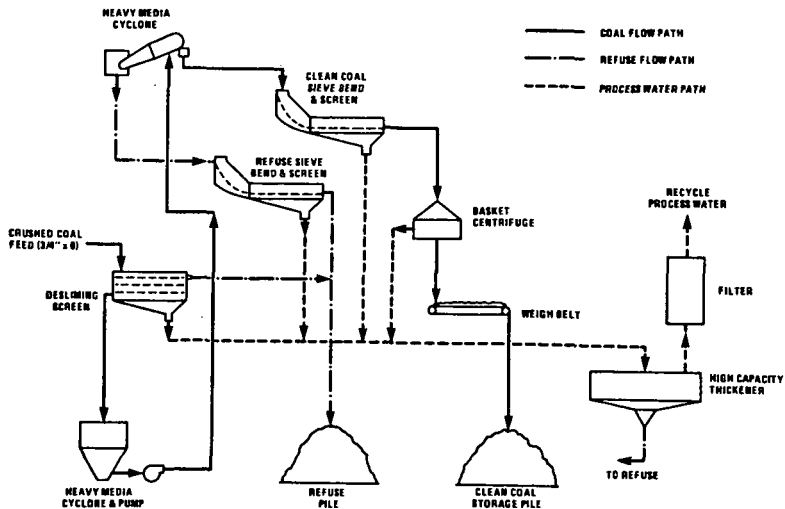


Table 1

Analysis of Parent Coal After Cleaning  
at EPRI's Homer City Coal Cleaning Test Facility

	"AS RECEIVED"	"MOISTURE FREE"
<u>PROXIMATE ANALYSIS, %</u>		
Moisture	6.4	--
Volatile Matter	37.6	40.1
Fixed Carbon	53.1	56.8
Ash	2.9	3.1
<u>ULTIMATE ANALYSIS, %</u>		
Moisture	6.4	--
Carbon	74.5	79.6
Hydrogen	5.4	5.8
Nitrogen	1.5	1.6
Sulfur	.9	.9
Ash	2.9	3.1
Oxygen (diff.)	8.4	9.0
<u>GROSS HEATING VALUE</u>		
BTU/lb	13,790	14,730

Table 2

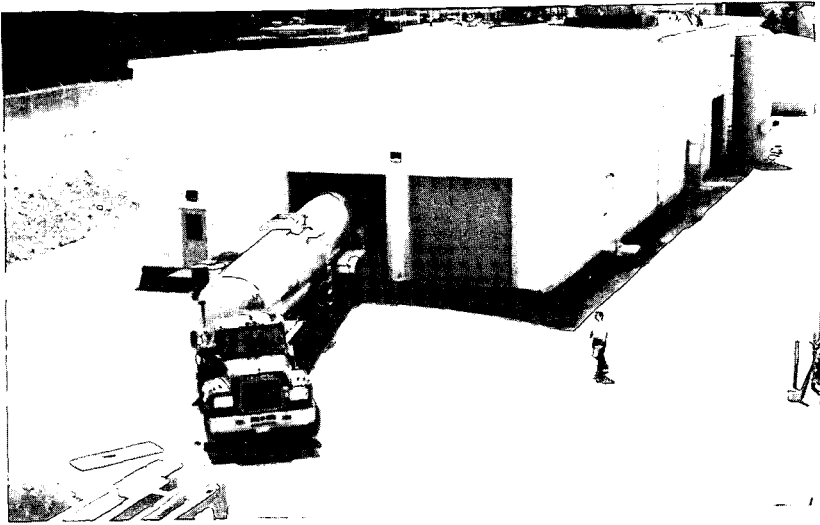
Coal-Water Slurry Properties  
CE/AFT CWS Specification

<u>Particle Size</u>	100% minus 100 Mesh
<u>Viscosity</u>	less than 2800 Centipoise at 113 sec <sup>-1</sup> and 25°C (Haake Method) Newtonian or Pseudo Plastic Behavior
<u>Volatile Matter</u>	Greater than 30% by weight (dry)

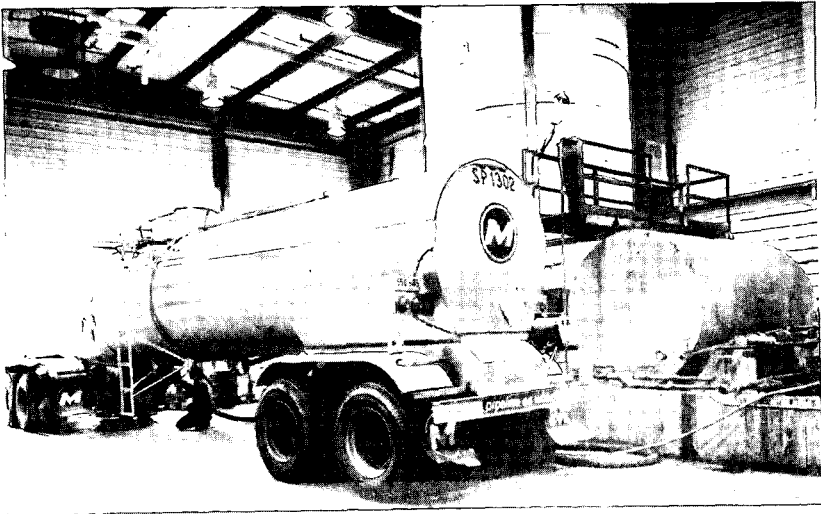
AFT Coal-Water Slurry Analysis

Total Moisture, %	31.0
Solids Content, %	69.0

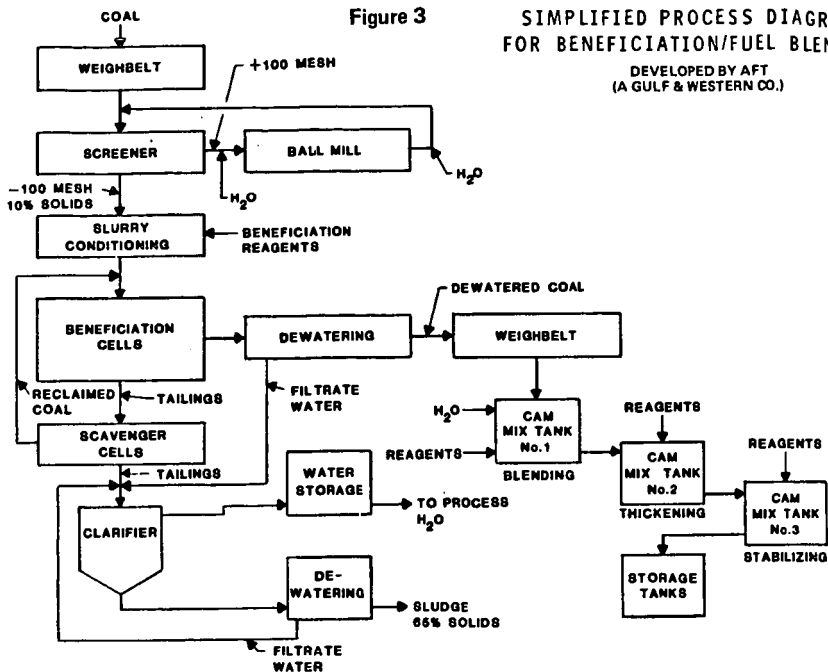
	"AS RECEIVED"	"MOISTURE FREE"
<u>Proximate Analysis, %</u>		
Moisture	31.0	--
Volatile Matter	27.1	39.3
Fixed Carbon	40.1	58.1
Ash	1.8	2.6
<u>Ultimate Analysis, %</u>		
Moisture	31.0	--
Hydrogen	3.8	5.5
Carbon	56.1	81.3
Sulfur	.6	.9
Nitrogen	1.1	1.6
Oxygen (diff.)	5.6	8.1
Ash	1.8	2.6
<u>Gross Heating Value</u>		
BTU/lb	10,170	14,740



**Photo 1**  
**TANK TRUCK ARRIVING AT ALTERNATE FUELS HANDLING**  
**FACILITY WITH A LOAD OF COAL-WATER-SLURRY**



**Photo 2**  
**TRANSFERRING COAL-WATER-SLURRY FROM TANKER TO**  
**THE 15,000 GALLON STORAGE TANK**



**Figure 4**

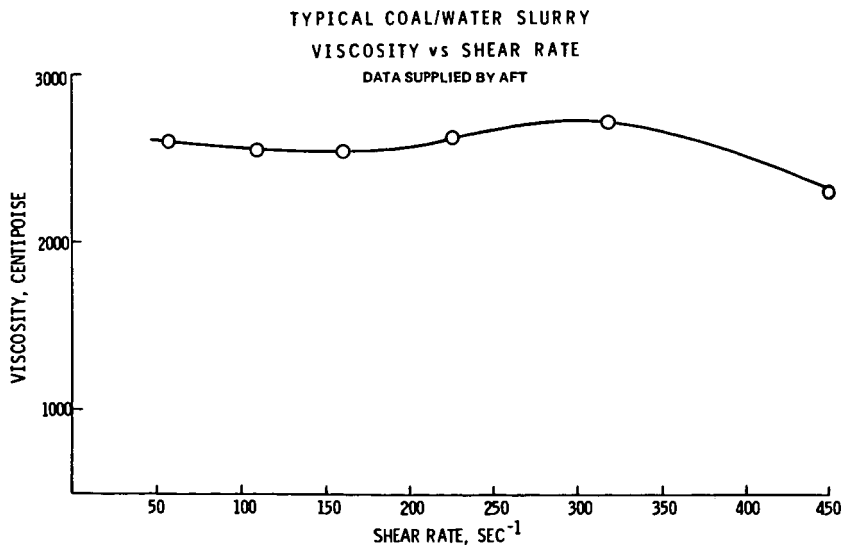


Figure 5

ALTERNATE FUELS HANDLING AND FIRING SYSTEM SCHEMATIC

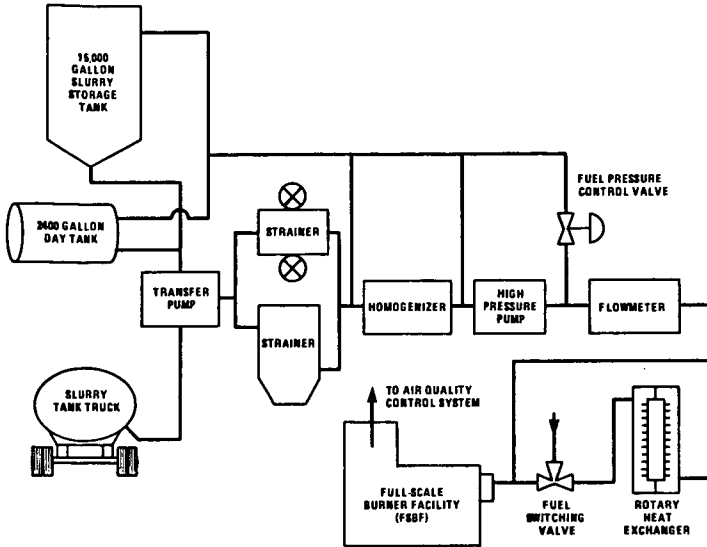


Figure 6

SIMPLIFIED COAL-WATER-SLURRY FIRING SYSTEM SCHEMATIC

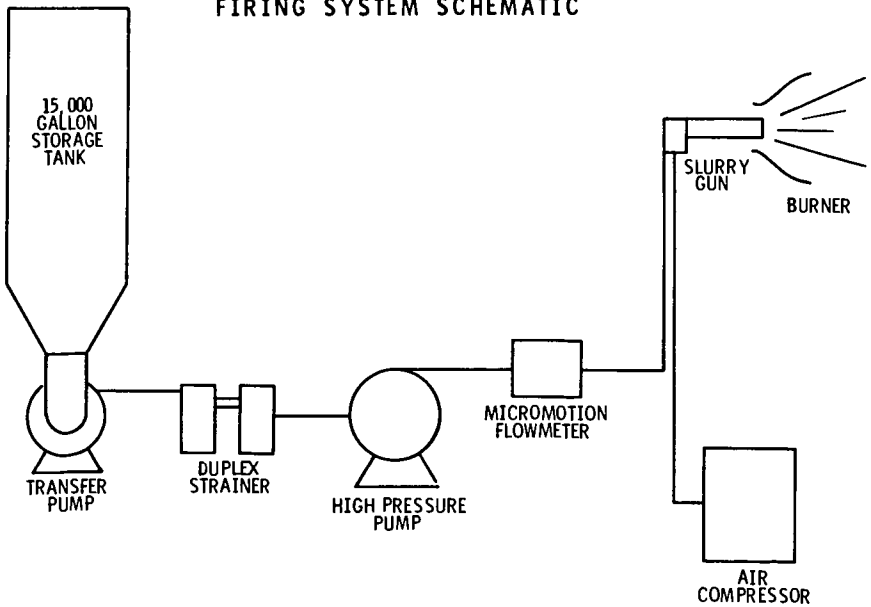


Figure 7

CRITICAL DIMENSIONS "Y" JET ATOMIZER DESIGN  
CROSS-SECTIONAL VIEW

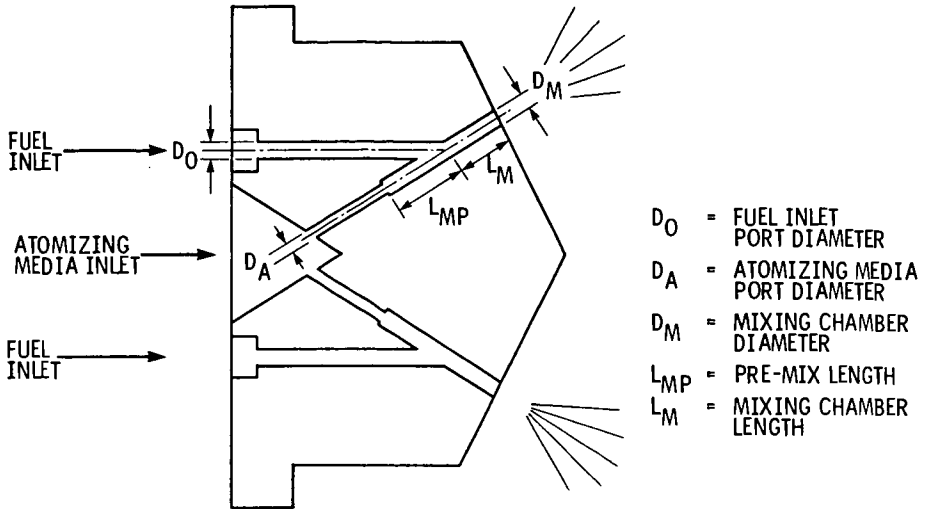
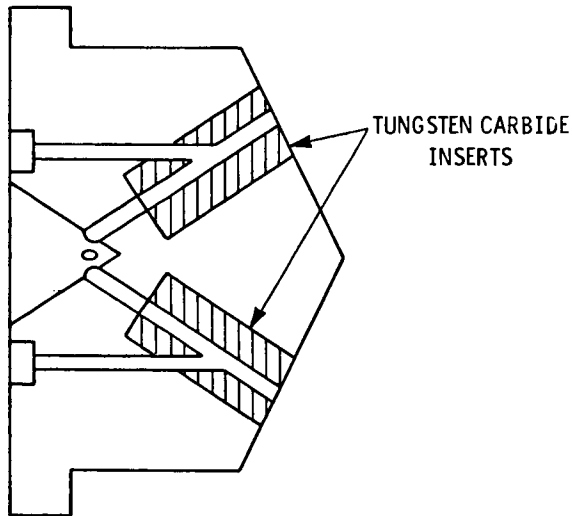


Figure 8

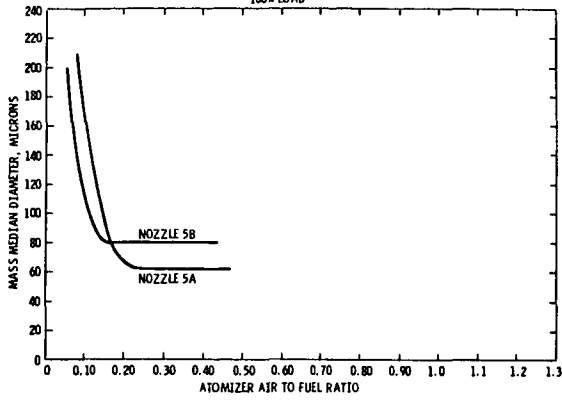
WEAR RESISTANT ATOMIZER DESIGN





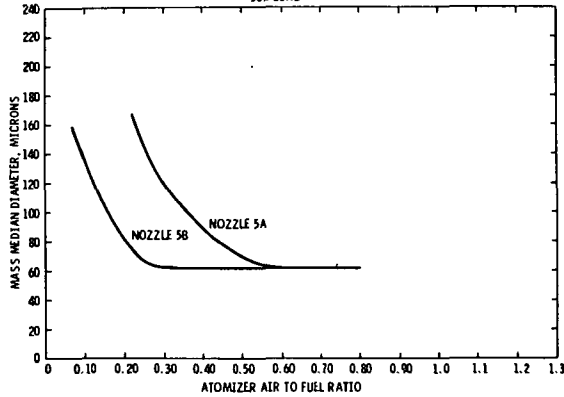
**Figure 12**

INFLUENCE OF ATOMIZER GEOMETRY ON  
ATOMIZATION QUALITY  
100% LOAD



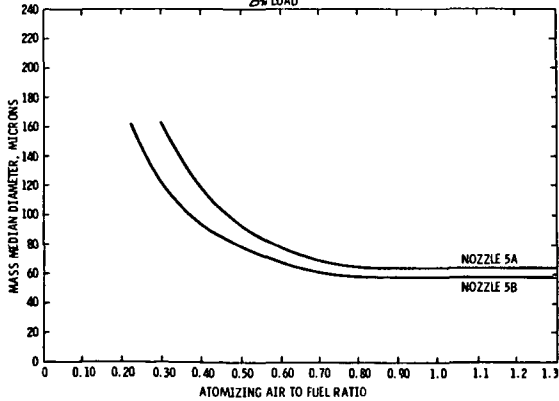
**Figure 13**

INFLUENCE OF ATOMIZER GEOMETRY ON  
ATOMIZATION QUALITY  
50% LOAD



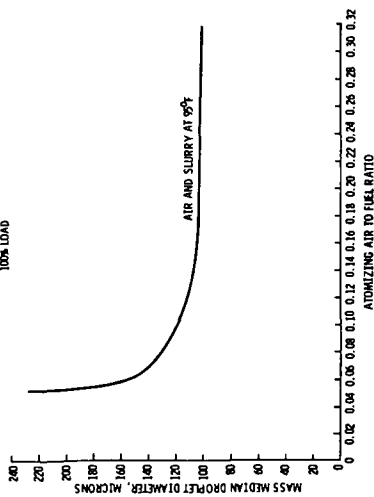
**Figure 14**

INFLUENCE OF ATOMIZER GEOMETRY ON  
ATOMIZATION QUALITY  
25% LOAD

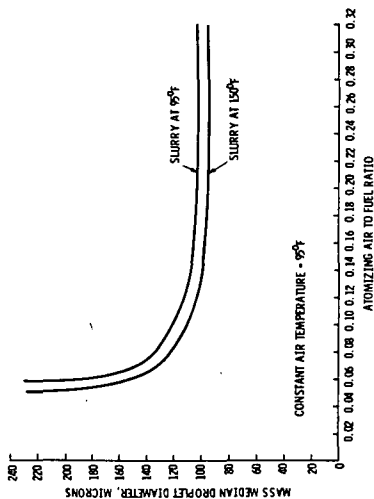




**Figure 15**  
INFLUENCE OF ATOMIZING AIR/SLURRY MASS  
FLOW RATIO ON ATOMIZATION QUALITY  
100% LOAD

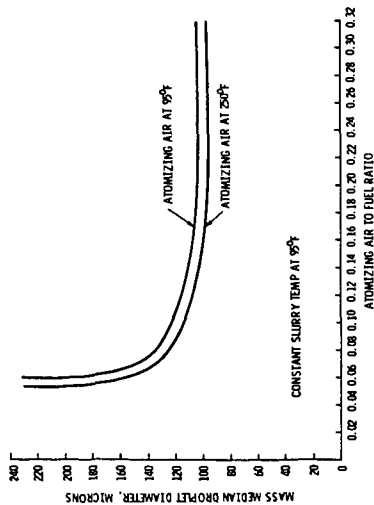


**Figure 16**  
EFFECT OF SLURRY TEMPERATURE



**Figure 17**

EFFECT OF ATOMIZING AIR TEMPERATURE



**Figure 18**

EFFECT OF SLURRY AND AIR TEMPERATURE

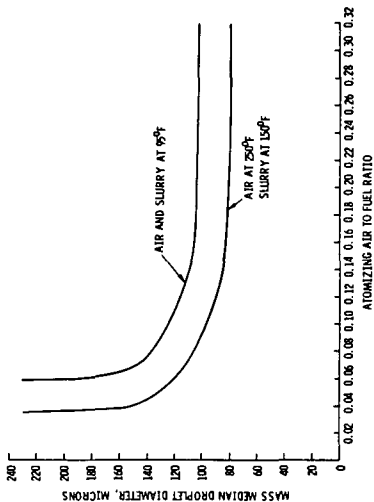


Figure 19

C-E/EPRI CWS BURNER - COLD FLOW MODEL  
INDICATED FLAME PATTERN FROM  
AERODYNAMICS OBSERVATIONS

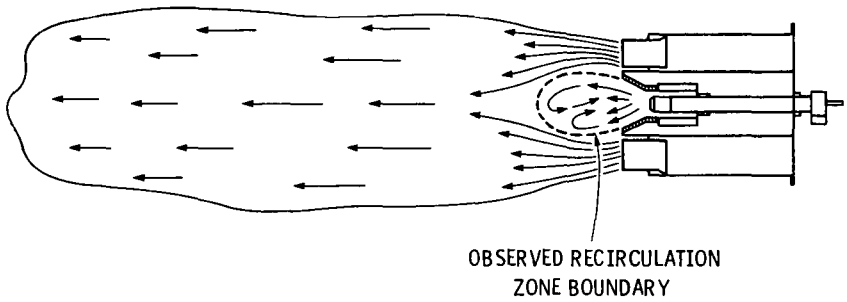


Figure 20

C-E COAL-WATER-SLURRY BURNER SCHEMATIC

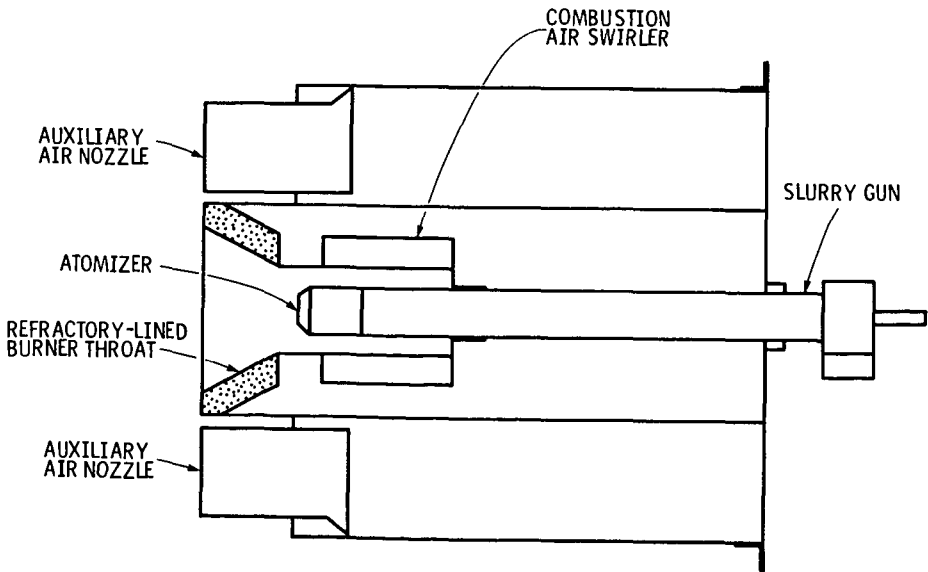


TABLE 3

## Coal-Water Slurry Combustion Test Matrix

100% Load =  $80 \times 10^6$  BTU/HR

INDEPENDENT VARIABLES				MEASURED DEPENDENT VARIABLES															
TEST NO.	LOAD	EXCESS AIR	COMB. AIR TEMP.	CO	CO <sub>2</sub>	NO <sub>x</sub>	O <sub>2</sub>	SOLIDS LOADING	CARBON BURNOUT	STACK FLYASH SIZE DISTRIBUTION	INSTUT FLYASH RESISTIVITY	FLAME				ATOMIZER AIR			
												HEAT FLUX	HEAT CALC. COMB. FLUX	HEAT CALC. COMB. FLUX	COMB. FLUX	TEMP	TEMP	FUEL	AIR
1	100	40	250	X	X	X	X					X	X	X	X	X	X	X	X
2	50	40	250	X	X	X	X					X	X	X	X	X	X	X	X
3	25	40	250	X	X	X	X					X	X	X	X	X	X	X	X
4	100	30	250	X	X	X	X					X	X	X	X	X	X	X	X
5	50	30	250	X	X	X	X					X	X	X	X	X	X	X	X
6	25	30	250	X	X	X	X					X	X	X	X	X	X	X	X
7	100	SP	250	X	X	X	X					X	X	X	X	X	X	X	X
8	50	SP	250	X	X	X	X					X	X	X	X	X	X	X	X
9	25	SP	250	X	X	X	X					X	X	X	X	X	X	X	X
10	75	30	250	X	X	X	X	X	X			X	X	X	X	X	X	X	X
11	75	30	400	X	X	X	X	X	X	X		X	X	X	X	X	X	X	X
12	100	30	250	X	X	X	X	X	X	X		X	X	X	X	X	X	X	X

Table 4

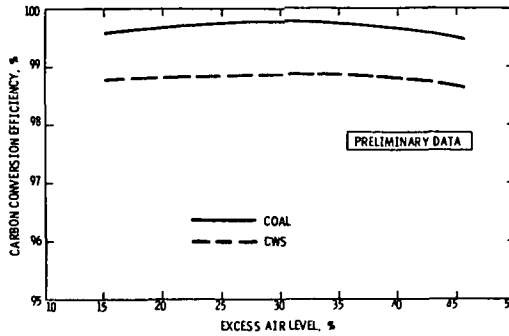
## Parent Coal Combustion Test Matrix

100% Load =  $80 \times 10^6$  BTU/HR

INDEPENDENT VARIABLES				MEASURED DEPENDENT VARIABLES														
TEST NO.	LOAD	EXCESS AIR		AIR TEMP.	CO	CO <sub>2</sub>	NO <sub>x</sub>	O <sub>2</sub>	SOLIDS LOADING	CARBON BURNOUT	STACK FLYASH SIZE DISTRIBUTION	INSTU FLVASH RESISTIVITY	FLAME QUALITY	HEAT FLUX COMB.	HEAT CALC. COMB. FLUX	FUEL FLOW	AIR FLOW	COMB. TEMP
1	100	40	250	X	X	X	X	X					X	X	X	X	X	X
2	50	40	250	X	X	X	X	X					X	X	X	X	X	X
3	25	40	250	X	X	X	X	X					X	X	X	X	X	X
4	100	30	250	X	X	X	X	X					X	X	X	X	X	X
5	50	30	250	X	X	X	X	X					X	X	X	X	X	X
6	25	30	250	X	X	X	X	X					X	X	X	X	X	X
7	100	SP	250	X	X	X	X	X					X	X	X	X	X	X
8	50	SP	250	X	X	X	X	X					X	X	X	X	X	X
9	25	SP	250	X	X	X	X	X					X	X	X	X	X	X
10	75	30	250	X	X	X	X	X	X		X		X	X	X	X	X	X
11	75	30	400	X	X	X	X	X	X	X			X	X	X	X	X	X
12	100	30	250	X	X	X	X	X	X	X	X		X	X	X	X	X	X

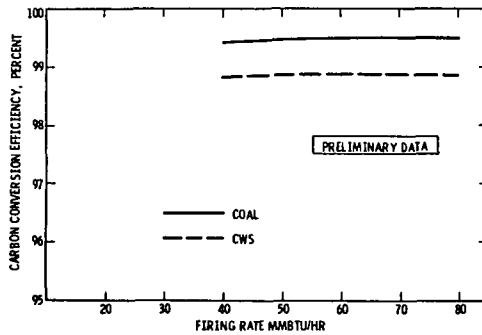
**Figure 21**

COMPARISON OF CARBON CONVERSION EFFICIENCY OF  
PARENT COAL VS COAL-WATER-SLURRY AS A FUNCTION  
OF EXCESS AIR LEVEL AT  $80 \times 10^6$  BTU/HR



**Figure 22**

COMPARISON OF CARBON CONVERSION EFFICIENCY OF  
PARENT COAL VS COAL-WATER-SLURRY AS A FUNCTION  
OF FIRING RATE AT 30% EXCESS AIR



**Figure 23**

CARBON CONVERSION EFFICIENCY vs ATOMIZING MEDIA RATIO  
FOR COAL-WATER-SLURRY

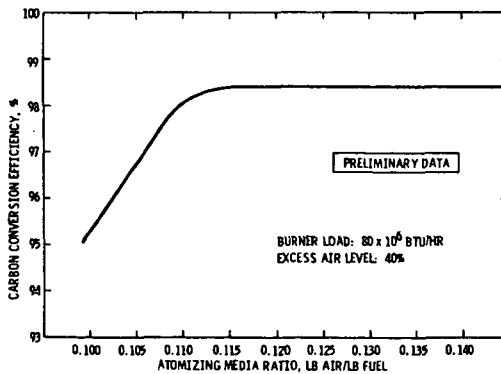


Table 5

FLY ASH RESISTIVITY MEASUREMENTS

<u>FUEL</u>	<u>LOAD</u> (10 <sup>6</sup> Btu/hr)	<u>EXCESS AIR</u>	<u>COMBUSTION AIR TEMPERATURE</u> (°F)	<u>FLY ASH RESISTIVITY</u> (OHM-CM)
CWS	40	30%	250	1.8 x 10 <sup>8</sup>
CWS	60	30%	250	2.1 x 10 <sup>8</sup>
CWS	60	30%	400	2.9 x 10 <sup>8</sup>
Parent Coal	40	30%	250	2.0 x 10 <sup>8</sup>
Parent Coal	60	30%	250	3.7 x 10 <sup>8</sup>
Parent Coal	60	30%	400	2.4 x 10 <sup>8</sup>
Parent Coal	80	30%	250	3.0 x 10 <sup>8</sup>

Table 6

FUEL SYSTEM POWER CONSUMPTION

One Elevation 800 MMBTU/HR Heat Input

(BASED ON LARGE SCALE LABORATORY TESTING)

	<u>Oil</u> (MMBTU/HR)	<u>Coal-Oil</u> (MMBTU/HR)	<u>Coal-Water</u> (MMBTU/HR)
STORAGE	NONE	0.13	0.02
TRANSPORT/FEED	1.71	2.24	2.24
BURNER/ATOMIZER	4.40	5.00	4.60
TOTAL	6.11	7.37	6.86

SMALL (5 MILLION BTU/HR) AND LARGE (300 MILLION BTU/HR) THERMAL TEST RIGS  
FOR COAL AND COAL SLURRY BURNER DEVELOPMENT

J W Allen - BSc, PhD, CEng, M Inst E  
P R Beal - BSc  
P F Hufton - BSc, CEng, MI Mech E

NEI International Combustion Ltd  
Sinfin Lane  
Derby  
DE2 9GJ  
England

1. INTRODUCTION

Thermal test rigs have been used by NEI International Combustion over the past 25 years for the evaluation and development of burner systems for both industrial and utility boilers. Initially, the rigs were little more than open brick containers which have evolved to the water-cooled gas-tight chamber currently in use to enable the development of low excess air combustion systems as demanded by market forces and the need for more effective fuel utilisation. A major step forward in thermal test rig facilities occurred in 1973 with the construction of what is probably the largest and most comprehensively instrumented burner test rig in the Western Hemisphere. The rig design had to meet all of the known oil burner performance requirements at that time, and also be sufficiently flexible to meet the predicted requirements of the succeeding 10 - 12 years. This rig is still in operation today and is currently undergoing the next major step change in conversion to enable pulverised fuel, coal slurries and gas burner systems, sized up to 300 million BTU/Hr, to be developed.

A complementary small scale thermal test rig facility, rated at around 5 million BTU/hr was also provided in 1975 to allow fundamental combustion studies and the development of new ideas in burner design and operation to take place at a more economical level in comparison with the operation of the large test rig.

Both these major step changes in the large scale thermal test rig capabilities have been dictated by market forces. Initially the need was to develop low excess air oil burners utilising the almost continuously deteriorating quality fuel oils supplied to the utility boiler industry. The current need is to meet the renewed interest in coal utilisation now that it is realised that fuel oil supplies are not infinite and consequently will be subject to continual increases in price with little or no guarantee as to quality and availability.

Although it is not universal practice to test burner systems for large boilers prior to site installation, the availability of a full-scale thermal test rig enables the development of a tailor-made burner system to suit a particular installation. Customers can see a proposed burner system in operation and any changes required, because of alterations in operating procedures or variations in fuel properties, can be accommodated. These investigations, into altered conditions, can be made quickly and economically compared with on site investigations and without interruption to the customers operating schedule. Markets for new fuels, such as coal slurries, can be pursued without relying on potential customers to provide full-scale test facilities. In fact, until the firing of coal-water and coal-oil slurries becomes universally accepted, there should be an increasing demand for off-site demonstrations of the capabilities of these new burner systems. The operation of a full-scale thermal test rig is therefore an essential piece of equipment for any burner manufacturer to achieve and maintain a leading position in the supply of combustion systems to the International utility boiler market.

## 2. The Large (300 million BTU/Hr) Thermal Test Rig at Derby

### 2.1 General Description of the Rig and its Capabilities

The original design of the large thermal test rig at Derby was ambitious, as it had to meet the requirement of NEI International Combustion to maintain its leadership in oil burner performance in the Western Hemisphere. A major requirement was that of sheer size. The combustion chamber dimensions had to be such that complete combustion could be obtained, upstream of gas sampling positions, with burner systems (firing up to 9 tonnes/hr of fuel oil) designed to produce long narrow flames typical of burners designed for tangential firing applications and those designed to produce more compact large diameter flames typical of front wall firing applications. These considerations resulted in a combustion chamber of internal dimensions 21.34 m (70 ft) long by 5.49 m (18 ft) square cross section. Cooling of the combustion chamber is achieved by means of static water sandwiched between inner and outer steel skins on the side walls and end wall of the chamber remote from the burner. The centre section of the burner wall is built entirely of refractory to enable easy changing of burner configurations, the roof is also entirely water-cooled and the hearth covered with a layer of refractory pebbles on a bed of sand.

Oil storage is provided by two lagged and steam heated storage tanks, each of 45460 litres (10,000 gallons) capacity. Oil is transferred from the tanks, via a low pressure transfer pump, to a primary pumping and heating circuit capable of delivering oil at a pressure of 44.8 bar (650 lbs/in<sup>2</sup>) at up to 13640 kg/hr (30,000 lbs) and a viscosity of 70 Redwood No 1 seconds (16 cS, 80 SSU). A second pumping and heating circuit was installed, at a later date, enabling an oil delivery pressure up to 83 bar (1200 lb/in<sup>2</sup>) and oil temperatures up to 200°C (392°F) to be achieved. This secondary pumping heating system was used particularly in a study of the combustion of fuel oils containing a high percentage (up to 14%) of hard asphaltenes.

Combustion air is supplied to the burner windbox by a four-stage axial flow fan capable of supplying 37.77 m<sup>3</sup>/sec (80,000 ft<sup>3</sup>/m) of combustion air at a maximum pressure of 44.8 mbar (18 ins water gauge). Noise levels from the fan are controlled by axial flow silencers immediately upstream and downstream of the fans and air flow rate is indicated by a venturi meter. Coarse air flow control is via the number of fan stages brought into operation and fine control is achieved by a remotely controlled butterfly damper.

All the flows to the rig are controlled from an operating console situated at the end of the combustion chamber remote from the burner. From this position the rig operator can observe an end view of the flame through a glass porthole. A comprehensive gas analysis system is also housed adjacent to the control console.

During the operation of a burner test, gases are sampled from the 2.74 m (9 ft) diameter 18.29 m (60 ft) high refractory lined stack, at a point some 10.67 m (35 ft) above ground level located in the stack. At this same point a platform has been erected to enable the isokinetic sampling of the flue gases for determination of the solids burden. The gas analysis instrumentation provides a continuous record of O<sub>2</sub>, CO, CO<sub>2</sub> and NO<sub>x</sub> in the flue gases throughout a test. A smoke density meter and facility for determining the Bacharach smoke number is also available. Observation ports are provided along the side wall of the combustion chamber to enable photographs to be taken of the flames as required.

Steam for oil heating and atomisation is available from a package boiler of 4994 kg (10,980 lb) per hour steam capacity at a delivery pressure of 17.24 bar (250 lb/in<sup>2</sup>).

Most oil burner test work is carried out using cold combustion air. However, combustion air preheat can be achieved by means of duct burners located in the combustion air supply ducting after the axial flow fans. With this system in operation oxygen has to be supplied to the combustion air stream to maintain a 21% O<sub>2</sub> content in the combustion air at the burner windbox.

In order to provide a complete burner test facility, comprehensive laboratory facilities and expertise are available to provide chemical and physical analysis of fuels and particulates and also isothermal test facilities to assess the quality of atomisation of the various atomiser designs under test.

Figure 1 indicates the general layout of the test rig and the ancillary supply and analysis equipment.

## 2.2 Conversion of the Rig to Provide a Coal and Coal Slurry Firing Capability

The object of the conversion exercise is to maintain the existing oil firing capability and provide the facility for firing pulverised fuel, coal slurries (e.g. coal water or coal oil mixtures) and gas at similar maximum heat input rates of around 300 million BTU/hr. Both light and dense phase systems for the firing of pulverised fuel are incorporated and the coal slurry firing facilities are designed to handle coal water mixtures containing up to 75% coal and coal oil mixtures with up to 50% coal. A typical British East Midlands steam raising coal of 15% ash content (dry basis) and 7220 Kcal/kg (13,000 BTU/lb) calorific value, was used as the basis of design calculations for the conversion exercise.

The problems to be overcome in the conversion exercise were the deposition and collection of ash, both within and outside the test rig (to satisfy Local Authority regulations), the provision of a combustion air pre-heating capability, and the design of conveying systems for dense phase and lean phase pulverised fuel and for coal slurries.

Local Authority environmental requirements restrict solids discharge from the rig stack to 72 kg/hr (158 lb/hr). Therefore, in order to cope with the maximum coal firing rate of 10 tonnes/hr with a 15% ash coal, the waste gases leaving the rig, at about 1000°C (1830°F), must be conditioned and cleaned before being dispersed to the atmosphere. The system decided upon for gas conditioning and cleaning comprised a high pressure hot water waste heat boiler followed by a multi-cyclone dust collector. An induced draught fan after the dust collector conveys the cooled clean gases into the stack and thus to atmosphere. The incorporation of the waste heat recovery system allowed the provision of pre-heat to the combustion air and primary air (conveying lean phase pulverised fuel) via high pressure hot water heat exchangers located in the appropriate air ducts. Surplus heat from the waste heat boiler is dissipated via a series of forced draught dump coolers located remotely from the test rig and operating in the closed circuit mode in line with the waste heat boiler. Water is supplied from the waste heat boiler to the heat exchangers at a temperature of 218°C (425°F) and pressure of 30 bar (440 lbs/in<sup>2</sup>) providing 121°C (250°F) pre-heat for the primary air lean phase pulverised fuel conveying and 177°C (350°F) preheat for the secondary combustion air. The system of duct burners and oxygen injection is retained in order to provide increased secondary (or combustion) air pre-heat as required.



In addition to collection of ash outside the combustion chamber it is anticipated that up to 50% of the total ash content of the coal could be collected inside the chamber. To facilitate the removal of this ash and any spillages of unburnt pulverised fuel the existing refractory pebble floor is to be replaced by a water-cooled floor of similar design to the side walls as mentioned in section 2.1. As the existing mode of operation for the development of low excess air oil burners is to be maintained a water-cooled door has been provided in the rig back wall enabling combustion gases to be diverted either directly, or via the waste gas conditioning system, to the existing stack

Coal conveying is to be based on a dense phase system either feeding directly to a purpose designed burner system or into a pre-heated primary air system giving the required air dilution to provide a lean phase pulverised fuel firing facility.

The dense phase system comprises a pressurised double-blow tank unit fed from a 20 tonne pulverised coal storage silo. Nitrogen purge facilities and continuous temperature monitoring of the storage silos are provided in order to minimise the explosion risk. The dense phase system will allow pulverised fuel to be conveyed in relatively small diameter pipelines, compared to the more conventional lean phase firing systems, which could be an important consideration when boiler changeovers from oil to coal firing are contemplated and the existing access to the boiler fronts is limited. Fuel flow rates from the dense phase system will be monitored by load cells located in the blow tank system.

The slurry feed system comprises a storage tank which can be stirred and heated continuously, and a mono-pump with facilities for flushing out the complete system after any particular firing exercise. Slurry flow will be monitored by a 'Doppler Effect' flow meter, with the slurry continuously circulated around the pump and storage tank and taken off as required to the burner system.

A facility for continuous data logging of fuel flows, gas flows, gas analysis and temperature is to be provided and this microprocessor controlled unit will also provide a central control over all the operating parameters, giving a continuous visual display of the levels of the parameters throughout a test run. An instant print-out of these parameters can be obtained at any selected point in the test run. Figure 2 shows the general layout of the test rig after the conversion to provide this multi-fuel burner development facility and Figures 3 and 4 show details of the pulverised fuel and coal slurry conveying systems.

The conversion programme is to take place in two phases - the first phase will provide facilities to enable a maximum of 3.5 tonnes/hr of coal to be fired either in dense phase or slurry form. Limiting the firing rate to this level removes the necessity for the provision of gas cleaning to meet the environmental emission levels and enables experience of operating the rig under coal firing conditions to be obtained more quickly. Phase 2 of the conversion involves installation of the gas conditioning dust cleaning plant to allow the operation at the full fuel rating. The conversion work is expected to be completed and the rig fully operational during the first half of 1983.

Attention has also had to be given to the sound levels from equipment to be provided in the conversion work. Firstly, for the protection of operating personnel, the sound pressure level from any individual item of plant will not exceed 90 dBA at 1 metre and secondly, because the rig will operate within the proximity of a local housing estate, the maximum sound power level from the complete plant is limited to 117 dBA, ref.  $10^{-12}$  watts, with a boundary condition of 65 dBA at 200 metres.

### 3. The Small (5 million BTU/hr) Thermal Test Rig at Derby

Fundamental combustion studies and particular aspects of burner systems development work can be carried out quickly and economically on this small rig. The rig is linked to the same gas analysis system as the large rig and is equipped for oil, gas and coal slurry firing, additionally a combustion air preheater is available capable of delivering combustion air at up to 425°C (800°F).

The combustion chamber comprises a water-cooled mineral wool lined steel cylinder 4 m (13 ft) long by 1.1 m (3.75 ft) diameter, with a 5.2 m (17 ft) refractory lined stack equipped with gas sampling and temperature measurement points. Observation ports are provided on the combustion chamber axis, close to the burner and in the chamber rear wall. Compressed air and steam are available for fuel atomisation purposes as are pumping and circulating trains for oil fuels and coal slurries. At a 5 million BTU/hr rating this rig is capable of burning 125 kg/hr (275 lbs) of gas oil and 205 - 230 kg/hr (450 - 500 lbs) of coal water slurry or their equivalent. Figure 5 shows the general layout of the small scale rig and its ancillary equipment.

### 4. Work on Coal Slurry Utilisation

#### 4.1 Coal Water Mixtures

Recent work based on the small scale rig has concentrated on investigations into the properties of coal water mixtures and their influence on handling equipment and burner design. In the initial stages of the work considerable problems were encountered with blockages in pipelines and burner heads because of the instability and excessive proportion of over-size coal particles (ca 500µm) in the coal water mixtures.

These early experiences enabled the compilation of a general specification for coal water mixture properties and associated handling equipment to be used as a basis for the successful development of a coal water combustion system. These desirable features can be listed as follows:-

##### 4.1.1 Combustion and Handling Equipment

Atomisers should be based on an external mix air atomiser design avoiding sudden changes in direction and diameter in the coal water mixture conveying system which tends to deposit the coal from the slurry and can be points of excessive wear, particularly in atomiser components. Steam atomisation is to be avoided since the additives used to stabilise the coal water mixture can break down at temperatures above 60°C (140°F).

Coal water mixtures should be fed to the burners via a continuous recirculation system (see Fig. 5) and particularly in the case of intermittent rig work, facilities should be provided for water flushing of all the feed lines and valves after each run. It should also be noted that a coal water mixture can freeze in ambient temperatures of 0°C (32°F) or less and provision should

be made for some form of trace heating, subject to the temperature limitations mentioned above, where these conditions can occur.

#### 4.1.2 Coal Water Mixture Properties

Coal particle size in the coal water mixture should be a maximum of 250µm and the coal volatile matter (dry basis) a minimum of 25%. There should be little or no settling out during transportation and any settling which does occur should be easily overcome by a simple recirculation system as described earlier.

The properties of the coal water mixture used in the small scale test work at Derby are given in Table 1.

TABLE 1

#### Coal Water Mixture Properties

##### 1.1 Proximate Analysis

	<u>Original Coal</u>	<u>Coal in Slurry</u>
Ash % (dry basis)	3.0	1.8
Volatile Matter (dry basis)	35.5	37.4
Fixed Carbon	61.5	60.8
Sulphur	1.24	1.02

Inherent coal moisture 4%

##### 1.2 Ultimate Analysis

	<u>Original Coal</u>	<u>Coal in Slurry</u>
C	83.4	84.5
H <sub>2</sub>	5.2	5.4
N <sub>2</sub>	1.8	1.8
Ash	3.0	1.8
S (pyritic)	0.55	0.34
S (sulphatic)	0.04	0.05
S (organic)	0.65	0.63
O <sub>2</sub> (by difference)	5.36	5.48

##### 1.3 Confirmatory Analysis

The above analyses were supplied by the coal water mixture supplier, confirmatory proximate analysis carried out at the Derby laboratories on the coal slurry was as follows:-

	<u>As Received</u>	<u>Dry Basis</u>
Moisture %	26.9	-
Ash %	1.36	1.86
Volatile Matter %	28.85	35.36
Fixed Carbon %	45.89	62.78

#### 1.4 Physical Analyses

<u>Sieve Analysis of Dry Sample</u>	<u>%</u>
+ 30 mesh (570 $\mu$ m)	Nil
- 30 mesh + 60 mesh (250 $\mu$ m)	0.42
- 60 mesh +100 mesh (150 $\mu$ m)	5.02
-100 mesh +200 mesh ( 75 $\mu$ m)	18.55
-200 mesh +300 mesh ( 45 $\mu$ m)	9.93
-300 mesh	66.08

#### Viscosity Data up to 60°C

Taken by a Contraves RM15 viscometer shear prior to measurement 30 sec<sup>-1</sup>.

<u>Temperature (°C)</u>	<u>Viscosity (centistokes)</u>
19.5	989
30.0	765
40.5	621
50.0	641
60.0	576

#### Surface Tension

Liquor extracted from the slurry 57 dyne cm<sup>-1</sup>.

The coal water slurry is in fact derived from a coal beneficiation process and the properties of the original coal are included in Table 1 for comparison purposes. The coal water mixture meets the desired specification levels with regard to coal particle size, coal volatile matter and stability and has proved very easy to handle through the small scale thermal test rig pumping system described earlier.

#### 4.2 The Influence of Coal Water Mixture Properties on Burner Design

Although, generally speaking, coal water mixtures can, as claimed by the proprietary slurry producers, be handled like a fuel oil there is a significant difference in the viscosity temperature relationship of the fuels which must be taken into consideration in designing a burner to handle a coal water mixture. Normally, to produce good atomisation, heavy fuel oils are heated to around 140°C (280°F), which helps to achieve oil drop-let sizes ex - the atomiser in the 60 - 100 $\mu$ , mean size range. Equally good atomisation is required for coal water mixture combustion in order to achieve rapid evaporation of the water content and release of the coal volatiles necessary to establish stable ignition conditions.

Typical viscosity/temperature curves for fuel oil and coal water mixtures are shown in Figure 6 and these, together with the slurry temperature/stability relationships mentioned in Section 4.1.1, preclude heating as a method of significant viscosity reduction with coal water mixtures.

Two possibilities were considered for the required viscosity reductions:

1) the addition of viscosity reducing chemicals, and 2) aeration of the coal water slurry. In order to be effective both techniques have to be applied to the fuel as close to the atomiser tip as possible and aeration was chosen as the more practical proposition being more compatible with known twin fluid atomiser design techniques.

Figure 7 shows the theoretical viscosities obtainable by aeration of coal water mixtures, based on calculation techniques used in viscosity blending of oils<sup>1</sup>.

#### 4.3 Development of a Coal Water Mixture Burner

Figures 8 and 9 show the general arrangement of the burner used for the small scale development work and a diagrammatic representation of the burner nozzle configuration, incorporating the viscosity reduction by aeration principle.

For the initial exercise on burner nozzle development cold combustion air was used with the gas burner (Figure 8) supplying the initial preheating, ignition and stabilisation of the coal water mixture flame, as required.

The nozzle design incorporates two sets of atomising air holes designated 'shear holes' which give rise to the initial aeration (or viscosity reduction) process and 'swirl holes' which produce a coherent spray from the nozzle tip. Initial qualitative spray trials resulted in three nozzles, designated C, D and E, of varying shear hole/swirl hole diameter ratios, being selected for thermal tests.

Isothermal spray work, using glycerine to represent the viscous coal water mixture, indicated that the nozzles produced good quality atomisation. Figure 10 shows the results of these isothermal tests. Extrapolation of the curves indicates that perhaps nozzle E will produce better atomisation at higher fuel flow rates.

The results of these initial thermal tests together with the variations in nozzle geometry are given in Table 2. In this table the 'apparent viscosities' calculated are based on the assumption that the atomising air supplied to the nozzle divides into shear and swirl air in direct proportion to the shear/swirl hole area ratios.

TABLE 2

Results of Preliminary Small Scale Thermal Tests on

Coal Water Mixture Atomisers

2.1 Nozzle C - Shear Hole/Swirl Hole Area Ratio 0.50

Coal Water Mixture (CWM) feed rate kgs/hr (lbs/hr)	110 (242)	148 (325)	192 (400)
Coal Water Mixture feed pressure bar (psi)	0.6 (8)	0.9 (12.5)	1.2 (16)
Atomising air pressure bar (psi)	4.1 (60)	4.1 (60)	4.1 (60)
Atomising air ratio			
wt air : wt CWM	0.48	0.36	0.29
Heat input to test rig % MCR	58	76	92
Heat input ratio CWM : gas	6.8	9.2	11.3
Excess O <sub>2</sub> % in flue gas	1.6	1.5	1.4
Flue gas temperature °C	779	805	820
Apparent aerated CWM viscosity cS	300	350	400

2.2 Nozzle D - Shear Hole/Swirl Hole Area Ratio 0.98

Coal Water Mixture (CWM) feed rate kgs/hr (lbs/hr)	110 (242)	148 (325)	182 (400)
CWM feed pressure bar (psi)	0.6 (8)	0.9 (12.5)	1.2 (16)
Atomising air pressure bar (psi)	4.1 (60)	4.1 (60)	4.1 (60)
Atomising air ratio			
wt air : wt CWM	0.48	0.36	0.29
Heat input to rig % MCR	58	76	92
Heat input ratio CWM : gas	6.8	9.2	11.3
Excess O <sub>2</sub> % in flue gas	1.5/4.4	1.5/4.7	1.5/4.6
Flue gas temperature °C	803/795	806/806	820/817
Apparent viscosity aerated CWM cS	100	150	250

2.3 Nozzle E - Shear Hole/Swirl Hole Area Ratio 2.0

Coal water mixture (CWM) feed rate kgs/hr (lbs/hr)	110 (242)	148 (325)	182 (400)
CWM feed pressure bar (psi)	0.6 (8)	0.9 (12.5)	1.2 (16)
Atomising air pressure bar (psi)	4.1 (60)	4.1 (60)	4.4 (60)
Atomising air ratio			
wt air : wt CWM	0.48	0.36	0.29
Heat input to rig % MCR	58	76	92
Heat input ratio CWM : gas	6.8	9.2	11.3
Excess O <sub>2</sub> % in flue gas	1.5/4.0	1.5/4.0	1.5/4.0
Flue gas temperature °C	792/820	846/862	925/937
Apparent viscosity aerated CWM cS	60	100	150

The results indicate that at a heat input equivalent to the rated maximum of the small rig (5 million BTU/hr) the ratio of heat input by coal water mixture to that of stabilising gas is 11.29 : 1 when firing with cold combustion air in a relatively cold furnace, which is equivalent to supplying pre-heated combustion air in the temperature range 200 - 315°C (400 - 600°F) depending upon the excess air ratios required for combustion.

Although no heat balances were performed during these first atomiser development tests, the flue gas temperature in Table 2 indicates a tendency for improved burning of the coal water mixtures as the apparent viscosity of the fuel was reduced by aeration. E.g. at the maximum firing rate of 182 kg/hr (400 lbs) of coal water mixture flue gas temperature increased from 820°C - 925°C (1500 - 1700°F) at 1.5% excess oxygen for viscosity changes from 400 - 150 cS.

The thermal work was carried out on the small scale rig with some of the refractory wool lining removed in an attempt to produce conditions similar to those in utility boiler practice with the flame exposed to cool surfaces and adjacent hot flame gases.

A completely refractory brick lined combustion chamber would obviously facilitate combustion stability when firing coal water mixtures, but work is continuing at Derby to study the effect of gas recirculation, the use of pre-heated air and possible a refractory quarl as an aid to combustion stability.

Gas recirculation is controlled by swirler design. The current swirler has a 45° vane angle and overall dimensions giving a swirl number of 1.1. A range of swirlers will be tested to assess the affect of recirculation of hot flame gases on the flame development. Pre-heated combustion air, in the range 100°C - 427°C (200°F - 800°F) will be utilised for this purpose also. It is considered that these two methods of increasing combustion stability are the important factors when considering the application of coal water mixture firing in utility boilers. If further initial heating is considered necessary the use of a refractory quarl to supply radiant heat to the flame root will also be studied.

##### 5. Large Scale Thermal Test Rig Work

The availability of the large rig for coal water mixture work depends on the progress of the conversion programme outlined in Section 2.2. However, it is probable that this will be one of the first exercises carried out on the converted rig, using firing rates in the 2 - 5 tonnes/hr range. The burner design will be based on that used for firing a 40% coal 60% oil mixture on the rig and subsequently on a utility boiler, but incorporating the design features discussed in Section 4.3, in order to produce a coherent coal water mixture spray. The current small scale test work will indicate the level of combustion air preheat and swirl required to achieve stable combustion conditions. With the larger flames it is anticipated that radiation from the main body of the flame, back to the flame root, will obviate the need for incorporation of a refractory quarl.

##### Reference

1. Technical Data on Fuel - H M Spiers (Editor)  
Sixth Edition 1961 (p. 150)

## Acknowledgement

The authors would like to thank all their colleagues at NEI International Combustion who have contributed to the preparation of this paper.

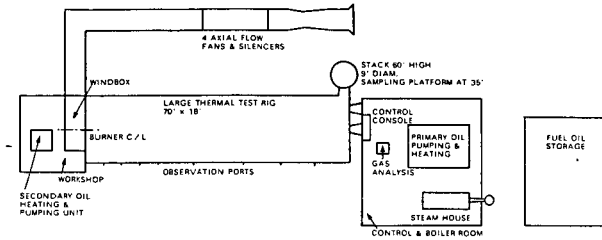


FIGURE 1  
GENERAL LAYOUT OF LARGE THERMAL TEST RIG FOR LOW EXCESS AIR OIL BURNER DEVELOPMENT

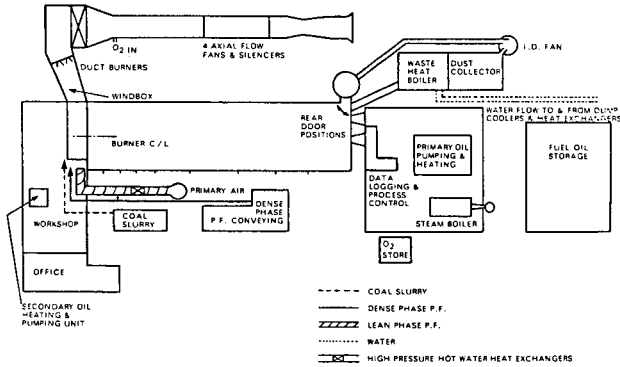


FIGURE 2  
GENERAL LAYOUT OF LARGE THERMAL TEST RIG FOR MULTI-FUEL BURNER DEVELOPMENT



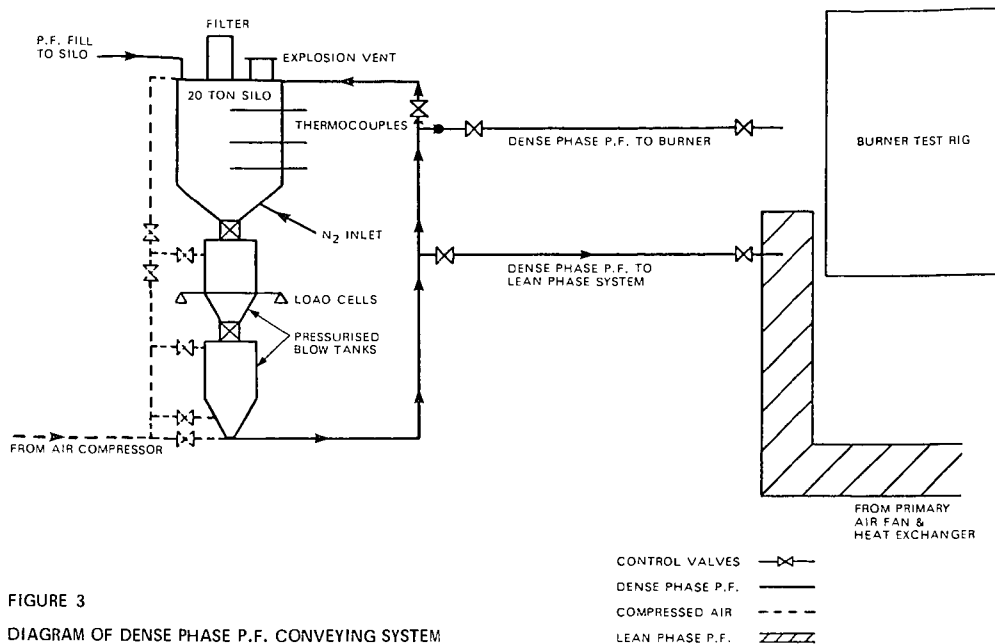


FIGURE 3  
DIAGRAM OF DENSE PHASE P.F. CONVEYING SYSTEM

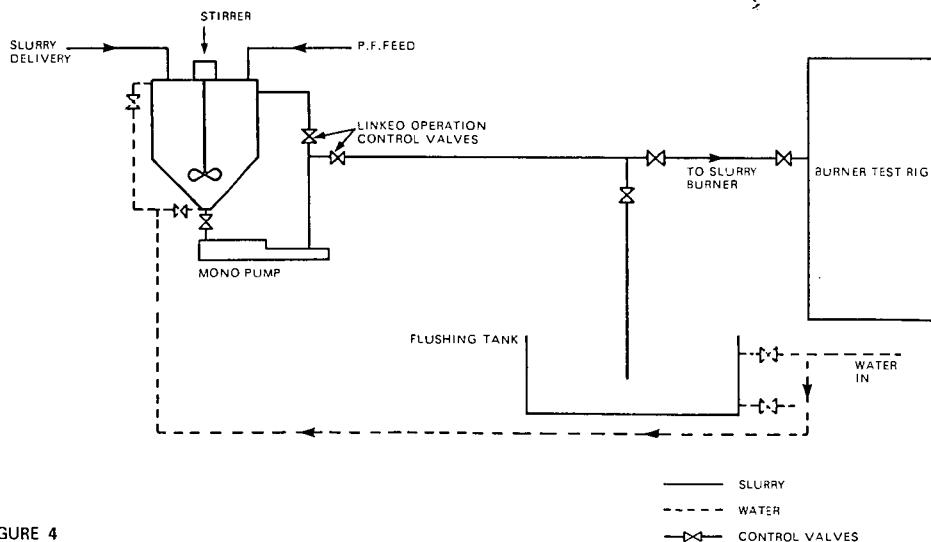


FIGURE 4  
DIAGRAM OF COAL SLURRY CONVEYING SYSTEM

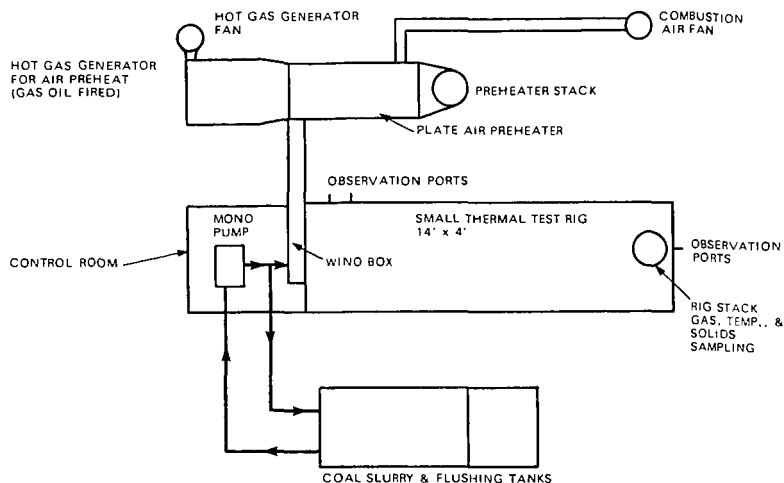


FIGURE 5  
GENERAL LAYOUT OF SMALL SCALE THERMAL TEST RIG

FIGURE 6  
COMPARISON OF COAL WATER MIXTURE & HEAVY FUEL OIL VISCOSITIES

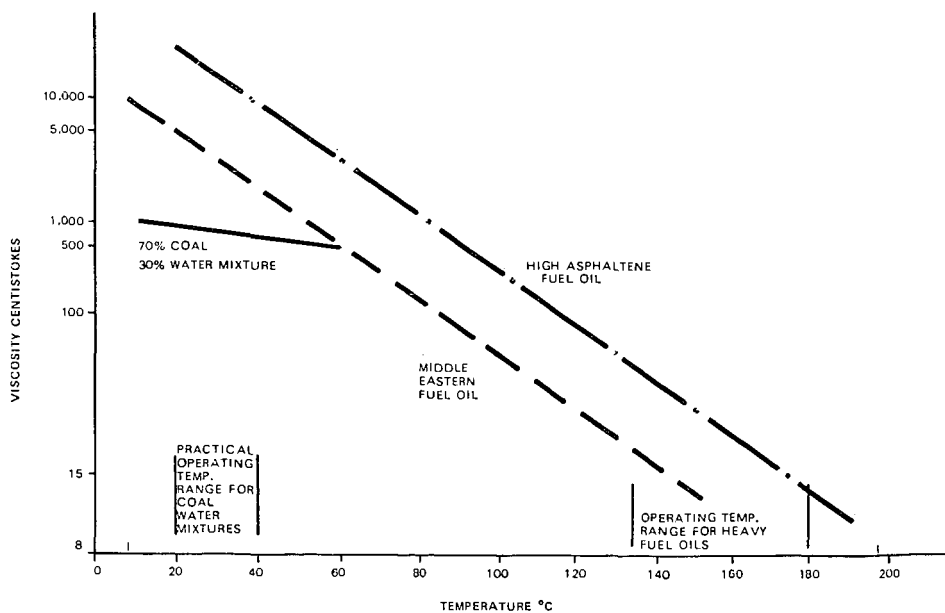


FIGURE 7  
VISCOSITY VARIATION, BY AERATION, OF COAL WATER MIXTURES AT 20°C

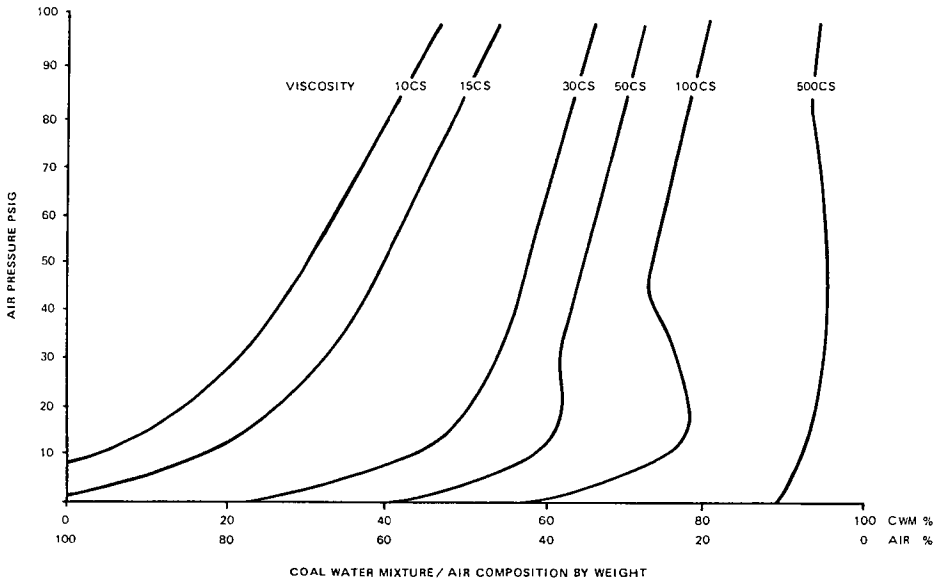
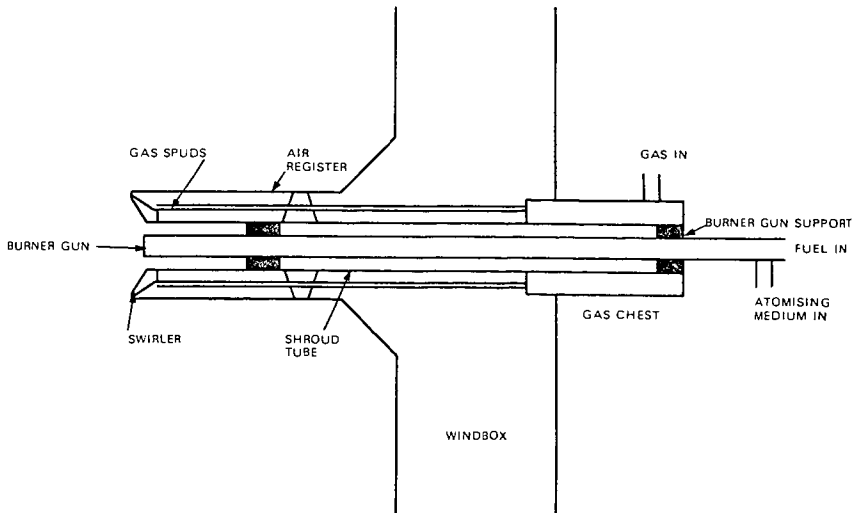


FIGURE 8  
GENERAL ARRANGEMENT OF SMALL SCALE RIG BURNER



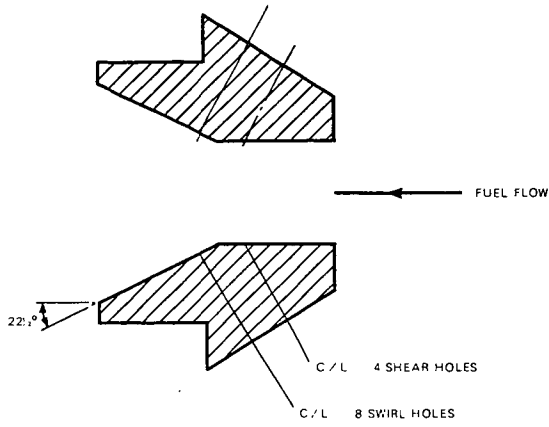
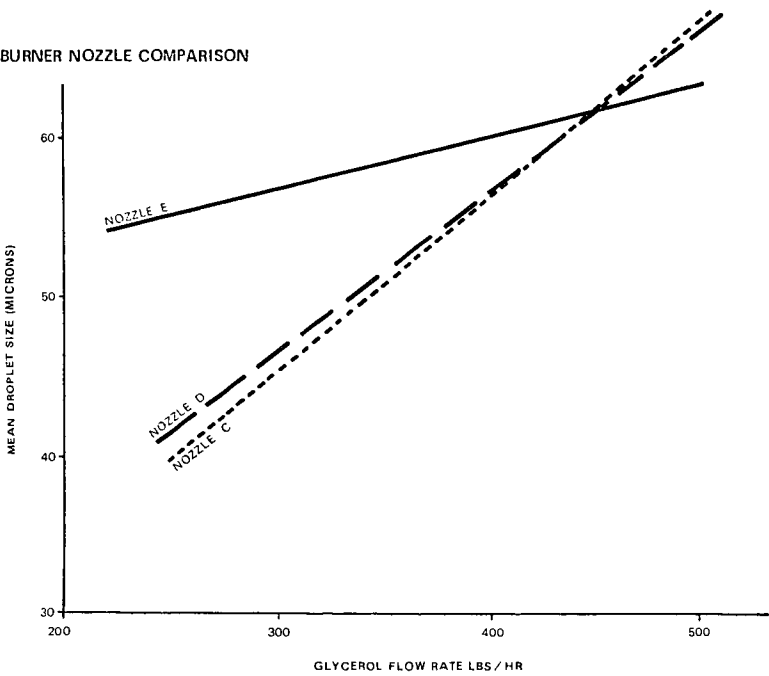


FIGURE 9  
 DIAGRAM OF COAL WATER MIXTURE BURNER NOZZLE

FIGURE 10  
 ISOTHERMAL BURNER NOZZLE COMPARISON



CHEMICAL AND PHYSICAL PROPERTIES OF HIGHLY-LOADED  
COAL-WATER FUELS AND THEIR EFFECT ON BOILER PERFORMANCE

By

G. A. Farthing, Jr.,  
R. D. Daley,  
S. J. Vecchi,  
E. R. Michaud

BABCOCK & WILCOX COMPANY  
Alliance Research Center  
Alliance, Ohio

and

R. K. Manfred, Project Manager  
ELECTRIC POWER RESEARCH INSTITUTE  
Palo Alto, California

ABSTRACT

Coal-water fuels (CWF) are being developed as substitute fuels for industrial and utility boilers presently burning oil. The chemical and physical properties of CWF vary widely depending on the coal and preparation process used. Also, the traditional methods for characterizing fuels and existing correlations between boiler performance and fuel properties may not be applicable to CWF. Babcock & Wilcox is working under contract to the Electric Power Research Institute to determine the range of properties a CWF should have to qualify as a boiler fuel. Laboratory fuels characterization methods are being developed for use as standard procedures for measuring the key properties related to storage, atomization, combustion, handling in various transport systems, and deposition tendencies on boiler heat transfer surfaces. The relationship between laboratory-measured rheological characteristics of CWF's and their pipe flow and combustion performance is being determined. Atomization studies are being performed in a newly constructed atomization facility having the capability of testing atomizers at fuel flows equivalent to 5-50 million Btu/hr. Atomization quality is assessed using laser diagnostics to determine droplet size and velocity distributions. Flame stability and combustion efficiency are being correlated with atomization quality through combustion testing at  $5 \times 10^6$  Btu/hr. The status of these studies is reported.

## INTRODUCTION

### Background

The use of residual fuel oil as a utility boiler fuel is coming to an end. Its price has increased by more than a factor of 5 since 1973. Its availability has become a matter of uncertainty. Federal policy prohibits its use in new baseload utility boilers, and the Congress has been considering mandatory conversion of existing oil-fired units to coal. Not surprisingly, then, utilities are aggressively searching for alternative fuels.

One such alternative may be coal-water fuel (CWF). Comprised of finely pulverized coal particles suspended in water, CWF may contain 65 to 80 percent dry coal by weight. The important and somewhat surprising characteristic of these highly loaded slurries is that they are quite fluid. They are also stable suspensions: the coal particles do not settle during storage for several weeks or even several months. Although producers differ in their methods, these properties are generally obtained by using a particular coal particle size distribution for efficient particle packing coupled with the use of certain chemical additives to provide good fluidity and stability.

One of the first applications of these fuels in the utility industry may be in boilers which were originally designed for coal firing, but because of the price, availability, and convenience of fuel oil, have been firing oil instead. In many cases these utilities never purchased, or have removed coal handling equipment, and many no longer have room for coal storage piles. If these utilities could be offered a coal-water fuel which could be fired with only minor modifications to their fuel oil handling systems, their conversion to coal firing would be greatly simplified and less costly. The environmental problems associated with coal storage piles would also be avoided.

Another possible short-term application for coal-water fuels is in utility boilers which were designed for oil firing. However, since coal-water fuel firing is similar to firing a moist pulverized coal, a number of problems arise.

The coal particle residence time in the boiler may not be long enough, at full load, to permit good carbon burnout. The boiler may not have an adequate ash removal system. Finally, there are problems associated with slagging, fouling, deposition, and erosion which must be addressed. All of these factors, which are strongly boiler-dependent, must be used to determine whether and by how much a boiler must be derated when firing coal-water fuel. Use of coal beneficiated to circa 1% ash may lessen the derating penalty enough to make slurries more viable for this application.

In the future CWF could fuel new utility boilers. Such factors as land availability, coal transportation costs, and relative capital costs of fuel handling and combustion systems will dictate the fuel choice.

Before coal-water fuels can fulfill this potential role, large-scale combustion tests must be performed. Also, large-scale fuel preparation facilities that can produce fuels of consistent quality and uniformity for a variety of coals must be designed and built.

To Babcock & Wilcox's (B&W's) knowledge, there are at least seven vendors of coal-water fuels who intend to market this product and who have subscale production facilities. It is suspected that many other organizations are currently pursuing the technology and could enter the marketplace in the near future. Prior to the work reported herein, B&W had performed preliminary fuel characterization, pumping, and combustion tests on CWF's from two of these vendors. The purpose of these feasibility studies was to determine whether these fuels, containing 67-72% dry solids, could be handled and burned in a manner similar to residual fuel oil. An existing 8-million Btu/hr oil burner fired at 4-million Btu/hr was used during these combustion tests. This burner is similar in design to burners provided in recent utility boiler offerings.

Results of these tests were encouraging. It was concluded that stable ignition of CWF could be obtained without the necessity of support fuel. The range of stable conditions, however, was more limited for the CWF tests than it was during combustion of the parent coals in the conventional pulverized form.

CWF properties had a profound influence on these combustion tests. For instance, large particles tended to plug the atomizer, and high CWF viscosities limited atomizer effectiveness. The ability to produce finely atomized droplets containing very few coal particles seemed to be the most important factor in achieving stable ignition. The effectiveness of atomization was greatly influenced by CWF viscosity, which could be decreased by preheating or diluting the fuel. Interestingly, while the viscosity of some CWF fuels decreases with increasing temperature, viscosity increases with increasing temperature for others. Clearly, more had to be learned about the effects of CWF properties on the combustion process prior to the eventual full-scale demonstrations of this new fuel.

### Objectives

The Electric Power Research Institute (EPRI), concerned about fuel procurement for its planned industrial and utility boiler CWF demonstrations, awarded B&W a contract to resolve some of these issues. The prime objective of the program is to provide EPRI with a standard coal-water fuel specification with which it can procure fuels for future tests. Since such a specification would be useless without standard fuel characterization test procedures, B&W will also recommend testing procedures for use with CWF's. B&W's work on this contract is in progress, and this paper presents some preliminary experimental results.



## EXPERIMENTAL APPROACH

In attempting to meet these goals, B&W is conducting an extensive experimental program consisting of work in four major areas:

- Laboratory fuel characterization tests
- Rheology testing
- Atomization characterization
- Combustion testing

EPRI has procured CWF's from five vendors to provide a range of physical properties representative of the expected commercial product. The vendors are each providing a CWF produced from a coal of their own choice. In addition, one vendor is producing a CWF from a coal provided by EPRI from its Homer City Coal Cleaning Plant. This "clean" coal was also supplied to B&W to be fired in the conventional pulverized form to provide a basis of comparison of combustion performance.

Experimental results in the four major areas of investigation will be correlated to link CWF combustion performance with CWF physical properties. This information will be used to determine the properties a CWF must have for use as a boiler fuel, and a standard CWF specification will then be generated.

### Fuels Characterization

The fuel analysis procedures listed in Table 1 were used to characterize the parent coals and CWF's. These tests provide a basis for comparing different CWF's and a basis for assessing the effects of coal properties on CWF properties. The results of these tests aid combustion tests and in interpreting handling and combustion test results.

The test procedures consist of standard ASTM methods, special methods developed by B&W for routine evaluation of fuels, and additional test methods specific for CWF's. The CWF viscosities were measured by a Haake Rotoviscometer, Model RV-100. The particle size distributions of the CWF's were measured by two Leeds & Northrup Microtrac Particle Size Analyzers covering a range of 0.3 to 300 microns.

The Laboratory Ashing Furnace (LAF), shown schematically in Figure 1, was used to study factors pertaining to ash deposit formation in boiler tube banks. Properties of fly ash produced in this unit are comparable to those of fly ashes obtained from commercial installations when similar combustion conditions are maintained. The LAF is designed to fire liquid, solid, slurry, and gaseous fuels. The LAF has a nominal heat input of 200,000 Btu/hr. The LAF consists of pulverized coal and liquid/slurry feed systems, an appropriate burner for specific fuel type, a refractory combustion chamber with a three-zone electric guard heater, a water-cooled heat exchanger, and a fly ash collection system. The CWF feed system includes a heated 55-gallon storage tank with an air powered mixer, a Moyno pump with variable-speed drive, feed lines, and a water-cooled burner with internal-mix atomizers.

The CWF dynamic stability test equipment consists of CWF sample containers, a Ling shaker table, a G-force generator, and a random frequency generator. The simulated transportation modes and test conditions included ship (5-20 HZ and 0.6 G's), rail (5-20 HZ and 0.6 G's), truck under normal road conditions (20-100 HZ and 0.6 G's), and truck under severe road conditions (100-200 HZ and 0.6 G's). The dynamic and static test results provide information on the storage and transportation properties of CWF's.

### Rheology

Many of the key physical properties of a CWF are associated with its flow properties. Not only do they determine its handling characteristics during transport and pumping, but the quality of atomization is also expected to be controlled by these properties. Since atomization quality has been shown to have a tremendous influence on the combustion performance of CWF's, the link between rheological properties and atomization quality must be established.

Since it is expected that the combustion characteristics of CWF fuels will be strongly dependent on the quality of atomization, and atomization quality will depend on the CWF flow properties, a support activity has been included to investigate the rheology of CWF's. In the development of a CWF working specification, it will be important to understand how slurry rheology affects

the other phenomena of interest in this study. To facilitate this analysis it is important to verify that the rheological behavior of coal-water fuels can be understood in terms of the available theoretical models of non-Newtonian fluids. In particular, it is important to show that the flow properties of these slurries in process pipelines, etc., can be predicted well enough for design purposes using theory and certain key laboratory physical property measurements.

It is believed that the time-independent rheology of coal-water fuels can be modeled in the following way:

$$\tau - \tau_y = k\dot{\gamma}^n$$

where:

- $\tau$  = shear stress
- $\tau_y$  = yield stress (empirical constant)
- $k$  = empirical constant
- $\dot{\gamma}$  = shear rate
- $n$  = empirical constant

It is known, for example, that most CWF's exhibit a yield stress (will not flow until the applied shear stress reaches some critical value) and show decreasing viscosity with increasing shear rate ( $n < 1$ ). Both of these characteristics can be handled in a straightforward manner using this model.

There are complicating factors, however. All of the empirical constants in the model are functions of temperature and quite possibly functions of time as well. Slurry fuels are known to exhibit thixotropy (viscosity decreases with increasing time at constant shear rate) meaning that the constants in the rheological model change as the slurry flows down the length of the pipeline.

The approach taken in this study was to use extensive laboratory viscometer measurements to determine the effect of temperature, shear rate, and time at constant shear rate on the apparent viscosity of the various coal-water fuels tested. This information will be used to determine the appropriate values for the constants in the rheological model corresponding to various flow conditions. Eventually, these results will be correlated with pipe flow results and results from the other areas of investigation.

## Atomization

Atomization characterization tests are performed in B&W's recently completed Atomization Facility (Figure 2). This facility is equipped with state-of-the-art laser diagnostics, and permits local droplet velocity, size distribution, and relative number density measurements to be made in large-scale sprays. The inside dimensions of the spray chamber are 8 feet x 8 feet x 10 feet. Mounted on opposing walls are two 4-foot x 8-foot plate glass windows which provide optical access to the spray for laser measurements, visual observation, and still and motion picture photography.

A uniform, axial flow of air continually sweeps through the chamber to prevent the build-up of a "fog" of very fine droplets. This air flow is provided by a large, forced draft fan, and is straightened and uniformly distributed by the windbox. The atomizer barrel is inserted through the windbox as shown. A gas cleanup system attached to the downstream end of the chamber removes most of the spray droplets from the air stream before it is exhausted back into the atmosphere. In the case of CWF, the fuel collected in the gas cleanup system is pumped into a large holding tank for subsequent disposal.

A 2000-gallon storage tank holds the CWF to be tested. The tank is equipped with a low-rpm stirrer. A variable speed, progressing cavity pump is used to supply CWF to the atomizer, and is capable of delivering 2-20 gallons/minute of CWF at a discharge pressure of 400 psig. The system is also equipped with an electric CWF heater which has a 100 KW capacity. With this heater the CWF can be heated to temperatures in excess of 250°F.

Local droplet velocity, size distribution, and relative number density can be obtained from the laser diagnostics using particle sizing interferometry (commonly referred to as the visibility technique). The method requires the same basic optical equipment as the dual-beam Laser Doppler Velocimeter (LDV) technique. The visibility and LDV techniques can provide non-intrusive local measurements of individual droplet size and velocity.

A schematic of a dual-beam LDV is shown in Figure 3. It consists of a laser, beam splitter, focusing lens, collection optics, photodetector, and signal processor. At the intersection of the two beams, which defines the measurement volume, a fringe pattern is formed by the interference of the two coherent beams. As a droplet moves across the measurement volume, it scatters light which is collected and processed by the signal processor. A typical signal is also shown in Figure 3, and is known as a Doppler burst.

The Doppler burst is made up of two components - an AC signal superimposed on a Gaussian "pedestal". The period of the AC signal and the fringe spacing can be used to determine the droplet's velocity. Droplet size can be determined from the "visibility" defined as

$$V = \frac{I_{\max} - I_{\min}}{I_{\max} + I_{\min}}$$

where  $I_{\max}$  and  $I_{\min}$  are defined as shown on the figure. It turns out that visibility is a simple function of (D/S) (where D = droplet diameter and S = fringe spacing) over a droplet diameter range of about 10:1. By changing the fringe spacing, a different range of droplet diameters can be measured.

The Atomization Facility is used to characterize the droplet size distribution obtained from the same atomizer being used for the combustion tests for each of the CWF's. A variety of atomization conditions (fuel flow rate, air/fuel ratio, fuel temperature) is investigated. Again, these results will be correlated with the results from the other areas of investigation.

### Combustion

Combustion tests are performed in B&W's Basic Combustion Test Unit (BCTU) shown in Figure 4. It is a water-cooled horizontal furnace with a nominal firing rate of about 5 million Btu/hr when firing pulverized coal. The combustion chamber is cylindrical with a diameter of 4-1/2 feet, and is 8 feet long. It is

partially lined with refractory brick to bring flame temperatures more in line with larger units. Two separately-fired air heaters are capable of supplying 800°F combustion air. A number of viewports mounted on the furnace permit visual observations, and provide access for various probes for detailed in-flame measurements.

Coal-water fuel is supplied to the furnace with a system consisting of a 500-gallon storage tank equipped with a stirrer, a variable-speed progressing-cavity pump, and a mass flow meter. An electric heater is also available for heated CWF tests. A dual-fluid, internal-mix atomizer is used to inject the CWF into the furnace in the form of a fine spray. Compressed air is used as the atomizing fluid.

The burner being used is a research burner having four concentric air zones which provide flexibility in how the air enters the furnace. Two of the zones are equipped with devices for imparting swirl to the flow, and another is equipped with a natural gas burner for firing the furnace at full load on natural gas. The burner is also equipped with a bluff body stabilizer for improved ignition stability.

The combustion characteristics of coal-water fuels must be comprehensively studied in order to achieve EPRI's principle objective -- the establishment of specifications for such fuels with which EPRI can confidently procure the large quantities of CWF that will be needed for future large-scale demonstrations. For B&W, determining combustion characteristics of CWF means performing a standard fuel characterization program similar to many such programs the company has performed in the past to determine the characteristics of other potential boiler fuels. Of course, each program must be tailored to fit the peculiarities of the fuel being tested.

In the case of CWF, there are a number of important areas in which further information is needed before these fuels can be demonstrated on a utility boiler. Ignition stability, the excess air and residence time needed for good carbon utilization, ash handling and deposition characteristics, flame temperature, and pollutant formation must all be addressed. And for the purpose of determining the specifications of a CWF boiler fuel, the way these factors are affected by changes

in the various CWF properties such as, moisture content, particle size distribution, chemical additives, slurry rheology, and parent coal characteristics must be delineated. It is the purpose of the combustion test program to address all of these factors and provide a maximum amount of the needed information.

Using the BCTU, B&W will relate combustion performance in terms of ignition stability, turndown, excess air requirements,  $\text{NO}_x$  emissions, and carbon burnout, to slurry characteristics such as solids loading, particle size distribution, viscosity vs. shear rate, viscosity vs. time, viscosity vs. temperature, and coal type. This information will be combined with an evaluation of slurry pressure drop, slurry storage and handling characteristics, and qualitative characterization of atomizer wear to provide the basis for recommending an acceptable range of slurry properties to guide future development work.

## PRELIMINARY RESULTS

At the time of writing much of the testing has been completed, but only a small fraction of the data has been analyzed. A detailed presentation of the results of the entire program is therefore not possible. Rather, it is our intention to present in this section some examples of the type of results being obtained, and to indicate some of the trends that have been noted thus far.

### Fuels Characterization

ASTM and B&W fuel analysis procedures were applied to samples of the parent coals and coal-water mixtures as show in Table 1. The results of selected procedures for the CWF's are shown in Table 2. All the CWF's were prepared from high volatile eastern bituminous coals. Based on the volatile content and burning profile of the CWF's, ignition and a stable flame would be expected in a burner and furnace designed for similar coals. Other things being equal, ignition and flame stability of CWF's are strongly dependent on both volatile content and atomization quality. It is safe to state that CWF should be made from high volatile bituminous coals with volatile contents as high as possible.

The five CWF's had a wide range of solids contents from 69.3 to 75.3% and viscosities from 510 to 1955 cp @ 100 sec<sup>-1</sup> shear rate. Examples of viscosity curves (viscosity versus shear rate) will be presented in the discussion of the CWF rheology. All the CWF's tested were thixotropic (decreasing viscosity with time at constant shear), but some appeared dilatant (increasing viscosity with increasing shear), while others appeared pseudoplastic (decreasing viscosity with increasing shear). A slurry which is both thixotropic and pseudoplastic is more desirable from a handling and atomizing standpoint. The fuels exhibited different responses as a function of temperature. The viscosity of several CWF's decreased with increasing temperature, while several did the opposite.

The particle size distribution (PSD) of the CWF's were not drastically different. All the fuels had at least 98.5% passing 50 mesh (300 microns). All the fuels, in general, were coarser than normal pulverized coal (PC) which has a mass mean diameter of approximately 40 microns. Four of the slurries contained



more fine material than normal PC, which has an average Sauter mean diameter of 15 microns. Four CWF's had at least 70% of the material less than 200 mesh (75 microns). In general, the CWF's had a wider particle size distribution than PC. Example particle size distributions are presented in a later section.

All the CWF's had sulfur contents less than 1%, ash contents varied from 1.8 to 7.9%. Some of the coals used to prepare the slurries were beneficiated to decrease ash and sulfur levels. The CWF's had almost identical densities. Four of the slurries had a pH in the range of 7.3 to 8.6, and the fifth had a pH of 6.0.

The fuels were subjected to several tests in order to predict the deposition potential of each. Deposition potential and ash chemistry is particularly important because of the effect on the size of industrial and utility boilers, furnace heat release rates, the design of heat transfer surface, and the number and placement of boiler cleaning equipment for ash and slag deposit removal. The deposition potential of the parent coals and CWF's is shown in Table 3.

Slagging potential is indicated by  $R_s$  values (based on elemental ash analysis) and  $R_{vs}$  values (based on actual slag viscosity/temperature relationship). These slagging indexes indicate that full-scale slagging behavior of these fuels would be low or medium. Some important observations, however, can be noted. Slurries A and D showed a substantial increase in sodium content as compared to the parent coal. The softening temperature of the CWF's were 230 and 350°F lower than the parent coal.

Fouling potential is indicated by  $R_f$  values (based on elemental ash analysis) and sintering strength values (based on crushing strength of simulated full-scale boiler fly ash produced in the LAF). The most important observation from Table 3 is the increase in fouling potential of the CWF's A and D compared to that of their parent coals. Since it has been well documented that the sodium content of a fuel plays a major role in its fouling behavior, the severe fouling classification of the two CWF's is probably due to the increased sodium content. The CWF of vendor E also had a high fouling potential based on elemental analysis.

The increased deposition potential of two of the CWF's and the higher deposition potential of the CWF made from a highly beneficiated coal are important from a utilization point of view. The type and quantity of chemical additives used in the preparation of the coal-water fuel can have a significant influence on the deposition characteristics. While the total quantity of mineral matter in the coal can be reduced by beneficiation, the relative quantities of chemical elements in the remaining minerals may be altered. This may increase the potential for formations of troublesome, difficult-to-remove boiler deposits in spite of the lower ash loading during utilization.

An important CWF property is that related to the settling of coal particles under storage (static) and transportation (dynamic) conditions. Figures 5 and 6 show typical static and dynamic test results for three CWF's (A, B, and D). Several general trends can be stated based on these figures and other test results. All the fuels exhibited little settling (based on solids content) of the liquid portion of the sample, but all contained settled material on the bottom of the container. This material was approximately 2 to 4% of the total weight of slurry.

The settled material ranged from a soft-pack in which the slurry could be easily resuspended to a hard-pack which required significant effort to resuspend. The dynamic stability of the CWF's appear independent of frequency (up to 200 HZ) and acceleration (up to 0.6 G's). The dynamic test results for simulated truck transportation agreed with the condition of the as-received slurries subjected to actual truck transport. The static and dynamic test results for times of 1, 2, and 3 days were almost identical. This would suggest that the stability of CWF's is not dependent on the transportation mode, but can be predicted from static test conditions. Stability was shown to be dependent on storage time because the amount of settled material increased during a test period of 6 weeks. There was essentially no difference in the particle size distribution of the slurry throughout the sample container including the settled material on the bottom.

## Rheology

A first step in the analysis of the rheological properties of the various CWF's is to verify that the pipe flow characteristics of these fuels are predictable from laboratory viscometer measurements. A viscometer generates a "flow curve" relating the rate of shear ( $\dot{\gamma}$ ) to the shear stress ( $\tau$ ) applied, or alternatively, to the apparent viscosity  $\mu_a (= \tau / \dot{\gamma})$ . Generally, such a curve can be used with the equations of motion and continuity to predict pressure losses for pipe flow. The procedure can be reversed, however, to generate a flow curve from pipe line pressure drop measurements which can then be compared with the viscometer-generated curve.

The results of such an analysis for CWF - D are shown in Figure 7. The solid line represents the flow curve generated with a rotational viscometer. It indicates a complicated, non-Newtonian, time-dependent rheology. The time dependence, as evidenced by hysteresis, is typical of a thixotropic fluid (its apparent viscosity drops with time at shear). The data points shown in the figure are generated from pipeline pressure drop data. It can be seen that the two sets of results are in reasonably good agreement. Over the common range of shear rates they indicate a fluid whose viscosity increases with increasing shear rate (a dilatant fluid). The small difference in apparent viscosity between the two results is probably due to a slight difference in water content of the two samples, although it may be a result of the time-dependent behavior (thixotropy). A difference in water content of as little as 0.1 percent could account for the difference.

It can be concluded from these results that the flow behavior (pipeline pressure losses, etc.) of this CWF can be predicted from laboratory viscometer measurements and existing non-Newtonian flow models. Rheology test results such as these will be used extensively to understand atomization and combustion results.

### Atomization and Combustion

Unfortunately, few results from the atomization and combustion tasks are available at the time of writing. It is partly for this reason that the two have been combined into a single section. Beyond this reason, however, the combination is a natural consequence of the inseparable nature of the two phenomena. It has become apparent that the quality of atomization has a tremendous influence on the combustion performance of a CWF. Production of very fine droplets is essential if stable, unassisted ignition of the fuel is to be obtained. Production of large droplets (in excess of 300 microns) which will not completely burn, means a lower carbon utilization efficiency.

It should be apparent from the last two statements that droplet size, and not coal particle size, determines the size of burning particles in a boiler. We believe that is the case. Even at this early stage in the data analysis, such a conclusion seems unavoidable.

As an example, consider the results shown in Figures 8, 9, and 10. Figure 8 shows droplet size distributions for a CWF generated using the Atomization Facility. Two curves are shown -- one for a CWF flow rate equivalent to full-load conditions at the BCTU ( $4 \times 10^6$  Btu/hr), and the other for approximately one-quarter of that flow. Note that the low-load droplet size distribution is finer than that for full load. This is as expected since the atomizing air flow rate was held constant for the two tests, resulting in a higher air/fuel ratio for the low load condition.

Figure 9 shows fly ash particle size distributions collected during the BCTU combustion tests. Fly ash size for full load conventional pulverized coal firing, full load CWF firing, and lower load CWF firing are shown. Coal particle size distributions for a conventional pulverized coal and CWF-A are shown in Figure 10. By comparing the figures, it can be seen that CWF firing at full load produces a coarser fly ash than conventional pulverized coal firing, while firing at low load produces a finer fly ash. Since carbon conversion in the BCTU is generally poorer at low load than at full load when firing pulverized coal, the finer fly ash at low load must be due to a better quality of atomization -- which is consistent with the atomization results presented above.

This is only one example of the kind of information B&W is generating as part of the EPRI program. A tremendous amount of data is being taken in all four areas of investigation, and on all the CWF's. It is expected that much of this information will be available for presentation at the National Meeting in Seattle.

#### ACKNOWLEDGEMENTS

The authors acknowledge the support of the Electric Power Research Institute whose funding made this work possible.

The advice and assistance of R. F. DeVault, J. M. McCoury, Jr., H. R. Oyster, M. E. Oyster, J. Santi, E. D. Scott, and E. W. Stoffer is also acknowledged.

A special note of thanks goes to R. T. Bailey whose expertise and diligent efforts made the laser droplet size measurements possible.

TABLE 1  
Fuels Characterization Tests

<u>FUEL ANALYSIS PROCEDURE</u>	<u>PARENT COAL</u>	<u>CWF</u>	<u>METHOD</u>
Total Moisture	X	X	ASTM (D3173, D3302)
Solids Content		X	ASTM (D3173, D3302)
Hardgrove Grindability	X		ASTM (D409)
Proximate Analysis	X	X	ASTM (D3172)
Ultimate Analysis	X	X	ASTM (D3176)
Higher Heating Value	X	X	ASTM (D2015, D3177)
Sulfur Forms	X	X	ASTM (D2492)
Ash Fusion Temperatures	X	X	ASTM (D1857)
Elemental Ash Composition	X	X	B&W
Ash Sintering Strength	X	X	B&W
High Temperature Slag Viscosity	X	X	B&W
Burning Profile	X	X	B&W
Volatile Release Profile	X	X	B&W
BET Surface Area	X	X	B&W
Slurry Density		X	B&W
Slurry Viscosity vs. Temperature		X	B&W
Particle Size Distribution			
• Microtrac		X	B&W
pH	X	X	B&W
Slurry Stability			
• Static		X	B&W
• Dynamic		X	B&W

TABLE 2  
CWF Properties

FUEL PROPERTY	SLURRY VENDOR				
	A	B	C	D	E
Solids (%)	75.3	69.3	69.4	69.9	74.9
Viscosity (cp @ 100 <sup>-1</sup> sec)	1955	1575	1550	510	520
HHV (Btu/lb, as received)	10730	9910	10180	10180	11380
HHV (Btu/lb, dry)	14250	14300	14670	14560	15190
VM (% , as received)	24.7	26.5	24.8	22.9	28.0
VM (% , dry)	32.8	38.2	35.7	32.7	37.4
Ash (% , dry)	7.9	6.3	5.9	6.9	1.8
Sulfur (% , dry)	0.84	0.87	0.81	0.77	0.91
Particle Size Distribution					
% < 200 Mesh	70	78	63	78	73
Mass Mean Diameter (microns)	59	44	67	48	53
Sauter Mean Diameter (microns)	7	9	15	8	11
pH	8.6	7.6	7.3	8.1	6.0
Density (g/cc)	1.23	1.22	1.20	1.23	1.23

TABLE 3

## Deposition Potential of Parent Coals and CWF's

	V E N D O R									
	A		B		C M F		C o a l		D	
	Coa l	C M F	Coa l	C M F	C M F	C o a l	C M F	C M F	C M F	E
Slagging Parameter										
R <sub>s</sub> (Classification)	.14 (Low)	.12 (Low)	.10 (Low)	.05 (Low)	.19 (Low)	.12 (Low)	.79 (Med)			
R <sub>vs</sub> (Classification)	(Low)	.24 (Low)	(Low)	.22 (Low)	.81 (Med)	(Low)	.45 (Med)			
Fouling Parameter										
R <sub>f</sub> (Classification)	.18 (Low)	.61 (High)	.05 (Low)	.03 (Low)	.74 (High)	.06 (Low)	.80 (High)			
Sintering Strength, psi	2290	17900	500	2072	16200					
@ 1700°F (Classification)	(Med)	(Severe)	(Low)	(Med)	(Severe)					
Other Indicators										
Na as Na <sub>2</sub> O (%)	0.85	2.56	0.39	0.61	3.02	0.40	0.92			
Fe as Fe <sub>2</sub> O <sub>3</sub> (%)	9.02	9.37	5.43	5.93	9.20	8.20	40.26			
Softening Temp. (°F)	2630	2400	2750+	2750+	2400	2750+	2140			
(reducing atmosphere)										



# Babcock & Wilcox LAB ASHING FACILITY

1. ELECTRIC FURNACE
2. ELECTRIC FURNACE CONTROL CABINET
3. STEAM DRUM
4. PULVERIZED FUEL TWIN-SCREW FEEDER
5. NATURAL GAS
6. COAL TRANSPORT LINE
7. EXHAUST FAN
8. SECONDARY AIR HEATER
9. FLY ASH BAG
10. SLAG COLLECTOR
11. CYCLONE ASH COLLECTOR
12. MAIN CONTROL PANEL
13. COMBUSTION PRODUCTS
14. HEAT EXCHANGER
15. SECONDARY AIR
16. HIGH PRESSURE TREATED WATER PUMP
17. BLOW DOWN DRAIN
18. PLANT STEAM
19. FEED RATE MONITOR
20. RELIEF VALVE (250 PSIG)
21. MANUAL STEAM VENT
22. EXHAUST TO ATMOSPHERE (FLUE GASES)
23. HEATED SECONDARY AIR
24. SLAGGING, FOULING, AND SOOTBLOWING TEST SECTION

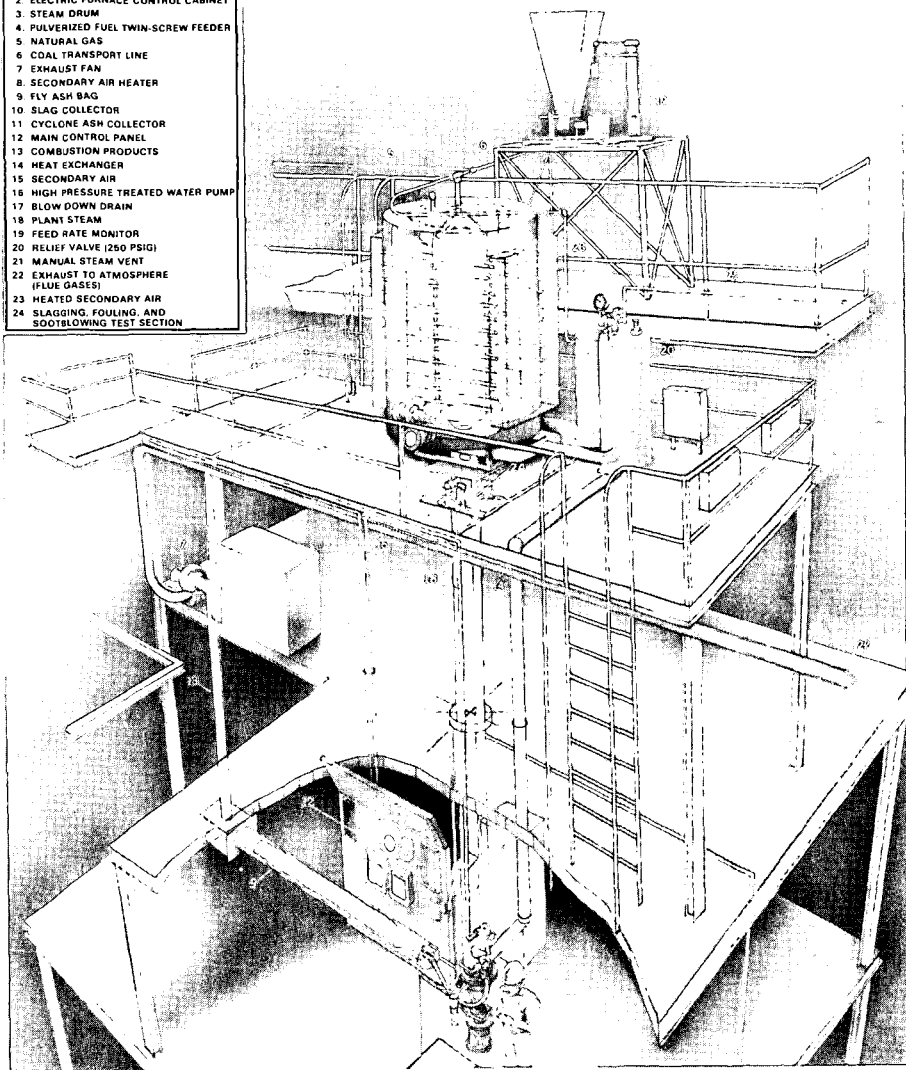


Figure 1. Laboratory Ashing Furnace.



Figure 2. Atomization Facility.

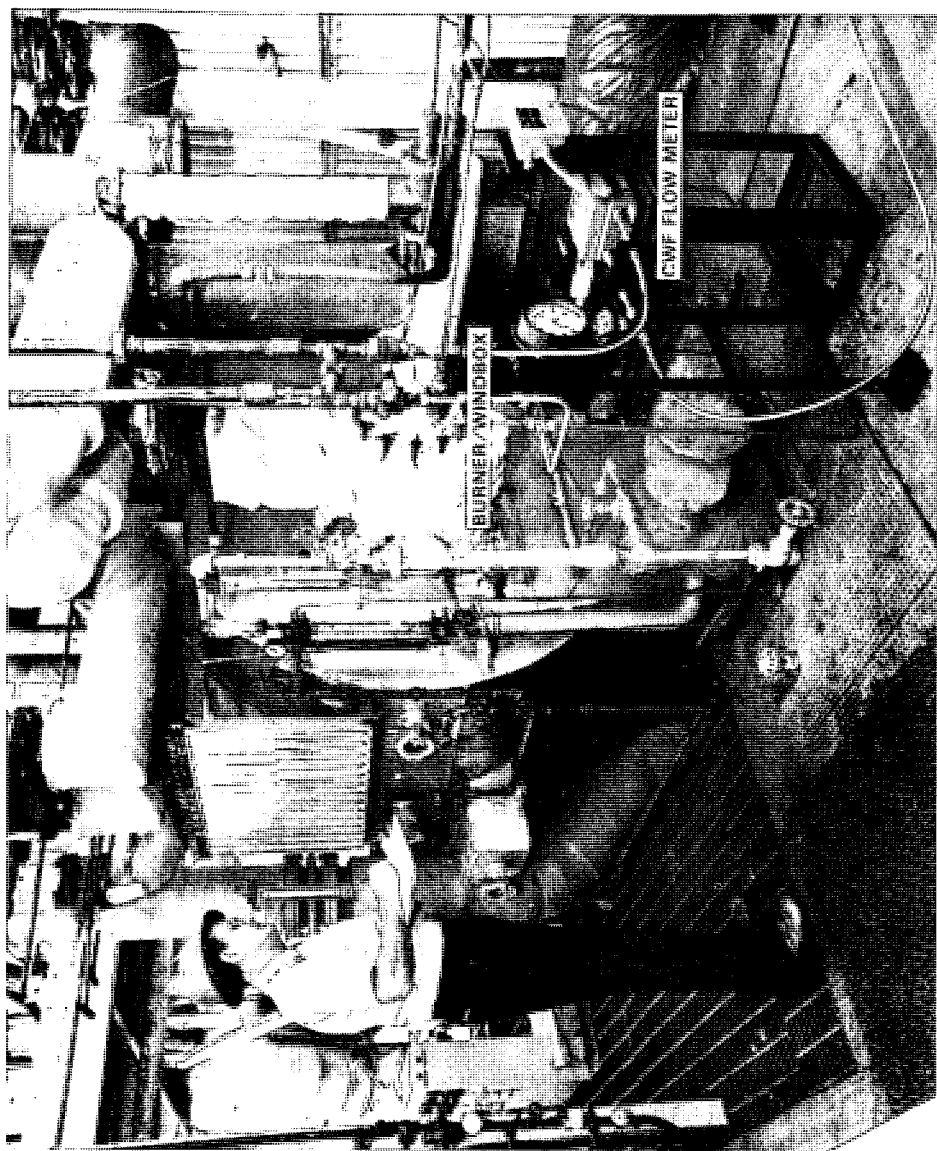


Figure 4. Basic Combustion Test Unit.

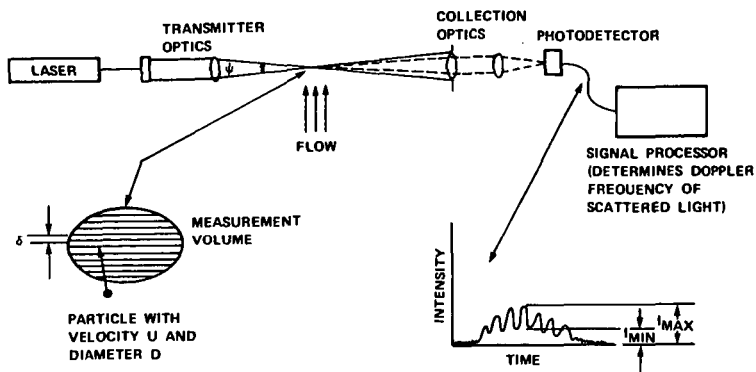


Figure 3. Laser Doppler Velocimeter (LVD) System  
Used to Size Particles by the Visibility  
Technique.

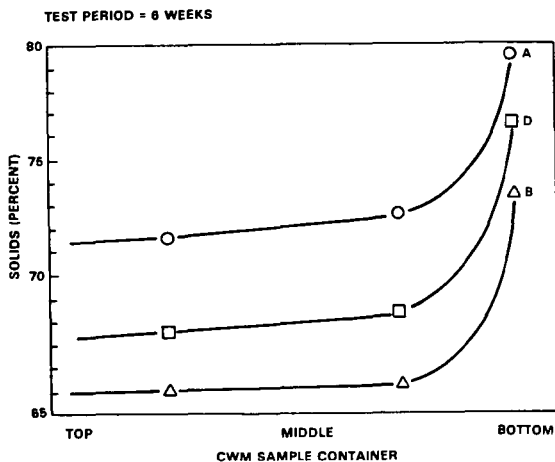


Figure 5. Static Stability Test Results.

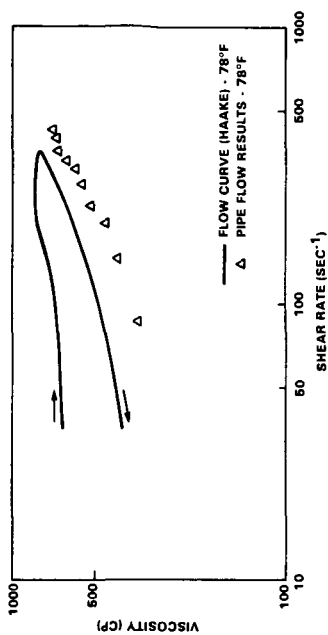


Figure 7. Rheology Test Results - CWF - D.

TRANSPORTATION MODE - TRUCK  
 TEST CONDITIONS: 100 - 200 HZ.  
 0.6 g  
 3 DAYS

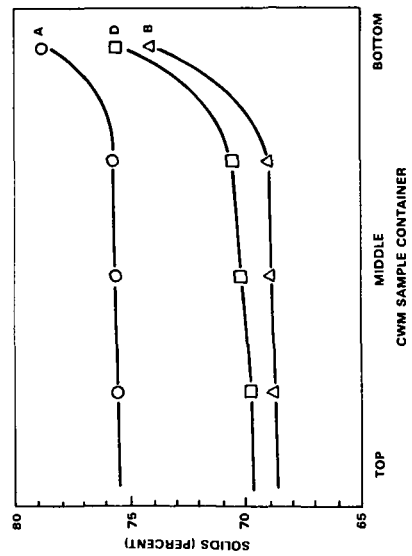


Figure 6. Dynamic Stability Test Results.

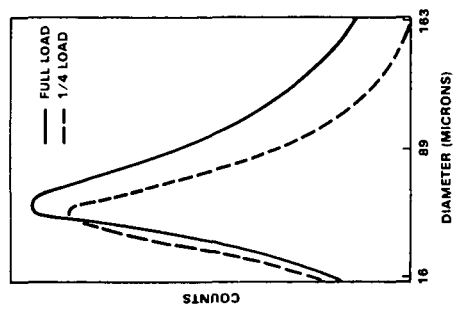


Figure 8. Droplet Size Distributions for CWF Sprays.

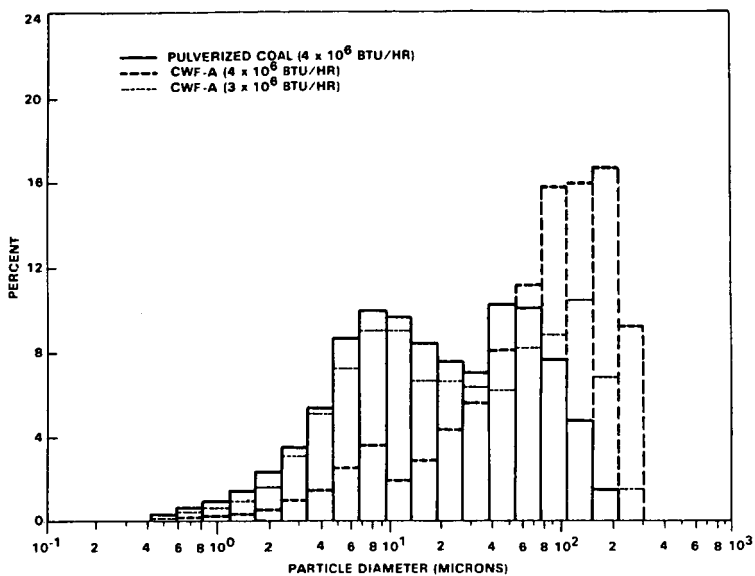


Figure 9. Fly Ash Particle Size Distributions.

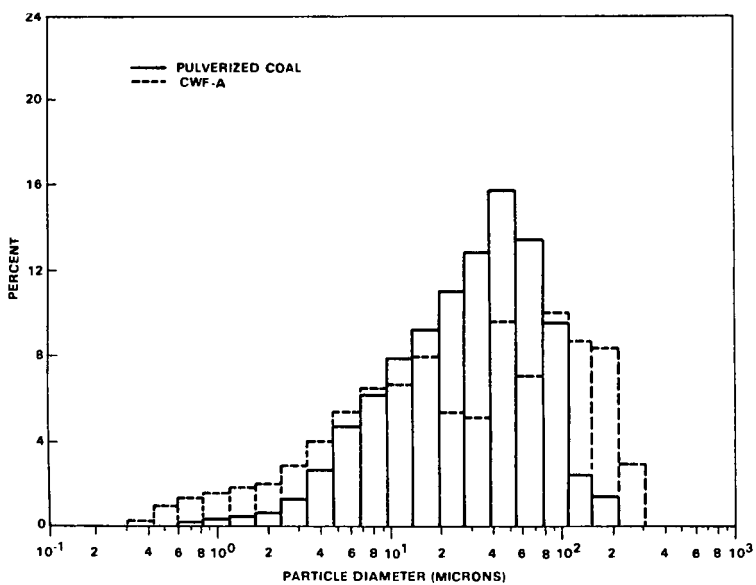


Figure 10. Particle Size Distributions - Pulverized Coal and CWF - A.

PROGRESS IN THE DEVELOPMENT OF A COAL/WATER MIXTURE  
AS A FUEL OIL SUBSTITUTE

R. E. Sommerlad, Vice President  
Foster Wheeler Development Corporation  
12 Peach Tree Hill Road  
Livingston, New Jersey 07039

R. H. Hickman, Manager  
Mechanical Engineering  
Forney Engineering Company  
P. O. Box 189  
Addison, Texas 75001

N. R. Raskin, Proposal Manager  
Steam Department  
Foster Wheeler Energy Corporation  
9 Peach Tree Hill Road  
Livingston, New Jersey 07039

INTRODUCTION

Coal/water mixtures (CWM) provide boiler and furnace operators with the opportunity to replace natural gas or oil with coal. CWM can be pumped, stored, and atomized like a liquid fuel; thus it has advantages over pulverized coal. However, unlike natural gas or oil, coal contains significant quantities of inorganic material (ash) which can adversely influence boiler performance and fuel-handling equipment. Burners can be modified to provide satisfactory ignition and flame stability characteristics with CWM and problems associated with nozzle lifetime can be solved. However, to solve problems associated with ash, we will probably have to resort to coal beneficiation, derating, or both. Based on available data, the optimum level of coal beneficiation cannot be defined. It will be determined from trade-offs among beneficiation, burner, and boiler/furnace-related costs.

CWM is clearly outside the range of fuel parameters used to design most oil and gas-fired units. Not only are the physical properties of the fuel different, but the ash and sulfur content of CWM is at least several orders of magnitude higher than it is in most oil and gas fuels. The differences in fuel properties can cause problems in virtually every portion of the firing system/furnace. Figure 1 illustrates some of these problems, which must be addressed and solved if CWM is to be used successfully.

EFFECTS OF FUEL PROPERTIES

Fuel properties and the extent of coal cleaning will affect the potential cost of firing CWM in boilers. Fuel properties will affect:

- Ignition and stability of CWM flame
- Emission of pollutants
- Availability.

Ignition and Flame Stability

Satisfactory ignition and flame stability with adequate turndown ratio are essential to the successful use of CWM. Ignition and flame stability are related and are controlled by the aerodynamics of the flame, heat transfer in and out of the ignition zone, and fuel properties. The most important fuel property is volatility. To achieve adequate ignition and flame stability, the coal must be heated to the point where the fuel devolatilizes and ignites. Although water in

CWM makes it more difficult to ignite than coals with less moisture, naturally occurring coals and wood bark with up to 60-percent moisture have been successfully burned commercially.

### Emissions

Many oil- and gas-fired boilers are located in areas that already have significant emissions problems. Hence steps must be taken to control particulate emissions from CWM firing which, although greater than from gas or oil, can be adequately controlled by electrostatic precipitators or bag filters.

Temperatures in CWM-fired boilers may be somewhat lower than in oil- or gas-fired boilers, tending to suppress the formation of thermal  $\text{NO}_x$ . However, fuel  $\text{NO}_x$  is temperature insensitive, and CWM will have a higher fuel nitrogen content than oil or gas. Thus  $\text{NO}_x$  emissions are expected to be higher.  $\text{NO}_x$  can be controlled by a range of techniques. Burner and combustion modifications have been successfully applied to reduce  $\text{NO}_x$  emissions when combusting coal to levels comparable to those with oil firing.

The potential for sulfur oxide ( $\text{SO}_x$ ) emissions can be higher when firing CWM than for oil or gas firing. Even though most of the coals considered for CWM will be cleaned to some extent, they will be higher in sulfur than most oils. Although  $\text{SO}_x$  can be controlled by flue gas desulfurization (FGD), this technique is expensive and troublesome and is rarely used on oil-fired units. The anticipated low flame temperatures in the boiler and intimate mixing of water in CWM firing offer potential for removing sulfur compounds in the furnace by injection of calcium compounds. Furnace injection of the sorbent is much less expensive than FGD. There is an additional advantage to this approach for use with beneficiated CWM. For new, large units, Federal regulations require a 90-percent reduction of  $\text{SO}_x$  when firing high-sulfur coals. This level of removal cannot be achieved solely by sorbent injection in a boiler. However, sulfur removed during beneficiation of the coals is credited toward total sulfur removal. Therefore, if capture in the boiler can remove a significant fraction of the sulfur, the required  $\text{SO}_x$  reduction can be achieved.

### Availability

Fuel properties definitely affect boiler availability. The potential problems from firing CWM in boilers designed to fire oil or gas are worse than they will be when firing it in boilers designed for coal. The cost of an inoperative 500-MWe boiler exceeds \$100,000/day. The down time of an average coal-fired boiler in the United States is almost 30 days a year--at a cost of \$3 million. About 60 percent of the down time is caused by boiler problems; ash characteristics--both quantity and quality of constituents--account for a significant portion of this time.

Table 1 compares parameters for gas-, oil-, and coal-fired boilers. Heat-release rates and tube-bank velocities are smaller and tube spacings in the superheater are greater in a coal-fired boiler. CWM introduces more ash, which can promote fouling, slagging, and erosion and it may contain corrosion-promoting materials.

Figure 1 shows potential problem areas where slagging and fouling can occur when firing coal in a utility-size boiler.



Table 1 Characteristics of Gas-, Oil-, and Coal-Fired Boilers

Description	Gas	Oil	Coal
Furnace Volume, Relative	1	1.3	1.9
Furnace Surface Area, Relative	1	1.3	1.7
Heat Release/Volume ( $10^6$ Btu/h·ft <sup>2</sup> )	25-50	25-50	10-22
Heat Release/Cooled Surface ( $10^6$ Btu/h·ft <sup>2</sup> )	200	200	70-120
Tube Bank Velocities (ft/s)	120	90	40-70
Superheater Spacing (in.)	2	4-6	8-16+

Difficult-to-remove slag deposits reduce heat flux through the wall, increasing furnace temperature. This deposit/temperature cycle can result in load reduction or shutdown.

As coal firing rates are increased to provide heat-release rates equivalent to those required in an oil-fired boiler, slagging may result. The higher heat-release and heat-transfer rates promote melting of particles flung to the wall above the burners. This action reduces the furnace heat extraction rate, allows higher temperatures to exist in the upper furnace, and increases the prospects of fouling the superheater. Consequently, slagging could inhibit the use of CWM in boilers designed to fire oil or gas.

#### TESTING

Hydraulic and burner testing have been performed at Forney Engineering Company in Addison, Texas. A test program initiated in 1981 in collaboration with a major United States CWM vendor included requirements to store, pump, transport, and burn CWM. The hydraulic test loop had typical connectors and piping, including two 10-ft sections of 1- and 2-in. Schedule 40 pipe. The test furnace is an 8-ft-dia cylindrical furnace with a water jacket. It is capable of  $70 \times 10^6$  Btu/h for short durations and up to  $40 \times 10^6$  Btu/h continuously. The furnace system includes a forced-draft fan with an in-line combustion air heater (gas fired), a steam generator for atomizing steam, an air compressor for atomizing air, and an ignitor system that uses No. 2 oil or natural gas. The windbox can be easily disconnected from the furnace and air duct to facilitate changing configurations.

Several pumps were tested. Diaphragm and vane types were troublesome, with discharge pulsations and accumulations in the liquid end. The progressive cavity pump was the most successful but required special care during extended periods of shutdown.

Based on CWM properties, the following needs were identified for burner tip design:

- Rapid mixing of the air and fuel to dry and ignite the coal in the primary recirculation zone.
- A strong recirculation zone maintained to create a highly radiant burning zone in the burner throat to dry the coal.
- No flame contact on any burner part because of anticipated slagging problems.
- Conventional burner parts for ease in retrofit applications.

Forney has several commercial burner designs for various applications:

- Parallel Air Flow (PAF)
  - Fast mixing
  - Low excess air applications
- Rotating Air Register (RAR):  
Highly turbulent
- Variable Flame Pattern (VFP): Variation of PAF with flame-shaping ability with rotational secondary air register.

Historically, Y-jet (YJ) and internal mix (IM) atomizers had been successfully used with high-gravity fuels. We attempted to adopt the basic features of each in two different atomizer designs--both incorporating a conical plug rather than individual orifices. Concepts for both atomizer tips, shown in Figure 2, have been patented.

After a matrix of tests including YJ and IM atomizers in RAR and VFP air registers, the following requirements were noted:

- Burner with two airflow paths with the primary path having a rotational, low flow
- Secondary airflow with high swirl to provide the recirculation zone
- Means of providing a highly radiant zone at burner exit.

These considerations were included in the design shown in Figure 3. This patented design provides dual velocities and two-throat configuration to maintain a radiant zone at the burner exit. A series of tests were successfully conducted under the usual burner performance parameters.

## BOILER DESIGN VS. CONVERSION POTENTIAL

Designs of existing utility steam generators vary substantially depending upon the original design fuel. Generally, the pressure-part arrangement of a boiler can be classified as one of the following types:

- Category A Unit--Two pass (Coal/Oil-Gas)
- Category B Unit--Two pass (Oil/Gas)
- Category C Unit-- Box type (Oil/Gas or Gas only).

The design configuration of each type of unit greatly affects its conversion potential in terms of both capital expenditure and derating requirements. Figure 4 shows a comparison of unit configurations that will be discussed.

### Category A Unit-- Two Pass (Coal/Oil-Gas)

Design Features. This type unit is characterized by a generously sized furnace (i.e., large plan area and a substantial distance from the burner zone to the first vertical radiant surface at the furnace exit). These features result in a sufficient radiant absorption in the furnace area, which lowers the furnace exit gas temperature entering the vertical convection sections, thus limiting slag formation. Also typical of this type of unit is a lower furnace hopper slope of at least 45 to 50 deg and a hopper throat opening of approximately 3 to 4 ft, both of which facilitate bottom ash collection and removal. The horizontal convection passes of a Category A steam generator are designed with adequate tube-to-tube clear spacing to prohibit fouling and possible plugging and to alleviate excessive flue gas velocities and associated tube erosion possibilities.

Conversion Potential. This type of unit was originally intended for burning coal as its primary fuel. Therefore, it should achieve full load output if reconverted to a similar type of coal or a CWM. The capital expense of the boiler portion of the conversion would be limited to refurbishment of original equipment, normal maintenance, and pollution control upgrading, if required.

### Category B Unit-- Two Pass (Oil/Gas)

Design Features. The Category B classification includes those steam generators with a furnace configuration similar to that of a Category A unit but with a less conservative convection pass arrangement. This type of unit was originally designed for oil or gas firing. The similarities in furnace arrangement when compared with the unit previously discussed are readily apparent. Generally, the furnace of a Category B steam generator is smaller than that of a Category A steam generator. Specifically, the former has a lower furnace hopper slope and opening and the furnace plan area is not as conservative. However, the overall furnace design for this type of unit is conducive to the firing of an ash-laden fuel. For this reason, based solely on furnace design criteria, a Category B unit is a viable candidate for conversion to pulverized-coal or CWM firing with minimal or no unit derating.

However, the convection pass arrangement in this unit can present several major obstacles when converting to coal or a coal-derived fuel. The clear spacings between tube sections of a Category B unit are less than those of a Category A unit. If such a unit were to fire coal or a coal-derived fuel, excessive fouling or erosion of the tubes could result, since the flue gas temperature and velocity of the unit would exceed the acceptable values for oil firing. To decrease flue gas temperatures and velocities so that the potential for fouling or erosion of existing convection pass tube banks can be reduced, the maximum unit load must be restricted. These design constraints are directly related to the fuel being considered, particularly the quantity and quality of its ash. Therefore, as might be expected, the derating requirements for coal and CWM vary.

Conversion Potential--Coal. Coal inherently has the highest ash content of the fuels being considered and will also exhibit the highest furnace exit gas temperature for any particular boiler load and furnace size. Consequently, the potential for convection pass fouling and tube erosion can restrict the maximum allowable output to approximately 70 percent of the design rating of a Category B Unit. This derating requirement can often be minimized or eliminated through substantial pressure-part modification. As indicated previously, the furnace of such a unit is normally capable of supporting full output while firing coal, and thus modifications to the furnace (which would be prohibitively expensive) would generally not be required.

Conversion Potential--CWM. Because of the ash and sulfur reductions that occur during the fuel preparation process, a Category B unit can be converted to CWM firing with less derating than would be required with coal. Reductions in ash (approximately 70 to 90 percent) and sulfur (50 to 70 percent) are possible during CWM beneficiation. Furthermore, the ash fusion temperatures of a beneficiated CWM are 100 to 200°F higher than those of the parent coal.

Consequently, higher furnace exit gas temperatures are allowable when firing CWM as opposed to coal. In a Category B boiler, higher temperatures translate to an allowable load of approximately 80 to 90 percent of full unit output. Again, convection pass pressure-part modifications could possibly restore such a unit to full load capability while firing a CWM.

#### Category C Unit--Box Type (Oil/Gas or Gas Only)

A Category C unit could be subject to a considerable derating if converted to coal or CWM. The horizontal convection passes of such a unit have closer tube-to-tubeside spacings than those of either Categories A or B boilers. The most critical disparity lies in the furnace design. A Category C unit has little or no provision for ash collection or removal, and the furnace is inadequately sized to reduce the potential for slagging associated with coal firing. The hopper slope is very shallow (or nonexistent), and the lower furnace throat opening (if any) is minimal. Burner spacings are generally close, and the distance from the lowest burner level to the hopper knuckle (or to the furnace floor) is generally inadequate. Both of these features result in a high furnace slagging potential. However, the most critical design limitation in evaluating the conversion of a Category C unit to firing coal or a coal-derived fuel is the inadequate furnace plan area. Modifications to the furnace hopper and burner pattern in many cases prove feasible and can minimize derating. This is also often the case with respacing of the convection passes, as was indicated in the previous discussion concerning a Category B unit.

However, furnace plan area enlargement is not feasible either physically or economically. Thus the derating for a Category C unit is more severe than that associated with the previously discussed boiler designs. Moreover, pressure-part modifications, within the realm of technical and economic feasibility, cannot alleviate these load restrictions.

Conversion Potential. Typically, conversion of a Category C unit to firing pulverized coal would involve a derating to 50 to 60 percent of design output because of furnace and convection pass design limitations previously identified. CWM presents the better conversion alternative for a Category C unit. Because of the ash and sulfur reduction that occurs during the fuel preparation process, slagging and fouling potential is considerably reduced. Even so, unit output may be restricted to approximately 70 to 80 percent of design rating.

Table 2 presents a summary of the typical feasible unit deratings for coal and CWM and for each type boiler.

Table 2 Maximum Allowable Load, %

<u>Fuel</u>	<u>Category</u>		
	<u>A</u>	<u>B</u>	<u>C</u>
Coal	100	70	50 - 60
CWM	100	80 - 90	70 - 80

#### Balance-of-Plant Considerations

The utilization of either coal or CWM in a boiler fuel conversion project significantly affects the required balance-of-plant equipment, impacting both the capital cost of the conversion and the site requirements. Each of the fuels studied has been examined in terms of the balance-of-plant considerations arising from a potential conversion project. The scope and costs of such equipment vary, depending on the original design fuel for each specific unit.

Balance-of-plant considerations must, at the very least, include:

- Refurbishment of coal-handling equipment (if it exists)
- Fuel handling
- Land requirements (coal yard and ash disposal)
- Fan systems

- Ash collection, storage, and removal systems
- Fly ash collection
- FGD system.

Compared with total plant conversion costs, boiler/island-related work is approximately 10 to 20 percent of the total project cost. However, the steam generator remains the primary consideration for potential derating.

### ECONOMICS OF CONVERSION

An evaluation of the capital expenses vs. the fuel savings of a potential conversion project is unique to the steam generator under consideration. Some general observations regarding the effect of basic unit design criteria and site considerations have been discussed. Such generalities are not possible regarding the specific economics of a conversion. To provide an indication of these economics, a specific unit has been selected as a test case for comparison of conversion to coal or CWM. The analysis is specific to that unit but the methods will be common to any conversion project.

The selected Category B steam generator is a natural-circulation, balanced-draft, reheat unit utilizing a parallel pass gas flow arrangement. The unit, originally designed to fire oil as the primary fuel, could be converted to coal firing in the future, because of the relatively large furnace plan area, the lack of lower furnace radiant superheater surface, and the presence of a lower furnace hopper with an adequate angle of slope.

As discussed earlier a unit of this type--even with these design features--requires some pressure-part modification to achieve full load output if converted to coal or CWM firing. In this instance, these modifications consist of:

- Some horizontal convection surface respacing
- An upper furnace radiant superheater installation (to reduce furnace exit gas temperature)
- Burner respacing.

The cost of these items, although high, is not substantial when compared with total project costs or with the cost of replacement power purchased in the event of a derating.

Table 3 summarizes an economic evaluation of the conversion alternatives being considered. Several conclusions are evident from a detailed review of the table:

- As indicated previously, the cost of the boiler modifications necessary to avoid derating of a unit of this type is approximately 10 percent of total conversion costs and is thus, in this case, economically justifiable.

- Both fuels present viable conversion options, even if only 50 percent of the accrued fuel savings are recoverable toward payback of capital investment.
- The total capital cost of a conversion to pulverized coal is significantly higher than conversion to CWM, primarily because of the expense of a coal yard.
- Based on the comparison of benefit-to-cost ratios of the conversion fuels considered, CWM is the more economically justifiable conversion option.

Foster Wheeler and its family of companies is dedicated to the commercialization of CWM as a boiler fuel, as evidenced by our participation in:

- Boiler conversion design studies
- Burner development
- Coal cleaning and slurry preparation
- Fuel-production plant design
- Small utility conversion demonstration.

Foster Wheeler views CWM as one of the most promising alternatives to foreign oil dependence while using one of the most abundant resources available in the Western Hemisphere.

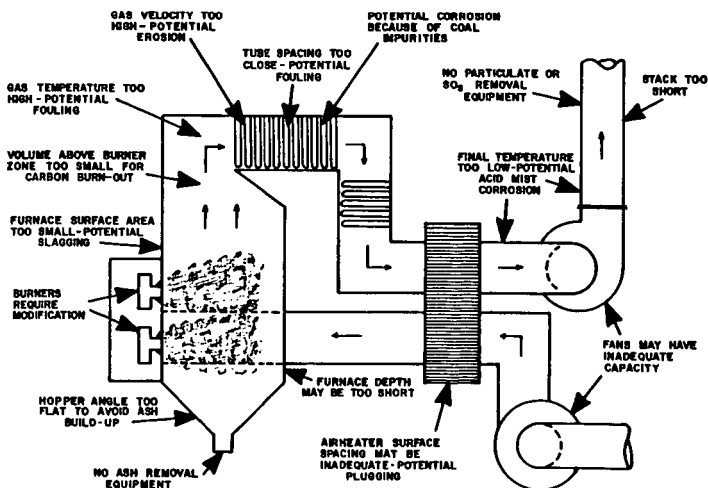
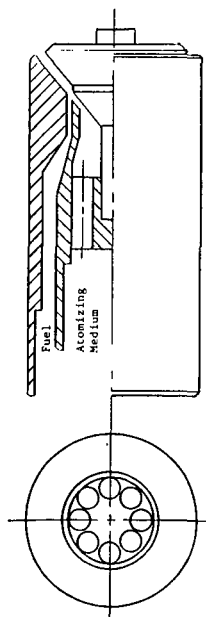


Figure 1 Potential Problem Areas in Retrofitting an Oil-Fired Furnace to CWM Firing

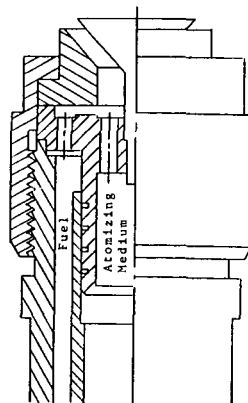
Table 3 Conversion Economics Evaluation

Fuel	\$ Million	
	Coal	CWM
Annual Fuel Costs	39.1	70.1
Annual Fuel Savings (vs. Oil)	67.4	36.4
Recoverable Portion of Savings	33.7	18.2
Levelized Annual Present Worth of Recoverable Savings	51.9	28.1
Capital Equivalent of Recoverable Savings	259.5	140.5
Conversion Costs		
Fuel System	96.4	9.3
Boiler Modification	4.7	2.3
Ash Systems	18.4	16.2
FGD System	41.7	41.7
Total	161.2	69.5
(w/o FGD)	(119.5)	(27.8)
<hr/>		
Capital Payback Period, years	3.1	2.5
(w/o FGD)	(2.3)	(1.0)
Benefit-to-Cost Ratio	1.6:1	2:1
(w/o FGD)	(2.2:1)	(5.1:1)





Conical Y-Jet Atomizer



Conical Internal-Mix Atomizer

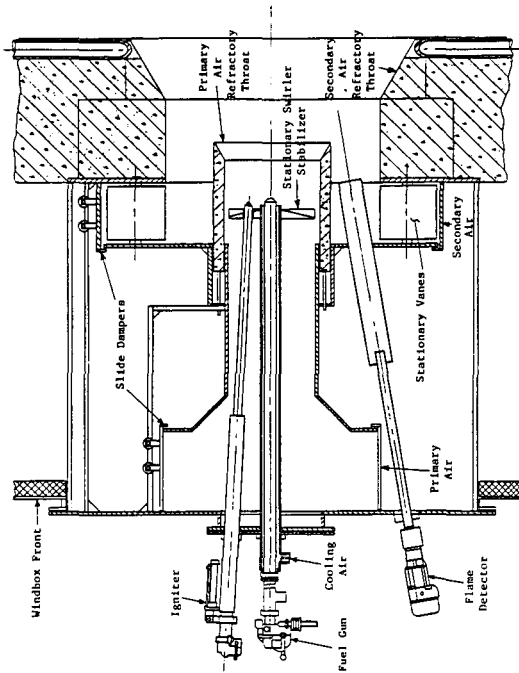


FIGURE 3 FORNEY CWF BURNER

FIGURE 2 SPECIAL CONICAL ATOMIZERS

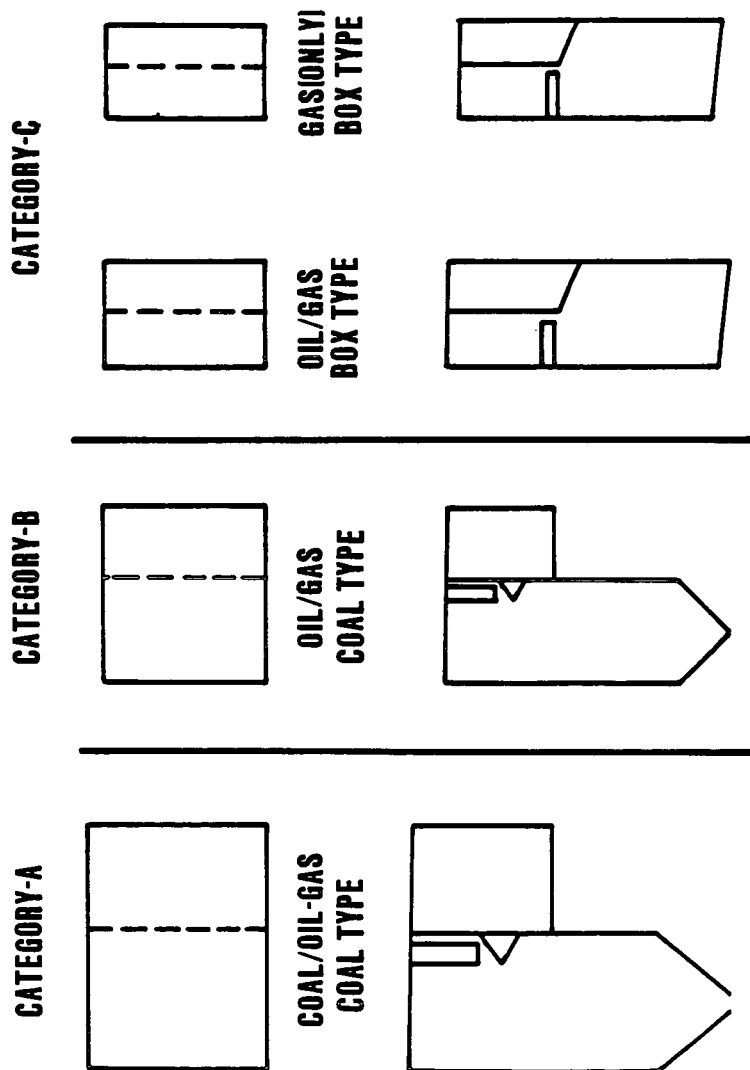


Figure 4 Comparison Boiler-Fuel Configurations

Symposium on Shape Selective Catalysis and Synthesis Gas Chemistry.

The Fuels Division of the American Chemical Society would like to acknowledge the generous financial support of the following institutions and corporations:

Air Products and Chemicals Inc.  
Amoco Oil Company  
Chevron Research Company  
E. I. duPont de Nemours and Company  
Exxon Corporation  
Mobil Oil Corporation  
Petroleum Research Fund  
Phillips Petroleum Company  
Strem Chemicals, Inc.  
Union Carbide Corporation  
W. R. Grace and Company

## SHAPE-SELECTIVE CATALYSIS IN ZEOLITES

Sigmund M. Csicsery

Chevron Research Company, Richmond, California 94802

### Introduction

Zeolites have four properties that make them especially interesting for heterogeneous catalysis: (1) they have exchangeable cations, allowing the introduction of cations with various catalytic properties; (2) if these cationic sites are exchanged to  $H^+$ , they can have a very high number of very strong acid sites; (3) their pore diameters are less than 10 Å; and (4) they have pores with one or more discreet sizes. These last two account for their molecular sieving properties. Zeolites have been applied as catalysts since 1960.

Pore diameters in molecular sieves depend on the number of tetrahedra in a ring (Figure 1). The actual pore size also depends on the type of cation present. Molecules like ammonia, hydrogen, oxygen, and argon can go through the pores of practically every type of molecular sieve. Type "A" sieves have cubic structure with pores just about big enough to allow normal paraffins through. Cations, however, occupy positions which block part of the pores. Monovalent cations (e.g., sodium, potassium) restrict the pore size to below ~4 Å. None of the organic molecules (except methane) would be able to penetrate NaA, or LiA zeolites. Divalent cations, however, occupy only every other cationic position leaving enough space for normal paraffins to diffuse through. Isobutane is slightly wider than the pores of CaA so cannot enter. However, molecules with nominal dimensions of perhaps half an angstrom too large can make their ways through narrower pores than expected because molecular vibration allows them to wiggle through. In addition, bond cleavage, followed by reconstruction of the broken bond, could facilitate the diffusion of larger molecules through narrow pores (1).

If almost all of the catalytic sites are confined within this pore structure and if the pores are small, the fate of reactant molecules and the probability of forming product molecules are determined mostly by molecular dimensions and configurations. Only molecules whose dimensions are less than a critical size can enter the pores, have access to internal catalytic sites, and react there. Furthermore, only molecules that can leave appear in the final product.

### Types of Shape Selectivities

We can distinguish various types of shape selectivities, depending on whether pore size limits the entrance of the reacting molecule, or the departure of the product molecule, or the formation of certain transition states.

Reactant selectivity occurs when only part of the reactant molecules are small enough to diffuse through the catalyst pores (Figure 2).

Product selectivity occurs when some of the product formed within the pores are too bulky to diffuse out as observed products. They are either converted to less bulky molecules (e.g., by equilibration) or eventually deactivate the catalyst by blocking the pores (Figure 2).

Restricted transition state selectivity occurs when certain reactions are prevented because the corresponding transition state would require more space than available in the cavities. Neither reactant nor potential product molecules are prevented from diffusing through the pores. Reactions requiring smaller transition states proceed unhindered.

Molecular traffic control may occur in zeolites with more than one type of pore system. Reactant molecules here may preferentially enter the catalyst through one of the pore systems while products diffuse out by the other. Counter-diffusion is, thus, minimized here.

Examples will be discussed for each type of shape selectivity.

### Diffusion

The importance of diffusion in shape-selective catalysis cannot be overemphasized. In general, one type of molecule will react preferentially and selectively in a shape-selective catalyst if its diffusivity is at least one or two orders of magnitude higher than that of competing molecular types (2-5). Too-large molecules will be absolutely unable to diffuse through the pores. Even those molecules which react preferentially have much smaller diffusivities in shape-selective catalysts than in large-pore catalysts.

### Reactant- and Product-Type Shape Selectivities

Shape selectivity was first described by Weisz and Frilette in 1960. P. B. Weisz, N. Y. Chen, V. J. Frilette, and J. N. Miale were not only the pioneers of shape-selective catalysis; but in their subsequent publications they demonstrated its many possible applications. They have described many examples of reactant- (and product-) type shape selectivity. Examples are selective hydrogenation of n-olefins over CaA-type (6-7) and Pt ZSM-5 (8) molecular sieves (Figure 4).

Most applications and manifestations of shape-selective catalysis involve acid-catalyzed reactions such as isomerization, cracking, dehydration, etc. Acid-catalyzed reactivities of primary, secondary, and tertiary carbon atoms differ. Tertiary carbon atoms react inherently much easier than secondary carbon atoms. Primary carbon atoms don't form carbonium ions under ordinary conditions and therefore do not react. Therefore, in most cases isoparaffins crack and isomerize much faster than normal paraffins. This order is reversed in most shape-selective acid catalysis; that is, normal paraffins react faster than branched ones which sometimes do not react at all.

### Restricted Transition State-Type Selectivity

In restricted transition state-type selectivity, certain reactions are prevented because the transition state is too large for the cavities of the molecular sieve. An example is acid-catalyzed transalkylation of dialkylbenzenes (9) (Figure 3). In this reaction one of the alkyl groups is transferred from one molecule to another. This is a bimolecular reaction involving a diphenylmethane transition state.

Meta-xylene in this reaction will yield 1,3,5-trialkylbenzene. Mordenite does not have enough space for the corresponding transition state. Thus, whereas the 1,2,4-isomer can form, the 1,3,5-isomer cannot (10,11). Symmetrical trialkylbenzenes are absent from the product, although they are the predominant components of the trialkylbenzene isomer mixtures at equilibrium (12-13). Figure 5 shows product distributions over Zeolon H-mordenite. Isomerization rates of the symmetrical mesitylene and the smaller hemimellitene over mordenite and HY are almost identical. This shows that symmetrical trialkylbenzenes are themselves not hindered within the pores of H-mordenite. In isomerization, the transition state involves only one molecule; so there is enough space to form the transition state in the internal cavity of the sieve.

Another example for transition state-type selectivity is isobutane isomerization over HZSM-5 (14-16).

One can distinguish experimentally between reactant and product-type selectivities and restricted transition state-type selectivities by studying particle size effects. Observed rates depend on the intrinsic, uninhibited rate constant and, if mass transfer is limiting, on the diffusivities of the reactant (or product) molecules and on the catalyst particle size. Reactant and product selectivities are mass transfer limited and, therefore, affected by crystallite size whereas restricted transition-state selectivity is not. Haag, Lago, and Weisz used this method to determine the causes of shape selectivity in the cracking of  $C_6$  and  $C_9$  paraffins and olefins over HZSM-5 (17).

The crystallite size effects observed allowed Haag, Lago, and Weisz to calculate effective diffusivities. This was the first known case for determination of molecular diffusivities in a zeolite at steady state and actual reaction conditions (Figure 6). Diffusivities decrease by four orders of magnitude from normal to gem-dimethyl paraffins. While branching has a large effect, the influence of the length of the molecule is small. Olefins have similar diffusivities to the corresponding paraffins. One surprising observation is that these diffusivities are about an order higher than the calculated Knudsen diffusivities.

An important consequence of the lack of space for the bulky transition state for transalkylation within HZSM-5 is that xylene isomerization proceeds without trimethylbenzene formation. This improves xylene yields and increases catalyst life.

The most important example of restricted transition state-type selectivity is the absence (or near absence) of coking in ZSM-5 type

molecular sieves. This has great significance because certain reactions can occur in the absence of metal hydrogenation components and high hydrogen pressure. Coking is less severe in ZSM-5 because the pores lack enough space for the polymerization of coke precursors. On ZSM-5 the coke is deposited on the outer surface of the crystallites, whereas in offretite and mordenite most of the coke forms within the pores (18) (Figure 7). Activity is barely affected in the first case, while it decreases rapidly in the second.

In large pore zeolites (e.g., HY, mordenite) the most significant step in coking is probably the alkylation of aromatics (19-22). These alkylaromatics cyclize or condense into fused-ring polycyclics, which eventually dehydrogenate to coke. Paraffins could also contribute to coking via conjunct polymerization, which leads to naphthenes.

### Molecular Traffic Control

Molecular traffic control is a special type of shape selectivity. It could occur in zeolites with more than one type of intersecting pore systems. Reactant molecules here may preferentially enter the catalyst through one of the pore systems while the products diffuse out of the other. This may minimize counterdiffusion and, thus, increase reaction rate (23-24).

ZSM-5 has two types of channels, both of which have ten-membered ring openings. One channel system is sinusoidal and has nearly circular (5.4 Å x 5.6 Å) cross-section. The other channel system has elliptical openings (5.2 Å x 5.8 Å). These are straight and perpendicular to the first system (25-26). Whereas linear molecules can occupy both channel systems, 3-methylpentane and p-xylene occupy only the linear, elliptical pores. These suggest that normal aliphatics can diffuse freely in both systems; but aromatics and isoparaffins prefer the linear, elliptical channels. Examples might be benzene alkylation with ethylene, and toluene alkylation with methanol over ZSM-5 catalysts (27).

In "reverse molecular traffic control" small product molecules diffuse out through pores too narrow for larger reactants, thus avoiding counterdiffusion (28). Examples might be catalytic dewaxing or xylene isomerization (27).

Sequential adsorption measurements did not support the concept of molecular traffic control (29). However, it is questionable whether such kinetic phenomena can be proven or disproven by adsorption measurements (30).

Product selectivity, restricted transition state-type selectivity, and molecular traffic control may all contribute to several reactions in which p-xylene is formed above its equilibrium concentrations over ZSM-5 zeolite (2,4,5,31,32,33).

### Control of Shape Selectivity

Shape selectivity can be improved by reducing the number of active sites on the external surface of zeolite crystallites. The external surface of a molecular sieve can be neutralized by poisoning with a

large molecule (34). The extent of shape selectivity can be also controlled by cations (35-38). Decreasing the aluminum content in the last stage of crystallization of ZSM-5 zeolites is another way to reduce the number of active sites on the outside surface of crystallites (39) and, thus, improve shape selectivity.

### Erionite

Erionite (41-42) can selectively distinguish between normal and isoparaffins. Over erionite the otherwise much-more-reactive 2-methylpentane reacts 50 times slower at 430°C than normal hexane at 320°C. The cavity of erionite has dimensions similar to the length of n-octane. This coincidence is responsible for the so-called "cage" or "window" effect (42-46).

### Quantitative Measure of Shape Selectivity

A quantitative measure of shape selectivity (called "constraint index") compares the cracking rates of normal-hexane and 3-methylpentane (46) (Figure 37). Silica-alumina has a constraint index of 0.6. This ratio represents the intrinsic cracking rates of normal paraffins and isoparaffins. Mordenite and rare earth Y are similarly unselective. Erionite has a very high "constraint index," and so do various ZSM catalysts.

### Applications

We could remove undesirable impurities by cracking them to easily removable molecules and distilling them away [such as in Selectoforming (47, 48) and catalytic dewaxing (49-52)]. Impurities can also be selectively burned inside molecular sieves and removed as CO<sub>2</sub> and CO. Or impurities can be converted to harmless molecules.

One important class of applications of shape selectivity is to avoid undesirable reactions. For instance, in xylene isomerization transition state-type selectivity limits transalkylation and coking over ZSM-5 sieve (53). In toluene alkylation or disproportionation reactions leading to the undesirable isomers (o- and m-xylenes) are avoided (52-53). Most of these applications will be discussed in detail by subsequent speakers of this Symposium.



## References

1. Rabo, J. A., "Salt Occlusion in Zeolite Crystals," in *Zeolite Chemistry and Catalysis*, Jule A. Rabo, ed., A.C.S. Monograph No. 171, 332 (1976).
2. Chen, N. Y., Kaeding, W. W., and Dwyer, F. G., *J. Amer. Chem. Soc.*, 101, 6783 (1979).
3. Védérine, J. C., Auroux, A., Dejaifve, P., Ducarme, V., Hoser, H., and Zhou, Sh., *J. Catal.*, 73, 147 (1982).
4. Kaeding, W. W., Chu, C., Young, L. B., Weinstein, B., and Butter, S. A., *J. Catal.*, 67, 159 (1981).
5. Kaeding, W. W., Chu, C., Young, L. B., and Butter, S. A., *J. Catal.*, 69, 392 (1981).
6. Weisz, P. B. and Frilette, V. J., *J. Phys. Chem.* 64, 382 (1960).
7. Weisz, P. B., Frilette, V. J., Maatman, R. W., and Mower, E. B., *J. Catal.* 1, 307 (1962).
8. Dessau, R. M., *J. Catal.*, 77, 304 (1982).
9. Csicsery, S. M., *J. Org. Chem.* 34, 3338 (1969).
10. Csicsery, S. M., *J. Catal.* 19, 394 (1970).
11. Csicsery, S. M., *J. Catal.* 23, 124 (1971).
12. Csicsery, S. M., *J. Chem. Eng. Data* 12, 118 (1967).
13. Venuto, P. B., private communication.
14. Hilaireau, P., Bearez, C., Chevallier, F., Perot, G., and Guisnet, M., *Zeolites*, 2, 69 (1982).
15. Valyon, J., Mihályfi, J., Beyer, H. K., and Jacobs, P. A., "Preprints of the Workshop on Adsorption of Hydrocarbons in Zeolites," Berlin (G.D.R.), 134 (1979).
16. Védérine, J. C., Auroux, A., Bolix, V., Dejaifve, P., Naccache, C., Wierzchowski, P., Derouane, E. G., Nagy, J. B., Gilson, J. P., Van Hoof, J. H. C., Van den Berg, J. P., and Wolthuizen, J., *J. Catal.*, 59, 248 (1979).
17. Haag, W. O., Lago, R. M., and Weisz, P. B., Faraday General Discussion No. 72, p. 317 (1982). "Selectivity in Heterogeneous Catalysis," September 14-16, 1981, University of Nottingham, Nottingham, England.

18. Dejaifve, P., Auroux, A., Gravelle, P. C., Védérine, J. C., Gabelica, Z., and Derouane, E. G., *J. Catal.*, 70, 123 (1981).
19. Walsh, D. E. and Rollmann, L. D., *J. Catal.*, 56, 195 (1979).
20. Rollmann, L. D., *J. Catal.*, 47, 113 (1977).
21. Walsh, D. E. and Rollmann, L. D., *J. Catal.*, 49, 369 (1977).
22. Rollmann, L. D. and Walsh, D. E., *J. Catal.*, 56, 139 (1979).
23. Derouane, E. G. and Gabelica, Z., *J. Catal.*, 65, 486 (1980).
24. Derouane, E. G., "Catalysis by Zeolites," (B. Imelik et al., Editors), p. 5, Elsevier, Amsterdam, 1980.
25. Meier, W. M. and Olson, D. H., "Atlas of Zeolite Structure Types." Structure Commission of IZA, 1978 (distributor - Polycrystal Book Service, Pittsburgh, Pennsylvania).
26. Flanigen, E. M., Bennett, J. M., Grose, R. W., Cohen, J. P., Patton, R. L., Kirchner, R. M., and Smith, J. V., *Nature* 271, 512 (1978).
27. Derouane, E. G., Gabelica, Z., and Jacobs, P. A., *J. Catal.*, 70, 238 (1981).
28. Lowe, B. M., Whan, D. A., and Spencer, M. S., *J. Catal.*, 70, 237 (1981).
29. Pope, C. G., *J. Catal.*, 72, 174 (1981).
30. Derouane, E. G., *J. Catal.*, 72, 177 (1981).
31. Chen, N. Y. and Garwood, W. E., *J. Catal.* 52, 453 (1978).
32. Young, L. B., Butter, S. A., and Kaeding, W. W., *J. Catal.*, 76, 418 (1982).
33. Wei, J., *J. Catal.*, 76, 433 (1982).
34. Anderson, J. R., Fogar, K., Mole, T., Rajadhyaksha, R. A., and Sanders, J. V., *J. Catal.*, 58, 114 (1979).
35. Namba, S., Iwase, O., Takahashi, N., Yashima, T., and Hara, N., *J. Catal.*, 56, 445 (1979).
36. Freeman, J. J. and Unland, M. L., *J. Catal.*, 54, 183 (1978).
37. Unland, M. L., U.S. Patent No. 4,115,424 (1978).

38. Sefcik, M. D., J. AM. Chem. Soc., 101, 2164 (1969).
39. Rollmann, L. D., U.S. Patent No. 4,148,713 (April 10, 1979).
40. Fraenkel, D. and Gates, B. C., J. Amer. Chem. Soc., 102, 2478 (1980).
41. Gard, J. A. and Tait, J. M. Advan. Chem. Ser., 101, 230; (1971) Intern. Conf. Molecular Sieve Zeolites, 2nd, Worcester, Massachusetts, September 8-11, 1970.
42. Gorrington, R. L., J. Catal., 31, 13 (1973).
43. Miale, J. N., Chen, N. Y., and Weisz, P. B., J. Catal., 6, 278 (1966).
44. Chen, N. Y., Lucki, S. J., and Mower, E. B., J. Catal., 13, 329 (1969).
45. Chen, N. Y. and Garwood, W. E., Advan. Chem. Ser. 121, 575; (1973) Intern. Conf. Molecular Sieves, 3rd, Zurich, Switzerland, September 3-7 (1973).
46. Young, L. B., U.S. Patent No. 3,962,364 (1976).
47. Chen, N. Y., Maziuk, J., Schwartz, A. B., and Weisz, P. B., Oil Gas J. 66, (47), 154 (1968).
48. Hydrocarbon Processing (September 1970) 192.
49. Chen, N. Y., Gorrington, R. L., Ireland, H. R., and Stein, T. R., Oil, Gas J., 75, (23), 165 (1977).
50. Chen, N. Y., Garwood, W. E., U.S. Patent No. 3,700,585 (1972).
51. Chen, N. Y., and Garwood, W. E., Ind. Eng. Chem. Process Des. Dev., 17, 513 (1978).
52. Smith, K. W., Starr, W. C., and Chen, N. Y., Oil, Gas J. 78, (21), 75 (1980).
53. Weisz, P. B., Pure and Appl. Chem., 52, 2091 (1980).

FIGURE 1  
PORE DIAMETERS IN ZEOLITES

No. of Tetrahedra in Ring	Maximum Free Dia., Å	Example
6	2.8	
8	4.3	Erionite, A
10	6.3	ZSM-5, Ferrierite
12	8.0	L, Y, Mordenite
18	15	Not Yet Observed

Typical Hydrocarbon Dimensions:

Benzene =  $5.7 \text{ Å} \times 2.2 \text{ Å}$

n-Hexane =  $3.5 \times 4.2 \text{ Å}$

FIGURE 2

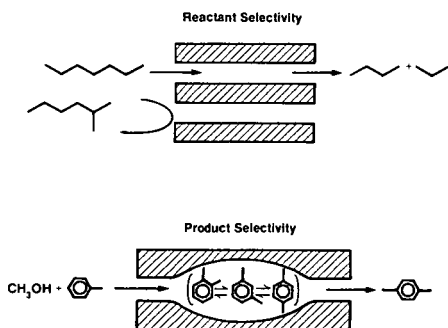
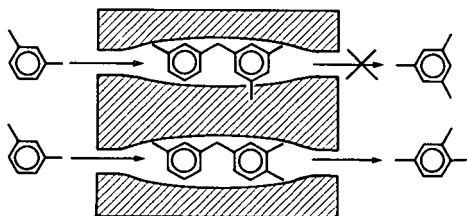


FIGURE 3

RESTRICTED TRANSITION STATE SELECTIVITY

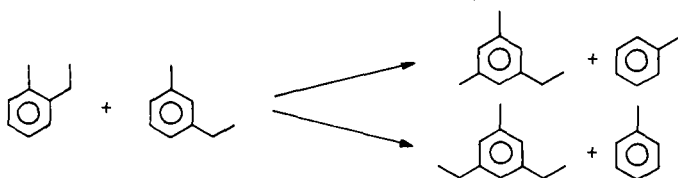


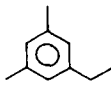
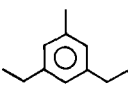
# **FIGURE 4** **SHAPE SELECTIVE HYDROGENATION** **OVER Pt - ZSM-5**

<u>Catalyst</u>	<u>Temp., °C</u>	<u>Pt - Al<sub>2</sub>O<sub>3</sub></u>	<u>Pt - ZSM-5</u>
<b>Hydrogenated, %</b>			
<b>Hexene</b>	<b>275</b>	<b>27</b>	<b>90</b>
<b>4,4-Dimethylhexene-1</b>	<b>275</b>	<b>35</b>	<b>&lt;1</b>
<b>Styrene</b>	<b>400</b>	<b>57</b>	<b>50</b>
<b>2-Methylstyrene</b>	<b>400</b>	<b>58</b>	<b>&lt;2</b>

Dessau, J. Catal., 77, 304 (1982).

FIGURE 5  
RESTRICTED TRANSITION STATE-TYPE SELECTIVITY IN THE  
TRANSALKYLATED PRODUCT DISTRIBUTION OF  
METHYLETHYLBENZENE



<u>Catalyst</u>	<u>Reaction Temperature, °C</u>	 <u>% of Total C<sub>10</sub></u>	 <u>% of Total C<sub>11</sub></u>
H-Mordenite	204	0.4	0.2
HY	204	31.3	16.1
Silica-Alumina	315	30.6	19.6
Thermodynamic Equilibrium	315	46.8	33.7

Csicsery, J. Catal. 19, 394 (1970).

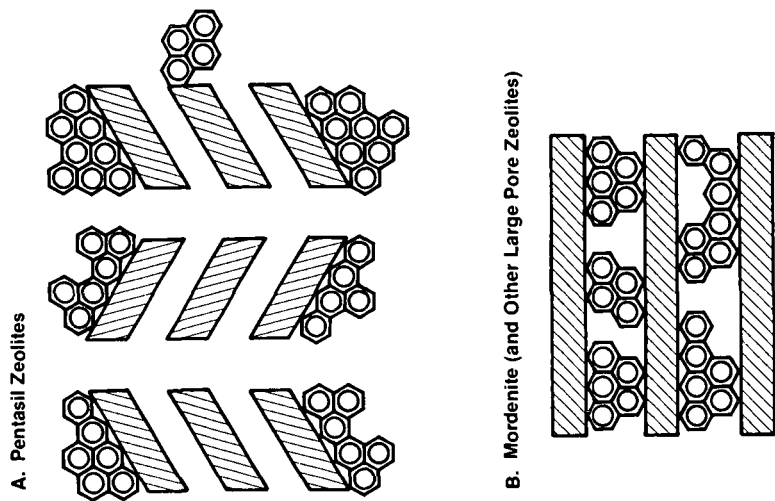
**FIGURE 6**  
**DIFFUSIVITIES IN ZSM-5**  
**538°C**

Structure	D at 538°C, cm <sup>2</sup> /S
<chem>C-C-C-C-C=C</chem>	$3 \times 10^{-4}$
<chem>C-C-C-C=C-C</chem>	$4 \times 10^{-5}$
<chem>C-C-C-C-C</chem>	$2 \times 10^{-8}$
<chem>C-C-C-C=C</chem>	$7 \times 10^{-8}$
<chem>C-C-C-C-C-C</chem>	$3 \times 10^{-8}$

Haag, Lago, and Weisz, Faraday General Discussions, 72, 317 (1982).

**FIGURE 7**

**COKE FORMATION IN ZEOLITES**



Dejaifve, et al., J. Catal., 70, 123 (1981).

## EXTENDED ABSTRACT

Symposium on "Shape Selective Catalysis, Route to Chemicals Fuels" ACS meeting 20-25 march 1983, Seattle.

## CATALYTIC, PHYSICAL AND ACIDIC PROPERTIES OF PENTASIL ZEOLITES

Jacques C. Védrine

Institut de Recherches sur la Catalyse, C.N.R.S.,  
2, av. Albert Einstein F 69626 Villeurbanne FRANCE

A large amount of efforts has been done in the recent years to understand the fascinating shape selective properties of ZSM-5 or ZSM-11 zeolites<sup>(1-4)</sup>. It has appeared that the acid strength of the Brönsted sites varies in a wide range for a same sample<sup>(5)</sup>. Moreover, depending on preparation conditions, the morphology and size of the zeolitic crystallites and the Al concentration within a crystallite and between crystallites may vary drastically<sup>(6-7)</sup>. It follows that it is somewhat difficult to rationalize the effects of particle size, of acid strength and of the nature of the zeolite (-5 or -11) on the catalytic properties of the catalyst for acid-type reactions like methanol conversion or alkylation of aromatics. The purpose of this presentation is to sum up some of our recent works in that field.

Experimental part : ZSM-5 and ZSM-11 samples have been prepared in the laboratory following the procedures described in ref. 8 and 9 respectively. For ZSM-5 samples the Al content of the samples was varied by using different Al concentration in the preparation mixture. For ZSM-11 samples the temperature and duration of the preparation were chosen to be 100°C, one month (sample 1) and 170°C, one week (samples 2 and 3). Chemical compositions were determined from atomic absorption measurements and are given in table 1. The samples were calcined under N<sub>2</sub> flow at 500°C and then at 540°C under air flow. Acidification was performed by exchanging Na cations by NH<sub>4</sub><sup>+</sup> in aqueous solution M/2 at 80°C, and by deammoniation at 540°C under air flow. One ZSM-5 sample was treated by a trimethylphosphite solution in n-octane at 120°C as described in ref. 10 resulting in a so called P-ZSM-5.

Table 1 : Physical characteristics of the different samples

Samples zeolite type modification	1 ZSM-11 no	2 ZSM-11 no	3 ZSM-11 no	4 ZSM-5 no	5 ZSM-5 no	6 P-ZSM-5 Phosphorus (1.1 wt%)
<u>Chemical analysis</u> atoms : Si : Al Na : (Si+Al)×10 <sup>2</sup>	37 0.3	31 0.5	43 0.1	23 0.2	9 0.7	10 0.7
<u>XPS data</u> atoms : Si : Al	24	30	70	26	10	9
<u>TEM analysis</u> Size of grains(μm) shape	0.6 <sup>+</sup> 0.2 aggre- gate  spheroi- dal	1-2 core + needles  spheru- litic	6 <sup>+</sup> 2 core + need- les spheru- litic	0.5-2 paralle- pipeds	0.5-2 paralle- pipeds	0.5-2 paralle- pipeds

Catalytic experiments were carried out in a flow microreactor (100 mg of catalyst) and analyses were performed on stream by gas chromatography.

Acidity characterization was performed using infra-red spectroscopy and micro-calorimetry of  $\text{NH}_3$  adsorption at  $150^\circ\text{C}$ . The morphology of the zeolite grains was determined using a high resolution transmission electron microscope JEOL 100 CX and Al distribution within the grain was determined with a high resolution EDX-STEM from Vacuum Generators (HB 5). Surface composition of the grains was measured by XPS using a monochromatized HP 5950 A spectrometer. X ray diffraction patterns were obtained using a conventional  $\text{CuK}\alpha$  X ray source. At last the capacity of n-hexane absorption at room temperature was measured by volumetry.

### Experimental results

The crystallinity of the samples prepared in the laboratory was determined by X ray diffraction, infra-red spectroscopy of the vibrational modes ( $550 : 450 \text{ cm}^{-1}$  ratios)<sup>(11)</sup>, high resolution electron microdiffraction and absorption capacity for n-hexane (11-12 wt %). All samples were found to be well crystallized materials except sample 1 which probably contained approximately 30 % of amorphous silica<sup>(10)</sup> and 70 % of aggregates of tiny crystallites (5-10 nm in size) as evidenced from i.r. and n-hexane absorption data. The other two ZSM-11 samples (samples 2 and 3) were formed of a core constituted by an aggregate of small 5-10 nm crystallites and of needles (500-1000 nm in size) emerging from the core with a spherulitic shape<sup>(7)</sup>. High resolution microdiffraction unambiguously showed that the tiny crystallites were well crystallized ZSM zeolite. ZSM-5 samples were formed of well crystallized parallel-pipes of 0.5 to 2  $\mu\text{m}$  in size. Physical and chemical characteristics of the samples are given in table 1. Their catalytic properties for methanol conversion and alkylation of toluene by methanol are summarized in tables 2 and 3.

Table 2 : Catalytic properties of ZSM-5 and ZSM-11 samples in the reaction of methanol conversion at  $370^\circ\text{C}$  with  $\text{N}_2$  as a carrier gas, flow rate =  $5 \text{ l h}^{-1}$ , WHSV =  $11 \text{ h}^{-1}$

Samples	1	2	3	4	5	6
Conversion (%)	90	84	70	89	89	89
<hr/>						
<u>Hydrocarbons %</u>						
aliphatics	80	84	75	78	70	84
aromatics	20	16	25	22	30	16
<hr/>						
<u>Aromatics (%)</u>						
xylenes	26	27	29	46	50	64
$\text{A}_6 + \text{A}_7$	6	7	5	9	6	8
Others	68	66	66	45	44	28
(m + p) : O xylenes	3	3	5	13	11	35



**Table 3** : Catalytic properties of ZSM-5 and ZSM-11 samples in the reaction of alkylation of toluene by methanol at 400°C, with N<sub>2</sub> as a gas carrier and a total flow rate equal to 1.85 l h<sup>-1</sup>, WHSV = 4.5/5 h<sup>-1</sup>

Samples Zeolite	2 ZSM-11	4 ZSM-5	5 P-ZSM-5
Conversion (%)			
methanol	100	98	100
toluene	18	16	10
Hydrocarbons (%)			
aliphatics	1.3	4.1	11.6
xylene	81.0	88.0	84.5
trimethylbenzenes	12.9	4.1	1.0
others	4.8	3.8	4.9
Selectivities (%)			
p-xylene	29.1	52.1	94.6
m-xylene	49.8	36.5	3.8
o-xylene	21.1	11.4	1.4
TMB 135	2.3	-	-
TMB 124	94.6	100	100
TMB 123	2.3	-	-

The main features of catalytic properties are that ZSM-5 samples present more shape selective properties than ZSM-11 whatever the particle size, presumably because ZSM-11 has more free space (+ 30 %) at the channel intersections. Detailed analysis of the methanol conversion reaction<sup>(7)</sup> shows that when the grain size of ZSM-11 samples increases more light hydrocarbons (C<sub>1</sub> + C<sub>2</sub>) and less heavier hydrocarbons (C<sub>6</sub><sup>+</sup> and A<sub>9</sub>) are formed. This very probably arises from the longer length path for the reactants when the particle size increases.

The i.r. OH bands at 3720-3740 and 3600-3605 cm<sup>-1</sup> were observed for all samples. The 3600 cm<sup>-1</sup> band was shown by NH<sub>3</sub> adsorption to be acidic while the 3720-3740 cm<sup>-1</sup> band was shown to have its relative intensity decreasing when the particle size increased due to a decrease in the number of terminal silanols. Modification by phosphorus was shown to decrease the number of OH groups by about one half but their strength remained comparable<sup>(10)</sup>. The EDX-STEM characterization showed that Al was not homogeneously localized in the zeolite framework. For spherulitic ZSM-11 grains the needles were shown to present in average about twice less Al than the core and even more an heterogeneous distribution of Al from the inner to the outer layers. For ZSM-5 samples heterogeneity in Al concentration within a same zeolitic grain or between grains was observed which precluded any rationalized law<sup>(7)</sup>.

Acidity strength and acid site concentration were determined by measuring microcalorimetrically the differential heat of ammonia adsorption at 150°C. It was observed that the strongest acid sites were obtained for relatively low Al content but obviously the number of strong acid sites decreased with the Al content decreasing. Acidity strength was observed to be heterogeneous which is in agreement with the heterogeneity in Al distribution. The number of strong acid sites was found to equal 1.6, 1.8, 1.8, 2.4, 2.3, 1.3 per u.c respectively for samples 1 to 6, after outgassing at 400°C.

Conclusions : These characterizations lead to the following conclusions :

- . Crystal growth of ZSM-11 particles seems to be particularly difficult leading to aggregates or core of tiny crystallites, 5-10 nm in size with a relatively high Al content (Si : Al  $\approx$  30 against 50 in the preparation mixture). When Al content is low the crystal growth is then sharply enhanced
- . ZSM-5 presents much more shape selectivity for less bulky aromatics than ZSM-11 in methanol conversion and toluene alkylation reactions. This is presumably due to larger free space at the channel intersections of ZSM-11 sample.
- . Acid strength and site distributions do not seem to play an important role in selectivity for the previous reactions as far as acid sites of sufficient strength are present.
- . The particle size which modifies the channel length plays only a secondary role in the selectivity for aliphatics and aromatics.
- . The preparation conditions particularly Al concentration and stirring during synthesis seem to play a great role in the crystal growth and in the morphology of the zeolitic grains.

References :

1. C.C. CHANG and A.J. SILVESTRI, *J. Catal.* 47, 249 (1977).
2. P.B. WEISZ in *Proceed, 7th Intern. Cong. on Catalysis*, Tokyo, Edit. by T. SEIYAMA and K. TANABE, Elsevier, Amsterdam 1981, p. 3.
3. E.G. DEROUANE, J.B. NAGY, P. DEJAIFVE, J.H.C. Van HOOFF, B.P. SPEKMAN, C. NACCACHE and J.C. VEDRINE, *C.R. Acad. Sci., Paris, Ser C* 284, 945, (1977) and *J. Catal* 53, 40 (1978).
4. E.G. DEROUANE and J.C. VEDRINE, *J. Molec. Catalysis* 8, 479 (1980).
5. A. AUROUX, V. BOLIS, P. WIERZCHOWSKI, P.C. GRAVELLE and J.C. VEDRINE, *JCS Faraday Trans II*, 75, 2544 (1979).
6. E.G. DEROUANE, S. DETREMMERIE, Z. GABELICA and N. BLOM, *Appl. Catal.* 1, 201 (1981), R. von BALLMOOS AND W.N. MEIER, *Nature* 289, 782 (1981).
7. A. AUROUX, H. DEXPERT, C. LECLERCQ and J.C. VEDRINE, Submitted to *Appl. Catal.* october 1982.
8. R.J. ARGAUER and G.R. LANDOLT, *US Patent*, 3702 886 (1972).
9. P. CHU, *US Patent* 3709 979 (1972).
10. J.C. VEDRINE, A. AUROUX, P. DEJAIFVE, V. DUCARME, H. HOSER and S. ZHOU, *J. Catal.* 73, 147 (1982).
11. G. COUDURIER, C. NACCACHE and J.C. VEDRINE, *JCS Chem. Commun.* 1982 in press.  
P.A. JACOBS, E.G. DEROUANE and J. WEITKAMP, *JCS Chem. Commun.* 1981, 591

A.C.S. Meeting, Seattle, March 1983  
Div. Fuel Chemistry

The bifunctional conversion of cyclooctane. A suitable reaction to test shape-selective effects in high-silica zeolites.

by : P.A. Jacobs, M. Tielen and R. Sosa Hernandez

## INTRODUCTION

It was reported earlier <sup>1</sup> that the bifunctional conversion of n-paraffines into feed isomers or hydro-cracked products was distinctly different over wide pore zeolites of the faujasite-type compared to those of the Pentasil-type. It was also established <sup>1</sup> that the rate of conversion of n-decane into its monomethyl branched feed isomers was determined by the pore structure in case of the Pentasil-zeolites. Branching at the paraffin-end was found to be favored in MFI-zeolites (ZSM-5) while in MEL-structures (ZSM-11) the pore intersections allowed also methyl-branching in the 3-position. This clearly indicates that the structure of the pores in medium or small pore zeolites can determine the product selectivity. Vice versa a well-choosen catalytic test reaction may give useful information on the dimensions and geometry of the zeolite pores.

It was therefore the aim of the present work to select a suitable probe molecule, the catalytic conversion of which will give useful information on the dimensions and geometry of zeolite pores in general and on the occurrence of transition state shape selectivity. More particularly, in the present work it is reported how cyclooctane is converted on Pt-loaded acid zeolites. Small amounts of

Pt are added in order to ensure constant activity in time and to avoid perturbation of the measurements by differences in rate of deactivation. Three zeolite structures (FAU, MFI and MEL) with identical chemical composition are compared.

## EXPERIMENTAL

The acid forms of HZSM-5 and HZSM-11 had a Si/Al ratio of 60. Ultrastable Y-zeolite was treated with  $\text{SiCl}_4$  and had the same chemical composition (FAU\*). These samples were impregnated with  $\text{Pt}(\text{NH}_3)_4\text{Cl}_2$  so as to obtain 1 % by weight loading with the metal.

The reaction with cyclooctane was carried out at atmospheric pressure in a continuous flow-reactor at a WHSV of  $0.5 \text{ h}^{-1}$ . Analysis of the reaction products was done on-line with high-resolution capillary gas-chromatography.

## RESULTS AND DISCUSSION

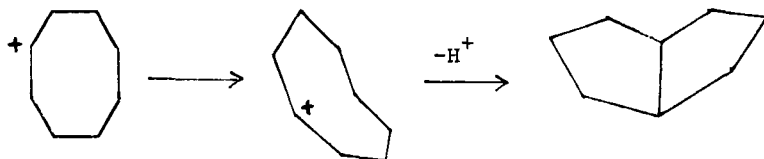
The activity sequence  $\text{MEL} > \text{MFI} > \text{FAU}^*$  for cyclooctane conversion (Fig. 1) is different from the one obtained for n-decane on the same samples :  $\text{MFI} > \text{MEL} > \text{FAU}^*$ . Comparison with the acid strength distribution measurements<sup>1</sup> shows that for the present reaction only acid sites of intermediate strength are needed. The same figure indicates that the catalysts show stable behavior in the temperature range investigated. Just as for the case of n-paraffin conversion, feed isomerization and cracking (Fig. 2) are consecutive phenomena.

When the individual product yield is plotted against cyclooctane conversion (Figs. 3 - 5), it was found that ethylcyclohexane, methylcycloheptane and bis[330]cyclo-octane are primary products. Methylcycloheptane may be formed via protonated cyclopropane intermediates, just as in the case of the ethylcyclohexane conversion <sup>2</sup>:

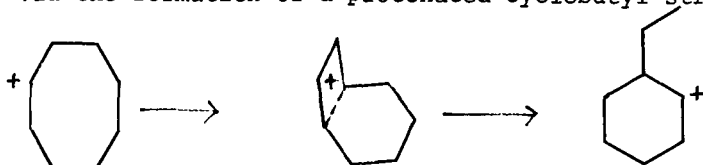


It is stabilized in the pentasil-type structures, more particularly in MEL.

The rate formation of bis[330]cyclooctanes (c + t) parallels the rate of isomerization to methylcycloheptane. The formation of a bicyclic molecule out of the cyclooctyl carbenium ion, requires that the ring is deformed to a chair-type form :



The direct formation of ethylcyclohexane without the formation of a primary carbenium ion, can only occur via the formation of a protonated cyclobutyl-structure :



The precursors of ethylcyclohexane and bis[330]cyclooctane from cyclooctane are therefore cyclooctyl cations deformed in a totally different manner, most probably under influence of the geometry of the zeolite pores. It is therefore straightforward that the transformation of cyclooctane will depend mainly upon the dimensions and structure of the zeolite pores.

#### REFERENCES

1. P.A. Jacobs, J. Martens, J. Weitkamp and H.K. Beyer, Disc. Faraday Soc., 1982, 353.
2. M. Nitta and P.A. Jacobs, Studies on Surface Science and Catalysis, 5, 1980, 251.

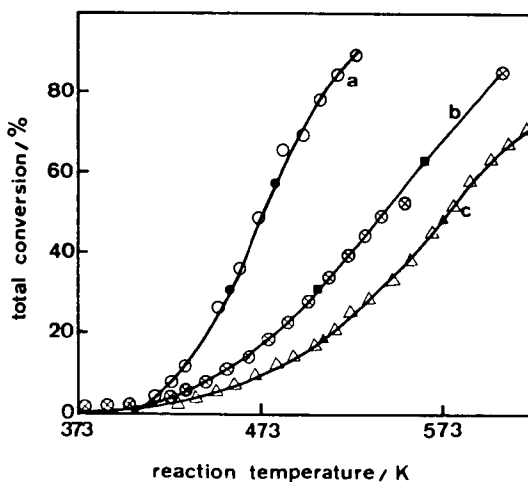


Figure 1

Total cyclooctane conversion in hydrogen over Pt-loaded acid a) MEL, b) MFI and c) FAU. Full points were obtained during a second cycle of temperature rise.

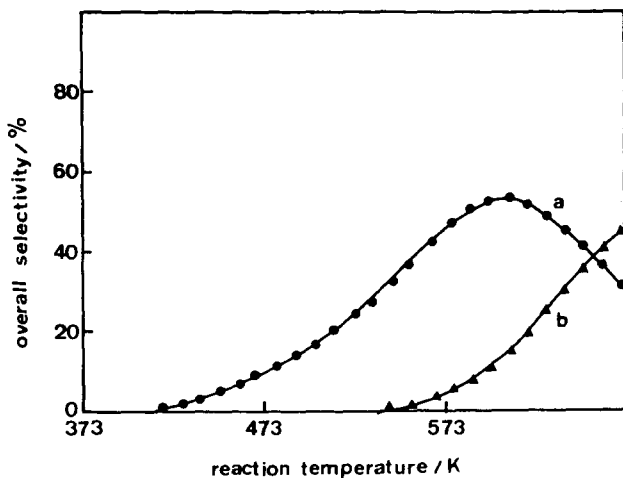


Figure 2

Overall selectivity of cyclooctane conversion over 1 Pt/H/MEL : a) feed isomers, and b) cracked products.

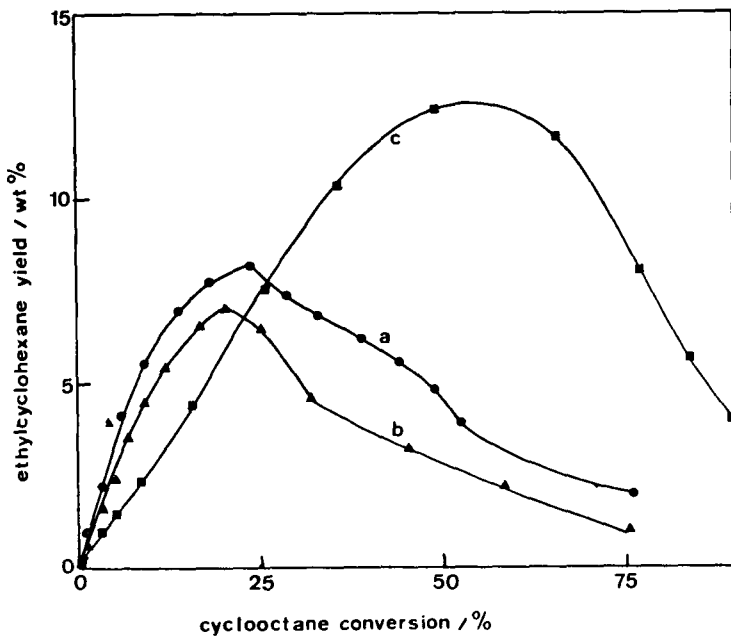


Figure 3

Yield of ethylcyclohexane from cyclooctane over FAU<sup>22</sup> (a), MFI (b), and MEL(c).

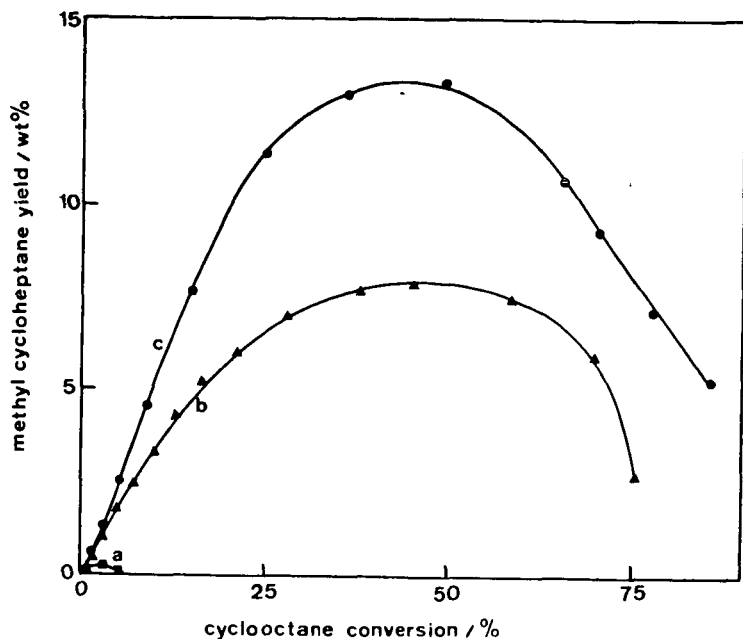


Figure 4

Yield of methylcycloheptane from cyclooctane on a) FAU<sup>2</sup>,  
b) MFI, and c) MEL - zeolites.

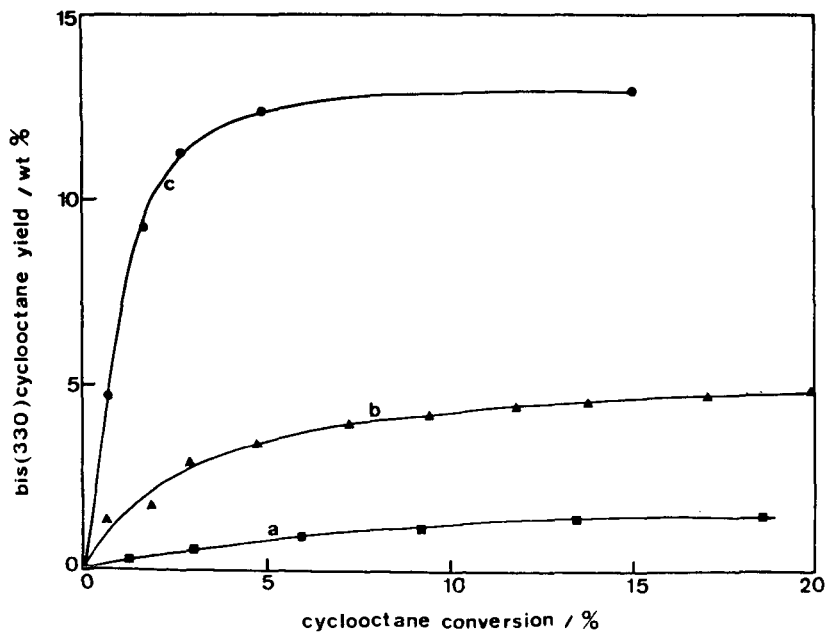


Figure 5

Yield of bis[330]cyclooctane from cyclooctane over a)  
FAU<sup>2</sup>, b) MFI, and c) MEL - zeolites.



# Shape Selective Catalysis and Reaction Mechanisms

M. GUISNET and G. PEROT

ERA CNRS Catalyse Organique, Université de Poitiers  
40, Avenue du Recteur Pineau, 86022 Poitiers Cedex, France

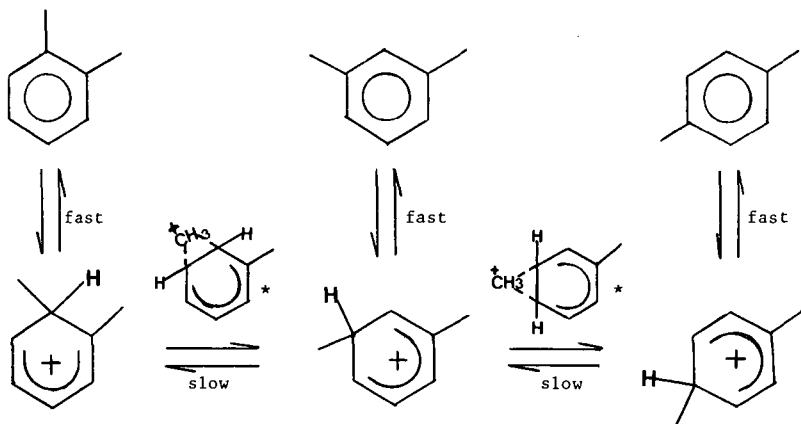
Thanks to the progress recently accomplished in the field of the synthesis and the modifications of zeolitic materials, the chemist now disposes of a large choice of acid catalysts. The problem lies in the selection, through a reliable method, of the one best suited for obtaining selectively a given reaction. The aim of this paper is to show that, by using model reactions, catalysts can be chosen on the basis of their shape selective properties. For this however the reaction mechanisms as well as the reasons for possible modifications in rate and orientation must be perfectly known.

## 1. Main factors governing reaction selectivity over acid zeolites

### 1.1. Isomerization and disproportionation of aromatic hydrocarbons over zeolites.

#### 1.1.1. Xylene isomerization

Over amorphous catalysts (1-3) xylene isomerization involves methyl shift in benzenium ion intermediates as the rate limiting step (scheme 1).



Scheme 1 : Isomerization of xylenes on acid catalysts \* Transition state according to (4).

With *m*-xylene as the reactant and over amorphous catalysts and Y zeolite, two parallel reactions leading to *o*-xylene and *p*-xylene can take place at similar rates. However over mordenite, offretite and ZSM5, the *p*-xylene formation is faster (5). This is mainly a matter of diffusion rate (6). The *p*-xylene molecule being smaller in size diffuses out of the porous structure more readily than *o*-xylene. It must be noticed that the intermediates and the transition states involved in the two reactions differ slightly in size and structure. Thus the possibility of steric effects cannot be excluded.

The isomerization of o-xylene into p-xylene involves two consecutive steps. At 350°C, the reaction is negligible over amorphous catalysts and Y zeolite but quite important over mordenite and very important over ZSM5 (5). Three factors converge to increase p-xylene selectivity from Y zeolite to mordenite and ZSM5 : i) the decrease in average pore dimension which increases residence time in the structure ; ii) the increase in acid strength which increases the rates of the two consecutive steps leading from o-xylene to p-xylene ; iii) the smaller size of p-xylene, favoring its desorption.

### 1.1.2. Xylene disproportionation

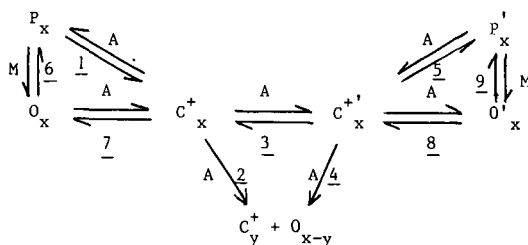
Xylenes can undergo simultaneously isomerization as well as disproportionation into toluene and trimethylbenzenes. The disproportionation mechanism involves bimolecular intermediates (1,7) much more bulky than the benzenium intermediates involved in isomerization. This is probably why the disproportionation/isomerization rate ratio ( $r_D/r_I$ ) increases as more space becomes available in the porous structure of the zeolite.

However  $r_D/r_I$  also seems to depend on the acidity of the zeolite. It decreases as the degree of exchange of protons for sodium cations in H-mordenite increases (8,9). This is more a matter of site density than acid strength. Indeed poisoning experiments with pyridine show that the acid strength required for both reactions is practically the same. But disproportionation requires probably two adjacent acid sites (1,7,10) while isomerization requires only one acid site. Hence the decrease in  $r_D/r_I$  from Y zeolite to ZSM5 may partly be explained by the site density decrease.

### 1.2. Alkane transformation

Over acid and bifunctional catalysts, alkanes undergo three main reactions : isomerization, cracking and disproportionation. All three of them involve carbocations as intermediates and their relative importance depends both on the characteristics of the alkane (size, degree of branching) and of the catalyst (acidity, porous structure, hydrogenation activity).

Scheme 2 shows the different chemical steps involved in the isomerization and the cracking of alkanes.



Scheme 2 : Isomerization and cracking of alkanes on acid and on bifunctional catalysts. P:paraffin , O:olefin , C<sup>+</sup>:carbocation , x,y:number of carbon atoms, A:acid step , M:metallic step.

#### 1.2.1. Alkane transformation on pure zeolite catalysts

Alkane cracking on pure acid catalysts occurs through steps 1, 2, 3 and 4 of scheme 2. The carbenium ion formation certainly results from intermolecular hydride transfer between a reactant molecule and a preadsorbed cation while steps 2, 3 and 4 are considered as monomolecular reactions.

In the absence of steric constraints or of diffusional limitations, the cracking rate is related to the stability of the intermediate carbenium ions ( $C_X^+$  and  $C_X^{*+}$ ). Thus over Y zeolite at 400°C isooctane cracking is 25 to 40 times faster than n-hexane cracking and 150 to 300 times faster than n-pentane cracking. The difference in reactivity of alkanes depends on the active sites: the greater their acid strength, the smaller the difference (12).

The intracrystalline structure has also a considerable influence on the relative reactivities of alkanes. Frilette et al (11) consider as shape selective the zeolites for which the "constraint index" CI (ratio of the apparent cracking rate constants of n-hexane and 3-methylpentane) is greater than 1. Due to the higher reactivity of 3-methylpentane towards carbenium ion formation, the CI of non-shape selective materials is smaller than 1. In the case of intermediate pore size zeolites the CI value ( $1 < CI < 12$ ) is determined by steric constraints in the bimolecular formation of the carbenium ion (step 1, scheme 2) (13,14). On the contrary for erionite which has small pore openings and large cavities the high value of CI is due only to differences in diffusional limitations for n-hexane on the one hand and 3-methylpentane on the other.

The acidity and the structure of zeolites also influence considerably the product distribution of alkane cracking (12). In the case of isooctane about 75 % of the cracking products can be considered as resulting from the successive steps 1 and 2 of scheme 2, the remaining 25 % result from one isomerization step followed by cracking of the rearranged carbocation (sequence 1,3,4). Over mordenite and ZSM5, direct cracking (sequence 1,2) is responsible respectively for 50 and 10 % of the products only, the remainder results from multiple transformations of isooctane. The differences between the three zeolites can be attributed to diffusional limitations.

In the case of pentanes and hexanes, the cracking steps (2,4) become so slow that the formation of isomers (step 5) is observed. The isomerization/cracking rate ratio depends on the zeolite. For n-pentane transformation at 400°C, it increases from almost zero over ZSM5 to about 0.7 over mordenite and 3.5 over Y zeolite (12). This may be due to the intrinsic selectivity of the catalytic sites but steric constraints to the bimolecular transition state of step 5 may also play an important role on ZSM5.

Over mordenite pentane cracking and isomerization are accompanied by some disproportionation into  $C_4$  and  $C_6$  products. With butanes this reaction is the only one that can be observed at low conversion (15). This is easily understandable since butane disproportionation involves secondary carbenium ions while its cracking or intramolecular isomerization necessarily involves primary cation (16). Disproportionation needing very strong acid sites (17), Y zeolite is less active than mordenite. Another explanation must be found for the inactivity of ZSM5. Probably the bimolecular  $C_8$  intermediate cannot be formed inside the porous structure of ZSM5. On the other hand, disproportionation is certainly a "demanding reaction" (requiring several sites) so that the low density of acid sites in ZSM5 could explain its inactivity.

#### 1.2.2. Isomerization and cracking of n-heptane over mechanical mixtures of platinum-alumina and zeolites (Y, mordenite, ZSM5).

The presence of the metallic component increases the carbocation formation ( $P_X + C_X^+$ ) and isomer desorption ( $C_X^{*+} + P_X'$ ) rates. On bifunctional catalysts,  $C_X^+$  formation involves successively i) the alkane dehydrogenation on the metallic sites (reaction 6) ii) the migration of the intermediate olefins from the metallic to the acid sites and iii) the adsorption of olefins on Brönsted acid sites (step 7). The isomer desorption involves the reverse sequence.

As has been mentioned by other authors (18-20) in the case of heavier n-alkanes, cracking always follows isomerization: the cracking of linear carbocations (step 2) compared to their isomerization (step 3) and to the cracking of branched cations (step 4) is very slow. In accordance with this step-by-step pathway, it can be observed that the isomerization/cracking rate ratio ( $r_i/r_c$ ) depends on the amount of platinum-alumina in the catalyst (i.e. on the residence time of the intermediate olefins on the zeolite). At low platinum-alumina contents the products result from a multistep

acid catalyzed reaction. This reaction leads to a total cracking of each individual molecule of dehydrogenated n-heptane : therefore, light products are largely predominant,  $r_c$  increases faster than  $r_i$ . At high platinum-alumina contents, the isocation cracking (step 4) now competes with its desorption to isoheptanes ( $C_7^{X+} \rightarrow P_7^X$ ) and  $r_i$  increases at the expense of  $r_c$ .  $r_i/r_c$  should in fact increase to a limit which would depend on the characteristics of the zeolite particles (size ; pore dimensions ; nature, strength and density of the acid sites).

Taking into consideration the above examples it can be concluded that the selectivity of the reactions on shape-selective materials depends on the frequently simultaneous influence of three well-known factors :

- a) own characteristics of the catalytic centers ;
- b) limitations to the diffusion of reactants and products ;
- c) steric constraints to the formation of transition states.

However, no evidence is found that diffusional limitations or steric constraints may lead to the formation of new intermediates.

## 2. Characterization of zeolites using model reactions.

The relationship between the structure of zeolites and their selectivity in a given reaction may be used to screen the best catalysts to characterize the porosity of synthetic or modified materials. The information that will be obtained will depend on the above factors. The ideal conditions for a good characterization of the porous structure are the following : i) factor a is known ; ii) the collected information concerns only one or other of factors b and c. Moreover in every case it is important that the influence of the external surface on the activity be known and if possible suppressed (21).

### 2.1. Diffusional limitations (factor b)

In order to limit the influence of steric constraints (factor c), reactions involving only monomolecular intermediates are recommended.

The relative reactivities of a series of organic compounds may be used. In this case the reactivity may vary according to the size of both the reactant and the products. Moreover as the reactants in one given series (alkanes, alcohols...) differ slightly, the reactivity can depend on the characteristics of the catalytic centers (factor a) which may change from one zeolite to the other.

One reactant undergoing competitive reactions can also be used. In this case, the selectivity depends only on the size of the products and a more precise determination of pore aperture can thus be obtained. Moreover, if the competitive reactions involved proceed through the same mechanism (as is the case for m-xylene isomerization) the influence of factor a can be considered as negligible.

Reactions involving consecutive steps (e.g. o-xylene isomerization) are not well adapted to the characterization of the porous structure of zeolites because their selectivity depends not only on pore size but also on the density and activity of acid centers.

### 2.2. Steric constraints in the neighbourhood of the active centers (factor c)

Reactions for which diffusional limitations (factor b) can be neglected must be chosen. Those involving bimolecular transition states are particularly well suited since the molecules of both the reactants and the products are generally much smaller than the transition states. However, even in this case the effect of factor b cannot always be excluded (see 1.2.1. constraint index).

In practice the inhibition to the transition state formation can be measured by comparing the rates of the bimolecular reaction and of another reaction without steric constraints.

To be free of the influence of factor a, it is convenient to choose a reactant offering the possibility of several competitive transformations through the same mechanism (e.g. formation of isomers) with one acting as the "shape sensitive" reaction and the other as reference. The disproportionation of m-xylene into 1,2,3- , 1,2,4- and 1,3,5-trimethylbenzenes offers such a possibility inasmuch as the formation of 1,3,5-trimethylbenzene suffers the intervention of a bulkier intermediate than that of 1,2,3- and 1,2,4-trimethylbenzenes (22).

However, if the mechanisms of the "shape sensitive" reaction and of the reaction taken as reference are different (e.g. disproportionation and isomerization of aromatics), factor  $\alpha$  becomes decisively important since the relative rates of transformation in the two directions may depend on the density and on the strength of the acid sites.

The differences in reactivities of reactants belonging to the same class of compounds can also be used (e.g. constraint index measurement). Again attention must be drawn to the fact that different reactants entail differences in reactivity which could be dependent on the acid strength of the zeolite.

It can be noticed finally that it is possible to characterize in one experiment factors  $b$  and  $c$  if the reactant undergoes several reactions whose selectivities depend for some only on factor  $b$ , for others only on factor  $c$ . Such is the case for *m*-xylene transformation (5) : the isomerization selectivity supplies information on pore size while the disproportionation/isomerization rate ratio as well as the distribution of the trimethylbenzenes supplies information on the space disposable in the neighbourhood of the active sites.

#### LITERATURE CITED

- (1) Poutsma, M.L., in *Zeolite Chemistry and Catalysis*, J.A. Rabo Ed., p. 437, ACS Monograph 171, American Chemical Society, Washington 1976.
- (2) Hanson, K.L. and Engel, A.J., *A.I. ChE Journal* **13**, 260 (1967).
- (3) Cortes, A. and Corma, A., *J. Catal.* **51**, 338 (1978).
- (4) Matsumoto, H., Take J.I. and YONEDA, Y., *J. Catal.* **11**, 211 (1968), *J. Catal.* **19**, 113 (1970).
- (5) Gnep, N.S., Tejada, J., Guisnet, M., *Bull. Soc. Chim.* **5** (1982).
- (6) Young, L.B., Butter, S.A. and Kaeding, W.W., *J. Catal.* **76**, 418 (1982).
- (7) Gnep, N.S. and Guisnet, M., *Appl. Catal.* **1**, 329 (1981).
- (8) Ratnasamy, P., Sivasankar, S. and Vishnoi, S., *J. Catal.* **69**, 428 (1981).
- (9) Tejada, J., Gnep, N.S., Guisnet, M., to be published.
- (10) Pukanic, G.W. and Massoth, F.E., *J. Catal.* **28**, 304 (1973).
- (11) Frilette, V.J., Haag, W.O., Lago, R.M., *J. Catal.* **67**, 218 (1981).
- (12) Hilaireau, P., Bourdillon, G., Perot, G., Guisnet, M., to be published.
- (13) Weisz, P.B., in *Proc. 7th Intern. Congr. Catalysis, Tokyo (1980)* ; Plenary Lectures, Preprint Pl.
- (14) Haag, W.O., Lago, R.M. and Weisz, P.B., *Faraday Discussions of the Chemical Society* **72**, 317 (1981).
- (15) Guisnet, M., Gnep, N.S., Bearez, C. and Chevalier, F., in *"Catalysis by Zeolites"* (B. Imelik et al Eds) Elsevier Scientific Publishing Company, Amsterdam **77** (1980).
- (16) Hilaireau, P., Bearez, C., Chevalier, F., Perot, G. and Guisnet, M., *Zeolites* **2**, 69 (1982).
- (17) Bearez, C., Chevalier, F., Guisnet, M., to be published.
- (18) Steinjs, M., Froment, G.F., Jacobs, P.A., Uytterhoeven, J.B., Weitkamp, J., Erdöl, Kohle, Erdgas, *Petrochem.* **31**, 581 (1978).
- (19) Steinjs, M. and Froment, G.F., Jacobs, P. and Uytterhoeven, J.B., Weitkamp, J., *Ind. Eng. Chem. Prod. Res. Dev.* **20**, 654 (1981).
- (20) Steinjs, M. and Froment, G.F., *Ind. Eng. Chem. Prod. Res. Dev.* **20**, 660 (1981).
- (21) Kibby, C.L., Perrotta, A.J. and Massoth, F.E., *J. Catal.* **35**, 256 (1974).
- (22) Csicsery, S.M., in *Zeolite Chemistry and Catalysis*, J.A. Rabo Ed., p. 680, ACS Monograph 171, American Chemical Society, Washington 1976.

# ON THE MECHANISM OF METHANOL CONVERSION OVER ZEOLITE

Yoshio Ono

Department of Chemical Engineering, Tokyo Institute of Technology, Meguro-ku, Tokyo, 152, Japan

## INTRODUCTION

Zeolites convert methanol into hydrocarbons. The most intriguing problem concerning the mechanism of the conversion is the way of forming carbon-carbon bonds from methanol. Chang and Silvestri(1) proposed the participation of carbenoid species, which is assumed to be produced by a concerted  $\alpha$ -elimination mechanism, involving both acidic and basic sites. Kaeding and Butter(2) proposed a mechanism involving the reaction of an incipient methyl carbenium ion from protonated dimethyl ether (or methanol) and the methyl group of dimethyl ether, at which a negative center is created by the aid of an anionic site on the catalyst. The attack of methyl carbenium ion on the C-H bond of methyl group is more stressed in the mechanism involving a pentacoordinated carbon center(3,4), as originally proposed in the polymerization or alkylation of methane in superacid chemistry(5,6). van der Berg et al.(7) suggested that the Stevens-type rearrangement of trimethyl oxonium ion could be the first step of the C-C bond formation. The intermediacy of methyl radical was proposed by Zatorski and Krzyzanowsky(8). Apart from the detailed mechanism of the C-C bond formation, the reaction is suggested to have an autocatalytic character(4,9,10). Here, the origin of the autocatalytic phenomena and its implication for the mechanism is discussed, and then the scheme of the first C-C bond formation is discussed to conclude that "methyl carbenium ion" species is the most plausible intermediate.

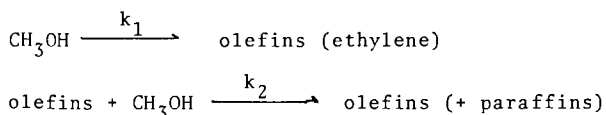
## RESULTS AND DISCUSSION

### Autocatalytic Phenomena

The autocatalytic behavior of the conversion was first pointed out by Chen and Reagan(9), who noticed that the rate of conversion of methanol was very slow at low conversion levels, but it accelerated rapidly as the concentration of hydrocarbons increased. Another feature of the autocatalysis is observed in the dependence of the hydrocarbon yield on the reaction temperature(10). Thus, the abrupt increase of the hydrocarbon yield is observed in a small temperature range, and the temperature of the jump depends on the acidity of ZSM-5 zeolite. The jump of the hydrocarbon yield with temperature is observed also for the conversion over ferrierite.

The autocatalysis was more clearly visualized in the reaction under low-pressure and low-temperature conditions(4). The reaction was carried out in a gas-recirculation system. At 492 K, only a small amount of hydrocarbons was formed for the first 8 h, though most of methanol was converted into dimethyl ether. After 12 h, the hydrocarbon yield increased abruptly, reaching 80 % at 18 h. At higher temperatures, the reaction proceeded in a similar fashion, but faster. The induction period lasted for 4-5 and 1.5-2 h at 512 and 531 K, respectively. These kinetic features indicate clearly the autocatalytic nature of the conversion.

In order to confirm that the reaction is autocatalytic, some of the reaction products were added to the starting methanol. The addition of ethylene or cis-2-butene (5 % of methanol in moles) decreased the "induction period" to 2 h at 512 K. This is about half of the period in the reaction with pure methanol. On the other hand, the addition of paraffins had no effect on the induction period. Therefore, it is concluded that the autocatalysis is caused by the reaction of methanol and olefins, which is much faster than the reaction to produce incipient olefins. Thus, as proposed by Chen and Reagen(9), the reaction can be divided into the following two steps.



The ratio of the rate constants ( $k_1/k_2$ ) for the two reactions was estimated as  $7 \times 10^{-4}$  and  $1.1 \times 10^{-3}$ , respectively(4). The abrupt change of the conversion with temperature, as observed in a flow system, may be caused at the temperature, at which the certain amount of olefins is accumulated in a reactor. As for the mechanism, one must consider the two steps separately. The second step, the propagation of the carbon-chain, plausibly involves the electrophilic methylation of olefins, for which Bronsted acid sites are responsible, as first pointed by Anderson et al.(11). The scheme of the first step will be discussed below.

#### Conversion of Methanol over Nafion-H and Heteropolyacids

To obtain information on the sites responsible for the conversion, the reaction was carried out in a gas-recirculation system over the catalyst with preadsorbed pyridine. Prior to the reaction, the catalyst was exposed to pyridine vapor for 2 h at 473 K, and then evacuated at 512 K for 1 h. The only product observed was dimethyl ether and no hydrocarbons were produced in 47 h. The reaction over Na-ZSM-5 give a similar result. These facts indicates that the acid sites plays a decisive role in the formation of hydrocarbons. This implies that the reaction should proceed also over strongly acidic solid other than zeolites.

Nafion-H, a perfluorinated resin sulfonic acid, is known to have high catalytic activities for the alkylation of benzene with alcohols and the methylation of phenol with methanol, and is reported to be a solid superacid. The conversion of methanol over Nafion-H was examined with a closed-recirculation system(4). Methanol of  $7.7 \times 10^5$  Pa was introduced over 1 g of Nafion-H at 512 K, and the gas-phase composition was analyzed at appropriate intervals. Dimethyl ether is the only product for the first 2 h, and after 2 h, the rate of hydrocarbon formation was accelerated with time, which is characteristic of an autocatalytic reaction. The fact that the features of the conversion over Nafion-H resembles those over ZSM-5 strongly indicates that Bronsted acid sites are active centers for the conversion.

It was found that dodecatungstophosphoric acid ( $\text{H}_3\text{PW}_{12}\text{O}_{40}$ ), a highly acidic solid, also had high activities for methanol conversion(12).

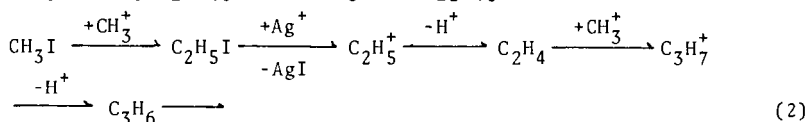
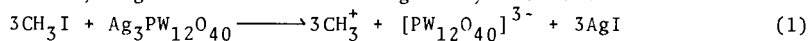
### Interaction of Methanol with ZSM-5, Infrared Study

Infrared spectroscopic study revealed that methanol ( $\text{CD}_3\text{OH}$ ) reacts with the acidic hydroxyl group of ZSM-5 to form methoxyl group ( $\text{CD}_3\text{O}-$ ) at 423 K. When the zeolite which beared  $\text{CD}_3\text{O}-$  groups was heated at 512 K, the  $\text{CD}_3$  bands completely disappeared and bands due to O-D stretching appeared, indicating that the desorption of methoxyl groups is accompanied with the cleavage of C-D bonds. The analysis of molecules desorbed from the surface revealed that the decomposition of the methoxyl groups leads to the formation of hydrocarbons.

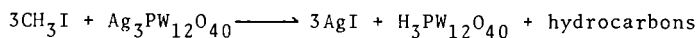
The reaction of the methoxyl group with benzene gave toluene, indicating that the surface methoxyl groups can be a source of "methyl carbenium ions". In other words, the "methoxyl groups" in ZSM-5 could be more properly comprehended as part of a methyl ester of the zeolitic acid than as part of a metal alkoxide, just as a methyl group in dimethyl sulfate, a good methylating agent.

### Selfcondensation of Methyl Iodide over $\text{Ag}_3\text{PW}_{12}\text{O}_{40}$

In order to ascertain the role of methyl carbenium ions in the formation of carbon-carbon bonds, the attempt to generate them was made; methyl iodide was reacted with  $\text{Ag}_3\text{PW}_{12}\text{O}_{40}$ . Methyl carbenium ions were supposed to be generated according to Eq.(1) because of the high tendency of forming silver iodide, and then to attack the carbon-hydrogen bonds of remaining methyl iodide.



The expected overall reaction is summarized as



Experiments were carried out as follows. The powder of  $\text{Ag}_3\text{PW}_{12}\text{O}_{40}$  (0.28 mmol) was reacted with methyl iodide vapor (1.80 mmol) at 423 or 573 K in a closed-recirculation system. The results are given in Table 1. The reaction was almost finished by the time when the first analyses were made, 15 and 5 min for the reaction at 423 and 573 K, respectively, the only minor change in the gas-phase composition being observed thereafter. About 3 moles of methyl iodide disappeared from the gas phase, and, at the same time, most of carbon atoms from consumed methyl iodide appeared as hydrocarbons, as was expected from Eq.(2). It should be noted that methyl iodide does not convert into hydrocarbons over  $\text{H}_3\text{PW}_{12}\text{O}_{40}$  or ZSM-5 even at 573 K. At 573 K, the distribution of the hydrocarbon products of the stoichiometric reaction of  $\text{CH}_3\text{I}$  and  $\text{Ag}_3\text{PW}_{12}\text{O}_{40}$  are very similar to that of the products in the catalytic conversion of methanol over  $\text{Ag}_3\text{PW}_{12}\text{O}_{40}$  supported on active carbon, indicating that the mechanism of the propagation of the carbon-carbon chain is the same in the two systems.

The results clearly shows that methyl carbenium ions play an essential role in the formation of carbon-carbon bonds. It is worthy of note that hydrocarbon formation is fast in the  $\text{CH}_3\text{I}-\text{Ag}_3\text{PW}_{12}\text{O}_{40}$  system even at 423 K. At the same temperature, methanol gives methoxyl group over ZSM-5 and yields dimethyl ether, but not



Table 1 Reaction Products of Reaction of  $\text{CH}_3\text{I}$  and  $\text{Ag}_3\text{PW}_{12}\text{O}_{40}$ 

Temperature/K	423		573		573 **
Reaction time/min	15	30	5	40	
$\text{Ag}_3\text{PW}_{12}\text{O}_{40}$ used/mmol(A)		0.28		0.28	
$\text{CH}_3\text{I}$ consumed/mmol(B)	0.95	1.04	0.80	1.22	
B/A	3.4	3.7	2.9	4.4	
Carbon atoms in hydrocarbons/mmol(C)	0.83	0.75	0.82	0.81	
C/A	3.0	2.7	2.9	2.9	
Distribution of Hydrocarbons *					
$\text{CH}_4$	0	0.2	6.3	5.9	6.8
$\text{C}_2\text{H}_4$	0.1	0	10.5	7.9	16.6
$\text{C}_2\text{H}_6$	—	—	—	—	0.6
$\text{C}_3\text{H}_6$	0.3	0.7	21.2	10.8	18.7
$\text{C}_3\text{H}_8$	0	0	8.4	28.3	5.6
$\text{C}_4\text{H}_8$	11.9	17.3	21.2	15.9	33.9
$\text{C}_4\text{H}_{10}$	33.7	34.1	12.5	17.8	
$\text{C}_5$	23.2	23.0	13.5	10.0	10.6
$\text{C}_6$	8.2	9.9	6.3	3.3	
$\text{C}_7$	18.2	13.9	0.1	0.1	7.2
$\text{C}_8$	4.3	0.9	0	—	

\* Distributions were calculated on carbon-number basis exclusive of ethane used as an internal standard. Separate experiments revealed that ethane yield was negligible at 423 K and 1.0 % at 573 K.

\*\* Hydrocarbon distribution in methanol conversion over  $\text{Ag}_3\text{PW}_{12}\text{O}_{40}$  supported on active-carbon under the conditions of W/F = 50 g h mol<sup>-1</sup> and methanol pressure of 10 x 1.3 kPa.

hydrocarbons. Difference in the temperature required for C-C bond formation in the two systems indicates that the reactivity of  $\text{CH}_3$  moiety depends on the chemical environment, where  $\text{CH}_3$  moiety is located. The less reactive  $\text{CH}_3$  in methoxyl groups in ZSM-5 need higher temperature to be reactive enough to attack on C-H bonds, in comparison with incipient  $\text{CH}_3^+$  from by the stoichiometric reaction.

#### REFERENCES

- (1) Chang, C. D., and Silvestri, A. J., J. Catal., 47, 249 (1977)
- (2) Kaeding, W. W., and Butter, S. A., J. Catal., 61, 155 (1980)
- (3) Kagi, D., J. Catal., 69, 242 (1981)
- (4) Ono, Y., and Mori, T., J. Chem. Soc., Faraday Trans. I, 77, 2209 (1981)
- (5) Olah, G. A., Klopman, G., and Schlosberg, R. H., J. Am. Chem. Soc., 91, 3261 (1969)
- (6) Olah, G. A., DeMember, J. R., and Shen, J., J. Am. Chem. Soc., 95, 4952 (1973)
- (7) van den Berg, J. P., Wolthuizen, J. P., and van Hooff, J. H. C., "Proceedings 5th Internat. Conf. on Zeolites, Naples, 1980" (L. V. Ree, Ed.) p.649, Hayden, New York, 1980
- (8) Zatorski, W., and Kryzanowski, S., Acta Phys. Chem., 24, 347 (1978)
- (9) Chen, N. Y., and Reagan, W. J., J. Catal., 59, 123 (1979)
- (10) Ono, Y., Imai, E., and Mori, T., Z. Phys. Chem., N.F., 115, 99 (1979)
- (11) Anderson, J. R., Mole, T., and Christov, V., J. Catal., 61, 477 (1980)
- (12) Baba, T., Sakai, J., and Ono, Y., Bull. Chem. Soc. Jpn., 55, 2657 (1982)

## Synergism in Acetic Acid/Methanol Reactions Over ZSM-5 Zeolites

Clarence D. Chang, Nai-Yuen Chen,  
L. R. Koenig and Dennis E. Walsh

Mobil Research and Development Corporation  
Central Research Division  
P. O. Box 1025  
Princeton, New Jersey 08540

### INTRODUCTION

Carboxylic acids are readily converted to aromatic hydrocarbons over ZSM-5 zeolites (1). The initial step of the reaction sequence involves oxygen elimination by decarboxylation, decarbonylation and/or dehydration. The residual hydrocarbon moiety is then aromatized, we believe, via classical carbenium ion pathways (2).

The reaction causes rapid catalyst deactivation, which can be alleviated by adding methanol to the feed (3). The synergistic effect of methanol on acetic acid aromatization is the subject of this study.

### EXPERIMENTAL DATA

#### A. FIXED BED RESULTS

##### Acetic Acid

Acetic acid was reacted over HZSM-5 at 316°C and 370°C, 1 atm., 1 LHSV. Results are shown in Table 1. At 316°C, activity is low (8% conversion). Decarboxylation is the principal mode of oxygen elimination, resulting in acetone and hydrocarbons, mainly isobutylenes and aromatics. At 370°C, both decarboxylation and dehydration are important, however, catalyst deactivation is rapid, with conversions dropping from 100% to 71.4% in 1.3 hr.

Again the main products are acetone, isobutylene and aromatics. Decarbonylation is a relatively minor reaction.

##### Acetic Acid/Methanol Mixture

A 4/1 molar mixture of methanol/acetic acid was reacted over HZSM-5 at 370°C, 1 atm., 1 As seen in Table 1, the conversion remains quantitative after 3 hr. No evidence of catalyst deactivation was seen during this period. The addition of methanol suppresses CO<sub>2</sub> formation, and dehydration becomes the main oxygen-elimination reaction. The hydrocarbons are mostly aromatic (79%).

## B. FLUID-BED RESULTS

Experimental data are presented in Table 2. Two conversions are presented for each run. "Total conversion" represents the conversion to all products, while "conversion to non-oxygenates" represents conversion to all hydrocarbon, COx and H<sub>2</sub>O products. The overall yields from the methanol experiment are in reasonable agreement with data obtained in the fluid bed MTG process (5). The hydrocarbon gas products, however, are higher in propene and lower in isobutane probably due to the lower reaction pressure used in this study.

### Acetic Acid and Methylacetate

The data obtained for acetic acid illustrate several interesting points which can be contrasted with the earlier continuous operation in a fixed bed. First, total conversions >90% may be maintained indefinitely provided periodic catalyst regeneration is employed. The experimental data show that decarboxylation takes place to a large extent.

On a weight basis, acetic acid yields less than 40% as much hydrocarbon as methanol. The lower yield is primarily due to carbon loss by decarboxylation, and to a small extent, to coke and CO production.

Methyl acetate has a higher carbon content (48.6% C) than acetic acid and methanol and despite decarboxylation and coke, the observed hydrocarbon yield remains comparable to that of methanol. Moreover, selectivity for direct conversion to C<sub>5</sub><sup>+</sup> hydrocarbons is higher than that of acetic acid or methanol (79.5%). Thus, the direct yield of C<sub>5</sub><sup>+</sup> liquid hydrocarbons is 32.1% on charge vs 23.3% for methanol.

### Acetic Acid/Methanol Mixtures

Processing a 1.9/1 or a 3.8/1 molar mixture of CH<sub>3</sub>OH and acetic acid provided observations similar to fixed-bed results, i.e. an enhancement in C<sub>5</sub><sup>+</sup> liquid yield at the expense of C<sub>4</sub><sup>-</sup> vs what might be expected if the mixture behaved as the average of its two components, the calculated values for which are shown in parentheses in Table 2. The selectivities of the hydrocarbon products amplify the observed synergism with respect to C<sub>5</sub><sup>+</sup> liquids. Furthermore, there is an enhancement in total hydrocarbon yield vs linear combination expectations.

This is illustrated in Figure 1 which shows the effect of increasing mole percent methanol in the MeOH/acetic acid charge and attendant decrease in oxygen rejection as CO<sub>2</sub> and increase in oxygen removal as H<sub>2</sub>O. Thus, more carbon remains available to form hydrocarbon products, much of it becoming C<sub>5</sub><sup>+</sup> liquids.

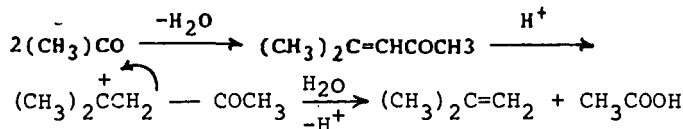
## DISCUSSION

### A. AROMATIZATION PATHWAY FOR ACETIC ACID

As shown previously, the major initial products of acetic acid reaction over HZSM-5 are acetone, isobutylene and CO<sub>2</sub>.

Acetone formation from acetic acid is a known reaction and is often referred to as "ketonization" (6,7). The reaction was originally observed on 3d-oxides, but has been reported for SiO<sub>2</sub>/Al<sub>2</sub>O<sub>3</sub> and mordenite (8,9) catalysts. The mechanism of ketonization via decarboxylation is discussed later.

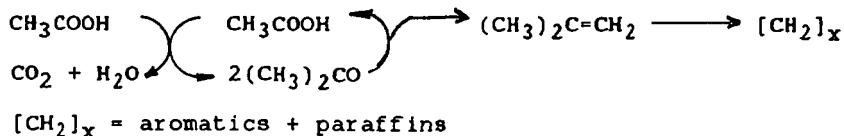
Isobutylene formation from acetone decomposition over silica gel and SiO<sub>2</sub>-Al<sub>2</sub>O<sub>3</sub> (8,9,10) and zeolites (1,12) has also been reported. The reaction mechanism over acid zeolites is believed to involve an aldol condensation followed by  $\beta$ -scission (12):



In the present case, the isobutylene is converted by HZSM-5 to aromatics and paraffins, while the acetic acid re-enters the catalytic cycle.

Neglecting catalyst deactivation for the moment, the main reactions of hydrocarbon formation from acetic acid over HZSM-5 are summarized in the following scheme:

Scheme A

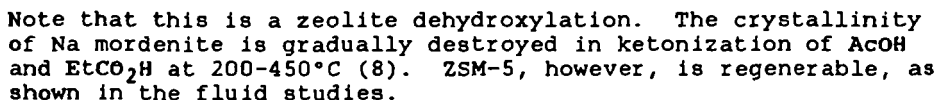
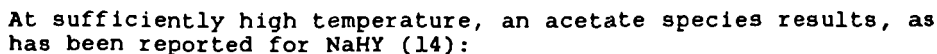


### B. MECHANISM OF CATALYST DEACTIVATION AND THE ROLE OF METHANOL

The ketonization of acetic acid over 3d-oxides such as chromia and TiO<sub>2</sub> at 350°-460°C has been shown to involve the bimolecular nucleophilic attack of an acylium ion by an acetate species with CO<sub>2</sub> elimination (7,13):



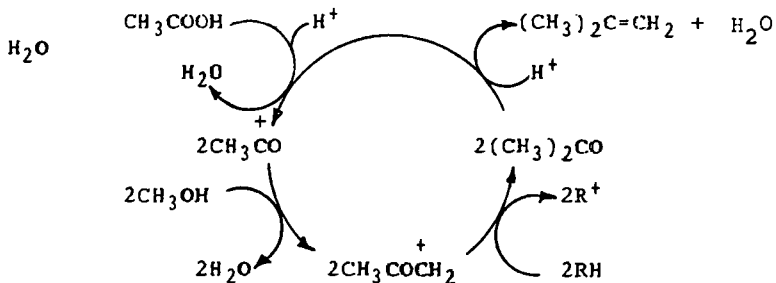
It seems reasonable to assume a similar mechanism for strongly acidic zeolites, except that in this case, the acylium ion may be directly generated:


$$\overset{+}{\text{CH}_3\text{CO}} \overset{-}{\text{O-zeol}} \xrightarrow{\Delta} \overset{-}{\text{CH}_3\text{COO}} + \overset{+}{\text{zeol}}$$
$$\begin{array}{l} \text{CH}_3\text{OH} \longrightarrow [\text{:CH}_2] + \text{H}_2\text{O} \\ \quad \quad \quad \uparrow \\ \text{CH}_3\text{CO} + \text{:CH}_2 \longrightarrow \text{CH}_3\text{COCH}_2 \end{array}$$
$$\text{CH}_3\text{COCH}_3 + \text{RH} \xrightarrow{+} (\text{CH}_3)_2\text{CO} + \text{R}^+$$
$$\begin{array}{c} \text{C} \\ \diagup \\ \text{C}-\text{C}=\text{O} \\ \diagdown \quad \diagup \\ \text{C} \quad \text{Cl} \end{array} \xrightarrow{-\text{Cl}^-} \begin{array}{c} \text{C} \\ \diagup \\ \text{C}-\text{C}=\text{O} \\ \diagdown \quad \diagup \\ \text{C} \quad \text{C} \end{array} + \text{C}=\text{O} \xrightarrow{\text{RH}} \begin{array}{c} \text{C} \\ \diagup \\ \text{C}-\text{C}=\text{O} \\ \diagdown \quad \diagup \\ \text{C} \quad \text{C} \end{array}$$

149

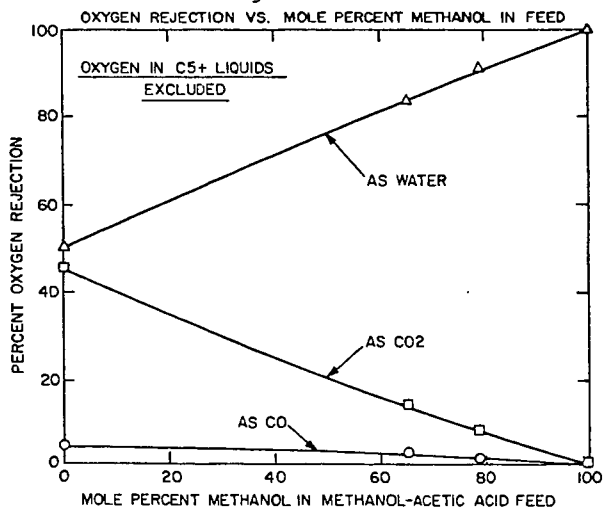
1

### Scheme B



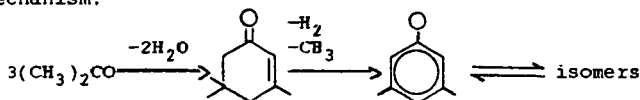
This scheme can obviously be adapted to methyl acetate conversion by including the equilibrium between methyl acetate, methanol and acetic acid.

Figure 1.



## References

1. Chang, C. D. and Silvestri, A. J., J. Catal. 47, 249, (1977).
2. Poutsma, M. L., in "Zeolite Chemistry and Catalysis", (Ed. J. A. Rabo), ACS Monograph 171, 1976, Ch.8.
3. Chang, C. D., Lang, W. H. and Silvestri, A. J., U.S. Patent 3,998,898.
4. (a) Argauer, R. J. and Landolt, G. R., U.S. Patent 3,702,886;  
(b) Olson, D. H., Kokotailo, G. T., Lawton, S. L. and Meier, W. M., J. Phys. Chem. 85, 2238 (1981).
5. Liederman, D., Jacob, S. M., Voltz, S. E. and Wise, J. J., 2nd. Eng. Chem. Process Des. Dev. 17(3), 340 (1978).
6. Kuriacose, J. C. and Jewur, S. S., J. Catal. 50, 330 (1977), and references therein.
7. Gonzalez, F., Munuera, G. and Prieto, J. A., J. Chem. Soc., Faraday Trans. 1, 74(6), 1517 (1978).
8. Sosnina, I. E. and Lysenko, S. V., Vestn. Mosk. Univ., Khim. 14(3), 354 (1973).
9. Sosnina, I. E., Zh. Fiz. Khim. 51, 2001 (1977).
10. Fujii, R., J. Chem. Soc. Japan 65, 181 (1944).
11. Kurganova, S. Ya., Rudenko, A. P. and Balandin, A. A., Zh. Org. Khim. 2(5), 804 (1966).
12. Chang, C. D., Lang, W. H. and Bell, W. K., in "Catalysis in Organic Synthesis, 1981", (Ed. W. E. Moser), in press.
13. Swaminathan, R. and Kuriacose, J. C., J. Catal. 16, 357 (1969).
14. Bielanski, A. and Datka, J., J. Catal. 32, 183 (1974).
15. Balaban, A. T. and Nenitzescu, C. D., Annalen 625, 66 (1959).
16. Dimethyl phenols are most likely formed according to the following mechanism:



Step A is well known (17,18). The dimethyl analogue of Step B has been described by Horning (19). Demethylation from a quaternary carbon upon dehydrogenation is a known reaction (20).

17. Whitmore, F. C., "Organic Chemistry", Van Nostrand, N.Y., 1937, p.253.
18. Szabo, D., Acta Chim. Acad. Sci. Hung. 33, 425, (1962).
19. Horning, E. C., J. Amer. Chem. Soc. 67, 1421 (1945).
20. Linstead, R. P., and Thomas, S. L. S., J. Chem. Soc., 1127 (1940).

TABLE 1  
Conversion of AcOH and AcOH/MeOH over HZSM-5  
Fixed Bed Data

Feed	AcOH	AcOH	AcOH (1 mol) + MeOH (4 mol)
T, °C	316	370	370
P, psig	0	0	0
LHSV, hr <sup>-1</sup>	1	1	1
WHSV, hr	1.5	1.3	3.0
Conversion, wt. %	8.0	71.4(a)	100
Products, wt. %			
H <sub>2</sub>	0.1	--	--
CO	1.7	1.6	1.3
CO <sub>2</sub>	32.9	15.7	3.2
H <sub>2</sub> O	tr	56.1	55.7
Acetone	33.4	6.0	--
Other n-cpds	2.7	0.7(b)	--
Hydrocarbons	29.2	19.9	39.8
Hydrocarbons, wt. %			
C <sub>1</sub>	--	0.1	0.2
C <sub>2</sub>	--	--	0.5
C <sub>2</sub> =	0.6	1.7	1.3
C <sub>3</sub>	--	2.7	0.1
C <sub>3</sub> =	1.8	2.7	3.3
C <sub>4</sub>	--	0.4	0.2
C <sub>4</sub> =	17.1(c)	7.1(c)	1.3
C <sub>5</sub>	--	0.1	--
C <sub>5</sub> =	--	0.3	0.3
C <sub>6</sub> aliphatic	--	0.3	0.1
Aromatics	80.5	84.6	68.1

(a) 100% conversion at 0.3 hr.  
(b) 570% dimethylphenols (16).  
(c) 29% isobutylene.  
(d) 81% conversion at 1.5 hr.

TABLE 2  
Conversion of AcOH, MeOH, and AcOH/MeOH over HZSM-5  
Fluid Bed Data

410°C, 1 atm, 1.0-1.1 WHSV, 20 min Reaction Intervals					
Fluid Bed Data					
Total Conversion	98.6	91.2	89.4	>91	(94.9)
Conversion to Non-Oxygenates	98.6	79.8	86.1	90.4	(89.2)
Products (Wt. % of Charge)					
CO	0.0	3.7	6.2	2.1	(1.8)
CO <sub>2</sub>	0.2	31.4	17.6	9.4	(15.8)
H <sub>2</sub> O	55.8	28.4	21.5	45.3	(42.1)
Oxygenates	1.4	20.2	13.9	9.6	(10.8)
C <sub>1</sub> Hydrocarbon gas	19.0	3.8	6.0	7.9	(11.4)
C <sub>2</sub> Liquid Hydrocarbon	23.3	10.6	32.1	24.9	(17.0)
Total Hydrocarbons	42.3	14.4	38.1	32.8	(28.4)
Coke	0.3	1.9	2.7	0.8	(1.1)
Wt. %s of Hydrocarbon					
C <sub>1</sub> + C <sub>2</sub>	5.4	1.5	5.6	7.2	7.6
C <sub>3</sub>	1.6	0.1	0.7	0.4	0.6
C <sub>3</sub>	25.9	5.2	6.7	13.8	14.2
iC <sub>4</sub>	5.5	0.5	0.3	0.4	0.5
nC <sub>4</sub>	0.4	0.3	0.0	0.1	0.1
C <sub>4</sub>	5.8	15.7	1.4	1.6	1.9
Total C <sub>4</sub>	44.6	23.3	14.7	23.5	(34.0)
C <sub>5</sub> + liquid	54.7	65.0	78.7	74.1	(59.8)
Coke	0.7	11.7	6.6	2.4	(6.2)



Extended abstract submitted for presentation at the  
185th ACS Meeting, Division of Fuel Chemistry,  
Seattle, Wash., March 20-25, 1983.

---

Hydroconversion of Long-Chain n-Alkanes on Pt/HZSM-5  
Zeolite

by Jens Weitkamp<sup>a)</sup> and Peter A. Jacobs<sup>b)</sup>

- a) Engler-Bunte-Institute  
Division of Gas, Oil, and Coal  
University of Karlsruhe  
Richard-Willstätter-Allee 5  
D-7500 Karlsruhe, West-Germany
- b) Centrum voor Oppervlaktescheikunde  
en Collöidale Scheikunde  
Katholieke Universiteit Leuven  
De Croylaan 42  
B-3030 Leuven, Belgium

Zeolite catalysts of medium-pore size are getting increasing acceptance in commercial processes, e.g., in hydrodewaxing of middle distillates. In this process *n*-paraffins and part of the isomers with one methyl branching are selectively hydrocracked in order to improve the low temperature properties, especially the pour point. Nonetheless, relatively little is known on the shape-selectivity effects occurring during hydroconversion of long-chain alkanes on medium-pore zeolites. Recently, the authors reported (1) on the shape-selective isomerization and hydrocracking of *n*-decane on Pentasil zeolites. The present paper extends these data to the homologous series of *n*-alkanes with 9 to 16 carbon atoms.

A Pt/HZSM-5 zeolite catalyst was employed throughout this study. The zeolite with a Si/Al ratio of 60 was prepared according to published methods (2). It was loaded with 0.5 wt.-% of platinum by contact with an aqueous solution of  $[\text{Pt}(\text{NH}_3)_4]\text{Cl}_2$ . The catalytic experiments were conducted with the pure *n*-alkanes in a hydrogen atmosphere at a total pressure of 2 MPa and a hydrocarbon partial pressure of 20 kPa except for *n*-hexadecane where the latter was 10 kPa to avoid condensation at low reaction temperatures. A fixed bed reactor was used.  $W/F_{n\text{-alkane}}$  was in the order of 100 g·h/mol. With each feed the reaction temperature was varied between 200 and 300 °C so that a wide range of conversion could be covered. Product analysis was achieved by capillary GLC techniques.

Two types of reaction occur during hydroconversion of *n*-alkanes on Pt/HZSM-5, viz. isomerization and hydrocracking. In Fig. 1 the yields of branched isomers and of hydrocracked products are plotted versus temperature for the experiments with *n*-nonane and *n*-pentadecane.

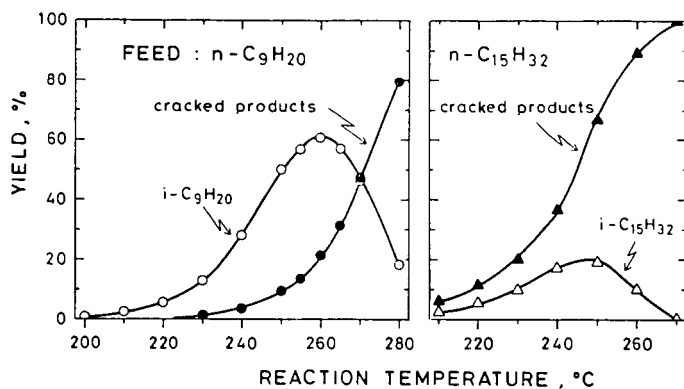


Fig. 1: Hydroconversion of n-Nonane and n-Pentadecane on Pt/HZSM-5

While n-nonane can be isomerized under mild conditions without significant hydrocracking the yield of i-pentadecanes from n-pentadecane is low throughout the whole range of temperature and, hence, of conversion. The quantitative evaluation of the influence of reaction temperature on conversion shows that the apparent energy of activation decreases with increasing chain length. This could indicate increasing diffusional resistances.

The distributions of i-alkanes formed by isomerization of the n-alkanes differ substantially from those observed over faujasite zeolites (3). In particular, methyl isomers strongly predominate on Pt/HZSM-5 up to 90 % conversion. Small amounts of dimethyl isomers with one branching in the 2-position are also formed while ethyl isomers are absent. These results are best interpreted in terms of product shape-selectivity.

Distributions of individual methyl isomers formed from three selected n-alkanes at moderate conversions around 10 % are given in Table 1. The main product from n-nonane is 2-methyl-octane. This is in principal agreement with our earlier results (1) of n-decane conversion on Pt/HZSM-5 and might reflect a restricted transition state shape-selectivity. On the other hand, roughly equal amounts of individual methyl isomers are formed from n-tridecane and n-pentadecane (Table 1). These distributions are probably close to equilibrium.

Table 1: Distributions of Methyl Isomers Formed from Various n-Alkanes (Values in mol-% of total methyl isomers)

Feed	n - C <sub>9</sub> H <sub>20</sub>	n - C <sub>13</sub> H <sub>28</sub>	n - C <sub>15</sub> H <sub>32</sub>
Temperature, °C	230	220	210
Conversion, %	14.6	10.6	9.3
Yield of i-C <sub>m</sub> H <sub>2m+2</sub> , %	13.2	8.2	2.8
	2-M-0c 42.6 3-M-0c 38.0 4-M-0c 19.4	2-M-Do 15.0 3-M-Do 22.3 4-M-Do 18.0 5-M-Do 22.8 6-M-Do 21.9	2-M-Te 14.6 3-M-Te 18.8 4-M-Te 15.4 5-M-Te 15.5 6-M-Te 18.0 7-M-Te 17.7

Hydrocracking on Pt/HZSM-5 is purely ionic, i.e., no hydro-genolysis on Pt-sites takes place. This can be concluded from the absence of methane and ethane. Typical carbon number distributions of the cracked products from n-tetradecane and n-pentadecane are depicted in Fig. 2. For comparison the corresponding distributions on a Y-type zeolite with a pure primary cracking selectivity are given.

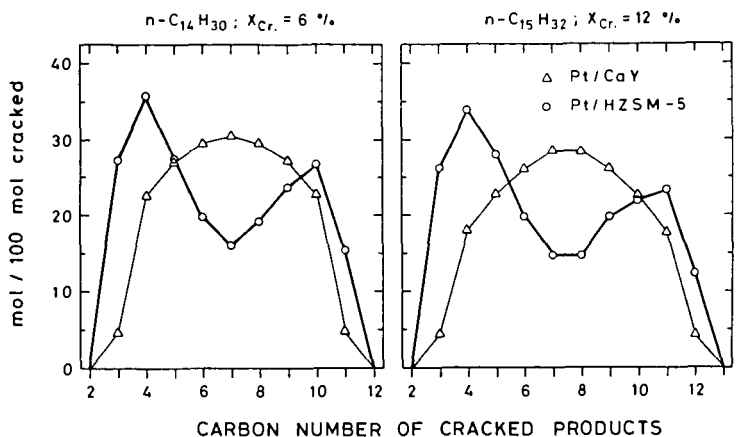


Fig. 2: Carbon Number Distributions in Hydrocracking of n-Tetradecane and n-Pentadecane

The curves for Pt/HZSM-5 are not fully symmetrical which is indicative of some secondary cracking. It is evident that the cracking selectivity on Pt/HZSM-5 deviates considerably from the one on faujasites. In particular, more  $C_3$  and  $C_4$  as well as  $C_{m-3}$  and  $C_{m-4}$  ( $m$  = carbon number of feed) are formed on ZSM-5. Moreover, the distribution curves for the medium-pore zeolite exhibit distinct minima.

The cracked products on Pt/HZSM-5 consist of n-alkanes and methyl isomers. Detailed isomer distributions will be given in the paper. A reaction network for shape-selective rearrangements and  $\beta$ -scissions in the pores of ZSM-5 will be developed.

#### References

- (1) P.A. Jacobs, J.A. Martens, J. Weitkamp, and H.K. Beyer, Farad. Discuss. Chem. Soc. 72, 353 (1982)
- (2) R.J. Argauer and G.R. Landolt, US Patent No. 3 702 886 (1972)
- (3) J. Weitkamp, Ind. Eng. Chem., Prod. Res. Devel., in press

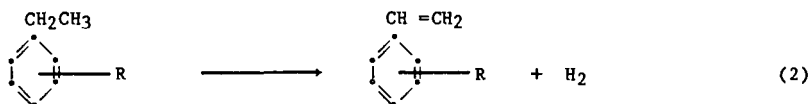
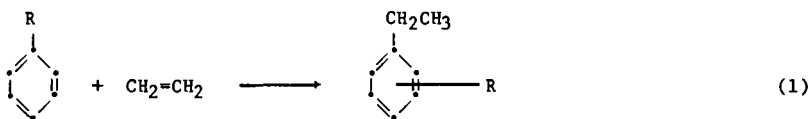
## Para-Methylstyrene - A New Monomer and Polymer for Industry

Warren W. Kaeding, L. Brewster Young and A. G. Prapas

Mobil Chemical Co., P. O. Box 1028, Princeton, N.J. 08540

**INTRODUCTION.** The present large volume styrene industry began during World War II as part of the effort to produce synthetic rubber to replace supplies of natural rubber which were suddenly cut off from sources in Asia (1,2). A rapid growth in polymer technology eventually followed. A considerable number and variety of new monomers were synthesized, purified and polymerized to establish the principles and products of the large volume styrenics plastics industry as we know it today.

**VINYLTOLUENE.** When toluene was substituted for benzene in the alkylation step, ethyltoluene was produced, Equation 1 ( $R=CH_3$ ). The corresponding vinyltoluene was obtained by a subsequent catalytic dehydrogenation, Equation 2, in a manner analogous to the process for producing styrene (3). By contrast with styrene, however, a mixture of three isomers was formed. Different polymer



properties of these individual isomers and various mixtures were observed giving rise to more complex separation and purification steps. The vinyltoluene of commerce which eventually emerged from this work is composed of approximately 35% para and 65% meta isomers determined primarily by the ratio produced during alkylation with an  $\text{HCl-AlCl}_3$  catalyst and practical isomer separation limitations (4).

Styrene is the simplest vinyl aromatic with the fewest production and purification problems. Polymer properties of styrene were also favored by comparison with the vinyltoluene mixtures which could be efficiently produced with the catalysts and processes available. As a result, styrene has become the dominant vinyl aromatic monomer and polymer in the marketplace.

**ZEOLITE CATALYSTS.** During the past three decades, interest and knowledge of the structure and catalytic properties of the naturally occurring zeolites has grown (5,6). More recently, this effort has expanded dramatically with the development of techniques for manufacture of many of these materials and especially with the discovery of unique, new synthetic zeolites not found in nature which have demonstrated desirable catalytic properties (7).

Zeolite catalysts are crystals composed of silicon and aluminum oxides which contain pores and channels of precise and uniform dimensions. Chemical reactions occur primarily within the pores at catalytic sites, often acidic protons, present on the internal framework structure. The dimensions of Mobil ZSM-5 class zeolite pores are sufficient to admit certain substituted benzene derivatives.

However, analogues with bulky side-chains or polycyclic rings can not diffuse in or out of the pores to undergo a chemical reaction or be produced within the pores. Zeolite catalysts have shape selective properties by virtue of the limited space within the pores (7).

Toluene can be alkylated with ethylene to produce ethyltoluene over (unmodified) HZSM-5 catalyst containing acidic sites, Equation 1 (8). The starting materials and products can diffuse in and out of the pores. The composition of products observed, however, differs significantly from that found with an  $\text{HCl-AlCl}_3$  catalyst. The amount of ortho isomer was reduced by an order of magnitude, Table 1. An examination of the relative minimum dimensions of the ethyltoluene isomers, Table 2, indicates that the para isomer is smallest (9). The small difference between the ortho and meta isomers is also significant. We believe that the product mix observed was a result of the precise dimensions of the zeolite catalyst pores. A subtle distinction was made between the meta and ortho isomers based on size, favoring the smaller isomer, either by rate of formation and/or rate of diffusion out of the pore (10).

PARA-SELECTIVITY. To magnify this effect, methods have been developed for reducing the effective pore and channel dimensions as originally synthesized by modification of the catalyst with physical treatments and chemical reagents. Para-selective alkylation catalysts were produced. A dramatic difference was observed for the alkylation reaction. Ninety-seven percent of the ethyltoluene product produced was the smallest para isomer. The largest ortho isomer was virtually eliminated. The rates of diffusion between the para and ortho/meta isomers were increased by three orders of magnitude with modified para-selective catalysts (10).

The use of a modified zeolite catalyst offers several advantages for production of ethyltoluene by comparison with the  $\text{HCl-AlCl}_3$  catalyst. The undesired ortho isomer, which is produced, and must be separated and recycled is virtually eliminated. Production of di- and polyethylated toluene is inhibited because of the confined space within the pores. In addition, all of the problems of corrosion, disposal and separation encountered with the use of  $\text{AlCl}_3$  are eliminated.

POLY-PARA-METHYLSTYRENE. Samples of 99+% p-methylstyrene were prepared in the laboratory. However, we have selected a 97% para-, 3% meta-methylstyrene mixture, designated PMS, for initial polymerization studies. A comparison of typical monomer properties of PMS with styrene and commercial vinyltoluene is shown in Table 3. In broad terms, PMS is similar to styrene in its polymerization behavior. PMS polymers, with a variety of molecular weights and melt flow properties, have been prepared. Analogous copolymers were also made by substituting PMS for styrene. A study of polymer properties reveals some differences as well as similarities with polystyrene, Table 4.

A potentially important advantage of poly-PMS is its lower density relative to styrene which translates to a 4% reduction in weight required to fabricate a desired product. Poly-PMS has a glass transition temperature of  $113^\circ\text{C}$ ,  $11^\circ\text{C}$  higher than polystyrene, Table 4. In addition to providing an extra margin of safety for higher temperature use and storage, decreases in molding cycle times, better mold fill properties and higher melt strengths have been observed.

A potential application where poly-PMS can give a significant improvement compared with polystyrene is in the area of flame retardancy (FR) or ignition resistance. PMS-based impact resins require lower loadings of FR reagents to meet the desired ratings.

Polystyrene is very difficult to crosslink by radiation without destroying its properties. As a result, applications using this property have not been developed. The methyl group of poly-PMS, however, provides susceptible positions for crosslinking at commercially viable levels of electron beam radiation. This

converts a thermoplastic to a thermoset resin, significantly improving its grease resistance and flammability behavior.

SUMMARY. Styrene has enjoyed a special position among vinylaromatic monomers because of its lack of isomers and consequent ease and simplicity of production. Our discovery of novel technology to produce p-ethyltoluene has enabled us to manufacture a substituted vinyl aromatic monomer selectively. Since much benzene is produced from toluene, the direct use of toluene for PMS eliminates the first process step for styrene. Quantities of PMS from a semi-commercial plant are now available for the critical cost/performance test in the marketplace to eventually determine its place in the polymer industry.

#### REFERENCES

1. Baruch Committee Report, "The Rubber Situation", House Document No. 836, U.S. Printing Office, Sept. 12, 1942; p. 28.
2. Boundy, R.H.; Stoesser, S.M. In "Styrene - Its Polymers, Copolymers, and Derivatives"; Reinhold: New York, 1952; p. 11.
3. Boundy, R.H.; Boyer, R.F. In "Styrene - Its Polymers, Copolymers, and Derivatives"; Reinhold: New York, 1952.
4. Coulter, K.E.; Kehde, H.; Hiscock, B. F. "High Polymers"; Leonard, E.C., Ed.; Wiley-Interscience: New York, 1971; Vol. 24, pp. 548-549.
5. Weisz, P.B.; Frillette, V.J. J. Phys. Chem. 1960, 64 382.
6. Plank, C.J.; Rosinsky, E.J.; Hawthorne, W.P. Ind. Eng. Chem. Prod. Res. Dev. 1964, 3 165.
7. (a) Meisel, S.L.; McCullough, J.P.; Lechthaler, C.H.; Weisz, P.B. CHEMTECH 1976, 6 86; (b) Meisel, S.L. Philos. Trans. R. Soc. London 1981, A300 157; (c) Csicsery, S. M. "Zeolite Chemistry and Catalysis"; ACS Monograph No. 171, Rabo, J.A.; Ed.; American Chemical Society: Washington, D.C., 1976; (d) Weisz, P.B. Pure Appl. Chem. 1980, 52 2091.
8. Kaeding, W.W.; Young, L.B.; Prapas, A.G. CHEMTECH 1982 12 556.
9. (a) Kaeding, W.W.; Chu, C.; Young, L.B.; Weinstein, B.; Butter, S.A. J. Catal. 1981, 67 159; (b) Kaeding, W.W.; Chu, C.; Young, L.B.; Butter, S.A. J. Catal. 1981, 69 392.
10. Chen, N.Y.; Kaeding, W. W.; Dwyer, F.G. J. Am. Chem. Soc. 1979, 101 6783.



**Table 1.** Alkylation of Toluene with Ethylene  
Composition of Typical Product Streams

Compound, wt%	HCl-AlCl <sub>3</sub> <sup>a</sup>	Catalysts	
		ZSM-5	Class Zeolite
		Unmodified	Modified
Light gas and Benzene	0.2	1.0	0.9
Toluene <sup>b</sup>	48.3	74.4	86.2
Ethylbenzene and Xylenes	1.2	1.2	0.5
p-Ethyltoluene	11.9	7.0	11.9
m-Ethyltoluene	19.3	14.7	0.4
o-Ethyltoluene	3.8	.3	0
Aromatic C <sub>10</sub> <sup>+</sup>	14.4	1.4	0.1
Tar	0.9	0	0
Total	100.0	100.0	100.0
Ethyltoluene Isomers, %			
Para	34.0	31.8	96.7
Meta	55.1	66.8	3.3
Ortho	10.9	1.4	0

(a) Ref. 4

(b) Excess toluene is used to prevent polyalkylation and resultant build-up of C<sub>10</sub><sup>+</sup> and tars.

**Table 2.** Minimum Dimensions of Alkyl Aromatics<sup>a</sup>

Hydrocarbon	Minimum Cross Section Å
Benzene	7.0
Toluene	7.0
Ethylbenzene	7.0
o-Xylene	7.6
m-Xylene	7.6
p-Xylene	7.0
o-Ethyltoluene	7.7
m-Ethyltoluene	7.6
p-Ethyltoluene	7.0

(a) From Fischer-Hirschfelder-Taylor hard sphere molecular models.

Table 3. Typical Monomer Properties

	<u>PMS</u>	<u>Styrene</u>	<u>Vinyltoluene</u>
Purity (wt% vinyl)	99.7	99.7	99.2
Isomer Distribution			
Para	97	--	33
Meta	3	--	66.7
Ortho	--	--	0.3
Refractive Index (np <sub>D</sub> <sup>25</sup> )	1.5408	1.5440	1.5395
Density, g.cm <sup>-3</sup> (25°C)	0.892	0.902	0.893
Viscosity, cps (25°C)	0.79	0.72	0.78
Surface Tension, dynes-cm <sup>-1</sup> (25°C)	34	32	31
Boiling Point (°C @ 760 mmHg)	170	145	168
Freezing Point (°C)	-34	-31	-77
Volume Contraction on Polymerization (% Calculated @ 25°C)	12	14	12
Heat of Polymerization (Kcal mole <sup>-1</sup> )	15-17	17	15-17

Table 4. Properties of Typical Polymers

<u>Properties</u>	<u>Poly PMS</u> <sup>a</sup>	<u>Polystyrene</u>
Specific gravity, gm/ml	1.01	1.05
Melt flow rate (condition G)	2.5	2.5
Thermal		
Glass transition temp. (°C)	113	102
Vicat Softening (°C)	116	109
Heat distortion temp. (°C)	95	89
Mechanical		
Tensile strength at break (psi x 10 <sup>-3</sup> )	7.0	7.6
Elongation (%)	3.0	3.0
Tensile modulus (psi x 10 <sup>-5</sup> )	3.2	3.6
Flexural strength (psi x 10 <sup>-5</sup> )	12	13
Hardness (Rockwell M)	82	74
Izod impact (ft.lbs./in.)	0.3	0.3

(a) 97% para, 3% meta isomers

## CO/H<sub>2</sub> CHEMISTRY IN A CHANGING ENVIRONMENT

Roy L. Pruett

Exxon Research and Engineering Company  
Corporate Research Laboratories  
P. O. Box 45,  
Linden, NJ 07036

The catalytic chemistry of CO/H<sub>2</sub> has been the subject of concentrated research during the past 10 years, and especially during the past 3. This effort has been based on several assumptions, which include two that are key: (a) the cost of petroleum and petroleum-derived chemical raw materials (e.g., ethylene) will continue to escalate at a rapid pace; (b) the partial oxidation of coal to CO/H<sub>2</sub> for both fuel and chemical purposes will become economically competitive.

In keeping with this activity, a large number of potential products have been synthesized from CO/H<sub>2</sub>. These vary from the simplest molecules, such as methanol, methane and ethylene, to much more complicated molecules, such as vinyl acetate, durene, long-chain  $\alpha$ -olefins, etc.

At the present time, there have been significant changes in the projected timing for some CO/H<sub>2</sub> applications. These are caused by: (a) decreased demand for crude, due to conservation efforts and the accompanying oversupply and price stabilization; (b) increased emphasis on natural gas and natural gas liquids as sources for methanol and other basic commodity chemicals, especially in certain parts of the world rich in these resources.

The result of the changing environment has been a decrease in development efforts toward chemicals and fuels, except for those areas in which special situations exist. This presentation will include discussions of a number of processes which have been experimentally demonstrated, a number which are proceeding toward commercialization, some recently publicized results in key areas, and a discussion of how the changing environment has altered the outlook on CO/H<sub>2</sub> chemistry.

## Synthesis Gas Conversion With a Transition Metal-Zeolite Catalyst

H. W. Pennline, V. U. S. Rao, R. J. Gormley, and R. R. Schehl

U. S. Department of Energy  
Pittsburgh Energy Technology Center  
P. O. Box 10940  
Pittsburgh, PA 15236

### INTRODUCTION

Recently, much interest has been generated in the synthesis of hydrocarbon fuels from low ratio hydrogen-to-carbon monoxide mixtures using indirect liquefaction catalysts. Studies have shown that a low  $H_2:CO$  ratio synthesis gas is produced by the more efficient, second generation gasifiers (1). One of the objectives of the catalyst research program of the U. S. Department of Energy/Pittsburgh Energy Technology Center is to investigate various indirect liquefaction catalyst systems that are capable of using low ratio synthesis gas mixtures.

Of particular interest are catalysts that exhibit shape-selective properties. With the advent of the Mobil methanol-to-gasoline process, ZSM-5 and other medium pore zeolite systems have been investigated (2,3,4). Work at PETC has involved the direct conversion of low ratio hydrogen-to-carbon monoxide synthesis gas to liquid fuels via transition metal-zeolite combinations. In past experimentation, cobalt and iron, either promoted or unpromoted, have been investigated in tubular microreactors or in bench-scale mixed reactors. Due to the interesting preliminary results obtained with a Co-Th-ZSM-5 catalyst, a process variable study with this catalyst system was undertaken.

### EXPERIMENTAL

The catalyst was prepared by physically mixing the transition metal-promoter coprecipitate with the zeolite. Cobalt-thoria in a ratio of about 10/1 was coprecipitated from a solution of the nitrates of these metals with sodium carbonate, washed, dried, and sieved through 200 mesh. The ammonium form of ZSM-5 was fabricated according to information in the patent literature (5). The dried  $NH_4$ -ZSM-5 with a silica/alumina ratio of 30/1 was then sieved through 200 mesh, mixed with the dried coprecipitate, and rolled overnight for intimate mixing. Initially this mixture was pelleted for testing. However, due to the frangibility of the pellets, further testing was conducted with catalyst that was extruded with Catapal SB alumina and dried. The structural integrity of the extrudates was greatly enhanced by the alumina binder. Microreactor tests of the pelleted versus the extruded catalyst indicated that the addition of the alumina binder did not significantly affect the catalyst behavior. Extrudates were 1/8-inch-diameter cylinders with random lengths of approximately 1/8-inch, and the final catalyst composition was 12.5 percent cobalt, 1.2 percent thoria, 10-15 percent alumina, and the remainder ZSM-5.

The studies were carried out in a mixed reactor system as described by Berty (6). The catalyst extrudates were loaded into a 2-inch-diameter basket and supported by a stainless steel screen. Impeller speed was 1240 rpm. An outer furnace heated the reactor, while excellent bed temperature control was obtained by a modification that involved the installation of a coil in the reactor head through which air could flow for faster heat removal.

The schematic of the system is shown in Figure 1. Synthesis gas is stored in large gas holders at ambient conditions. The gas is then boosted to high pressures after going through a silica gel trap for dehumidification and an activated carbon trap to remove sulfur impurities. The high-pressured gas is stored in a bank of aluminum cylinders rather than carbon steel cylinders to prevent carbonyl formation. Before entering the system, the gas is again flowed through an activated carbon trap. The flow is metered and controlled by a mass flow meter, and hydrogen can be blended with the  $\text{H}_2$ : $\text{CO}$  synthesis gas via a similar apparatus. Products exit the reactor via a downward sloping heated line ( $200^\circ\text{C}$ ) and enter a hot trap ( $200^\circ\text{C}$ ) where heavy hydrocarbons, if produced, are condensed. Lighter products are condensed in water-cooled or air-cooled traps. The product gas is metered by a wet test meter and can be directed to an on-line gas chromatograph that can analyze hydrocarbons up to  $\text{C}_8$ .

The catalyst was brought to synthesis conditions in an identical manner for each test. Initially the reactor was pressurized to 300 psig with hydrogen. The activation procedure began by flowing hydrogen at  $1000\text{ hr}^{-1}$  space velocity over the catalyst while rapidly heating to  $200^\circ\text{C}$ . After maintaining this temperature level for two hours, the catalyst was heated to  $350^\circ\text{C}$  for twenty-one hours under the hydrogen flow. It has been reported in the literature that a  $350^\circ\text{C}$  reduction greatly enhances the hydrogen adsorption capacity of a cobalt catalyst (7). Afterwards, the catalyst temperature was reduced to  $250^\circ\text{C}$  and then the pressure was decreased to 100 psig. At these conditions the synthesis gas flow rate was incrementally increased over an hour until the design space velocity for the test was reached. Care was taken at this critical point so that temperature runaway did not occur. After this induction step, the pressure was increased to operating conditions, and afterwards the temperature was increased ( $10^\circ\text{C/hr}$ ) to synthesis conditions. Trap drainings, flow, and gas analyses were performed on a 24-hour basis for a material balance determination. All tests in this study used a  $\text{H}_2$ : $\text{CO}$  feed gas.

The gaseous and liquid products were characterized by various techniques. Product gas exiting the system was analyzed for hydrocarbons up to  $\text{C}_8$  by gas chromatography. Liquid hydrocarbon samples, after a physical separation from the aqueous phase, were characterized by simulated distillation ASTM D-2887, fluorescent indicator adsorption ASTM D-1319, and bromine number ASTM D-1159. The aqueous fraction was analyzed by mass spectroscopy, and the water content was determined by the Karl Fischer reagent technique.

## RESULTS AND DISCUSSION

To determine if deactivation would be a problem in the study, one of the first experiments in the process variable scan was a life test conducted at  $280^\circ\text{C}$ , 300 psig, and  $1000\text{ hr}^{-1}$  space velocity of  $\text{H}_2$ : $\text{CO}$  synthesis gas. Data listed in Table 1 for test 1-39 at different times on stream indicate that catalyst deactivation is significant. The initial high ( $\text{H}_2$ + $\text{CO}$ ) conversion of 83.8 percent decreases after 417 hours on stream to 56.6 percent. The hydrocarbon product distribution also shifts to a lighter fraction with time, as noted by the increase in percent  $\text{CH}_4$  (23.4 to 42.4) and by the decrease in  $\text{C}_5$ + weight percent (61.0 to 38.5), which corresponds to the decreasing liquid product yield. The functionality of the liquid oil was constant throughout the test, with a high olefin (76) and low paraffin (20) and aromatic (4) percentages. Aqueous analyses indicated that +99 percent of this fraction was water. It

was concluded from this test that deactivation was a key factor, and subsequently all comparisons would be done after the same time on stream using a different catalyst charge for each test.

Test 1-42 was conducted to elucidate the role of the zeolite function of the bifunctional catalyst at the lower temperature of 280°C. Coprecipitated cobalt and thorium were added in the same proportion as the ZSM-5 based catalyst to calcined Catapal SB gamma alumina, and the mixture was then extruded with uncalcined alumina. When this test is compared to 1-39, the conversion versus time curves are almost identical, indicating that the Fischer-Tropsch component, Co-Th, is responsible for the synthesis activity of the catalyst and also is the functional component deactivating with time. However, the hydrocarbon distribution is different in each case, with the alumina based cobalt-thorium yielding a heavier product than the ZSM-5 based catalyst. This is evidenced in Table 1 by the greater wax fraction in the hydrocarbons with the alumina based catalyst (10.3 percent versus 1.8 percent) and less of the liquid oil fraction boiling in the gasoline range, as determined by simulated distillation (68 percent versus 89 percent).

The functionality of the liquid product oils indicates that more olefins are produced with the ZSM-5 based catalyst than with the alumina based catalyst. Proton NMR studies of the oils indicate that the ZSM-5 based catalyst produces a high degree of branching, whereas the alumina based catalyst product is linear. Also,  $\beta$ -olefins with negligible  $\alpha$ -olefins are formed with the ZSM-5 based catalyst, whereas the opposite occurs with the alumina based catalyst.

The effect of reaction temperature was observed in four separate tests at 260°, 280°, 300°, and 320°C at process conditions of 300 psig and 4000 hr<sup>-1</sup> space velocity. Results are listed in Table 1. With an increase in temperature, the hydrocarbon distribution shifts to a lighter product, as indicated by the increasing CH<sub>4</sub> fraction, the decreasing C<sub>5</sub><sup>+</sup> fraction, and the increasing fraction boiling in the gasoline-range. Also interesting is the functionality of the product oil. With a decrease in reaction temperature from 280°C, the olefin/paraffin ratio decreases and approaches a paraffinic product, which is characteristic of cobalt catalysts, thus indicating that at the lower temperature (< 260°C), the zeolite function does not significantly influence the reaction mechanism. The test at 300°C yielded an oil fraction not too different functionally from the 280°C test. However, at 320°C, a significant amount of aromatics was formed (46%), which can be attributed to the acid-catalyzed reactions within the zeolite framework at the higher temperature. No hydrocarbons above a carbon number of 12 were formed.

Unfortunately, at the elevated temperatures, the rate of deactivation is quite significant, as seen in Figure 2. As expected, initial conversions are greater at the higher temperatures, but the rate of deactivation is also greater at the higher reaction temperatures. Accelerated carbon or coke formation at the higher temperature could explain the rapid deactivation.

The effect of the promoter thorium can be determined by comparing test 1-57 (12.5% Co-ZSM-5) and test 1-41 (12.5% Co-1.2% ThO<sub>2</sub>-ZSM-5), which are at the same process conditions. The thorium increases the activity of the cobalt-ZSM-5, as evidenced by the conversion data. Liquid products are more olefinic with the promoted catalyst. Also, the thorium shifts the product to a heavier hydrocarbon distribution, as noted by the decrease in the methane fraction, the increase in the C<sub>5</sub><sup>+</sup> fraction, and the increase in the wax fraction.

The effects of different methods of catalyst pretreatment, which included calcination in air of only the zeolite component before mixing and extrusion, calcination in air of the total extruded catalyst, and chemically treating the zeolite before mixing and extrusion, were investigated. After the standard activation procedure and at process conditions of  $4000 \text{ hr}^{-1}$  space velocity, 300 psig, and  $280^\circ\text{C}$ , the activities of all catalysts tested, as characterized by conversion, were identical. A catalyst air-calcined at  $350^\circ\text{C}$  exhibited similar results to an uncalcined catalyst activated in hydrogen at  $350^\circ\text{C}$ , and no major differences existed between the calcination of only the zeolite component as compared to calcination of the total catalyst.

Three tests with Co-Th-ZSM-5 were conducted at identical process conditions, with the only difference being the calcination temperatures of the respective catalysts:  $538^\circ\text{C}$  (test 2-6),  $450^\circ\text{C}$  (test 2-2), and no calcination (test 1-41). The simulated distillation results in Table 1 indicate that a lighter gasoline range liquid product is formed after the two higher temperature calcinations, although the conversions and liquid oil yields for all three tests are very similar. The aromatic fraction in the liquid oil increases (2, 7, and 10 percent) with the increasing temperature of calcination. Calcination evidently increases the strength of the acid sites in the zeolite component, and this leads to a greater aromatic formation.

In another comparison, the ZSM-5 component was exchanged with HCl (test 1-54) rather than the usual  $\text{NH}_4\text{Cl}$  exchange (test 1-41) with the purpose of increasing the strength of the acid sites. The uncalcined zeolites were then individually mixed with equal amounts of cobalt - thorium and extruded. Each catalyst was tested in a Berty reactor as in the previous preparative work: a space velocity of  $4000 \text{ hr}^{-1}$  with  $\text{H}_2:\text{CO}$  synthesis gas,  $280^\circ\text{C}$ , and 300 psig. Results indicate the activity of both catalysts was the same with time on stream. However, the product selectivity for the two catalysts was different. The product from the HCl-exchanged catalyst was much lighter than that from the  $\text{NH}_4\text{Cl}$ -exchanged catalyst, as seen by the difference in gasoline-range hydrocarbons (89 versus 70 percent). Although the functionality of the liquid product is still high in olefin content for both catalysts, the aromatic content from the HCl-exchanged catalyst was higher (11 percent) than that from the  $\text{NH}_4\text{Cl}$ -exchanged catalyst (2 percent).

#### SUMMARY

From this study with the promoted transition metal-zeolite combination, several conclusions can be made. At medium temperature and with a low  $\text{H}_2:\text{CO}$  ratio synthesis gas, the cobalt-thorium-ZSM-5 synthesizes a highly branched olefinic product. Deactivation at these conditions can be attributed to the Fischer-Tropsch component of the catalyst. As the higher optimum temperature for the catalytic activity of the zeolite component is approached, a high fraction of aromatics is formed in the liquid product. The effect of the addition of the promoter thorium to the transition metal-zeolite catalyst is to increase olefin production and to increase the amount of liquid hydrocarbon formation. A pretreatment step (calcination or chemical), which does not alter the synthesis activity of the catalyst, activates the acid sites of the zeolite component and thus increases production of aromatics.

#### DISCLAIMER

Reference in this report to any specific commercial product, process, or service is to facilitate understanding and does not necessarily imply its endorsement or favoring by the United States Department of Energy.

#### ACKNOWLEDGEMENTS

The authors wish to thank R. E. Tischer for the catalyst extrusions and the Analytical Chemistry Branch for the analyses of the liquid products.

#### REFERENCES

1. Hildebrand, R. E., and Joseph. L. M., 1979. Presented at the Methanol Symposium, 13th Middle-Atlantic ACS Meeting.
2. Chang, C. D., Lang, W. H., and Silvestri, A. J., 1979. J. Catal. 56:268.
3. Caesar, P. D., Brennan, J. A. Garwood, W. E., and Ciric, J., 1979. J. Catal. 56:274.
4. Rao, V. U. S., Gormley, R. J., Pennline, H. W., Schneider, L. C., and Obermyer, R., 1980. ACS Div. Fuel Chem., Prepr. 25:119.
5. Argauer, R. J., and Landolt, G. R., 1972. U. S. Patent 3,702,886.
6. Berty, J. M., 1974. Chem. Eng. Prog., 70:68.
7. Kibby, C. L., Pannell, R. B., and Kobylinski, T. P., 1980. Presented at 7th Canadian Symposium on Catalysis, Alberta, Canada.



TABLE 1. Process Conditions and Synthesis Results

CFSTR Test No.	1-39	1-39	1-39	1-42	2-10	1-41	1-44	1-43	1-57	2-6	2-2	1-54
Hours on Stream	33	201	417	33	37	40	32	33	37	36	36	38
Space Velocity, hr <sup>-1</sup>	1000	1000	1000	1000	4000	4000	4000	4000	4000	4000	4000	4000
Temperature, °C	280	280	280	280	260	280	300	280	280	280	280	280
(H <sub>2</sub> +CO) Conversion	83.8	67.9	56.6	80.5	25.9	61.4	66.7	54.8	55.4	64.4	66.7	63.7
H <sub>2</sub> Conversion	93.3	87.1	76.0	91.7	33.9	77.9	82.3	68.8	72.9	82.5	84.8	82.3
Hydrocarbon Distribution, wt%												
CH <sub>4</sub>	23.4	34.5	42.4	22.5	17.6	18.1	38.8	65.5	26.5	20.0	18.5	21.2
C <sub>2</sub> H <sub>6</sub> +C <sub>2</sub> H <sub>4</sub>	3.9	5.4	6.1	4.1	2.4	3.1	5.7	9.7	4.0	3.9	3.2	3.1
C <sub>3</sub> H <sub>8</sub> +C <sub>3</sub> H <sub>6</sub>	5.9	6.4	7.8	5.9	5.1	5.2	5.2	5.2	7.4	4.9	4.0	3.7
C <sub>4</sub> H <sub>10</sub> +C <sub>4</sub> H <sub>8</sub>	4.0	3.8	5.2	4.6	4.6	6.0	6.9	5.1	7.7	3.7	3.6	6.5
C <sub>5</sub> +	61.0	49.6	38.5	52.6	54.7	62.9	43.3	14.5	54.4	66.4	70.0	65.4
Wax	1.8	0.3	0	10.3	15.6	4.8	0.1	0	0	1.1	0.8	0
Liquid Oil Product Composition, wt%												
Aromatics	4	2	2	2	3	2	4	46	4	10	7	11
Olefins	76	83	80	43	36	82	74	25	29	72	76	68
Saturates	20	15	18	55	61	16	22	29	67	18	17	21
Liquid in Gasoline Range (BP < 204°C), wt%												
Liquid Yield, gm oil/gm cat-hr	0.13	0.08	0.05	0.09	0.13	0.39	0.27	0.07	0.27	0.41	0.42	0.38

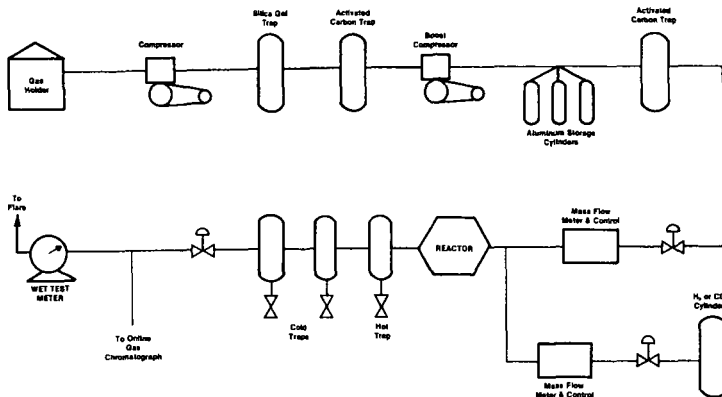


FIGURE 1. SCHEMATIC OF REACTOR SYSTEM

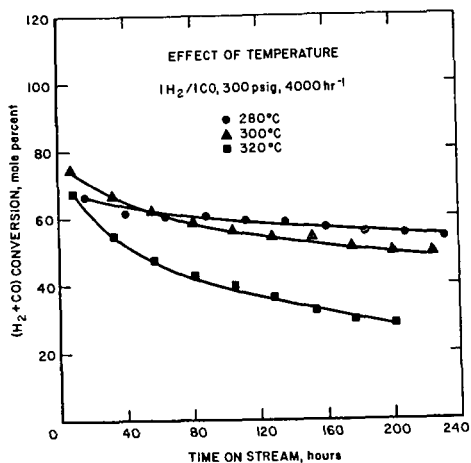


FIGURE 2. EFFECT OF REACTION TEMPERATURE ON CONVERSION WITH TIME

## R. S. Sapienza and W. A. Slegeir

Even with the recent interest in synthesis gas chemistry, the mechanisms of the various reactions and the role the catalyst plays has yet to be unequivocally established. A review of the research work carried out to elucidate the reaction mechanisms does not yield consistent conclusions in spite of the great efforts of many investigators and the use of many different scientific tools. A comparison of reaction results does not make it probable to assume basically different reaction mechanisms for different catalysts. The subtle differences noted should show greater potential for interpretation but present theories fall short of providing a unified picture capable of explaining or predicting catalyst behavior.

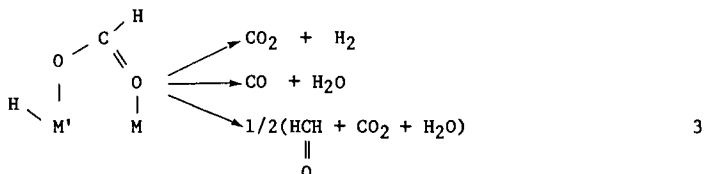
$$\begin{array}{c}
 \text{H} - \text{C} = \text{O} \\
 | \quad | \\
 \text{H} \quad \text{O} \\
 | \quad | \\
 \text{M} \quad \text{M}' \longleftarrow \text{M} - \text{M}' + \text{CO} + \text{H}_2 \\
 \uparrow \\
 \text{M}' + \text{M} + \text{CO} + \text{H}_2\text{O} \\
 \text{M}' + \text{M} + \text{CO}_2 + \text{H}_2
 \end{array}
 \quad
 \begin{array}{c}
 \boxed{\begin{array}{c} \text{O} = \text{CH}_2 \\ | \\ \text{M} \end{array}} \\
 \swarrow \\
 \begin{array}{c} \text{C} = \text{O} \\ | \quad | \\ \text{M} \quad \text{M} + \text{M} \begin{array}{c} \text{H} \\ \diagup \quad \diagdown \\ \text{H} \end{array} \end{array}
 \end{array}
 \quad
 \text{M} + \text{CO} + \text{H}_2$$
$$M + CO + H_2 \longrightarrow \begin{array}{c} C = O \\ | \quad | \\ M \quad M \end{array} \longrightarrow \begin{array}{c} O = CH_2 \\ | \\ M \cdot \end{array} \begin{array}{l} \nearrow \text{methane} \\ \longrightarrow \text{methanol} \\ \searrow \text{hydrocarbons} \end{array} \quad 2$$

171

This mechanism which integrates features of the carbide and carbenol intermediate theories<sup>(2)</sup> has been successful in developing a new series of highly active Fischer-Tropsch (F-T) catalysts.

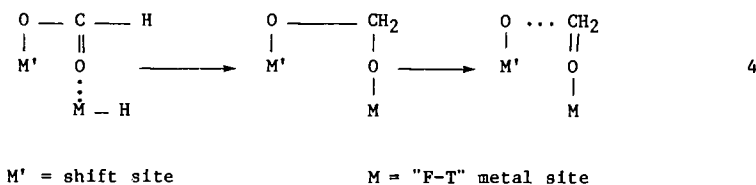
The reversibility between reduced and various oxidized states of the catalyst is an essential feature for catalyst activity in the Kolbel-Engelhardt (K-E) synthesis.<sup>(3)</sup> Active catalysis demands some sites which promote water-gas shift activity and other sites which generate F-T intermediates. It seemed probable to us that the interaction of the water-gas shift intermediates with F-T active metal sites could explain experimental observations.

Spectroscopic studies of zinc oxide, magnesia, alumina, and iron-chromia catalysts suggest that the water-gas shift reaction proceeds through surface metal formate species.<sup>(4)</sup> Other work on the decomposition of metal formates is also revealing. Their decomposition is thought to need vacant sites to occur and is enhanced by the presence of foreign metal ions.<sup>(5)</sup> A bicoordinated structure can be visualized which reacts by one of three pathways.



In such decompositions, most interest in the literature has focussed upon the dehydrogenation and dehydration reactions but the minor reaction which leads to the formation of formaldehyde became the center of our attention. Although little data on this byproduct and other organics are available and little is known about the mechanism involved, appreciable amounts (~10%) of formaldehyde are formed in formic acid decompositions catalyzed by thoria, alumina, and zinc oxide.<sup>(6)</sup>

Mechanistic studies at Brookhaven National Laboratory (BNL) indicate that the water-gas shift formate intermediate may be the important transfer agent in the Kolbel-Engelhardt synthesis, generating the surface oxymethylene intermediate on a separate "F-T" metal site.<sup>(7)</sup>



As described for the F-T reaction the metal site will determine the eventual product character and distribution (Table 1) and may explain the promoting effects of alkali metals in F-T catalysis, i.e., enhanced formate formation.

Table 1  
The Use of Various Metals for the Hydrogenation of Zinc Formate

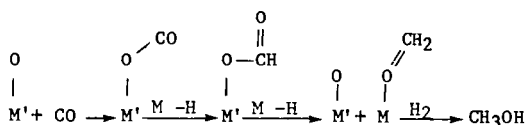
M	tCH <sub>3</sub> OH	tC <sub>x</sub> H <sub>y</sub>
Cu/ZnO	11.7	trace
Pt/Al <sub>2</sub> O <sub>3</sub>	11.5	trace
Pd/Al <sub>2</sub> O <sub>3</sub>	22.6	0.1
Ni/SiO <sub>2</sub>	trace	8.9
Co/SiO <sub>2</sub>	0.1	14.8
Fe/Al <sub>2</sub> O <sub>3</sub>	trace	2.4

---

water as solvent, 500 psi, H<sub>2</sub>, 245°C, t = mole prod/mol M'

The link between metal and metal oxide catalyzed reaction of carbon monoxide are also tied to the formate transfer reaction. (In general metal oxide syngas reactions proceed via similar reaction path with methanol as the main product.)

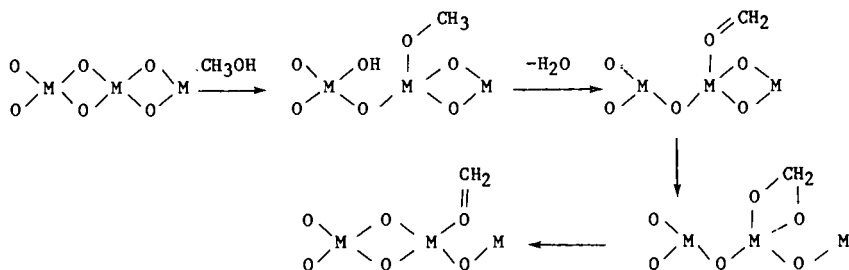
The formaldehyde-formate relationship leads to a plausible mechanism for the formation of methanol from synthesis gas. In fact, the high yield of formaldehyde (~25%) from the decomposition of zinc formate was actually considered as a commercial synthetic preparation, but was never realized. However, the reduction of the surface formaldehyde (oxymethylene) so produced was likely the cornerstone of the earliest methanol synthesis.



5

As can be seen from this hypothesis, each of the metal centers in a methanol catalyst will have a particular function. One metal can be thought of as a formate center, the other as a hydrogenating center. This description of the role of formate has been used at BNL to design new K-E and methanol catalysts.

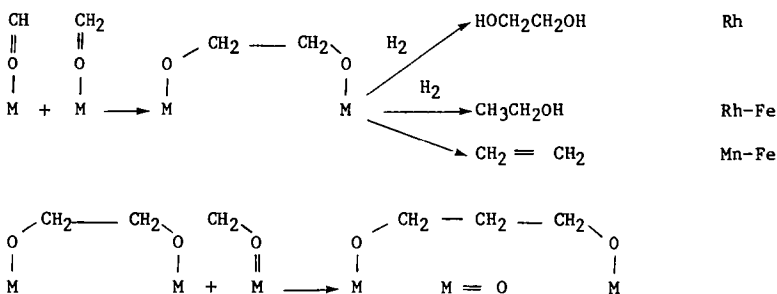
Finally, the oxymethylene species may also be involved in the initial hydrocarbons formed from methanol over non-reducible oxide catalysts. This would include products derived in the isosynthesis<sup>(2)</sup> as well as the zeolite controlled methanol conversions.<sup>(8)</sup> In both chemistries the formation of a carbenoid species from methanol seems likely. This species may be an oxymethylene formed on an acid site. As mentioned earlier, the oxide surface would allow mobility of the carbene (eq.6) and reaction with itself or other methanol molecules would be expected to yield ethylene and dimethyl ether respectively. Carbene addition to the double bond of formed olefins can also occur. This explanation is consistent with recent deuterated water observations in the conversion of methanol to ethylene<sup>(9)</sup> and is in accord with the mechanistic findings of Chang.<sup>(8)</sup>



In summary, we have proposed that a common intermediate may be involved in many synthesis gas and related conversions. This oxymethylene moiety can be derived directly from carbon monoxide and hydrogen over a metal catalyst or indirectly from a formate intermediate in reaction involving steam or on metal oxide surfaces. We believe that the oxymethylene species symbolizes the link between these chemistries and the potential route to developing new synthesis gas catalyst systems.

#### References

1. R. S. Sapienza, M. J. Sansone, L. D. Spaulding, and J. F. Lynch, "Fundamental Research in Homogeneous Catalysis", Vol. 3, M. Tsutsui, Ed., Plenum, p. 129, 1979.
2. H. H. Storch, N. Golumbic, and R. B. Anderson, "The Fischer-Tropsch and Related Synthesis", Wiley, New York, 1951.
3. H. Kolbel and F. Engelhardt, Erdöl u. Kohle 3, 529 (1950).
4. a) e.g., Y. Amenomiya and G. Pleizier, J. Catal. 76, 345 (1982).  
b) W. A. Slegeir, R. S. Sapienza, and B. Easterling, "Catalytic Activation of Carbon Monoxide", ACS Symposium Series No. 152, P.C. Ford, et., Washington, 1981.
5. a) P. Mars, J. J. F. Schotten, and P. Zwietering, Adv. in Cat., Vo. 14, 35 (1964).  
b) G. M. Shaborwa, Doklady Akad Nauk SSR 133, 1375 (1960).  
c) R. E. Eischens and W. A. Plisken, "Actes Du Deuxieme Congre's Intern. de Catalyse, Paris, 1960, pp. 789, Ed. Technip, Paris (1961).
6. a) P. Sabatier "Catalysis in Organic Chemistry" translated by E.E. Reid, Van Nostrand, NY 1923.  
b) K. Hofman and H. Schibsted, Chem. Ber. 51, pp. 1389, 1398 (1918).
7. W. A. Slegeir, Final Report, BNL-51423, October 1980.
8. a) C. D. Chang and A. J. Silvestri, J. Catal. 47, 249 (1977).  
b) C. D. Chang, J. Catal. 74, 203 (1982).
9. T. Mole and J. A. Whiteside, J. Catal. 75, 284 (1982).



175

INTERMEDIATES TO ETHYLENE GLYCOL:  
CARBONYLATION OF FORMALDEHYDE CATALYZED BY NAFION®  
SOLID PERFLUOROSULFONIC ACID RESIN

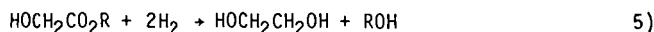
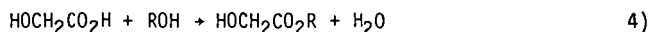
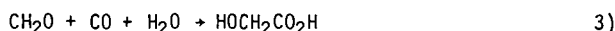
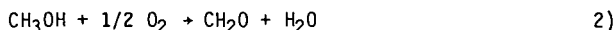
Dan E. Hendriksen

Corporate Research-Science Laboratories  
Exxon Research and Engineering Company  
P.O. Box 45  
Linden, New Jersey 07036

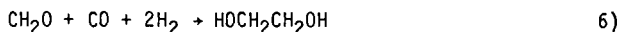
INTRODUCTION

Carbon monoxide and hydrogen can be converted to ethylene glycol by a variety of direct and indirect routes. This work explores an indirect route proceeding through the acid-catalyzed carbonylation of formaldehyde, using a novel strong acid catalyst, Nafion solid perfluorosulfonic acid resin. The glycolic acid product of this carbonylation may be esterified and then hydrogenated to yield ethylene glycol. Ethylene is presently the feedstock for ethylene glycol production; the ethylene is partially oxidized to ethylene oxide,<sup>(1a)</sup> which is then hydrolyzed to yield ethylene glycol.

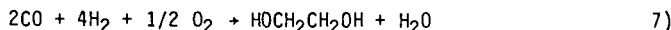
In this work, the following sequence of reactions is envisioned.



Equations 3, 4, and 5 may be combined to yield equation 6,



and the sum of equations 1 - 5 is equation 7.



In this sequence, equations 1 and 2 are the conventional processes for methanol<sup>(1b)</sup> and formaldehyde<sup>(1c)</sup> production, respectively. Both are high volume chemicals whose production technology is well-developed. The remaining transformation desired, starting with formaldehyde, is shown as equation 6. This is accomplished through the carbonylation of formaldehyde to yield glycolic acid, as shown in equation 3, followed by the esterification of this acid, equation 4, and the hydrogenolysis of the ester to ethylene glycol, equation 5.



The overall reaction from carbon monoxide and hydrogen, equation 7, is instructive since it reveals that this process essentially couples two reactions, the direct synthesis of ethylene glycol from CO/H<sub>2</sub>, equation 8,



and the burning of hydrogen, equation 9.

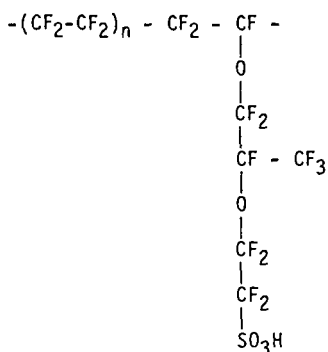


While conversion to ethylene glycol is severely limited by the unfavorable thermodynamics of the direct synthesis, equation 8, the coupling of this reaction with the highly exothermic equation 9 results in a sequence in which the high-energy intermediate formaldehyde may be quantitatively converted to ethylene glycol with no thermodynamic constraints.

It is well known that strong acids catalyze the carbonylation of formaldehyde to yield glycolic acid. Solid acid catalysts for this reaction have been explored to some extent, but there is only a single example in the patent literature of catalysis by Nafion®. In this case, the carbonylation of formaldehyde was carried out in acetic acid solvent to yield acetylglycolic acid.<sup>(2)</sup> The present work significantly extends the reaction chemistry accessible with this novel acid catalyst.

## RESULTS AND DISCUSSION

"Nafion-H" Resin.<sup>a</sup> There are several properties of DuPont's "Nafion-H" perfluorosulfonic acid resin which make it an ideal candidate for the strong acid-catalyzed carbonylation of formaldehyde. First, it is a superacid; i.e., stronger in intrinsic acidity than 100% sulfuric acid. The resin is a copolymer of tetrafluoroethylene and perfluoro-3, 6-dioxo-4-methyl-7-octensulfonic acid, resulting in a structure:



<sup>a</sup>"Nafion-H" is a convenient notation to indicate the acid form of this ion exchange resin. "Nafion" is a registered trademark of DuPont.

By analogy, one might expect the resin to be nearly as acidic as trifluoromethane sulfonic acid,  $\text{CF}_3\text{SO}_3\text{H}$ . DuPont claims that its acidity is of the same order as  $\text{AlCl}_3 \cdot \text{HCl}$ . Second, the resin is thermally very stable. DuPont states that there should be no problem with deterioration below  $175^\circ$ , and their safety data show significant decomposition only above  $270^\circ$ . Others have found the material to be stable and useful to at least  $220^\circ$ .<sup>(3)</sup> Third, the resin is swelled by polar organic solvents, allowing reactants to diffuse into the resin granules. This makes the interior acid sites available, as well as the acid sites on the catalyst surface. Furthermore, the resin is chemically inert, being deactivated only by ion exchange with e.g.,  $\text{Fe}^{3+}$ . Such deactivated catalysts are readily regenerated by the same technique used to prepare the acid form of the resin. The resin can be prepared in a range of equivalent weights from 1000 to 1800 to fit specific needs, and offers all the classic advantages of a solid catalyst in the ease of separation of products.

The choice of a solvent to use with Nafion-H is nontrivial. As stated, polar organic solvents are desired because they swell the resin. Acetic acid is useful but is not inert in the reactions studied here. Water and alcohols are found to decrease the activity of the catalyst when present in excess. Ethers such as glyme or diglyme were found not to be inert under reaction conditions, while THF is known to be polymerized over Nafion-H at room temperature.<sup>(4)</sup> However, p-dioxane was found to yield no GC-observable decomposition products when heated at  $150^\circ$  for 3 hours over the Nafion-H resin, and was used in most of the experiments reported here.

Carbonylation in the Presence of Water. With water present in the dioxane solvent, glycolic acid is presumably the product of formaldehyde carbonylation, as in equation 3. The most extensive series of experiments was done using these reactants. The series of experiments shown in Table I illustrates several aspects of this reaction. First, the reaction occurs readily under these conditions, giving routine yields of ca. 70% at  $150^\circ$ . The first two experiments may be compared to see that the reaction remains incomplete even after 3 hours at  $130^\circ$ , indicating a substantial temperature effect in this range. The series was run primarily to test the durability of the Nafion-H catalyst during these five reactions. The same Nafion-H catalyst was used in each of these reactions, and was only rinsed with dioxane and sucked dry on a filter between reactions. The yield of glycolic acid does indeed stay constant at  $150^\circ$ , with only a slight unexplained dip in the fourth reaction, indicating that the Nafion-H did maintain its catalytic activity through all the reactions. A different measure of this catalytic activity is the equivalent weight of the resin before and after the series. The initial equivalent weight was 1282 g/ equivalent, and afterwards was 1315 g/equivalent, a decrease in available acidity of less than three percent. This could conceivably be accounted for by washout of monomer during the first reaction.

A number of reactions were run in order to determine the effect of carbon monoxide pressure on the yield of glycolic acid in this system. The results are shown in Table II. With the other reaction conditions constant, the yield did increase from 50% to 80% upon increasing the pressure from 1500 psi to 4500 psi. While this does indicate that increasing the pressure of CO results in higher yields, the data should not be interpreted as showing that high pressures are required for high yields. The equipment used here was a rocking autoclave, and more efficient stirring may well enhance the efficiency of the reaction.

One reaction was done with a mixture of hydrogen and carbon monoxide to verify that the presence of hydrogen would have no effect on the yield. This run is also shown in Table II. The yield, 73%, is slightly higher than in comparable runs without hydrogen, but no significance is attached to this. In the presence

of this Nafion-H acid catalyst the hydrogen is expected to act only as a diluent, requiring proportionately higher total pressures to achieve the same carbon monoxide partial pressure as in the absence of the hydrogen.

The effect of water on the yield of glycolic acid in this reaction system was also explored. These data are shown in Table III-1. The amount of formaldehyde in these runs was reduced so that the initial mole ratio of water to Nafion-H could be varied and held approximately constant during a run, without being affected by the reaction. This molar ratio of water to Nafion-H was expected to change the effective acidity of the Nafion-H, which would in turn affect the yield in a given time. The reaction with the most water present, a 20:1 ratio of  $\text{H}_2\text{O}$  to  $\text{H}^+$ , did not result in complete conversion of the formaldehyde. Decreasing the ratio results in an optimum yield at a 5:1 ratio of water to acid. Decreasing the ratio still further to 2:1 and even 1:1 surprisingly results in a constant yield of about 50% glycolic acid (analyzed as methyl glycolate after conversion to the ester). Such yields in the presence of only half as much water as formaldehyde raise the question of whether glycolic acid is truly the reaction product, or whether dehydrated forms of glycolic acid such as the cyclic dimer glycolide, Figure 1a, or oligomers, Figure 1b, might not be the actual products.

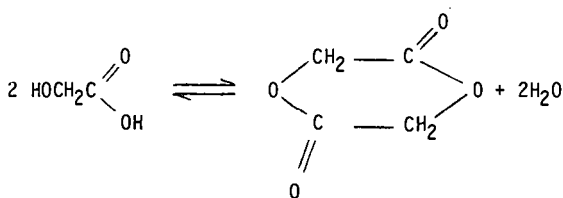


FIGURE 1a. Formation of Glycolide

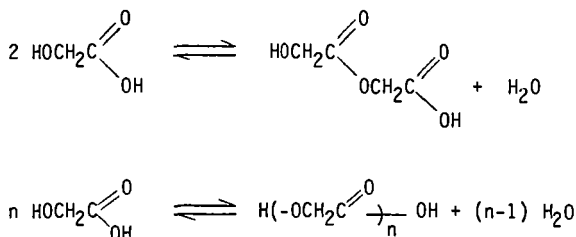


FIGURE 1b. Formation of Glycolic Acid Oligomers

An indication that these dehydrated forms of glycolic acid are the actual products under these reaction conditions was gained from a semi-quantitative GC analysis of these reaction solutions for water. This analysis showed that all the water initially added to the reaction solution was still present in solution at the end of the reaction, and consequently could not be combined as glycolic acid. A reaction with no water added was included in an earlier series, shown in Table III-2. These three reactions also indicate that there is an optimum water to acid ratio, but a yield of even 25% with no water added is somewhat surprising. All these data demonstrate that too much water in the reaction solution reduces formaldehyde

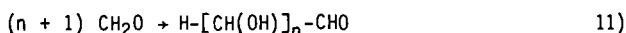
conversion and concomitantly glycolic acid yield, but the results at the lower levels of water are less definitive.

The preceding data show that in these reactions the conversion of formaldehyde is complete, or nearly so, while the yield of glycolic acid is always substantially less than quantitative. There are obviously by-products in this reaction. This subject has not been extensively investigated, but some comments on the suspected by-products and their mode of formation can be made.

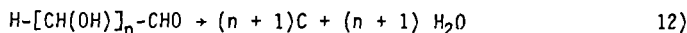
The most likely side reaction is the acid-catalyzed reaction of formaldehyde with itself, instead of the desired acid-catalyzed reaction with carbon monoxide. One such reaction is the formation of methyl formate from formaldehyde,<sup>(6a)</sup> equation 10,



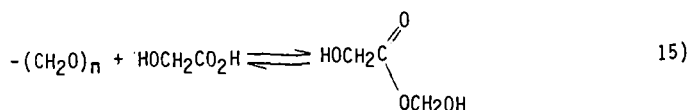
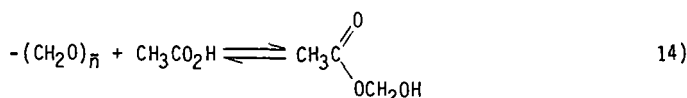
but no evidence has been found to support this. Another possibility is the acid-catalyzed condensation of formaldehyde to polyhydroxy aldehydes, equation 11.



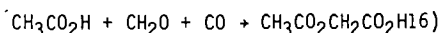
This reaction would be similar in stoichiometry to the formose reaction,<sup>(5)</sup> the base catalyzed condensation of formaldehyde to sugars and a mixture of polyhydroxy aldehydes. The solutions after reaction were varying shades of brown, and the Nafion-H sometimes turned a dark brown or even black, especially when the reaction contained little water or was exposed to high temperatures. This is reminiscent of the acid-catalyzed carbonization of sugars, equation 12.



If these ideas about the nature of the byproducts are correct, then one approach to suppress the condensation of the formaldehyde would be to chemically separate the formaldehyde monomers with a solvent or an added component. The Nafion-H, as a strong acid, rapidly catalyzes polymerization of formaldehyde to polyoxymethylene (paraformaldehyde), and catalyzes the corresponding depolymerization at higher temperatures as well.<sup>(6a)</sup> Therefore, a reversible chemical interaction is needed to separate the formaldehyde monomers while permitting the carbonylation to proceed. Examples of such interactions to form unstable adducts are reaction with water, equation 13, to form methylene glycol;<sup>(6b)</sup> with acetic acid, equation 14), to form the unstable methylene glycol ester;<sup>(6c)</sup> and analogously with glycolic acid, equation 15.



Other investigators have disclosed the use of acetic acid as a solvent to yield acetyl glycolic acid, equation 16, using a Nafion-H catalyst.<sup>(2)</sup> In the sulfuric

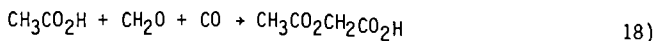
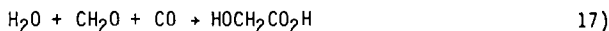


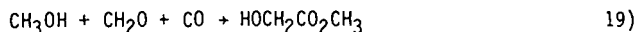
acid catalyzed reaction, glycolic acid has been disclosed as a useful solvent for enhancing yields.<sup>(7)</sup> However, data obtained in this study and shown in Tables IV-1 and IV-2 indicate that an equimolar amount of acetic acid has no effect in this reaction. In the absence of water the acetic acid actually decreases the yield. Glycolic acid, whether added wet or dehydrated, also decreases the yield of glycolic acid from formaldehyde. The reason for this decrease in yield is not readily apparent.

This Nafion-H catalyzed carbonylation of formaldehyde in dioxane/water has a number of aspects which make it an attractive intermediate reaction in a process for ethylene glycol preparation. A summary of these favorable aspects is as follows:

1. The Nafion-H solid acid catalyst is easily separated from the reaction products, a classic advantage of heterogeneous catalysts.
2. As demonstrated by others, solid acid resins similar to Nafion-H appear to be virtually non-corrosive.<sup>(2)</sup>
3. The catalyst is thermally stable, has shown no loss of activity with use, and is easily regenerable if necessary, e.g., due to contamination with other cations. Polar solvents swell the catalyst, which allows utilization of interior acid sites.
4. The acid catalyst retains its activity in the presence of substantial amounts of water; therefore, dry formaldehyde (as trioxane or paraformaldehyde) is not required.
5. The reaction is not affected by hydrogen, which acts only as a diluent for the carbon monoxide. The catalyst has no activity for the undesired reduction of formaldehyde to methanol. Consequently, synthesis gas could be used without separation or the carbon monoxide could be concentrated before use, and the separated hydrogen subsequently used for hydrogenolysis of the glycolic acid ester.
6. The reaction proceeds under reasonable conditions of temperature and pressure.
7. The glycolic acid product is stable to further reaction.
8. The dioxane solvent appears inert under reaction conditions.

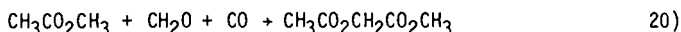
Carbonylation in Ester Solvents. The acid-catalyzed carbonylation of formaldehyde has been carried out with water as discussed above, equation 17, with acetic acid, equation 18, and with methanol,<sup>(8),(9)</sup> equation 19.



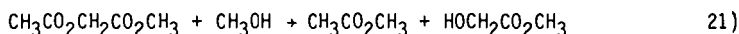


The reaction with acetic acid as solvent is reported to be efficient and specific, but the acetyl glycolic acid product must be hydrolyzed and then esterified before it can be hydrogenated to ethylene glycol. The reaction with methanol as solvent would be ideal if it yielded only the methyl ester. However, substantial yields of alkoxy acids and their esters are also invariably produced in the presence of alcohols. These may be hydrogenated to glycol ethers, useful as solvents, but cannot serve as intermediates to ethylene glycol.

The reaction using an ester as solvent, e.g. methyl acetate in equation 20, appears not to have been reported before.



The product of the reaction with an ester, in this case methyl acetyl glycolate, can be transesterified, e.g. with methanol as in equation 21 to yield methyl glycolate and regenerate methyl acetate.

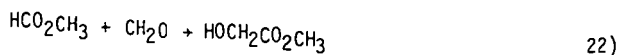


The methyl acetate can then be separated and the methyl glycolate hydrogenated to ethylene glycol.

Some formaldehyde carbonylations using methyl acetate as solvent are shown in Table V-1. It may be seen from the first reaction that the yield of methyl acetyl glycolate, intermediate to ethylene glycol, is over 60%, but there is also some production of methyl methoxyacetate, 15% in this case. In the analysis of the reaction products from this run it was noted that some acetic acid was formed, presumably from the methyl acetate. The second reaction demonstrates that adding a small amount of acetic acid at the beginning of the reaction does not affect the yields of the two products. Addition of methanol at the beginning of the reaction has a profound effect, however, as shown in the third reaction. This may be because the formaldehyde is converted to methylal,  $(\text{MeO})_2\text{CH}_2$ , by the added methanol. All the formaldehyde not accounted for in the products was recovered as methylal. Addition of water at the beginning of the reaction also decreases the yield of methyl acetyl glycolate, and results in the formation of some free acids, notably methoxyacetic acid.

Methyl formate was also tested as an ester solvent, with typical results shown as the first reaction in Table V-2. The main reaction product expected here is methyl formyl glycolate,  $\text{HCO}_2\text{CH}_2\text{CO}_2\text{CH}_3$ , but methyl glycolate, possibly derived from the former product by decarbonylation, is also found. Methyl methoxyacetate is formed in even greater yield than with methyl acetate as solvent.

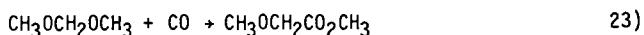
A unique aspect of the reactions using methyl formate as solvent is that no CO pressure needs to be applied, as the second reaction in Table V-2 confirms. The methyl formate presumably acts as a source of CO, and the overall reaction in equation 22 results.



This reaction has been investigated by others using different strong acids.

The carbonylation of formaldehyde using Nafion-H resin does proceed in ester solvents, but not with complete selectivity to intermediates to ethylene glycol. The reaction might nevertheless be interesting as a means of coproducing ethylene glycol and glycol ethers.

Reactions of Methylal. In the preceding work using ester solvents the focus was on intermediates to ethylene glycol, avoiding the alkoxy esters or acids which can be produced as byproducts. These alkoxy esters or acids do have value, however, since they can be hydrogenated to glycol ethers, which are articles of commerce and are useful as solvents. Consequently, some reactions were run to determine if methylal could be carbonylated to methyl methoxyacetate efficiently and selectively over Nafion-H resin, as in equation 23.

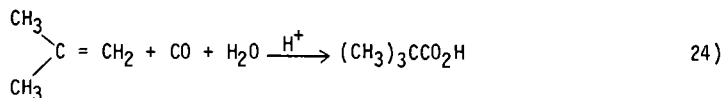


The results are shown in Table VI. The first reaction was carried out in dioxane solvent and resulted in only modest yields of both methyl methoxyacetate and methyl glycolate. Using a mixed methanol/dioxane (50:50) solvent resulted in no reaction at all. When methyl acetate was used as the solvent though, a good yield of both methyl methoxyacetate and methyl acetyl glycolate resulted; the former was not produced selectively.

There could be some question over whether methyl glycolate is inert to further reaction in this catalyst system, or if it can be methylated by the Nafion-H to form methyl methoxyacetate. One reaction was run in order to test this possibility. Methyl glycolate was reacted in a mixed methanol/dioxane solvent (10/40 by volume) over the Nafion-H resin using standard reaction conditions. No methyl methoxyacetate was found in the reaction solution, and the methyl glycolate was recovered quantitatively.

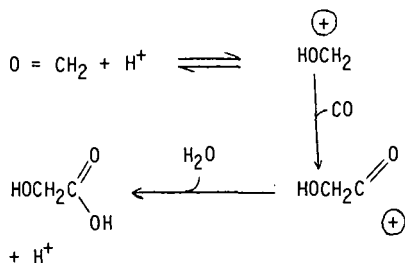
These results indicate that methylal can be carbonylated efficiently to methyl methoxyacetate, especially in ester solvents, but the reaction is not selective and results in substantial amounts of intermediates to ethylene glycol as well.

Aspects of the Mechanism. The acid-catalyzed reaction of formaldehyde with carbon monoxide belongs to the class known as Koch reactions.<sup>(10)</sup> The Koch reaction usually refers to the reaction of an olefin with carbon monoxide, as exemplified by the reaction of isobutene with CO and water, equation 24, to product pivalic acid.



The first step in a Koch reaction is formation of a carbonium ion from the substrate and the acid catalyst. The carbonium ion then adds carbon monoxide to form a more stable acylium ion. This finally reacts with water to form the

free acid, or with an alcohol to form an ester. The reaction with formaldehyde is:



The ease with which the Koch reaction takes place depends on how easily the substrate is protonated. Protonation of formaldehyde requires a strong acid; some data on the proton affinity of formaldehyde have been obtained.<sup>(11)</sup>

## EXPERIMENTAL

**Materials:** Glycolic acid was obtained as wet crystals (Aldrich) or 70% aqueous solution (Pfaltz & Bauer). It was analyzed by titration with 0.1 M NaOH using a phenolphthalein indicator. The "Nafion" 501 perfluorosulfonic acid resin was obtained as a sample from the Plastic Products Division of DuPont. This material consists of granules nominally 0.2 to 0.5 mm in diameter, and has an equivalent weight of about 1200. It was received as the potassium sulfonate and was converted to the acid form and analyzed essentially as recommended by DuPont. Conversion to the acid form is achieved by soaking the resin about five times in 4 M HCl, allowing time for exchange and with superficial washing with distilled water between HCl treatments. This is followed by washing with distilled water until the washings show a neutral pH, after which the material is dried in a vacuum oven overnight at about 110°. The Nafion-H was stored in sealed jars or in a desiccator as it can absorb appreciable amounts of water from the air. Analysis of the acid form was carried out by soaking the resin in water with an excess of sodium chloride, and titrating the liberated HCl with 0.1 M NaOH. Dioxane was dried by refluxing over calcium hydride followed by distillation. All other materials were reagent grade and used as received.

**Reactions:** The reactions with carbon monoxide were carried out in a 300 cc rocking autoclave equipped with a glass liner, which contained 50 cc of reaction solution over the Nafion-H. Carbon monoxide was introduced before heating. The starting time of the reaction was taken as the time the autoclave reached temperature (after approximately 30 minutes) and the autoclave was allowed to cool and rock overnight after the heat was turned off at the end of the reaction time. Formaldehyde was added as trioxane, the cyclic trimer; 8g, or ~6 mequiv Nafion-H was used in each run, and ~50 ml of p-dioxane was used as solvent.

**Analysis of Reaction Products:** Analysis of the products was by gas chromatography using peak area integration and a hexadecane internal standard. Since glycolic acid gave poor sensitivity and reproducibility, this product was analyzed as methyl glycolate by refluxing the entire reaction solution, including the Nafion-H, with an excess of methanol before GC analysis. A semi-quantitative estimate of the unreacted formaldehyde could be made through analysis of the methylal resulting from reaction of methanol with the formaldehyde. These analyses used a 6' x 1/8" Carbowax 20 M column, programming from 80° to 225° at



2°/min. A blank run, substituting a known amount of glycolic acid for formaldehyde, verified the utility of this analysis for glycolic acid. The reaction (mole ratios: glycolic acid, 10: water, 3.5: Nafion-H, 1; 150°, 3h,  $P_{CO} = 2500$  psi) resulted in analysis for 96% of the added glycolic acid. This result also indicates that the glycolic acid, once formed, is inert to further reaction under these conditions. This is in contrast to a catalyst system in which further carbonylation to malonic acid followed by decarboxylation to acetic acid proved to be a major problem.<sup>(12)</sup>

#### Preparations:

(1) Methyl glycolate,  $HOCH_2CO_2CH_3$ , (MG), was prepared by thermal reaction between dehydrated glycolic acid and excess methanol at 210° for 10 hours in a rocking autoclave.<sup>(13)</sup> The glycolic acid was dehydrated in a rotary evaporator by raising the temperature slowly to 180°. <sup>(13)</sup> Methyl glycolate was distilled under vacuum (22 mm, 61°) b.p. 150°, lit. 151.1°. <sup>(14a)</sup>

(2) Acetylglycolic acid,  $CH_3CO_2CH_2CO_2H$ , was prepared by heating dehydrated glycolic acid with excess acetic acid 10h at 200°. The product was recrystallized from ether/toluene. m.p. 63-65°; lit. 66-68°. <sup>(14b)</sup>

(3) Methyl acetylglycolate,  $CH_3CO_2CH_2CO_2CH_3$ , (MAG), was prepared by reaction of methyl glycolate with acetyl chloride in methyl acetate solvent. The product was distilled under vacuum; b.p. 82-83° at 22 mm.

(4) Methyl methoxyacetate,  $CH_3OCH_2CO_2CH_3$ , (MMAc), was prepared by refluxing commercially obtained methoxyacetic acid with an excess of methanol over Nafion-H and distilling the product; b.p. 128°, lit 131°. <sup>(14c)</sup>

#### ACKNOWLEDGMENTS

I would like to thank Joseph A. Olkusz, Jr., for experimental assistance and also Theodore Gaydos and Raymond Kacmarcik for help during the final stages of this work. I also thank Drs. Daniel Vaughan and Charles Fischer of the Plastic Products Division of DuPont for information about "Nafion" 501 and for the sample used in this work.

TABLE I

CARBONYLATION OF FORMALDEHYDE TO GLYCOLIC ACID  
DURABILITY TEST USING THE SAME NAFION-H CATALYST<sup>a</sup>

Temperature	Time	$P_{CO}$	Unreacted Formaldehyde	Yield Glycolic Acid
130	3 h	2600	29%	38%
150	3 h	2700	5%	63%
150	5 h	2600	4%	68%
150	5 h	2700	6%	56%
150	5 h	2700	4%	69%

<sup>a</sup>Mole ratios:  $H_2O$ , 10:  $CH_2O$ , 10:  $H^+$ , 1.

TABLE II

CARBONYLATION OF FORMALDEHYDE TO GLYCOLIC ACID.  
DEPENDENCE OF YIELD ON CARBON MONOXIDE  
PRESSURE, AND A REACTION IN THE PRESENCE OF HYDROGEN<sup>a</sup>

<u>P<sub>CO</sub> (psig)</u>	<u>Yield Glycolic Acid</u>	<u>Time</u>
1500	48%	5 h
2500	61%	5 h
4600	79%	3 h
<hr/>		
3000 <sup>b</sup>	73%	3 h

<sup>a</sup>Mole ratios: H<sub>2</sub>O, 10: CH<sub>2</sub>O, 10: H<sup>+</sup>, 1; Temperature 150+°C.

<sup>b</sup>The gas used was 4000 psi of 25:75 H<sub>2</sub>:CO.

TABLE III

CARBONYLATION OF FORMALDEHYDE TO GLYCOLIC ACID.  
DEPENDENCE OF YIELD ON H<sub>2</sub>O/H<sup>+</sup> RATIO<sup>a</sup>

MOLE RATIOS						
	<u>H<sub>2</sub>O</u>	:	<u>CH<sub>2</sub>O</u>	:	<u>H<sup>+</sup></u>	<u>Yield Glycolic Acid</u>
1.	20		2		1	36% <sup>b</sup>
	10		2		1	44%
	5		2		1	57%
	2		2		1	49%
	1		2		1	48%
- - - - -						
2.	20		10		1	61%
	10		10		1	72%
	0		10		1	25%

<sup>a</sup>Time, 3h; P<sub>CO</sub>, 2500 psi; Temperature 150+°C

<sup>b</sup>Incomplete conversion

TABLE IV-1

EFFECT OF ADDED ACETIC ACID<sup>a</sup>

MOLE RATIOS						Yield Glycolic Acid	
<u>AcOH</u>	:	<u>H<sub>2</sub>O</u>	:	<u>CH<sub>2</sub>O</u>	:	<u>H<sup>+</sup></u>	
--		10		10		1	72%
10		--		10		1	40%
10		10		10		1	71%

<sup>a</sup>Time, 3h; Temperature, 150+°C; P<sub>CO</sub>, 2500 psi

TABLE IV-2

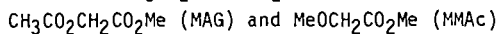
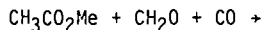
EFFECT OF ADDED GLYCOLIC ACID

<u>Time</u>	<u>P<sub>CO</sub></u>	<u>Initial HOCH<sub>2</sub>CO<sub>2</sub>H</u>	:	<u>H<sub>2</sub>O</u>	:	<u>CH<sub>2</sub>O</u>	:	<u>H<sup>+</sup></u>	<u>Yield Glycolic Acid<sup>a</sup></u>
2 h	2500	11		4		12		1	40%
3 h	4000	12		(-8) <sup>b</sup>		10		1	13%

<sup>a</sup>Yield = (total yield - amount added)/moles CH<sub>2</sub>O; Temperature, 150+°C

<sup>b</sup>The initial added glycolic acid was 66% dehydrated.

TABLE V-1

CARBONYLATION OF FORMALDEHYDE IN METHYL ACETATE<sup>a</sup>

Added Component	Added Comp/CH <sub>2</sub> O	% YIELDS		Notes
		MAG	MMAc	
--	--	61	15	b
Acetic Acid	1	63	13	
Methanol	2	18	23	c
Water	1	31	18	d

<sup>a</sup>Time, 3h; Temperature, 150°; P<sub>CO</sub>, 2500 psi; Mole ratios: CH<sub>2</sub>O, 10: H<sup>+</sup>, 1.

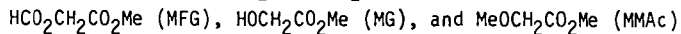
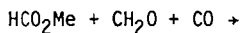
<sup>b</sup>Acetic acid found in reaction products.

<sup>c</sup>Methylal yield was 58%.

<sup>d</sup>Also substantial yields of methyl glycolate (18%) and methoxyacetic acid, CH<sub>3</sub>OCH<sub>2</sub>CO<sub>2</sub>H. Time = 0.5 h.

TABLE V-2

## CARBONYLATION OF FORMALDEHYDE IN METHYL FORMATE



% YIELDS			
MFG	MG	MMAc	Notes
11	11	31	a
5	17	21	b

<sup>a</sup>Temperature, 150°, P<sub>CO</sub>, 2500 psi; Time 3h.

<sup>b</sup>No CO added, ΔP = +200 psi; Temperature, 150°; Time, 5h.

TABLE VI

CARBONYLATION OF METHYLAL TO  
 $\text{MeOCH}_2\text{CO}_2\text{Me}$  (MMAc),  $\text{HOCH}_2\text{CO}_2\text{Me}$  (MG), and  $\text{CH}_3\text{CO}_2\text{CH}_2\text{CO}_2\text{Me}$  (MAG)<sup>a</sup>

<u>Solvent</u>	<u>% YIELDS</u>		
	<u>MMAc</u>	<u>MG</u>	<u>MAG</u>
dioxane	20	17	not a product
methanol/dioxane, 50:50	0	0	not a product
methyl acetate	49	trace	39

<sup>a</sup>Time, 3h; Temperature 150°;  $P_{\text{CO}}$ , 2500 psi; Mole ratios:  $(\text{MeO})_2\text{CH}_2$ , 10:  $\text{H}^+$ , 1.

## REFERENCES

- (1) Thomas, C. L., Catalytic Processes and Proven Catalysts. Academic Press, New York, 1970. a) p. 205; b) p. 149; c) p. 208.
- (2) Preparation of Hydroxy-carboxylic Acids and Their Derivatives. G. B. Patent 1,499,245 to D. R. Nielsen, January 25, 1978; Assignee PPG Industries, Inc., U.S. Application 570,691, filed April 23, 1975.
- (3) Pineri, M., Private communication, July 1979.
- (4) Poly(tetramethylene ether) Glycol. U.S. Patent 4,120,903 to G. Pruckmayr and R. Weir, October 17, 1978; Assignee DuPont.
- (5) Shigemasa, et al., J. Catalysis **58**, 296 (1979), and references therein.
- (6) Walker, J. F., Formaldehyde. 3rd edition, R. E. Krieger Publishing Company, Huntington, New York, 1975. a) p. 253; b) p. 55; c) p. 345.
- (7) Process for the Preparation of Glycolic Acid. U.S. Patent 2,153,064 to A. T. Larson, April 4, 1939; Assignee E. I. DuPont.
- (8) Process for the Preparation of Alkyl Glycolates. U.S. Patent 2,211,625 to D. J. Loder, August 13, 1940; Assignee DuPont.
- (9) Alkoxy Acid or Ester Preparation. U.S. Patent 3,948,977 to S. Suzuki, April 6, 1976; Assignee Chevron Research Company.
- (10) Falbe, J., Carbon Monoxide in Organic Synthesis. Springer-Verlag, New York, 1970. p. 123.
- (11) Hopkinson, A. C., Holbrook, N. K., Yates, K. and Csizmadia, I. G., J. Chem. Phys., **49**, 3596 (1968).
- (12) Catalytic Applications of Oxidative Addition of Alkyl Halides to Transition Metal Complexes. S. J. Lapporte and V. P. Kurkov in Organotransition-Metal Chemistry, Y. Ishii and M. Tsutsui, Eds., 1975, p. 199, Plenum Press, New York.
- (13) Process for the Production of Ethylene Glycol. U.S. Patent 4,087,470 to S. Suzuki, May 2, 1978; Assignee Chevron Research Company.
- (14) CRC Handbook of Chemistry and Physics, 49th edition. a) p. C-94; b) p. C-93; c) p. C-96.

## STRUCTURE AND REACTIVITY OF RHODIUM COMPLEX HYDROFORMYLATION CATALYSTS

Alexis A. Oswald, Dan E. Hendriksen, Rodney V. Kastrup  
Joseph S. Merola, Edmund J. Mozeleski and John C. Reisch\*

Exxon Research and Engineering Co., P. O. Box 45, Linden, NJ 07036  
and Exxon Chemical Co.,\* P. O. Box 241, Baton Rouge, LA 70821

### INTRODUCTION

In the present work, the reactivity and selectivity of various *t*-phosphine rhodium complex hydroformylation catalysts are correlated with their structures. Such a study is of particular interest at this time because there has been a rapid commercial development in this area during the last 10 years and because the structure of the catalyst complexes can now be well characterized by nuclear magnetic resonance spectroscopy (NMR) under simulated hydroformylation conditions.

Known triphenylphosphine rhodium carbonyl hydride and novel, more stable alkylidiphenylphosphine rhodium carbonyl hydride complexes were particularly investigated in this study. The catalyst behavior of various alkylidiphenylphosphine rhodium carbonyl hydrides was studied as a function of substitution and branching of the alkyl groups. As a result of this work rhodium complexes of alkylidiphenylphosphine were recognized as potentially highly attractive catalyst candidates of increased stability for continuous hydroformylation.

It should be recalled that the triphenylphosphine rhodium carbonyl hydride ( $\text{Ph}_3\text{P}$  complex) catalyst system was discovered by Professor Wilkinson and coworkers in the late 1960's as a low pressure, low temperature catalyst for the selective hydroformylation of 1-olefins to produce *n*-aldehydes (1). Pruett and Smith at Union Carbide Corp., and the Wilkinson group at Imperial College found in the same period that the selectivity of Wilkinson's catalyst to *n*-aldehydes was greatly increased by the addition of excess  $\text{Ph}_3\text{P}$  ligand, especially at low CO partial pressures (2). The discovery of these effects resulted in the commercial development by Union Carbide and Davy McKee of a low pressure propylene hydroformylation process based on a catalyst system containing the tris-phosphine complex and excess triphenylphosphine ligand (3,4,5).

The commercial rhodium hydroformylation process operates at about 100°C. The gaseous propylene,  $\text{H}_2$  and CO reactants are continuously introduced into a well stirred solution of the catalyst while a vapor mixture of unreacted reactants and products is being flashed off (Figure 1). The ratio of normal versus iso-butyraldehyde products in such an operation is high, in excess of ten. For an effective removal of high boiling aldehyde products in such a process, increased reaction temperatures are obviously advantageous.

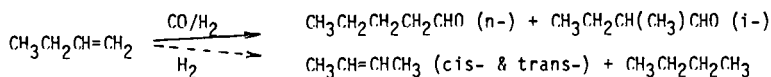
We have previously reported on our work relating to the mechanisms of triphenylphosphine rhodium complex catalyzed hydroformylations (6,7,8). We postulated that, in selective 1-*n*-olefin hydroformylation to *n*-aldehydes, the tris-(triphenylphosphine) rhodium carbonyl hydride complex is the stable precursor of the reactive trans-bis phosphine species. This postulate is based on correlating the data on equilibria among various  $\text{Ph}_3\text{P}$ -Rh complexes with hydroformylation rates and selectivities.

The structures of the various  $\text{Ph}_3\text{P}$ -Rh complexes and their equilibria were determined via NMR in the presence of varying amounts of excess  $\text{Ph}_3\text{P}$  and under different CO partial pressures. Studies of hydroformylation catalysis were carried out mainly using 1-butene as a reactant for the selective production of *n*-valeraldehyde at temperatures in excess of 100°C.

In the present work, the catalytic and structural studies were extended to various tris-(alkylidiphenylphosphine) rhodium carbonyl hydride complexes and related catalysts ( $\text{Ph}_2\text{PR}$  complexes). The previously described experimental methods were used

(6). Although the use of these catalysts was found to require higher temperatures than that of the  $\text{Ph}_3\text{P}$  complex catalysts, high selectivities toward valeraldehydes, particularly the n-isomer, could be maintained coupled with an increase in catalyst stability. Details of the work are described in Exxon patents (9). In this presentation, correlations of catalyst structure and activity are emphasized.

Using 1-butene instead of propylene in this laboratory allowed an additional insight into the reaction mechanism since isomerization side reactions producing 2-butenes could be also readily studied:

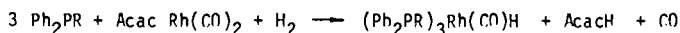


In contrast to the voluminous, prior patent literature, the present batch hydroformylation studies included not only the determination of the normal to iso (n/i) ratio of the aldehyde products but the paraffin hydrogenation and internal olefin isomerization by-products as well. A limited study of continuous hydroformylation, via a continuous product flash-off operation, was also made.

#### RESULTS AND DISCUSSION

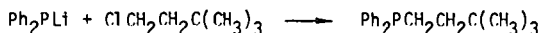
In contrast to  $\text{Ph}_3\text{P}$  complexes,  $\text{Ph}_2\text{PR}$  complexes were generally not considered for hydroformylation catalysis. For example, propyldiphenylphosphine, a  $\text{Ph}_3\text{P}$  degradation product during continuous propylene hydroformylation, was mainly regarded as a catalyst modifier rather than as a catalyst ligand on its own (10-12). In the present work, the structure and catalytic activity of  $\text{Ph}_2\text{PR}$  complexes was studied in detail and compared with those of the corresponding  $\text{Ph}_3\text{P}$  complexes.

Most of the  $\text{Ph}_2\text{PR}$  studies to be discussed were carried out with  $\text{Ph}_2\text{PCH}_2\text{CH}_2\text{C}(\text{CH}_3)_3$  and  $\text{Ph}_2\text{PCH}_2\text{CH}_2\text{Si}(\text{CH}_3)_3$  because they readily provided crystalline rhodium carbonyl hydride complexes. When an excess of these ligands was reacted with ethanolic solutions of rhodium dicarbonyl acetyl acetonate and then hydrogen at ambient temperature, the corresponding tris-phosphine complexes were formed as pure crystalline precipitates. The following overall reaction took place



The same reaction occurred when other alkylidiphenylphosphines were used. However, most of the products separated as oils.

Most of the alkylidiphenyl phosphine reactants used were prepared in our laboratory. The preferred displacement approach to these compounds involved the reaction of lithium diphenylphosphide with the appropriate alkyl chlorides in tetrahydrofuran, e.g.



The addition approach utilized the free radical chain addition of diphenyl phosphine to the corresponding olefins. The additions were initiated by irradiation with broad spectrum ultraviolet light and preferably employed activated olefinic reactants at a reaction temperature of about 15°, e.g.



On changing the structure of the alkyl group of the  $\text{Ph}_2\text{PR}$  ligands, major changes in catalyst activity were observed, primarily due to steric crowding. Steric crowding affected the structure and stability of the  $\text{Ph}_2\text{PR}$  complexes formed. The structure of the catalyst complexes, in turn, determined reactivity and selectivity.

All the findings including hydrocarbon by-product formation, could be corre-



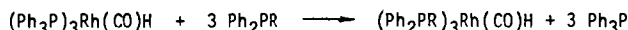
lated with changing equilibria between the catalyst complexes present in hydroformylation systems and with the steric and electronic effects of ligands on such equilibria. These equilibria and the critical reaction steps are shown by the outline of an overall mechanistic scheme in Figure 2.

According to the figure, coordinatively saturated alkyldiarylphosphine rhodium complexes of varying carbonylation degrees are the main components of such hydroformylation catalyst systems. Upon reversible dissociation, these unreactive complexes generate coordinatively unsaturated species which react with the olefin and in turn, with CO and H<sub>2</sub> to provide the normal and iso aldehyde products, with the regeneration of the catalyst.

### 1. Studies of Catalyst Complex Structures and Equilibria by NMR

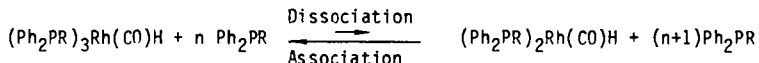
In comparative NMR studies, first the structure and stability of Ph<sub>2</sub>PR and Ph<sub>3</sub>P complexes were compared. Differences in the behavior of specific Ph<sub>2</sub>PR ligands were also studied to ascertain electronic and steric influences of substituting the R alkyl groups.

Ligand exchange studies of the tris-Ph<sub>3</sub>P complex using sterically non-crowded Ph<sub>2</sub>PR reactants generally showed substantial reaction:



The more basic Ph<sub>2</sub>PR ligand formed a more stable complex than Ph<sub>3</sub>P. In the above reaction, the ratio of complexed Ph<sub>2</sub>PCH<sub>2</sub>CH<sub>2</sub>C(CH<sub>3</sub>)<sub>3</sub> to complexed Ph<sub>3</sub>P in the -60 to + 35° temperature range was about 3.

Ligand exchange between complexed and free phosphine ligands also occurred, in a reversible manner, when there was only one phosphine present. Such an exchange took place via coordinatively unsaturated trans-bis-phosphine rhodium carbonyl hydride intermediates:



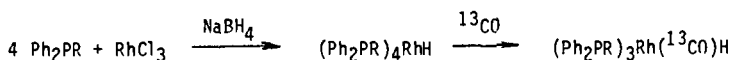
Since the equilibria strongly favor the coordinatively saturated tris-phosphine complexes, only the NMR spectra of these species could be detected. However, the rate of ligand dissociation could be determined by line shape analyses of the signals.

The qualitative aspects of the comparative <sup>31</sup>P NMR ligand exchange studies of the Ph<sub>2</sub>PCH<sub>2</sub>CH<sub>2</sub>C(CH<sub>3</sub>)<sub>3</sub>, Ph<sub>3</sub>P and Ph<sub>2</sub>PCH<sub>2</sub>CH<sub>2</sub>Si(CH<sub>3</sub>)<sub>3</sub> complex systems are indicated by the <sup>31</sup>P spectra in Figures 3a and b. At -60°C, the typical doublet signal of the tris-phosphine complexes plus singlet signals of the free phosphines were observed for all three systems. However, the doublet signal of the Ph<sub>2</sub>PR type complexes remained sharp at 35° while the Ph<sub>3</sub>P complex exhibited a broad doublet. Similarly, the Ph<sub>2</sub>PR complex still showed a very broad doublet at 60° where the doublet of the Ph<sub>3</sub>P complex had already collapsed. Further increases in the ligand exchange rates, resulted in a single composite signals for the Ph<sub>3</sub>P and Ph<sub>2</sub>PR systems at 90° and 120°, respectively.

Clearly higher temperatures in the Ph<sub>2</sub>PR complex systems were necessary to reach ligand exchange rates comparable to that of the Ph<sub>3</sub>P complex. Since the increase in ligand exchange rate parallels that of complex dissociation to yield coordinatively unsaturated species, these data indicate that in the Ph<sub>2</sub>PR complex systems a comparable generation of such reactive species occurs at higher temperatures. This suggests that to achieve comparable hydroformylation rates, higher temperatures are needed when complexes of Ph<sub>2</sub>PR are used in place of Ph<sub>3</sub>P. On the other hand, at the higher temperatures, the Ph<sub>2</sub>PR complexes are more stable than the Ph<sub>3</sub>P complex.

In view of recent suggestions, of a potential CO dissociation from the tris-Ph<sub>3</sub>P complex to generate hydride species leading to n-aldehyde products (13, 14), ligand exchange was also studied by <sup>13</sup>C NMR. For these studies, <sup>13</sup>CO enriched tris-

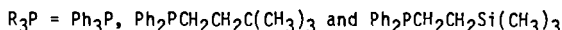
phosphine complexes were used. Such complexes could be readily derived by reacting the corresponding tetrakis-phosphine rhodium hydride complexes with  $^{13}\text{CO}$  at atmospheric pressure. For example, the following sequence of reactions was carried out with  $\text{Ph}_2\text{PCH}_2\text{CH}_2\text{C}(\text{CH}_3)_3$  and  $\text{Ph}_2\text{PCH}_2\text{CH}_2\text{Si}(\text{CH}_3)_3$ :



The first reaction to form the tetrakis-phosphine rhodium hydride was carried out in 10 minutes in refluxing ethanol solution in a manner reported for the  $\text{Ph}_3\text{P}$  derivative (15). The resulting crystalline hydride could be reacted with  $^{13}\text{CO}$  at room temperature either in toluene solution or ethanol suspension.

Variable temperature  $^{13}\text{C}$  NMR studies of tris-phosphine monocarbonyl hydride complexes are illustrated by Figure 4. The spectra indicate that at  $-30^\circ$ , the  $\text{Ph}_3\text{P}$  complex has the expected structure. The double quartet signals of the complexed  $^{13}\text{CO}$  show coupling to one rhodium and three phosphine ligands. At increased temperatures up to  $110^\circ\text{C}$ , this signal of the  $\text{Ph}_3\text{P}$  complex collapsed into doublets. That was the consequence of the exchange of the phosphine ligands. Rhodium coupling remained since no  $^{13}\text{CO}$  dissociation occurred. However, free  $^{13}\text{CO}$  could be detected in this system at  $140^\circ\text{C}$  when free triphenyl phosphine ligand was used as the solvent ( $\text{P/Rh} = 260$ ).

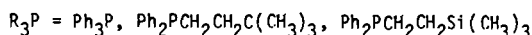
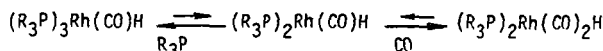
The  $^{13}\text{CO}$  NMR studies show that the CO ligand of these tris-phosphine monocarbonyl hydride complexes is very strongly bound. During hydroformylation, carbonyl free phosphine rhodium hydride complexes are not present, except under non-equilibrium CO starvation conditions. The main reaction in these systems is always phosphine rather than CO dissociation. Proton NMR studies of the hydride region of tetrakis-phosphine rhodium hydrides were known (16). The dissociation in d-toluene solutions of three tetrakis-phosphine rhodium hydrides was studied by  $^{31}\text{P}$  NMR ligand exchange methods in the presence of excess phosphine ligands in the present work.



In general, it was found that significant ligand exchange of these hydrides occurred at much lower temperatures than those observed for the corresponding carbonyl hydrides. The doublet signal of the tetrakis-triphenylphosphine rhodium hydride collapsed at  $-30^\circ$  while the corresponding  $\text{Ph}_2\text{PR}$  complexes gave broad singlet signals for complexed  $^{31}\text{P}$  at about  $+20^\circ$ . Thus it was found  $\text{Ph}_2\text{PR}$  ligands are more strongly complexed than  $\text{Ph}_3\text{P}$  in carbonyl free rhodium hydrides as well.

The increase in hydrogenation and isomerization side reactions during 1-butene hydroformylation under CO starvation conditions can be explained by the formation of carbonyl free rhodium hydride complexes. Tetrakis-triphenylphosphine rhodium hydride is a known hydrogenation catalyst (16). In the present work, it was found to be an effective 1-butene isomerization catalyst even at  $0^\circ$ . Its low temperature catalytic activity is attributed to its facile dissociation to provide the corresponding highly reactive tris-phosphine rhodium hydride.

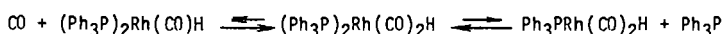
At increased CO partial pressure, tris-phosphine rhodium carbonyl hydrides are converted to the corresponding trans-bis-phosphine dicarbonyl hydrides via the following equilibrium reactions:



Complexes of  $\text{Ph}_3\text{P}$  and  $\text{Ph}_2\text{PR}$  type ligands showed similar equilibria between mono- and dicarbonyl hydride complexes.

Increased concentrations of excess phosphine ligand effectively reduced the amount of dicarbonyl hydride formed. This is illustrated by Figure 5. The figure shows that, in the absence of a significant excess of the  $\text{Ph}_2\text{PR}$  type ligand, conversion to the dicarbonyl hydride is essentially complete under about 200 kPa pressure of 1 to 1  $\text{H}_2/\text{CO}$ . However, at a five-fold excess of  $\text{Ph}_2\text{PR}$  (P/Rh ratio of 15/1) the ratio of dicarbonyl to monocarbonyl complex is only about 1 to 3.

In the case of bis-phosphine dicarbonyl hydride complexes, the relative dissociation rates of phosphine and carbonyl ligands were also studied by NMR:



A 1% solution of the bis- $\text{Ph}_3\text{P}$  complex plus excess  $\text{Ph}_3\text{P}$  to provide a P/Rh ratio of 9 were used for the study. This solution was prepared under 400 kPa  $\text{H}_2/^{13}\text{CO}$  pressure, from the tetrakis- $\text{Ph}_3\text{P}$  complex which was largely converted to the desired bis-phosphine rhodium dicarbonyl hydride. Variable temperature NMR studies indicated reversible CO and phosphine ligand dissociation.

As it is shown by Figure 6, the  $^{13}\text{C}$  NMR spectrum of the resulting solution showed the expected double triplet for the complexed  $^{13}\text{CO}$  ligand as well as the singlet signal of free  $^{13}\text{CO}$ . At +35°, the fine structure of the complexed CO disappeared. Also, the signals of complexed and free  $^{13}\text{CO}$  considerably broadened as a consequence of CO exchange. At 90°C, only one, broad  $^{13}\text{CO}$  signal was obtained due to further increased ligand exchange rates.

Similar variable temperature  $^{31}\text{P}$  NMR studies showed reversible phosphine ligand dissociation. However, a free versus bound  $\text{Ph}_3\text{P}$  ratio much below the expected value was found at low temperature. This suggests the presence of unidentified rhodium complex species undergoing rapid ligand exchange.

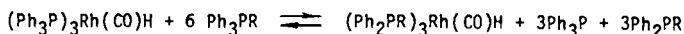
When 1-olefins are hydroformylated under conditions where the dicarbonyl hydride predominates in the above type of system, the n/i ratio of aldehyde products is greatly decreased but still remains above two. It is believed that most of the remaining preference of such catalyst systems for producing n-aldehydes is due to  $^{13}\text{CO}$  dissociation to provide the trans-bis-phosphine monocarbonyl hydride intermediate of linear hydroformylation.

The electronic effects on the properties of tris- $\text{Ph}_2\text{PR}$  rhodium carbonyl hydride catalyst complexes were studied by substituting groups of varying electrophilicity on the  $\beta$ -carbons of the alkyl groups of their ligands. The basicities of some of these ligands of general formula  $\text{Ph}_2\text{PCH}_2\text{CH}_2\text{R}'$  and their  $^{31}\text{P}$  NMR parameters of their complexes are shown by Table I.

The data of the table indicate that by appropriate electronegative  $\beta$ -substituents the proton basicity of aqueous alkylidiphenylphosphines was reduced to the level of triphenylphosphine. However, no apparent correlation could be observed between the inverse basicity values,  $\Delta\text{HNP}'\text{s}$ , and the NMR parameters. Most of the  $\text{Ph}_2\text{PCH}_2\text{CH}_2\text{R}'$  complexes showed little change of their chemical shift and coupling constant values. Also, all the  $\text{Ph}_2\text{PCH}_2\text{CH}_2\text{R}$  ligands displaced  $\text{Ph}_3\text{P}$  from its complex. Thus the observed basicity was not a major factor in the NMR data.

In view of the above study, the difference between the sterically non-hindered alkylidiphenylphosphine and triphenylphosphine complexes is apparently attributed to minor differences in their  $\pi$ -backbonding ability and steric hindrance.

Steric hindrance was found to have a major effect on the structure of the complexes formed when  $\alpha$ - and  $\beta$ - branched alkylidiphenylphosphine ligands were used. These effects were first studied by determining the degree of  $\text{Ph}_3\text{P}$  ligand displacement with such  $\text{Ph}_2\text{PR}$  ligands as indicated by the following simplified scheme



In the case of the monomethyl branched ligands, such as isobutyl-, secondary butyl- and cyclohexyl- diphenylphosphines, partial displacement occurred. The ratio of bound  $\text{Ph}_2\text{PR}$  to  $\text{Ph}_3\text{P}$  was about 3 to 2. However,  $\beta$ ,  $\beta$ - and  $\alpha,\alpha$ -dimethyl branched ligands such

as neopentyl- and t-butyl-diphenyl phosphines were not able to displace any of the  $\text{Ph}_3\text{P}$ .

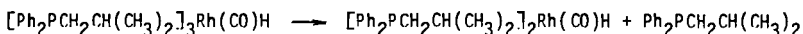
Displacement of  $\text{Ph}_3\text{P}$  by the above sterically hindered phosphine ligands could be enhanced under about 400 kpa  $\text{H}_2/\text{CO}$  pressure. This pressure results in the formation of major amounts of the bis-triphenylphosphine rhodium dicarbonyl hydride complex. The latter, in turn, was found to be more subject to displacement by the sterically demanding phosphine ligands:



Thus, at equilibrium the mixtures containing monosubstituted ligands showed the displacement of about 80% of the  $\text{Ph}_3\text{P}$  from the dicarbonyl complex. However, there was still no noticeable displacement by the neopentyl and t-butyl derivatives.

The above inhibition of ligand displacement is clearly due to steric effects. Electronic effects would result in increased ligand displacement since these branched alkylidiphenylphosphine ligands have higher basicities than their straight chain isomers.

Another effect of steric crowding is on the dissociation rate of the complexes formed. This is illustrated by the example of triphenylphosphine plus isobutylidiphenylphosphine rhodium complex catalyst system in Figure 7. The  $-30^\circ\text{C}$  spectrum of this system shows that both ligands participate in the complex formation to form four different tris-phosphine complexes. However, no distinct phosphorus signals of these complexes can be observed at ambient temperature. Only a broad phosphorus signal is observed in the complex region. This indicates a high ligand exchange rate at a relatively low temperature. This is clearly the consequence of increased phosphine dissociation due to steric decompression:



The increased dissociation rate to provide reactive coordinatively unsaturated complex species results in increased catalytic activity. However, steric crowding also results in a reduced ratio of monocarbonyl hydride versus dicarbonyl hydride complexes, i.e. reduced n/i ratio of products.

## 2. Hydroformylation Process Studies

The main aim of the present 1-butene hydroformylation studies was to determine the effect of the structure of phosphine-rhodium complex catalysts on activity, selectivity and stability. The well known  $\text{Ph}_3\text{P}$  complex catalyst system which we studied previously(6) was a catalyst primarily used for comparison in this work. As a  $\text{Ph}_2\text{PCH}_2\text{CH}_2\text{R}'$  type alkylidiphenylphosphine ligand, 2-trimethylsilyl ethyldiphenylphosphine (SEP), was studied in detail.

In the following at first, the  $\text{Ph}_3\text{P}$  and SEP based rhodium complex hydroformylation catalyst systems will be compared at different temperatures and excess phosphine concentrations. Thereafter, the detailed structural effects of various  $\text{Ph}_2\text{PR}$  ligands will be discussed with emphasis on steric crowding. The catalytic results will be correlated with the structural findings of the NMR studies.

The effect of temperature on the  $\text{Ph}_3\text{P}$  and SEP complex catalyst systems is shown in Table II. Most of the batch experiments were carried out at a one molal phosphine ligand concentration to maintain the selectivity and stability of the catalyst at increased temperatures. The results show that, at comparable temperatures, the triarylphosphine complex is always more active than the alkylidiphenylphosphine complex. However, the activity and selectivity of the latter is better maintained particularly at higher temperatures.

At the relatively low temperature of  $110^\circ$ , a lower n/i aldehyde product ratio is obtained with the SEP complex. However, there is no significant difference between

the higher n/i values of the two systems at 145°. In the 135 to 160° range, the use of the SEP complex leads to a higher total (n+i) aldehyde selectivity. This is mainly due to the reduced butene-1 to butene-2 isomerization side reactions in the presence of the more basic SEP ligand. The top temperature of 160° has generally less adverse effect on the selectivity of the SEP complex system.

The effect of increasing concentrations of the SEP and  $\text{Ph}_3\text{P}$  ligands at 145° is shown in Table III. This increase in both systems resulted in a decreased activity but increased n/i aldehyde selectivity. At high ligand concentrations, the n/i values depended on the phosphine concentration rather than on the P/Rh ratio. When these phosphines were used as the only solvents, the n/i ratios reached maximum values but the selectivities to total aldehyde products decreased.

The SEP and  $\text{Ph}_3\text{P}$  rhodium complex catalyst systems were also compared in continuous 1-butene hydroformylation, operating via product flash-off (PFO) from the reaction mixture (Figure 1). The reaction conditions and data obtained are shown by Table IV.

In the first three experiments, the SEP system was operated at 120° while the  $\text{Ph}_3\text{P}$  system was running at 100°. Most importantly the results indicate that the increased temperature of the SEP-Rh system is highly advantageous for achieving higher butene conversions without increasing the stripping gas rate. At the lower temperature of the  $\text{Ph}_3\text{P}$ -Rh system, a higher conversion operation was not feasible under these conditions because of the limited product flash-off capability due to vapor liquid equilibria. It is noted that the selectivities of the two systems are similar.

In the other three experiments, the stability of the SEP and  $\text{Ph}_3\text{P}$  based rhodium catalyst systems was compared in a six day continuous PFO operation at 145°C. The butene conversion achieved with the SEP system showed less than 10% change. The conversion in the case of the  $\text{Ph}_3\text{P}$  system dropped from 82 to 65% during the test period. About 1/2% per day of the  $\text{Ph}_3\text{P}$  ligand was converted to butyldiphenylphosphine via ortho-metalation(10). No similar degradation of the SEP ligand was observed. In addition, as shown by the table, the selectivity of the SEP complex system was somewhat higher and did not change significantly when a mixture of 1- and 2-butenes was used in place of the pure 1-butene feed. (The 2-butene is apparently of very low reactivity under these conditions).

In more detailed PFO process studies of the SEP-Rh catalyst system at 120°, complete maintenance for 30 days of both hydroformylation activity and selectivity was established. In these studies, the n/i ratios of the valeraldehyde products were correlated with the excess phosphine ligand concentration and CO partial pressure. As was expected on the basis of the NMR studies of catalyst structures, the n/i ratio was directly dependent on the [SEP] and inversely dependent on the pCO.

The catalytic properties of a high number of alkylidiphenylphosphine rhodium complexes were studied in batch experiments. Comparative results obtained with complexes of ligands of the formula  $\text{Ph}_2\text{PCH}_2\text{CH}_2\text{R}'$  and  $\text{Ph}_3\text{P}$  are shown by Table V.

The results show that, at the 1M phosphine concentrations, all the  $\text{Ph}_2\text{PCH}_2\text{CH}_2\text{R}'$  complexes are highly selective catalysts for hydroformylation at 145°. They provide aldehyde products having n/i ratios in the 8.9-18.9 range. In general, their product linearity is similar to that of the  $\text{Ph}_3\text{P}$  system (n/i = 11.2). The total aldehyde selectivity of the  $\text{Ph}_3\text{P}$  complex catalyst is higher. Their n + i aldehyde selectivity is in the 86.9 to 91.8% range while the corresponding n + i value of the  $\text{Ph}_3\text{P}$  system is 81.2. However, as expected on the basis of the NMR ligand dissociation rates, the  $\text{Ph}_3\text{P}$  system is more than twice as active.

The activity and selectivity of all these catalysts is highly dependent on the excess phosphine ligand concentration. When the phosphine ligand concentration was dropped to 0.14 M, the reaction rate usually increased about fourfold and the n/i ratio of the aldehyde products decreased to about a half of the previous value. Of course, these effects are expected on the basis of the catalytic mechanisms suggested by the NMR studies.

No definite correlation could be found between the basicity of the  $\text{Ph}_2\text{PCH}_2\text{CH}_2\text{R}'$  ligands and the catalytic properties of their rhodium complexes. Overall

the differences among these complexes were smaller than the difference between them as a group and the  $\text{Ph}_3\text{P}$  complex. The  $\text{Ph}_3\text{P}$  ligand stands out by virtue of its increased  $\pi$ -backbonding ability which weakens the CO coordination to the rhodium. Also,  $\text{Ph}_3\text{P}$  is a sterically more demanding ligand than  $\text{Ph}_2\text{PCH}_2\text{CH}_2\text{R}'$  ligands. Both properties increase the reactivity of the  $\text{Ph}_3\text{P}$ -Rh complex catalyst system.

The effect on catalysis of the steric crowding of alkyldiphenyl phosphine ligands by methyl substitution on the  $\alpha$ - or  $\beta$ -carbon atoms of their alkyl group was also studied. The comparative experiments were carried out using two different ligand concentrations at  $145^\circ$ . The results are shown by Table VI.

Compared to straight chain and  $\gamma$ -methyl substituted alkyldiphenylphosphines, the  $\alpha$ - and  $\beta$ -methyl substituted derivatives led to increased hydroformylation rates but reduced selectivities. The rate increasing effect was observed at the higher phosphine ligand concentration of 1M. The selectivities were decreased in terms of lower n/i ratios of aldehyde products and increased isomerization side-reactions to 2-butenes. The isomerization was particularly increased at the low ligand concentration of 0.14 M. At an extreme, this resulted in a reduced reaction rate since 2-butenes are much less reactive than 1-butene. The effect of steric crowding was further increased when the  $\alpha$ ,  $\alpha$ - and  $\beta$ ,  $\beta$ -dimethyl substituted alkyldiphenylphosphines were used in place of the monomethyl substituted ligands.

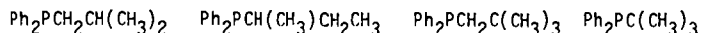
The increased reactivity of branched alkyldiphenylphosphine rhodium complexes is attributed to the accelerated dissociation via steric decompression of tris-phosphine rhodium carbonyl hydride complexes to provide reactive species. The reduced n/i ratio of the products is due to the increase of rhodium dicarbonyl hydride catalyst complexes. The increased isomerization to 2-butenes is apparently a consequence of the reversibility of reactions forming the secondary butyl rhodium complex intermediate.

#### CONCLUSIONS

The present correlation of the structure of  $\pi$ -phosphine rhodium carbonyl hydride complexes with high temperature hydroformylation catalysis data leads to the extension of our previously proposed rhodium hydroformylation mechanisms to alkyldiphenylphosphine ligand based catalysts. In view of their increased stability, alkyldiphenylphosphines are now recognized as rhodium complex catalyst ligands potentially superior to the commercially widely used triphenylphosphine.

Alkyldiphenylphosphines form remarkably stable tris-phosphine rhodium carbonyl hydride complexes of the formula  $(\text{Ph}_2\text{PCH}_2\text{CH}_2\text{R}')_3\text{Rh}(\text{CO})\text{H}$ . These act as a preferred reversible reservoir for the generation of the highly reactive, coordinatively unsaturated trans-bis-phosphine carbonyl hydride intermediates of 1-n-olefin hydroformylation to provide mostly n-aldehyde products. In accord with the complex equilibria found among variously carbonylated rhodium complex catalyst precursors, the stability and selectivity of such catalyst systems directly depends on the excess phosphine ligand concentration. It is inversely related to the partial pressure of the CO reactant. Changes in the  $\text{R}'$  group of such ligands did not result in any profound change of the catalytic properties of their rhodium complexes although they caused wide variations in their proton basicities.

In contrast branched alkyldiphenylphosphines having  $\beta$ - or  $\alpha$ - alkyl substituents e.g.



form rhodium carbonyl hydride complexes of widely differing stabilities. These complexes in turn exhibit a broad range of catalyst behavior. Tris-phosphine rhodium carbonyl hydride complexes of these ligands are thermally unstable due to steric crowding. This facilitates the generation of reactive species. Under CO pressure, complexes of these ligands are largely converted to bis-phosphine rhodium dicarbonyl hydride,  $(\text{Ph}_2\text{PR})_2\text{Rh}(\text{CO})_2\text{H}$ , intermediates of nonselective hydroformylation.

Thus profound electronic differences between sterically noncrowded alkylidiphenylphosphine and triphenylphosphine rhodium carbonyl hydride complexes resulted in two types of catalyst systems having distinct properties. In contrast, small changes in the electronic character of alkylidiphenylphosphine complexes did not cause significant changes in catalysis. However, small changes in the steric requirements of  $\alpha$ - and  $\beta$ -branched alkylidarylphosphines produced tremendous changes in the catalytic behavior of their rhodium complexes. Moderate steric crowding of such complexes may result in highly desired catalyst properties. However, such steric effects on catalysis are difficult to predict.

#### ACKNOWLEDGEMENTS

The authors wish to express their appreciation of the excellent technical assistance of R. A. Cook, M. P. Krivoshik and J. V. Vieira of the Exxon Research and Engineering Co. They also thank Exxon Chemical Co., for permission to publish this paper. Helpful discussions with Professor J. E. Bercaw of Caltech at Pasadena and Prof. E. L. Muetterties of the University of California at Berkeley are also acknowledged.

#### LITERATURE CITED

- Osborn, J. A., Jardine, F. H., Young, J. F. and Wilkinson, G., J. Chem. Soc. A, 1966, 171.
- Pruett, R. L. and Smith, J. A., Org. Chem. 1969, 34, 327; U. S. Patent 3,527,809; Evans, D., Osborn, J. A. and Wilkinson G., J. Chem. Soc. A, 1968, 3133.
- Brewster, E. A. V. and Pruett, R. L., U. S. Patent 4,247,486; Bryant, D. R. and Billig, E., U.S. Patent 4,277,627 (both assigned to Union Carbide Corp.).
- Chem. Eng. Dec. 5, 1977, 110.
- New Syntheses with Carbon Monoxide, Editor: Falbe, J., Springer Verlag, Berlin-Heidelberg-New York, 1980, Chapter 1 on "Hydroformylation, Oxo Synthesis Roelen Reaction" by Cornils, B.
- Oswald, A. A., Hendriksen, D. E., Kastrup, R. V. and Merola, J. S., Preprints, Div. Pet. Chem., Inc., Am. Chem. Soc. Natl. Meeting, Las Vegas, Nev., Spring 1982, 27 (2) 292. Advances in Synthesis Gas Chemistry Symposium, Presentation on "Rhodium Hydroformylation Mechanisms."
- Advances in Chemistry, Editors: Alyea, E. C.; Meek, D. W., American Chemical Society, 1982, 196, 78, Chapter on <sup>31</sup>P NMR Studies of Equilibria and Ligand Exchange in Triphenylphosphine Rhodium Complex and Related Chelated Bis-Phosphine Rhodium Complex Hydroformylation Catalysts" by Kastrup, R. V., Merola, J. S., Oswald, A. A.
- ACS Symposium Series Editors: Quin, L. D., Verkade, J. G., 1981, 171, 503, Chapter on <sup>31</sup>P NMR Studies of Catalytic Intermediates in Triphenylphosphine Rhodium Complex Catalyzed Hydroformylations," Oswald, A. A., Kastrup, R. V., Merola, J. S., Mozeleski, E. J.
- Oswald, A. A., Jermansen, T. G., Westner, A. A., Huang, I-D., Patent Cooperation Treaty (PCT) International Patent Publication No. WO/80/01690, August 21, 1980, British Patent Application 8,223,961, February 21, 1983, and U. S. Patent 4,298,541 (assigned to Exxon Research and Engineering Co.)
- Gregorio, G., Montrasi, G., Tampieri, M., Cavalieri d'Oro, P., Pagani, G., Andreetta, A., Chim. Ind. (Milan) 1980, 62 (5), 389.
- Paul, J. L., Pieper, L. W. and Wade, E. L., U.S. Patent 4,151,209 (to Celanese Corp.).
- Morrell, D. G. and Sherman, P. D., U.S. Patent 4,260,828 (to Union Carbide Corp.).
- Hughes, O. R. and Young, D. A., J. Am. Chem. Soc. 1981, 103, 6636.
- Unruh, J. D. and Christenson, J. R., J. Mol. Cat. 1982, 14, 19.
- Levison, J. J., and Robinson, S. D., J. Chem. Soc. A, 1970, 2947.
- Dewhurst, K. C., Keim, W. and Reilly, C. A., Inorg. Chem. 1968, 1, 546; Dewhurst, K. C., U. S. Patent 3,480,659 (assigned to Shell Oil Co.).
- Streuli, C. A., Anal. Chem. 1960, 32, 985.

Figure 1

**SCHEME OF CONTINUOUS HYDROFORMYLATION UNIT WITH  
CONTINUOUS PRODUCT FLASH-OFF**

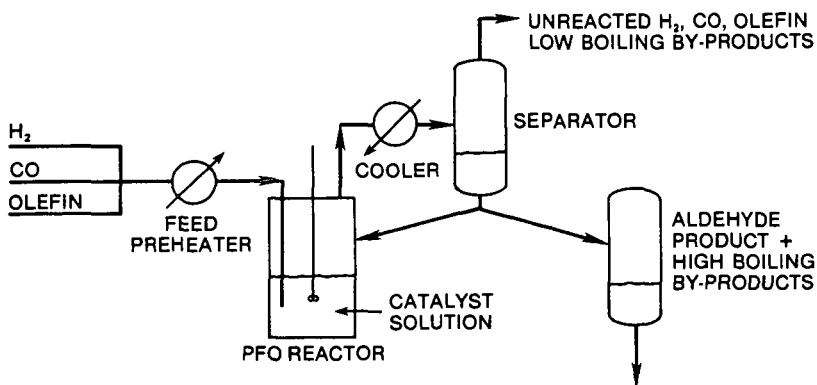


Figure 2

**CATALYTIC INTERMEDIATES IN PHOSPHINE RHODIUM  
COMPLEX CATALYZED HYDROFORMYLATION OF 1-BUTENE**

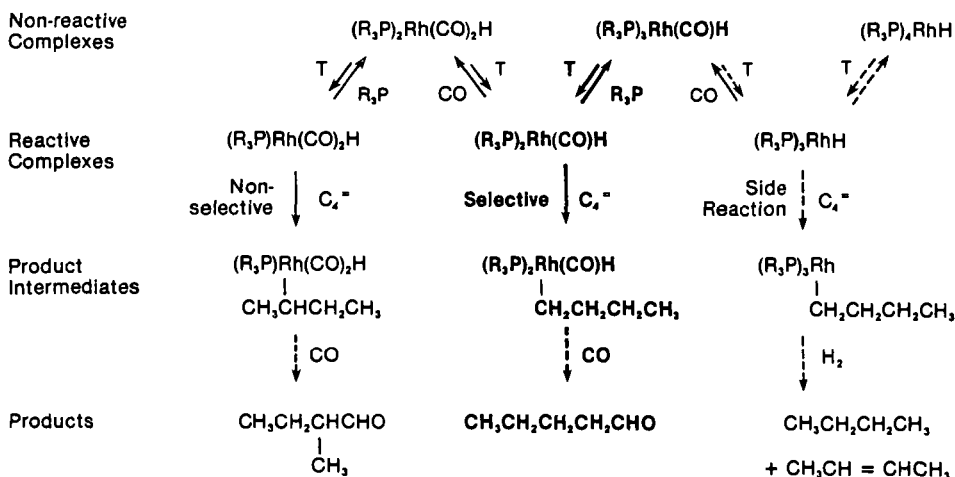




FIGURE 3  
<sup>31</sup>P NMR STUDY OF LIGAND EXCHANGE AT VARIOUS TEMPERATURES  
 (Ph<sub>3</sub>PR)<sub>3</sub>RhCOH + 6 Ph<sub>3</sub>PR  $\rightleftharpoons$  (Ph<sub>3</sub>PR)<sub>3</sub>RhCOH + 7 Ph<sub>3</sub>PR

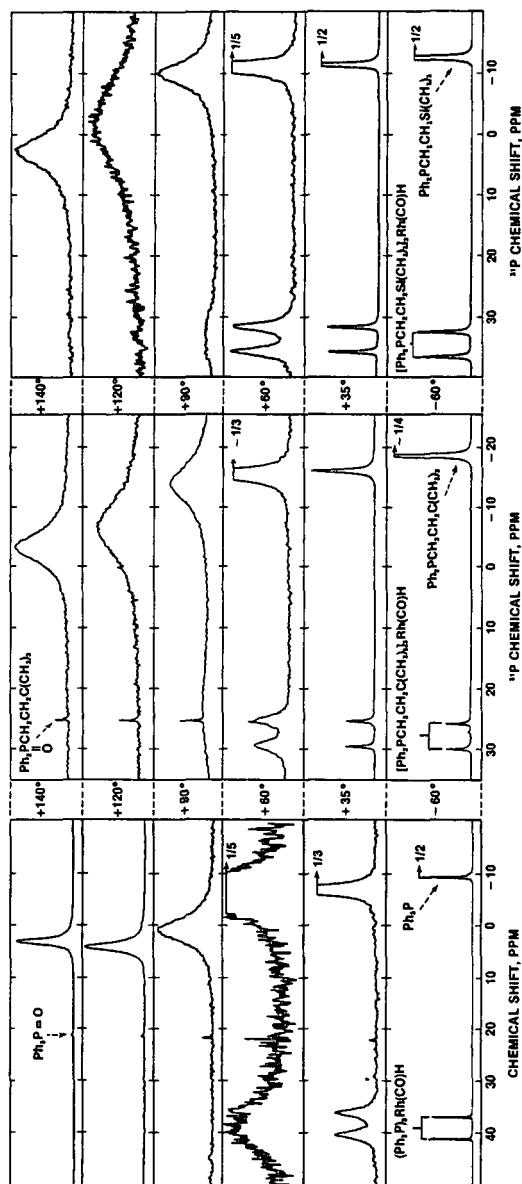


Figure 4

EFFECT OF TEMPERATURE ON  $^{13}\text{C}$  NMR SPECTRUM:  $\text{P/Rh} = 9$   
 $\text{CO} + (\text{Ph}_3\text{P})_3\text{RhH} \rightleftharpoons [(\text{Ph}_3\text{P})_3\text{Rh}(\text{CO})\text{H}] \rightleftharpoons (\text{Ph}_3\text{P})_3\text{Rh}(\text{CO})\text{H} + \text{Ph}_3\text{P}$

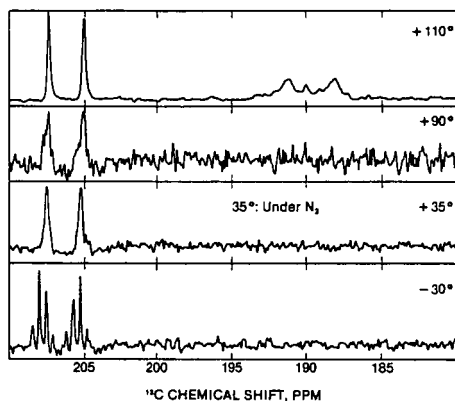


Figure 6

EFFECT OF TEMPERATURE ON  $^{13}\text{C}$  NMR SPECTRUM:  $\text{P/Rh} = 9$   
 $\text{CO} + (\text{Ph}_3\text{P})_3\text{Rh}(\text{CO})\text{H} \rightleftharpoons [(\text{Ph}_3\text{P})_3\text{Rh}(\text{CO})_2\text{H}] \rightleftharpoons \text{Ph}_3\text{PRh}(\text{CO})_2\text{H} + \text{Ph}_3\text{P}$

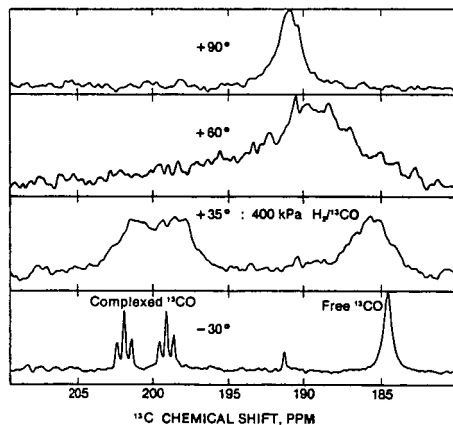


Figure 5

EFFECT OF EXCESS PHOSPHINE UNDER 200 kPa  $\text{H}_2/\text{CO}$  AT  $0^\circ$   
 $(\text{Ph}_3\text{P})_3\text{Rh}(\text{CO})_2\text{H} + n\text{Ph}_3\text{PR} \rightleftharpoons (\text{Ph}_3\text{P})_3\text{Rh}(\text{CO})\text{H} + (n-1)\text{Ph}_3\text{PR} + \text{CO}$

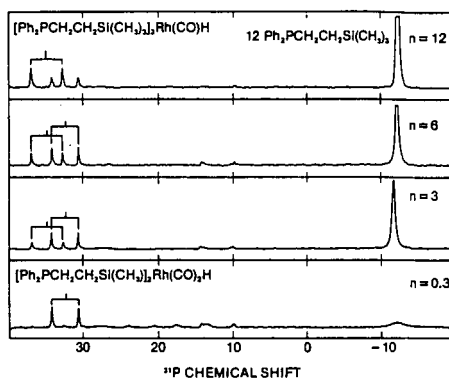


Figure 7

EFFECT OF MODERATE STERIC HINDRANCE  
 ON LIGAND DISPLACEMENT AND EXCHANGE

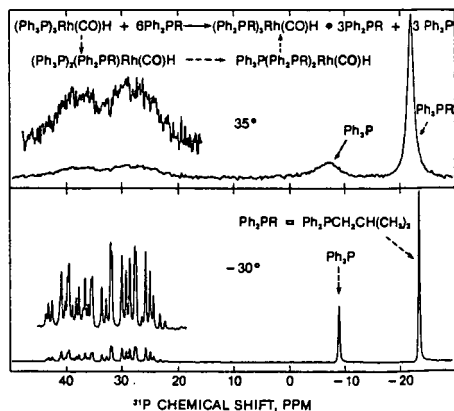


Table I

$\Delta$  HNP'S of  $\text{Ph}_2\text{PCH}_2\text{CH}_2\text{R}$  LIGANDS AND  $^{31}\text{P}$  NMR PARAMETERS<sup>a)</sup>  
OF THEIR  $(\text{Ph}_2\text{PCH}_2\text{CH}_2\text{R}')_3\text{Rh}(\text{CO})\text{H}$  COMPLEXES

Phosphine Ligand			Phosphine Complex	
Structure	Inverse Basicity, <sup>b)</sup> $\Delta\text{HNP}$	Chem. Shift ppm	Chem. Shift $\alpha$ , ppm	Coupling Constant $J_{\text{P-Rh}}$ , cps
$\text{Ph}_2\text{PCH}_2\text{CH}_2\text{Si}(\text{CH}_3)_3$	385	-12.2	34.6	150
$\text{Ph}_2\text{PCH}_2\text{CH}_2\text{C}(\text{CH}_3)_3$	412	-16.8	27.5	152
$\text{Ph}_2\text{PCH}_2\text{CH}_2\text{CH}_2\text{CH}_2\text{CH}_2\text{CH}_3$	392	-16.8	27.5	151
$\text{Ph}_2\text{PCH}_2\text{CH}_2\text{Ph}$	416	-16.6	27.6	153
$\text{Ph}_2\text{PCH}_2\text{CH}_2\text{-N} \begin{array}{c} \diagup \diagdown \\ \text{O} \end{array}$	450	-23.0	21.6	151
$\text{Ph}_2\text{PCH}_2\text{CH}_2\text{CO}_2\text{CH}_3$	455	-17.7	27.9	151
$\text{Ph}_2\text{PCH}_2\text{CH}_2\text{SO}_2\text{CH}_3$	543	-18.6	27.3	151
<hr/>				
$\text{Ph}_3\text{P}$	510	-7.5	38.3	155

- a) At 35° in toluene solvent, relative to 1M phosphoric acid.  
 b) Basicity determinations were carried out according to the modified method of Streuli(17) using perchloric acid as a titrant and pure nitromethane as a solvent. Half neutralization potentials (HNP's) were determined relative to the value of diphenyl guanidine.

Table II

EFFECT OF TEMPERATURE ON THE HYDROFORMYLATION OF 1-RUTENE WITH  
TRIS-PHOSPHINE RHODIUM CARBONYL HYDRIDE CATALYSTS USING TRIPHENYLPHOSPHINE  
(TPP) AND 2-TRIMETHYLSILYL-ETHYLDIPHENYLPHOSPHINE (SEP) AS LIGANDS

Reactions at 2500 kPa of 5/1H<sub>2</sub>/CO with 20g 1-Butene Plus 80g Mixture of 1 M Phosphine  
Ligand Plus 2-Ethylhexyl Acetate Using AcacRh(CO)<sub>2</sub> as Catalyst Precursor

Seq. No.	Li-gand	Temp. °C	Rh Conc. mM	H <sub>2</sub> /CO Feed	Ratio Final	H <sub>2</sub> /CO Consumption Dependent Factors (at 50% Conversion)				Product Parameters					
						Normal-ized at 1 M Rh	Rate Constant k min <sup>-1</sup>	Re-action Time min	Aldehyde Linearity		Aldehyde Selectivity %	By-Products Selectivity %	2-Bu-tenes	Ru-tane	
									n/i Ratio	100n					
										n + i	n				i
												Total n + i			
													n + i	n	
1	SEP	110	4.00	52/48	4.9	8	0.032	22	7.6	88.4	93.9	83.0	10.9	4.3	1.8
2		125	1.00	52/48	4.6	26	0.026	27	8.2	89.1	94.1	83.8	10.3	4.0	1.9
3		135	1.00	53/47	5.1	46	0.046	15	9.8	90.8	90.2	81.9	8.3	5.9	3.9
4		145	1.00	54/46	6.9	73	0.073	10	11.4	91.9	89.2	82.1	7.2	6.8	3.9
5		160	0.50	56/44	6.9	130	0.065	11	11.3	91.9	82.8	76.1	6.7	10.8	6.4
6		170	0.25	56/44	5.2	160	0.040	17	8.9	89.9	78.7	70.8	7.9	13.8	7.5
7	TPP	90	3.00	52/48	5.0	11	0.033	22	12.3	92.5	89.6	82.8	6.8	7.7	2.7
8		110	0.50	52/48	5.1	34	0.017	40	12.9	92.8	91.3	84.8	6.5	5.7	3.0
9		125	0.50	52/48	4.7	116	0.058	12	11.9	92.3	89.1	82.2	6.9	7.9	3.1
10		135	0.50	54/46	6.4	156	0.078	9	12.8	92.7	84.2	78.1	6.1	10.7	5.1
11		145	0.25	54/46	5.7	200	0.050	14	11.2	91.8	81.2	74.6	6.6	13.3	5.5
12		160	0.25	56/44	5.6	256	0.064	11	7.6	88.4	78.9	69.7	9.2	15.8	5.3

Table III  
EFFECT OF TRIPHENYLPHOSPHINE AND 2-TRIMETHYLSILYL-ETHYLDIPHENYLPHOSPHINE LIGAND CONCENTRATION ON THE RHODIUM HYDROFORMYLATION OF 1-RUTENE

Reactions at 145° at 2500 kPa of 5/1 H<sub>2</sub>/CO Initial Reactant (53/47 or 54/46 H<sub>2</sub>/CO Feed) and 20g 1-Rutene Plus 80g Mixture of Phosphine Ligand Plus 2-Ethylhexyl Acetate, Using Acacrh(CO)<sub>2</sub> as Catalyst Precursor [SEP Ligand: Ph<sub>2</sub>PCH<sub>2</sub>CH<sub>2</sub>Si(CH<sub>3</sub>)<sub>3</sub>]

Seq. No.	Catalyst System Parameters				H <sub>2</sub> /M Consumption Independent Factors (50% Conversion)				Product Parameters				By-Product Selectivity, %			
	Li-gand, L	M in Mixture at Start	Wt. % in Solvent	Rh Conc. mM	L/Rh Ratio	H <sub>2</sub> /O <sub>2</sub> Ratio Final	Normal- ized at 1 M Rh	k min <sup>-1</sup>	Rate found	Re- action Time min	Aldehyde Linearity			Aldehyde Selectivity, %		
											n/1 Ratio	100n n+1		n	i	
																Total n + i
1	TPP	0.14	4.7	0.05	2822	5.8	800	0.040	18	4.0	80.2	83.0	66.6	16.4	13.4	3.6
2				0.50	280	5.3	640	0.340	2	4.4	81.5	81.8	66.7	15.1	13.0	5.2
3		0.56	18.5	0.25	2240	5.1	320	0.080	9	7.6	88.4	82.3	73.6	9.7	11.7	5.1
4				2.00	200	4.9	285	0.570	1.5	7.2	87.0	80.0	70.3	9.7	14.0	5.9
5		1.00	32.9	0.25	4000	5.7	200	0.050	14	11.2	91.8	81.2	74.6	6.6	13.3	5.5
6				2.00	500	5.2	220	0.440	2	11.1	91.7	82.1	75.3	6.8	12.7	5.3
7		2.20	72.1	0.25	4400	5.9	92	0.023	32	21.7	95.6	80.0	76.5	3.5	14.3	5.7
8				2.00	1100	5.2	90	0.180	4	21.5	95.0	81.0	77.4	3.6	13.5	5.5
9		3.00	100.0	2.00	1500	3.6	48	0.096	9	31.0	96.9	73.3	71.0	2.3	19.6	7.1
10	SEP	0.14	5.0	0.10	1400	5.0	180	0.036	19	4.6	82.2	90.7	74.6	16.1	6.5	2.8
11				0.50	280	5.4	200	0.100	4	5.1	83.5	86.2	72.0	14.2	7.6	6.2
12		0.56	20.0	0.25	2240	5.5	132	0.033	21	8.0	88.8	89.6	79.6	10.0	7.0	3.4
13				2.00	200	6.0	105	0.210	3.5	9.9	90.9	86.1	78.2	7.9	8.2	5.7
14		1.00	35.9	0.50	2000	6.9	68	0.034	20	12.2	92.4	87.5	80.9	6.6	8.3	4.2
15				2.00	500	5.9	70	0.140	5	11.7	92.1	86.4	79.6	6.8	7.4	6.2
16		2.20	78.7	1.00	2200	5.1	38	0.038	18	14.6	93.6	86.9	81.3	5.6	8.7	4.4
17				2.00	1100	5.6	35	0.070	9	15.1	93.8	84.0	78.8	5.2	9.1	6.9
18		2.80	100.0	2.00	1400	5.6	25	0.050	15	20.1	95.2	82.8	78.9	3.9	9.1	8.0

Table IV

CONTINUOUS HYDROFORMYLATION OF 1-BUTENE IN THE PRODUCT FLASH-OFF MODE  
WITH SEP-Rh AND Ph<sub>3</sub>P-Rh COMPLEX CATALYST SYSTEMS

	<u>TPP</u>	<u>SEP</u>	<u>SEP</u>	<u>SEP</u>	<u>SEP</u>	<u>TPP</u>
• Temperature, °C	100	120	120	140	140	140
Pressure, kPa	800	1050	1050	1275	1275	1275
P <sub>H<sub>2</sub></sub> , kPa	565	675	760	724	775	724
P <sub>CO</sub> , kPa	69	90	83	138	149	138
• Rhodium Conc., mM	2.50	2.50	4.44	4.44	4.44	4.44
• Phosphine Conc., mM	310	600	360	1000	1000	1000
1-Butene Feed, mole/hr/L	4.0	4.0	4.0	2.8*	2.8	2.8
Aldehyde Product, mole/hr/L	1.0	1.0	1.5	1.6	1.6	2.3
• Conversion per Pass, %	26	26	38	56 52**	60 55**	82 65**
• n+i Selectivity %	92	92	91	90	90	84
n/i ratio	21	22	21	35	32	29
Hydrocarbon Selectivity, %	7	7	7	8	9	14
• Stripping Gas, mole/hr/L	35	25	38	24	24	21

\*Plus 3 mole/hr/L 2-butenes    \*\*After 6 days operation

Table V

## HYDROFORMYLATION OF 1-BUTENE WITH VARIOUS TRIS-PHOSPHINE RHODIUM CARBONYL HYDRIDE CATALYSTS

Reactions at 145° at 2500 kPa of 5/1  $H_2/CO$  (54/46) Feed and 20g 1-Rutene Plus 80g Mixture of 1M Phosphine Plus 2-Ethylhexyl Acetate Using  $AcacRh(CO)_2$  as a Catalyst Precursor


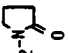


Ligand No.	Ligand Structure	Rh Conc. mM	Ligand Conc. M/kg	Final $H_2/CO$ Ratio	Rate Constant $k_p$ , min <sup>-1</sup>		Re-action Time min.	Linearity $n+1$		Selectivities, Mole %				By-Products 2-Rutene	
					Calcd. 1MRh	Found		n/1	Ratio	n+1	n	1		2-Rutene	Butane
1	$Ph_2PCH_2CH_2Si(CH_3)_3$	1.0 0.1	1 0.14	6.2 5.1	86 363	0.043 0.036	16 19	8.9 4.6	89.9 82.2	87.1 90.7	78.3 74.6	8.8 16.1		7.7 6.5	5.2 2.8
2	$Ph_2PCH_2CH_2C(CH_3)_3$	0.5 0.1	1 0.14	5.5 5.4	100 490	0.050 0.049	14 14	9.8 4.4	90.7 81.6	88.6 90.4	80.4 73.7	8.2 16.7		7.9 6.9	3.5 2.7
3	$Ph_2P(CH_2)_5CH_3$	0.5 0.5	1 0.14	5.3 5.9	96 282	0.048 0.141	14 5	8.8 4.3	89.8 81.0	89.7 88.9	80.6 72.0	9.2 16.9		6.7 6.9	3.6 4.2
4	$Ph_2PCH_2CH_2-$ 	0.5 0.25	1 0.14	5.2 4.9	90 552	0.045 0.138	16 5	10.7 5.5	91.5 84.6	90.9 90.2	83.1 76.3	7.8 13.9		6.4 6.2	2.7 3.6
5	$Ph_2PCH_2CH_2-N$ 	0.5 0.5	1 0.14	4.5 4.9	92 288	0.046 0.144	15 5	9.3 5.4	90.3 84.3	91.8 90.6	82.9 76.3	8.9 11.3		5.6 4.6	2.6 4.8
6	$Ph_2PCH_2CH_2SO_2C_2H_5$	0.5 0.25	1 0.14	5.2 5.8	26 64	0.013 0.016	52 44	18.9 5.7	95.0 85.2	88.1 86.8	83.7 73.9	4.4 12.9		8.1 9.3	3.8 3.9
7	$Ph_3P$	0.25 0.05	1 0.14	5.7 5.8	200 800	0.050 0.040	14 18	11.2 4.0	91.8 80.2	81.2 83.0	74.6 66.6	6.6 16.4		13.3 13.4	5.5 3.6

Table VI

## EFFECT OF THE BRANCHING OF ALKYL DIPHENYL PHOSPHINE LIGANDS ON THE RATE AND SELECTIVITY OF RHODIUM HYDROFORMYLATION

Reactions at 2500 kPa, with 5 to 1  $H_2/CO$  and 20g 1-Butene Plus 80g Mixture of Alkyl Diphenyl Phosphine Ligand and 2-Ethylhexyl Acetate Solvent, Using  $AcacRh(m)_2$  as Catalyst precursor at 145°C

Seq. No.	Catalyst System Parameters Ph <sub>2</sub> P <sup>R</sup> Structure of -R Group	Ligand		L/Rh Ratio	H <sub>2</sub> /CO Consumption Dependent Factors (50 % Conv.)										Aldehyde Linearity		Selectivities, Mole %		By-Products 2-Ru- Ru- tane
		Conc. M	Rh mM		H <sub>2</sub> /CO Ratio Feed	H <sub>2</sub> /CO Final	Normal- ized at 1 M Rh	Rate Constant k min <sup>-1</sup>	Re- action Time min	n/1 Ratio	100n n+1	Total	Aldehydes n-1-	Aldehydes n-1-					
1	-CH <sub>2</sub> CH <sub>2</sub> CH <sub>2</sub> CH <sub>3</sub>	1.0	0.25	4000	53/47	5.2	120	0.030	23	9.6	90.5	88.7	80.3	8.4	7.8	3.5			
2		0.14	0.010	1400	53/47	5.5	530	0.053	13	4.2	80.8	89.1	72.0	17.1	7.8	3.1			
3	-CH <sub>2</sub> CH <sub>2</sub> C(CH <sub>3</sub> ) <sub>3</sub>	1.0	0.50	2000	53/47	5.5	100	0.050*	14*	9.8	90.7	88.6	80.4	8.2	7.9	3.5			
4		0.14	0.10	1400	53/47	5.3	490	0.049	14	4.4	81.6	90.4	73.7	16.7	6.9	2.7			
5	-CH <sub>2</sub> C(CH <sub>3</sub> ) <sub>3</sub>	1.0	0.10	10000	54/46	4.9	250	0.025	27	2.6	72.5	62.9	45.6	17.3	34.7	2.4			
6		0.14	0.25	560	54/46	5.0	284	0.071*	23*	1.7	63.4	52.7	33.4	19.3	44.5	2.8			
7	-CH <sub>2</sub> CH(CH <sub>3</sub> ) <sub>2</sub>	1.0	0.25	4000	54/46	6.5	232	0.058	12	4.4	81.6	86.8	70.8	16.0	9.6	3.6			
8		0.14	0.10	1400	54/46	6.0	580	0.058	12	3.3	76.9	76.5	58.8	17.7	21.0	2.5			
9	-CH(CH <sub>3</sub> )CH <sub>2</sub> CH <sub>3</sub>	1.0	0.20	2800	53/47	5.4	220	0.044	16	3.4	77.2	86.5	66.8	19.7	10.5	3.0			
10		0.14	0.05	2800	53/47	5.3	460	0.023	30	3.2	76.2	69.3	52.8	16.5	28.1	2.6			
11		1.00	0.20	5000	53/47	5.3	40	0.008*	92*	3.6	78.2	87.5	68.4	19.1	9.4	3.1			
12		0.14	0.10	1400	53/47	5.5	370	0.037*	20*	3.2	76.2	75.4	57.5	17.9	22.0	2.6			
13		1.0	0.20	5000	53/47	5.4	190	0.038	18	5.4	84.5	88.1	74.4	13.7	8.4	3.5			
14		0.14	0.05	2800	53/47	5.5	500	0.025	27	3.4	77.1	8.2	63.4	18.8	15.0	2.8			

\*The rate of reaction was decreasing with time. The initial rate is listed.



# THE PREDICTION OF THE QUALITY OF COKE BY THE USE OF $V^r$ -G DIAGRAMS

Peng Chen

Department of Fuels Engineering, University of Utah, Salt Lake City, UT 84112

Permanent address: Central Coal Mine Research Institute, Hepingli, Beijing,  
People's Republic of China

All properties of coal are more or less related to the coalification metamorphism. However, caking properties (plasticity) also affect the coke strength. Upon heating, coal undergoes chemical changes, giving rise to the evolution of gas and condensable vapors and leaving behind a solid residue consisting almost entirely of carbon. In the temperature range 350-500° C, depending on the rank of the coal, coking coal softens, becomes plastic, and coalesces into a coherent mass which swells and then forms a solid porous structure. In this series of transformation, two important temperature zones can be distinguished. The first is that in which the coal is plastic and the second is that at higher temperature in which the resolidified material contracts. A strong contraction and resolidification, which is likely to occur with coals of high volatility and plasticity, produces many fissures in the coke, leading to lower mechanical strength. Coke strength is, therefore, closely associated with agglomeration of particles, pore size and its distribution, strength of cell wall and development of fissures. It is assumed that the coke strength may be expressed statistically as a function of these two parameters.

Many methods to predict the strength of coke have been proposed. These methods are as follows:

(1)  $R^{\circ}_{\max}$ --Log  $\alpha_{\max}$  diagrams put forward by Miyazu.<sup>(1)</sup> Here,  $R^{\circ}_{\max}$  is the mean maximum percent reflectance of vitrinite.  $\alpha_{\max}$  is the maximum percent fluidity measured by the Gieseler plastometer.

(2)  $V^r$ --b diagrams, put forward by Simonis.<sup>(2)</sup> Here,  $V^r$  is the percent by weight volatile matter on a dry, ash-free basis, and b is the total dilatation of the coal, measured by the Audibert-Arnu dilatometer.

(3) X--Y diagrams have been used in the Soviet Union.<sup>(3)</sup> Here, X is the final drop of the expansion-pressure curve which is function of V. Y is the thickness of the plastic layer of the Sapozhnikov test, which reflects the quantity of the plastic mass.

(4) S.I.--C.B.I. diagrams were used by Shapiro.<sup>(4)</sup> S.I. and C.B.I. are the abbreviations of Strength Index and Composition Balance Index. These values are obtained from petrographic analysis.

(5)  $V^r$ --G diagrams has been put forward by the Central Coal Mine Research Institute.<sup>(5)</sup> G is the caking index of coal, which is the modification of Roga Index.<sup>(6)</sup>

## Experimental

More than 400 samples of bituminous coals were selected from the main coal fields of China. Among these, 177 samples of 2 tons each were taken from bituminous coal mines and seams representing different ages of coal formation and periods of metamorphism. Examinations were made according to the requirements for coking tests on a semi-industrial scale using a washer, a 200kg coke oven, different sizes of automatic screens, a micum drum, etc. The raw coal was cleaned by a jig washer,

85% of the coal charged into the coke oven was less than 3mm in size and had a moisture content of 10%. The test coke-oven was constructed of aluminum and magnesium blocks. The carbonizing chamber has a width of 450mm. The coke strength was determined by the ISO/R 556-1967(E) test. The M40 index, crushing strength of coke; the M10 index, abrasive strength of coke; the F10 index, the yield of coke powder of less than 10mm, and the Q60 index, block coke of larger than 60mm after the drop-shatter test, were determined.

The proximate analysis, ultimate analysis, petrographic analysis and tests of caking and coking properties were determined. Most of the test methods adopted are similar in principle to the corresponding methods specified in the International Standards issued by ISO.

## Results

Statistical analysis on the coalification metamorphism-- Volatile matter and mean maximum reflectance of coal have been most commonly used as parameters to describe the coalification metamorphism.<sup>(7,8)</sup> There is a good correlation between these two indices as shown in Table 1. Although the volatile matter index is made on whole coal and reflectance solely on vitrinite, which is generally about 50-80% in coking coal, there is still a good correlation. Ultimate analysis, such as carbon content, hydrogen content, and atomic H/C and O/C ratios have also been used (Table 2).

Table 1. Correlation Between  $V^r$  and  $\bar{R}^o \max$

Source	Regression Equation	Correlation Coefficient
U.S.A.	$\bar{R}^o \max = 2.476 - 0.0402xV^r$	-0.944
Canada & Australia	$\bar{R}^o \max = 2.519 - 0.0465xV^r$	-0.884
China	$\bar{R}^o \max = 2.12 - 0.0357xV^r$	-0.917

Table 2. Correlation between  $C^r$ ,  $H^r$ ,  $O^r$  and  $V^r$   
(Samples 390)

Regression Equation	Correlation Coefficient
$V^r = 247.76 - 2.52xC^r$	-0.86
$V^r = 15.28xH^r - 49.57$	0.90
$V^r = 10.7 + 2.64xO^r$	0.79
$C^r = 108.28 - 4.15xH^r$	-0.72
$C^r = 94.32 - 1.11xO^r$	-0.98

Statistical analysis of the caking properties--Although caking properties of coal are not always proportional to the coking power, they play an essential role during carbonization in determining the strength of the coke.<sup>(9)</sup> Each test index has its own features. Most of them, such as Roga index (RI), Caking index (G), Gray-King index (GK), Crucible Swelling index Number (CSN), etc., reflect the overall result of the process which converts coal from the solid state into the plastic state and then resolidifies it into a solid coherent body with a porous structure. Some of them reflect the temperature range of the plastic state while others reflect the fluidity of the plastic mass. The

correlation of these indices, therefore, is sometimes good and sometimes poor. The correlation coefficients between indices of cohesiveness of coal are summarized in Table 3.

Table 3. Correlation Coefficients between Indices of Cohesiveness of Coal

	G	R.I.	C.S.N.	G.K.	Y	b	Log $\alpha$ max
G	1.00	0.98	0.78	0.94	0.83	0.73	0.86
R.I.	0.98	1.00	0.77	0.91	0.80	0.69	0.87
C.S.N.	0.78	0.77	1.00	0.80	0.63	0.58	0.37
G.K.	0.94	0.91	0.80	1.00	0.86	0.83	0.88
Y	0.83	0.80	0.63	0.86	1.00	0.92	0.66
b	0.73	0.70	0.58	0.83	0.92	1.00	0.76
Log $\alpha$ max	0.86	0.87	0.37	0.88	0.66	0.76	1.00

Relationship between components and properties of coal and coke strength--  
Among the 177 samples used in the coke-oven tests, 29 samples could not go through the tumbler test. After deducting the samples of charges containing >15% ash, there remained 134 coal samples. Organic components, coalification metamorphism and caking properties are internal variables characteristic of the coal used. In addition, the coke produced also depends on external variables such as the particle size of coal, the bulk density of the charge, the heating rate, the coking temperature, the coking time and the structure of the coke oven. In the present study, these external variables are constant. It was, therefore, possible to use a few parameters referring to the internal variable of coal coking to reflect the relation between the property of coal and coke strength.

Trend surface analysis can be used to solve this problem. It has been carried out for 134 coal samples. The results are listed in Table 4. The F-test demonstrated the following:

- (1) The second order equation, square trend-surface equation, is distinctly better than the linear equation, and
- (2) The cubic equation does not have a significant difference as compared with the second order equation.

Table 4. Goodness of Fit for  $V^r$ --G on Coke Qualities

Fitting Trend Equation	Indices of Coke Qualities				
	M40	M10	Q60	Q40	F10
Linear	0.53	0.68	0.36	0.62	0.56
Square	0.69	0.82	0.50	0.80	0.77
Cubic	0.70	0.82	0.53	0.85	0.77

Therefore, the second order equation is used to indicate the trend surface. From Figures 1 and 2, the following information may be obtained:

- (A) When a coal has a volatile matter (daf) of less than 30%, the coke strength is mainly controlled by the cohesiveness.
- (B) When a coal has a volatile matter (daf) of more than 30%, the coke strength is controlled by both the cohesiveness and the degree of metamorphism of coal.

(C) As the volatile matter (daf) increase, the strength is more affected by the degree of metamorphism of coal.

(D) The effect of the degree of coal metamorphism is greater on the M40 index than on the M10 index. The effect of the cohesiveness is larger on M10 than on M40.

It may be seen from Figures 3 and 4, that the percentage of lump coke is mainly affected by the degree of coal metamorphism. As  $V^r$  increases, the percentage of lump coke decreases.

It may be seen from Figure 5 that the percentage of coke breeze is mainly affected by the cohesiveness of the coal. The higher the  $V^r$ , the more it is affected by the cohesiveness of coal.

If other indices reflecting the degree of coal metamorphism and the cohesiveness were used, similar relations would be obtained (Table 5). The combinations of  $V^r$  and other indices reflecting cohesiveness usually did not show any difference in goodness of fit for the M40 index. As for the M10 index, the combination of  $V^r$ --G is distinctly better than  $V^r$ --Y or  $V^r$ --Log  $\alpha_{\max}$ , or C.S.N. Thus, it is evident that

(1) Caking index G, which we have improved, is better than other indices reflecting cohesiveness of coal.

(2) Index V is better than  $\bar{R}^{\circ}_{\max}$ . The former is based on whole coal and the latter is based on vitrinite in coal only.

Table 5. Comparison of Goodness of Fit when Fitting with Different Indices

Combination of Different Indices	Coke Strength			
	M40		M10	
	Square	Cubic	Square	Cubic
$V^r$ vis. G	0.69	0.70	0.82	0.82
$V^r$ vis. R. I.	0.69	0.70	0.78	0.81
$V^r$ vis. Log $\alpha_{\max}$	0.67	0.69	0.66	0.72
$V^r$ vis. Y	0.66	0.69	0.55	0.70
$V^r$ vis. C.S.N.	0.68	0.72	0.56	0.59
$V^r$ vis. b	0.63	0.67	0.44	0.62
$\bar{R}^{\circ}_{\max}$ -Log $\alpha_{\max}$	0.59	0.60	0.66	0.70
$\bar{R}^{\circ}_{\max}$ -( $\Sigma d$ ) $^{2/3}$ *	0.57	0.62	0.33	0.39

\* ( $\Sigma d$ ) $^{2/3}$ , vol. % of 2/3 semi-vitrinite in coal plus fusinite and semi-fusinite, then plus mineral impurities in coal.

Taking advantage of these results, we can estimate the strength of coke using the diagram of  $V^r$ --G. We must point out that these results have been obtained from a semi-industrial scale oven and are different from the results in a conventional coke oven. In general, the coke strength is slightly lower for the smaller oven, but it is not important in selecting the blending ratios of coals.

If the value of blending coals in the  $V^r$ --G diagram does not fall in the optimum area, we can add some coals to the blending coals to move the position

in the  $V^r$ -G diagram into optimum area. In addition, we may use further treatment to enhance the ability to make better coke or to improve the economics of manufacturing coke. The methods of further treatment are shown in Figure 6. We can, for example, use preheating to improve the caking ability of these blending coals, which are low in caking ability and have a position in the  $V^r$ -G diagram low on the optimum area. The optimum area for blending has  $V^r$  values from 28% to 32% and G values from 60 to 75.

ACKNOWLEDGMENTS: The author wishes to express his appreciation to Dr. Wang Yinren, Director, Beijing Research Institute of Coal Chemistry, Dr. D. M. Bodily, Chairman, Department of Fuels Engineering, University of Utah, and Dr. J. Y. Tong, Department of Chemistry, Ohio University, for their helpful suggestions. The author gratefully acknowledges cooperation and support from many colleagues at the Beijing Research Institute of Coal Chemistry.

#### REFERENCES:

1. Miyazu, T., Okuyama, Y., Sugimura, H. and Kumagai, M., J. Fuel Soc. Japan, 1970, 49, 736.
2. Simonis, W., Gnuschka, G., and Beck, K. G., Gluckauf-Forschungshefte, 1965, No. 4, 201, 1965, No. 6, 301.
3. Lowry, H. H.: "Chemistry of Coal Utilization" Vol. 1, New York, John Wiley and Sons, Inc. (1945), pp.280-297.
4. Shapiro, N., Gray, R. J., and Eusner, G. R., Iron and Steel Division, AIME Proceedings, 1961, 20.
5. Chen, Peng: Coking Chemistry, 1979, No. 6, 1.
6. Chen, Peng: Coal Geology and Prospecting, 1976, No. 4.
7. Huntzens, F. J. and Van Krevelen, D. W. " Fuel, 1954, 33, 88.
8. Keiichiro, K., Fuel, 1980, 59, 380.
9. Zimmerman, R. E.: "Evaluating and Testing the Coking Properties of Coal", Miller Freeman Publications, Inc., San Francisco (1979).

#### FIGURES:

1. Forecasting the M40 with the square trend surface.
2. Forecasting the M10 with the square trend surface.
3. Forecasting the Q60 with the square trend surface.
4. Forecasting the Q40 with the square trend surface.
5. Forecasting the F10 with the square trend surface.
6. Some methods of further treatment to improve the coke strength using  $V^r$ -G diagram.

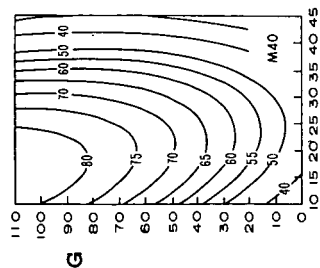


Figure 1

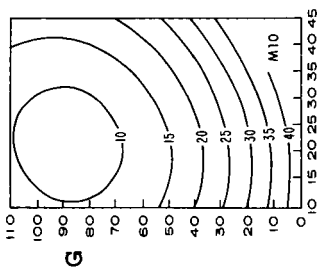


Figure 2

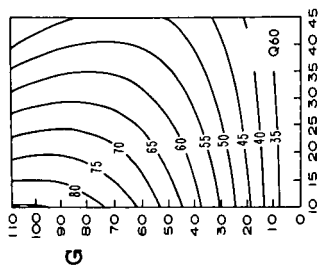


Figure 3

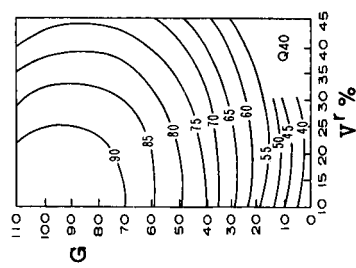


Figure 4

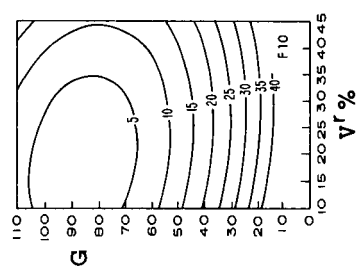


Figure 5

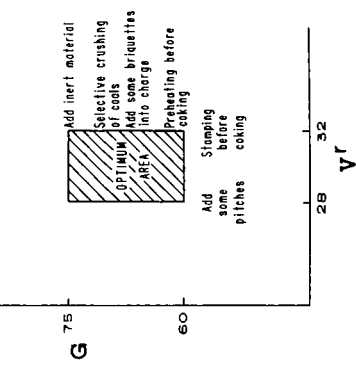


Figure 6

## MICROANALYTICAL CHARACTERIZATION OF NORTH DAKOTA FLY ASH

S.A. Benson, D.K. Rindt, G.G. Montgomery, and D.R. Sears

Grand Forks Energy Technology Center  
U.S. Department of Energy  
Grand Forks, N.D. 58202

### INTRODUCTION

Goals of particulate research at the Grand Forks Energy Technology Center (GFETC) include detailed characterization of fly ash with respect to those properties which relate to controllability as well as possible environmental hazards of emissions. The focus is entirely on low-rank western and Gulf Province coals, whose properties are distinctly different from those of eastern coals. Typically the western coals have high moisture, low sulfur, and large variations in the distribution of inorganic constituents.

Beulah, a North Dakota lignite, was used in the combustion tests of primary interest to this paper. This lignite is extraordinarily variable in its inorganic constituents. For example, the sodium content can have a tenfold variation within a few hundred meters in a single seam (1). The specific Beulah lignite used was selected for its high sodium content.

The fly ash was generated for this research using the GFETC Particulate Test Combustor (PTC), illustrated in the schematic in Figure 1. This unit is an axially-fired pulverized coal combustor with a nominal consumption of 34 kg coal/hr. The unit is designed to generate ash characteristic of that produced with similar fuel in a full-sized utility boiler. Axial firing maximizes the fly ash/(bottom ash + slag) ratio. The fly ash samples for analysis were collected at the inlet to the baghouse with two devices, a five-stage multicyclone and a source assessment sampling system (SASS). The flues are equipped with heat exchangers permitting delivery of flue gas to the chosen control device at temperatures from  $\sim 100^\circ$  to  $390^\circ\text{C}$ . During these tests, the PTC was equipped with an experimental baghouse because of on-going fabric filter research at GFETC. The PTC instrumentation permits measurement of flue gas condition such as temperature and concentrations of  $\text{SO}_2$ ,  $\text{NO}_x$ ,  $\text{O}_2$ , and  $\text{CO}_2$ .

The coal and fly ash were characterized by several analytical techniques. The inorganics of the coal were examined by an extraction technique which selectively removes the inorganics depending upon their association in the coal (2). Low temperature ashing with subsequent x-ray diffraction was used to identify the mineral phases of the coal. The fly ash was examined and analyzed by scanning electron microscope/microprobe, Electron Spectroscopy for Chemical Analysis (ESCA), x-ray diffraction and x-ray fluorescence.

### COAL CHARACTERISTICS

The inorganics associated with the Beulah lignite consist of a complex mixture of cations bound to the humic acid groups, possible chelates or coordination complexes, minerals formed during coalification, and minerals accumulated during deposition. Traditional and non-traditional methods were used to examine the coal characteristics. The traditional analysis of the lignite is summarized in Table 1 which lists the ultimate analysis, moisture, heating value, and major element ash analysis.

One of the two "non-traditional methods" used is low-temperature ashing in an oxygen plasma at  $150^\circ\text{C}$  with x-ray diffraction analysis to determine the crystalline

phases in the ash. The phases identified include  $\text{SiO}_2$  (quartz),  $\text{FeS}_2$  (pyrite), kaolinite, and  $\text{CaCO}_3$  (calcite). The second method involves a procedure which selectively removes inorganics (2). The ion-exchangeable cations and soluble salts are removed with 1M ammonium acetate. The coal is then extracted with 1M hydrochloric acid to remove chelated species, acid decomposable minerals such as carbonates, and oxides. The inorganics remaining in the coal can include  $\text{FeS}_2$ , organically bound sulfur, quartz, and clay minerals. The elements found to be extracted with ammonium acetate are Na (100% of the total Na content), Mg (88%), Ca (41%), and K (57%). The elements removed by HCl are Mg (20%), Al (61%), Ca (50%) and Fe (30%). The elements which remain are Si (100%), Fe (70%), Al (40%), and S (100%). Table 2 summarizes a study of the inorganic constituents in Beulah lignite and the geologic formation it is found in.

TABLE 1. TYPICAL COAL AND COAL ASH ANALYSIS OF BEULAH, N.D. LIGNITE

Ultimate Analysis, as Fired		Coal Ash Analysis, Percent	
Carbon	46.29%	$\text{SiO}_2$	22.3
Hydrogen	5.29	$\text{Al}_2\text{O}_3$	11.7
Nitrogen	.62	$\text{Fe}_2\text{O}_3$	9.8
Sulfur	.99	$\text{TiO}_2$	0.9
Ash	8.2	CaO	15.7
Moisture	27.2	MgO	5.3
Heating value	17,460 J/g	$\text{Na}_2\text{O}$	9.9
(7512 Btu/lb)		$\text{K}_2\text{O}$	0.7
		$\text{SO}_3$	23.0

#### ASH SAMPLING

Fly ash is sampled isokinetically in three ways in the PTC: 1) Using a modified U.S. EPA "method 5" (3) dust loading filters; 2) by collection in a Southern Research Institute\* 5-stage multicyclone which simultaneously samples isokinetically and size fractionates the ash (4,5); 3) by collection in a three-stage cyclone module of an Acurex\* Source Assessment sampling system or "SASS-Train" (6,7). Nominal aerodynamic size ranges for the multicyclone and the SASS-Train, at the stated flow rates, appear in Table 3. Nominal size ranges, expressed as aerodynamic diameters in  $\mu\text{m}$  are those corresponding to actual flow rates employed. The figures represent the mass median diameters ( $D_{50}$ ) or "cut points", of the size distribution entering or leaving the stage.

University of Washington Mark III\* cascade impactors were used to more precisely determine particle size distribution (7). The cumulative particle size distribution, expressed in aerodynamic diameters, appears in Figure 2. This data is used only for comparison. The bulk of the characterization work was done on the multicyclone and SASS Train samples because the masses of particles collected by the impactor are very small and inadequate for analysis.

\*Reference to specific brand names and models is done to facilitate understanding and neither constitutes nor implies endorsement by the Department of Energy.



TABLE 2. INORGANIC CONSTITUENTS IN BEULAH LIGNITE AND SENTINEL BUTTE FORMATION (2)

Constituent	Beulah Lignite		Sentinel Butte Formation		
	Whole Coal	Sink Fraction	Overburden	Lignite	Underclay
Alkali feldspars	XXX		XX	X	X
Augite				X	
Barute	X			X	
Biotite	X		X		
Calcite/dolomite	X	XX	XX	X	
Chlorite			XX	X	X
Galena	X				
Gypsum		XX		XXX	
Hematite		X		XX	
Hornblende			X		
Illite	XXX		XX	X	X
Kaolinite	XXX	X	XX	XXX	XXX
Magnetite	X				
Montmorillonite			XXX	X	XXX
Muscovite	X				
Plagioclase		X	XXX	X	X
Pyrite	XXX	XXX		XX	
Quartz	XXX	XXX	XXX	XXX	XXX
Rutile	X				
Volcanic glass			X		

XXX Abundant  
XX Common  
X Minor

TABLE 3. AERODYNAMIC SIZE RANGES (UPPER AND LOWER D<sub>50</sub> CUT POINTS) AND SAMPLE FLOW RATES OF GFETC'S ASH SAMPLING EQUIPMENT

Instrument	Southern Research Institute Multicyclone					Acurex/Aerotherm SASS Train*		
Flow rate employed STD l/min	9.36					113.2		
Stage No.	1	2	3	4	5	1	2	3
Nominal size range (upper and lower D <sub>50</sub> ), μm	>10.3	10.3-5.6	5.6-4.15	4.15-1.9	1.9-1.55	>10	10-3	3-1

## RESULTS AND DISCUSSION

Fly ash samples were collected by the SASS Train to provide larger masses but only 3 size cuts for x-ray fluorescence (XRF) and x-ray diffractions (XRD). The

elemental trends determined by XRF analysis show increasing concentration of  $\text{Na}_2\text{O}$  and  $\text{SO}_3$  and decreasing  $\text{SiO}_2$ ,  $\text{CaO}$ ,  $\text{Fe}_2\text{O}_3$ , and  $\text{MgO}$  with decreasing particle size. Very little change was noted for  $\text{Al}_2\text{O}_3$  or the minor elements ( $\text{TiO}_2$ ,  $\text{K}_2\text{O}$ , and  $\text{P}_2\text{O}_5$ ). These relationships are illustrated graphically in Figure 3. X-ray diffraction was used to identify the crystalline species in each size fraction. The trends show the following relationships.

1.  $\text{Na}_2\text{SO}_4$ ,  $\text{Na}_2\text{Ca}(\text{SO}_4)_2$  are present in the smaller size fractions.
2.  $\text{SiO}_2$ ,  $\text{CaO}$  noted in larger size fractions and not in smaller size fractions.  $\text{Fe}_3\text{O}_4$ - $\text{MgFe}_2\text{O}_4$ - $\text{MgO}$  phases decrease from larger to smaller size fractions.
3. Possible  $\text{Al}_2\text{SiO}_5$  and  $\text{K}_2\text{SO}_4$  phases noted in smallest size fractions.

These two bulk particle characterization methods show the trends of the elemental distribution versus particle size and how the elements are combined. The most interesting trend is the increasing amount of  $\text{Na}_2\text{O}$  and  $\text{SO}_3$  with decreasing particle sizes. This leads to the particle-to-particle characterization using the scanning electron microscope/microprobe for various sizes of particles collected with the 5-stage multicyclone.

The scanning electron microscope (SEM) equipped with an energy dispersive x-ray analyzer was used to image and analyze particles down to  $\sim 1\mu\text{m}$  in size. The particles were selected at random for analysis by using a grid overlay of points generated by random numbers on the SEM photomicrograph. A typical SEM photomicrograph is shown in Figure 4. One hundred particles for each stage were analyzed, determining 10 elements per particle, and sized. All data was entered into a computing system for correlation analysis.

The average particle size determined from the SEM photomicrographs for each stage are listed in Table 4. Table 4 also lists the  $\text{Na}_2\text{O}$  and  $\text{SO}_3$  concentration averages for all five stages along with the ratio of  $\text{Na}_2\text{O}$  to  $\text{SO}_3$ . The concentrations of  $\text{Na}_2\text{O}$  and  $\text{SO}_3$  increase as particle decreases and the ratio of  $\text{Na}_2\text{O}$  to  $\text{SO}_3$  is very close to that of pure  $\text{Na}_2\text{SO}_4$  for stages 1, 3, and 4. The particles collected in stage 5 are not consistent with the other stages in particle-size or in the ratio of  $\text{Na}_2\text{O}$  to  $\text{SO}_3$ . The reason for the inconsistency in the ratio could be due to the bimodal distribution of  $\text{SO}_3$  shown in Figure 5, and also to the presence of  $\text{Na}_2\text{Ca}(\text{SO}_4)_2$  noted by XRD in the small size fraction of the SASS samples.

The compositional relationships can be represented by plots of composition versus composition for selected constituent pairs. These plots can be used to ascertain the origin of certain species from the original mineral matter of the coal and the interactions that have occurred during combustion. For example, Figure 6 illustrates the compositional plots for several combinations. Figure 6-1 represents the plot of  $\text{Al}_2\text{O}_3$  versus  $\text{SiO}_2$  which reveals a cluster of points around a slope of approximately 0.8. Minerals having been identified in Beulah (2) include biotite, kaolinite, muscovite, and illite, where the  $\text{Al/Si}$  ratio is in the range of 0.67-1.0. From this it can be suggested that the aluminosilicate framework remains intact after combustion. The common clay minerals have a range in composition of 25-45%  $\text{Al}_2\text{O}_3$  and 35-50%  $\text{SiO}_2$ . Since most of the particles in Figure 6-1 contain less than these percentages, either the aluminosilicates somehow became combined with additional elements or became coated.

The plot of  $\text{Na}_2\text{O}$  versus  $\text{CaO}$  in Figure 6-2 shows inverse relationship which is supported by the XRF data in Figure 3.

In the plots of  $\text{SiO}_2$  versus  $\text{SO}_3$  and  $\text{Al}_2\text{O}_3$  versus  $\text{SO}_3$ , Figures 6-3 and 6-4, there is a crude negative correlation between  $\text{SiO}_2$  or  $\text{Al}_2\text{O}_3$  and  $\text{SO}_3$ . Despite considerable scatter, many of the points lie in the region along lines connecting clay minerals, at 0%  $\text{SO}_3$ , with  $\text{Na}_2\text{SO}_4$  or glauberite at 0%  $\text{SiO}_2$ . This is consistent with clay-like particles becoming coated with  $\text{Na}_2\text{SO}_4$ .

TABLE 4. SIZE, SODIUM, AND SULFUR RELATIONSHIPS  
FOR EACH STAGE OF THE MULTICYCLONE

Stage	Weight Average			
	Particle Size $\mu\text{m}$	$\text{Na}_2\text{O}, \%$	$\text{SO}_3, \%$	$\text{Na}_2\text{O}/\text{SO}_3$
1	5.48	8.60	10.98	0.79
2	1.99	10.78	12.53	0.86
3	1.29	13.20	17.02	0.78
4	1.20	13.98	19.43	0.72
5	1.38	14.99	23.05	0.65

$\text{Na}_2\text{O}/\text{SO}_3$  in pure  $\text{Na}_2\text{SO}_4 = 0.78$

Surface analysis of the particles was performed utilizing ESCA. The ESCA analysis technique analyzes to a depth of 20 to 30Å. A typical ESCA scan is shown in Figure 7 for Stage 5 particles. The major constituents found on the surface include Ba, O, Ca, Na, C, S, and Si. The published binding energies (8) of the elements detected by the detailed ESCA scans show that Na, Ca, and Ba are present as sulfates. The Na, Al, and Si may be tied up as silicates, but detailed binding energies for such compounds are unavailable in the literature.

The surfaces of the particles were characterized by a sputter-etching technique used to remove surface layers followed by subsequent ESCA analysis. It was found that carbon and sulfur were concentrated on the surface of all five stages of the multicyclone samples. Contamination of the surface of the particles can largely be attributed to the high concentration of carbon. The presence of sodium was noted on the surface of the larger particles but in the smaller size fractions ( $<1.5 \mu\text{m}$ ) the sodium concentration was more uniform throughout the depth analyzed by sputtering. Campbell and others (9) also showed that Na, S, and C were found on the surface of ash particles. In all cases, except for Stage 5, Ca, Al, and Si were found to increase after sputtering.

## CONCLUSIONS

The most significant trend noted by all techniques was the increase of sodium and sulfur with decreasing particle size. The relatively more volatile sodium salts may sublime to form very small particles of pure salt or they may condense on the surfaces of other particles such as aluminosilicates originating from clay minerals of the coal. The latter is supported by the results of the SEM data in Figures 6-3 and 6-4 and the ESCA results. These results support the validity of vaporization-condensation mechanisms of particulate formation. A summary of the possible mechanisms of particulate formation are described by Damle and others (10).

The work described here is part of an ongoing project at GFETC to develop a model for ash formation during the combustion of low-rank coals.

## ACKNOWLEDGMENTS

The authors would like to thank Robin Roaldson for his assistance in analyzing particles with the scanning electron microscope and Harold Schobert for his helpful comments in preparation of this paper.

## REFERENCES

1. S.A. Cooley, R.C. Ellman, "Analysis of the Northern Grest Plains Province lignites and subbituminous coals and their ash", U.S. Dept. of Energy DOE/GFETC/ RO-81/2, July 1981.
2. H.H. Schobert, S.A. Benson, M.L. Jones, and F.R. Karner, "Studies in the characterization of United States low-rank coals", Proceedings, International Conference on Coal Science, Dusseldorf, Sept 1981, p.10-15.
3. "Method 5-determination of particle emission from stationary sources", Code of Federal Regulators, Title 40 Part 60, Appendix A, July 1, 1979 pp 143.
4. W.B. Smith, R.R. Wilson, Jr., and R.B. Harris, "A five stage cyclone system for in situ sampling", Environmental Science and Technology, 13, 1387, (1979).
5. W.O. Lipscomb, "Survey of particulate emissions macro- and micro-sampling and sizing methods and real-time monitoring and sizing methods", U.S. Department of Energy, DOE/FC/10193-T1, February, 1981.
6. D.E. Blake, "Source Assessment Sampling System: Design and Development", U.S. Environmental Protection Agency EPA-600/7-78-018, February, 1978.
7. W.B. Smith, P.R. Cavanaugh, and R.R. Wilson, Technical Manual: A Survey of equipment and methods for particulate sampling in industrial process streams. U.S. Environmental Protection Agency, Research Triangle Park, N.C. EPA-600/7-78-043 March, 1978.
8. Handbook of X-ray photoelectron spectroscopy, Perkin-Elmer Corporation, Physical Electronic Division. 1979.
9. J.A. Campbell, R.D. Smith, L.E. Davis, and K.L. Smith, "Characterization of micron-sized flyash particles by X-ray Photoelectron Spectroscopy (ESCA)," The Science of the Total Environment, 12, 75-85, (1979)
10. A.S. Damle, D.S. Ensor, and M.B. Ranade, "Coal combustion aerosol formation mechanisms: A Review", Aerosol Science and Technology 1, 119-133 (1982).

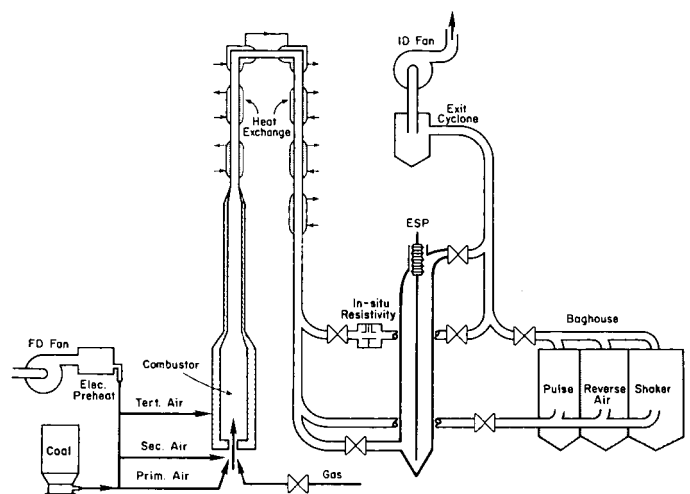


Figure 1. 34 kg/hr Coal Combustion Unit Employed for Ash Generation

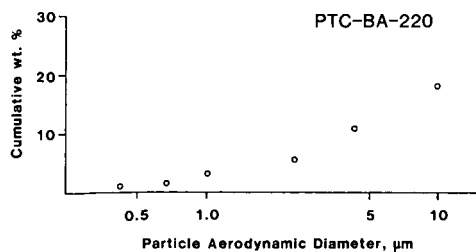


Figure 2. Baghouse Inlet Particle Size Distribution Determined with University of Washington's Mark III Cascade Impactor

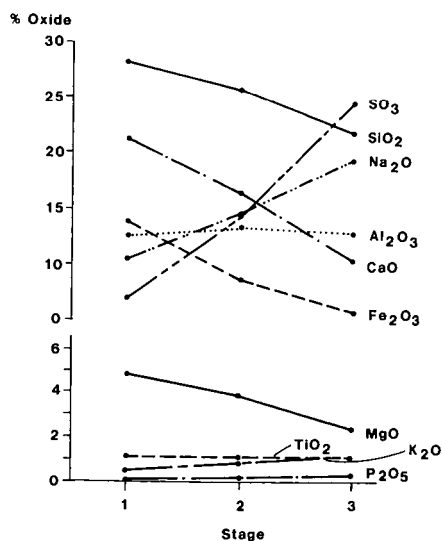


Figure 3. X-ray Fluorescence Analysis of Each Stage from the SASS Train Sampler

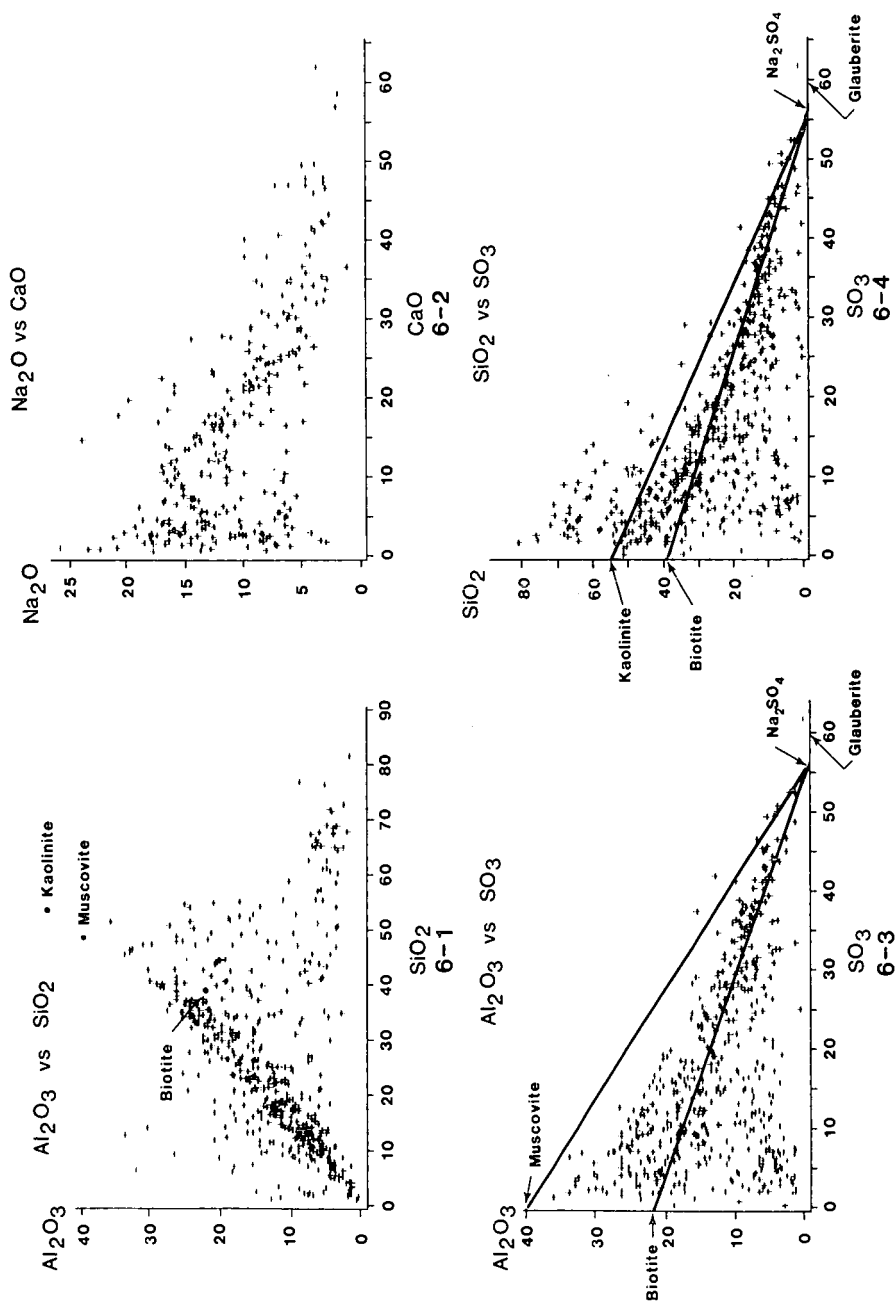


Figure 6. Compositional Relationships for SEM Data Combined from All Five Stages of the Multicyclone

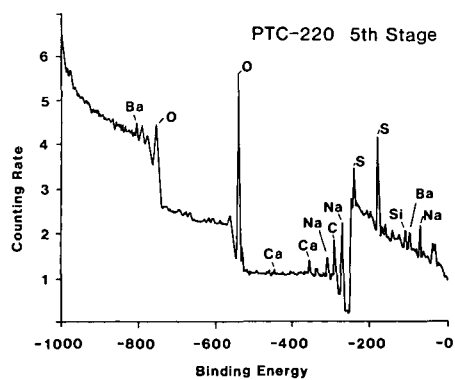


Figure 7. ESCA Scan of Stage 5 of the Multicyclone

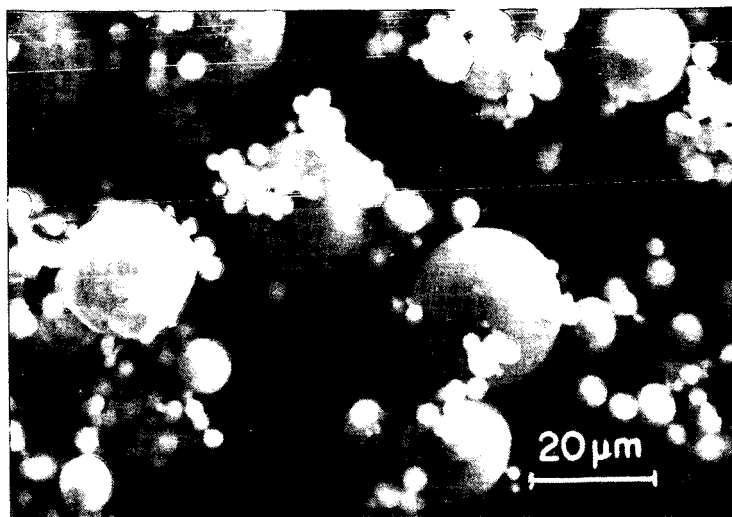


Figure 4. Secondary Electron Image of Particles from Stage 1 Multicyclone

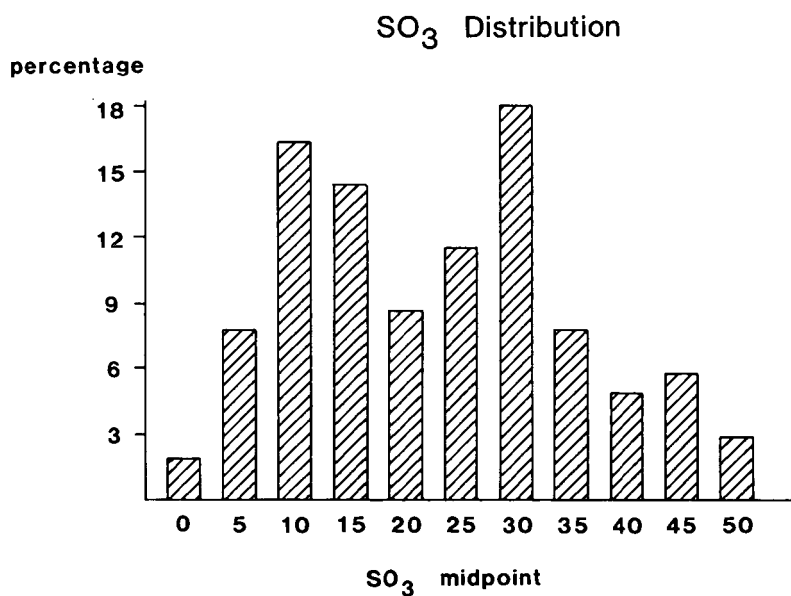


Figure 5. Concentration Population Distribution for SO<sub>3</sub> in Particles Collected in Stage 5 of the Multicyclone



# On the Application of Complex Equilibrium Calculations to the Study of Mineral Matter during Coal Combustion

R. W. Carling, R. W. Mar, and A. S. Nagelberg

Sandia National Laboratories  
Livermore, CA 94550

## Introduction

Coal is a complex mixture of organic and inorganic materials. The inorganic portion, the mineral matter, usually makes up a significant portion of a coal's composition. The contents vary from seam-to-seam but can be as high as 32 weight percent, with an average of 15 weight percent for North American coals. Mineral matter acts as a diluent and is clearly undesirable in mining and transportation. It is also the cause of many problems within a combustor, such as gaseous and particulate emissions, fouling, slagging, corrosion, and erosion. With the increased usage of coal to fulfill the nation's and the world's energy requirements, higher mineral content coals will play a more significant role in the future. Therefore, it has become important to understand the behavior of the mineral matter and its consequences in coal utilization systems.

In this report we discuss the application of complex thermochemical calculations to the study of mineral matter behavior during the combustion of pulverized coal. In principle, one can specify the conditions of combustion (e.g., temperature, total pressure, and oxygen partial pressure) and then calculate the chemical equilibrium between reactions involving all or selected fractions of the elements found in a coal particle. These calculations may be used to predict the ash and gaseous species formed during combustion. Practical problems such as submicron fly ash formation, deposit formation, fouling, and corrosion may be addressed in this manner. An understanding of the formation of chemical species and the effects of changes in operating parameters and system chemistry on stability ranges should aid in identifying control strategies to combat harmful species. Basically, one is seeking to improve and control the thermochemical environment of the coal particle by the proper selection of operating parameters conditions and chemical constituents.

At the outset, one might question the application of equilibrium calculations to a nonequilibrium process such as coal combustion. There might not be time for chemical equilibrium to be attained, and this is particularly true where the reactants are large particulates. Equilibrium calculations should be considered an important first step, to be followed by an examination and incorporation of kinetic aspects. That is, educated guesses must be made concerning the reactivity and release of chemical constituents of the coal. Kinetic factors may be

introduced by specifying the chemical state of the calculation, which may differ considerably from the total coal chemistry. Even if equilibrium conditions existed, uncertainties and variations in the calculated results may be introduced by a number of factors. In this paper we address the impact of three potential sources of error on mineral matter calculations, namely: 1) errors in the data, 2) selection of species, and 3) solution formation.

### COMPLEX EQUILIBRIUM CALCULATIONS

Numerous methods have been reported for computing complex thermodynamic equilibria, but all methods are based on the methods of Brinkley(1-2) or White, Johnson, and Dantzig(3). Brinkley's approach requires a formulation of independent chemical reactions and the simultaneous solution of equilibrium constant expressions. A superior approach, first suggested by White et al.(3), involves the computation of the composition that minimizes the Gibbs free energy of the system.

A number of independent computer programs to calculate complex equilibria by free energy minimization have been developed over the years(4-7). A major step forward was taken by Erickson(8-10) in his development of codes called SOLGAS and SOLGASMIX. These codes are capable of handling systems containing multiple condensed phases, ideal and nonideal solutions, and mixtures at constant total pressure and temperature. Bessman(11) modified SOLGASMIX to handle the additional case of equilibria at constant gas volume and variable pressure; his version is called SOLGASMIX-PV. Kee and Nagelberg(12) have taken SOLGASMIX-PV and interfaced it with CHEMKIN(13) that allows users at Sandia National Laboratories to share the vast thermochemical data base already available at Sandia.

While the equilibrium state of a complex chemical system is unique, there is no guarantee that all free energy minimization codes will provide the same answer. The Gibbs free energy surface may in fact consist of a number of local minima; thus, a free energy minimization routine could isolate on a local minimum rather than the grand minimum. Different numerical algorithms and convergence criteria selected for the iterative methods of free energy minimization and different programming structures may also lead to conflicting results. For example, Minkoff, Land, and Blander(14) have shown the NASA CEC code(4) to be incapable of converging on a solution when minor amounts of condensed phases are present in delicate balance. By using a primal geometric programming approach, Minkoff et al.(14) were able to eliminate convergence problems. Another cause of inaccurate results, perhaps the most obvious, is erroneous thermochemical data or poor data representation (curve fitting of the data).

A semianthracite coal composition obtained from the Penn State Coal Data Base (PSOC #627) was used in this study. The chemical composition of the coal is shown in Table I. A calculation was carried out in which

this coal was reacted with 20 percent excess oxygen at a pressure of one atmosphere over a temperature range of 1000 to 2000 K. The species considered in the calculation are given in Table II. Thermochemical data for these species were taken from JANAF(15). The sodium-containing species predicted to form in the gas phase during combustion are shown in Figure 1. The major species were NaCl, NaOH, and Na, with NaOH dominating at high temperatures.  $\text{Na}_2\text{SO}_4$  is predicted to form in lesser concentrations with a maximum peak at 1400 K. The condensed phases predicted to be present are shown in Figure 2. The principle condensed-phase species formed was  $\text{SiO}_2$  at all temperatures. Below 1400 K, 2 mole percent  $\text{Na}_2\text{SO}_4$  was observed as the only other phase. Above 1400 K, the sulfate was replaced by sodium silicate ( $\text{Na}_2\text{Si}_2\text{O}_5$ ).

The purpose of the calculations described above is not to identify ash formation and deposit formation mechanisms; rather, we will use the results in Figures 1 and 2 as a baseline from which we will illustrate the effects of errors in the data, the number of species considered in the calculation, and solution effects.

## EFFECTS OF VARIOUS CALCULATIONAL FACTORS

### Errors in the Thermochemical Data

The quality of the thermochemical data used in calculations are often not evaluated when computational codes are used. Durie, Milne, and Smith(16) in their study of salt deposition from hydrocarbon flames, showed a change of only a few kcal/mol in the free energy of formation of a species resulted in a significant rearrangement in the relative proportions of deposited phases. However, one cannot generalize Durie's observations because the effect of a change in the free energy will vary from situation to situation, depending upon the number of chemical constituents, their thermodynamic stabilities, and their relative concentrations.

To illustrate the effect of errors in the data on coal combustion calculations, let us examine the sensitivity of the results to the free energy of  $\text{Na}_2\text{SO}_4$ . Figure 3 shows the predicted distribution of the sodium containing species in the gas phase if the free energy of  $\text{Na}_2\text{SO}_4$  is reduced by 1 percent (1.2 kcal). It is seen that all curves exhibit the same qualitative behavior as those on Figure 1. In fact, except for the  $\text{Na}_2\text{SO}_4$  curve, all species were virtually unaffected by the free energy change. The absolute amount of  $\text{Na}_2\text{SO}_4$  is, of course, reduced.

The magnitude of the change is better illustrated in Figure 4, where the effect of varying the free energy by 1 and 5 percent is shown. In this illustration the situation appears to be buffered, and a drastic rearrangement of the relative proportions of all species does not result if the stability of just one species is modified. However, if one is

(15). Data for the rest of the minerals were taken from the work of Robie, Hemingway, Schafer, and Haas(17). The calculated gas phase composition is given in Figure 5, to be compared with that shown in Figure 1. It is seen that there is a major rearrangement of species, and as a whole, the species concentrations were all reduced by one to two orders of magnitude. Major changes also occurred with the condensed phases, as seen in Figure 6. While  $\text{SiO}_2$  remained as the primary condensed phase,  $\text{Na}_2\text{SO}_4$  and  $\text{Na}_2\text{Si}_2\text{O}_5$  were not stable. At temperatures between 1000 and 1220 K, the stable-condensed phases were  $\text{SiO}_2$ , pyrophyllite, and albite. At temperatures greater than 1220 K, the stable-condensed phases were silica, albite, and mullite. Thus, the results of complex equilibrium calculations can be significantly altered by the choice of species. Caution must be used when making the selection, and kinetic factors and experimental information should be carefully evaluated.

### Condensed Phase Solutions

Previous calculations pertaining to coal combustion have not allowed for the formation of condensed phase solutions. Solutions will obviously form when liquid silica, alkali silicates, and sulfates are present. The results on Figure 2 show that silica and sodium disilicate form, and the phase diagram information in the literature clearly suggest a solution will result(18). Let us now extend the baseline calculations on Figures 1 and 2 to include solution formation. For lack of better information, we will assume ideal solution behavior. The sodium-containing gas species formed in this case are shown in Figure 7. It is seen that the NaCl concentration is not affected, but noticeable changes in the behavior of NaOH, Na, and  $\text{Na}_2\text{SO}_4$  is seen. While their concentrations maintain the same qualitative behavior, they all form in lesser amounts. Another way of representing the effects of solution formation is seen in Figure 8, where the ratio of concentration without solution formation to that where no solution is formed is shown.

### SUMMARY

Complex equilibrium calculations may be a very useful tool in the study of mineral matter evolution in a coal combustor. Kinetic constraints must be applied but may be done within the context of equilibrium calculations; kinetic considerations may be used to define a more realistic chemistry for the system. Equilibrium calculations are only an approximate representation of the real situation since not all possible chemical species can be considered in a calculation and the thermodynamic data for many species are uncertain. In order to utilize the results of complex calculations, one must understand the caveats and uncertainties created by these problems.

It has been shown that the qualitative behavior of chemical species is fairly insensitive to errors in the thermochemical data. However, the absolute concentrations of the species can change by orders of magnitude if the free

concerned with absolute concentrations, great care must be taken to use accurate thermochemical data. A relatively small error of 1 kcal will change the concentration by a factor of two, and a change of two orders of magnitude is realized if a 5 kcal error is assumed. If the interest is in observing changes that occur as parameters are varied (i.e., the movement of phase boundaries), there is a smaller sensitivity to errors in the data.

Errors in data can also result from the misrepresentation of the data in the computer programs. Codes are generally constructed to be of generic use, and thus, a generalized approach to representing the data is used. For example, the NASA CEC code(4) and the Sandia code(12) use multiple-order polynomial fits over two-temperature ranges to represent the data. When dealing with complex condensed-phase mixtures, the free energies must be equal at transition temperatures. Failure to consider this constraint will result in an obvious error, such as a phase predicted to be present under conditions clearly out of its stability range (e.g., a solid phase predicted at temperatures above the melting point).

#### Species Considered in the Calculation

Complex equilibrium calculations are usually conducted with only a few species for several reasons. First and foremost, there are not many accurate self-consistent data. Also, calculations can become very time consuming, and the possibility of poor convergence behavior increases with the number of species, especially if many species are present in minor amounts(14).

When applying equilibrium calculations to the study of mineral matter behavior, one selects only a few species to consider by making assumptions concerning the reactive chemistry of the system. For example, aluminum is often found in coal but is usually not considered in the calculations because it is assumed to be present in kinetically and thermodynamically inert forms, such as alumino-silicates. If, however, Al is considered in the calculation, a significant change in the calculated results could occur.

To illustrate the point, let us repeat the equilibrium calculations of Figures 1 and 2, this time allowing the following aluminum-containing species to form:

gas phase: Al, AlO, Al<sub>2</sub>O, AlOH, Al<sub>2</sub>Cl<sub>6</sub>

solid phase: Al<sub>2</sub>O<sub>3</sub>, Al<sub>6</sub>Si<sub>2</sub>O<sub>3</sub>(mullite), NaAlO<sub>2</sub>,  
Al<sub>2</sub>Si<sub>2</sub>gH<sub>4</sub>(kaolinite), NaAlSi<sub>2</sub>O<sub>6</sub>(jaedite),  
Al<sub>2</sub>Si<sub>4</sub>O<sub>12</sub>H<sub>2</sub>(pyrophyllite), Al<sub>2</sub>SiO<sub>5</sub>(kyanite),  
NaAlSi<sub>3</sub>O<sub>8</sub>(albite)

For our calculations, the thermochemical data for Al, AlO, Al<sub>2</sub>O, AlOH, Al<sub>2</sub>Cl<sub>6</sub>, Al<sub>2</sub>O<sub>3</sub>, mullite, and NaAlO<sub>2</sub> were taken from JANAF

energy of formation is varied by just a few percent. Failure to account for the formation of condensed phase solutions will also change the absolute concentrations substantially; however, the qualitative behavior is not affected as much. The qualitative and quantitative behavior of product species can be strongly influenced by the selection of species to be considered in the calculation.

#### References

1. S. R. Brinkley, Jr., J. Chem. Phys., 14, 563 (1946).
2. S. R. Brinkley, Jr., J. Chem. Phys., 15, 107 (1947).
3. W. B. White, W. M. Johnson, and G. B. Dantzig, J. Chem. Phys., 28, 751 (1958).
4. S. Gordon and B. J. McBride, "Computer Program for Calculation of Complex Chemical Equilibrium Compositions, Rocket Performance, Incident and Reflected Shocks, and Chapman-Jonquet Detonations", NASA SP273, NASA-Lewis Research Center, 1971.
5. D. R. Cruise, J. Phys. Chem., 68, 3797 (1964).
6. B. Sundman, CALPHAD Conference XI, Argonne National Laboratory, May 1982.
7. H. B. Levine, JAYCOR, San Diego, CA (Private Communication).
8. G. Erickson, Acta. Chem. Scand., 25, 2651 (1971).
9. G. Erickson and E. Rosen, Chemica Scripta, 4, 193 (1973).
10. G. Erickson, Chemica Scripta, 8, 100 (1975).
11. T. M. Bessman, "SOLGASMIX-PV, a Computer Program to Calculate Equilibrium Relationships in Complex Chemical Systems", ORNL/TM-5775, Oak Ridge National Laboratory, 1977.
12. R. J. Kee and A. S. Nagelberg, Sandia National Laboratories, Livermore, CA (Private Communication).
13. R. J. Kee, J. A. Miller, T. H. Jefferson "CHEMKIN: A General Purpose, Problem-Independent, Transportable, Fortran Chemical Kinetics Code Package", SAND80-8003, Sandia National Laboratories, 1980.
14. M. Minkoff, R. H. Land and M. Blander, CALPHAD Conference XI, Argonne National Laboratory, May 1982.
15. JANAF Thermochemical Tables 2nd edition, D. R. Stull and H. Prophet, eds., U. S. Department of Commerce, National Bureau of Standards, NSRDS-NBS 37, 1971.
16. R. A. Durie, J. W. Milne, and M. Y. Smith, Combust. Flame, 30, 221 (1977).

17. R. A. Robie, b. S. Hemingway, C. M. Schafer, and J. L. Haas, Jr., "Heat Capacity Equations for Minerals at High Temperatures", U. S. Geological Survey Rep. 78-934, U.S. Department of the Interior, 1978.
18. E. M. Levine, C. R. Robbins, and H. F. McMurdie, Phase Diagram for Ceramists (The American Ceramic Society, Columbus, Ohio, 1964).
19. L. J. Wibberley and T. F. Wall, J. Inst. Fuel, 61, 87 (1982).
20. W. D. Halstead and E. Raask, J. Inst. Fuel, 42, 344 (1969).
21. R. M. Allen and J. B. VanderSande, "Analysis of Sub-Micron Mineral Matter in Coal via Scanning Transmission Electron Microscopy", SAND82-8677, Sandia National Laboratories, Livermore, CA, 1982.

TABLE I  
Chemical analysis of Pennsylvania #2 seam semianthracite coal  
(PSOC #627, provided by Pennsylvania State coal data base)

Elemental Analysis (dry)		Analysis of HTA dry coal	
77.08%	carbon	68.50%	SiO <sub>2</sub>
2.61	hydrogen	22.80	Al <sub>2</sub> O <sub>3</sub>
.73	nitrogen	2.93	TiO <sub>2</sub>
.52	organic sulfur	2.55	Fe <sub>2</sub> O <sub>3</sub>
.39	oxygen	.31	MgO
.01	chlorine	.33	CaO
18.67	mineral matter	.16	Na <sub>2</sub> O
		1.66	K <sub>2</sub> O
		.06	P <sub>2</sub> O <sub>5</sub>
		.25	SO <sub>3</sub>

TABLE II  
Chemical Species Considered in Complex Equilibrium Calculations

Gaseous	CO	CO <sub>2</sub>	Cl	Cl <sub>2</sub>	ClO	H	H <sub>2</sub>	H <sub>2</sub> O	HCl	H <sub>2</sub> S
Species	Na	Na <sub>2</sub>	NaCl	Na <sub>2</sub> Cl <sub>2</sub>	NaH	NaOH	NaOH	Na <sub>2</sub> SO <sub>4</sub>	Na <sub>2</sub> SO <sub>4</sub>	SiS
	O	O <sub>2</sub>	OH	S	S <sub>2</sub>	SO	SO <sub>2</sub>	SO <sub>3</sub>	SiO	SiO <sub>2</sub>
Condensed	C	NaCl	NaOH	Na <sub>2</sub> O	Na <sub>2</sub> S					
Species	Na <sub>2</sub> SO <sub>4</sub>	Na <sub>2</sub> SiO <sub>3</sub>	Na <sub>2</sub> Si <sub>2</sub> O <sub>5</sub>	SiO <sub>2</sub>	SiC	Si				

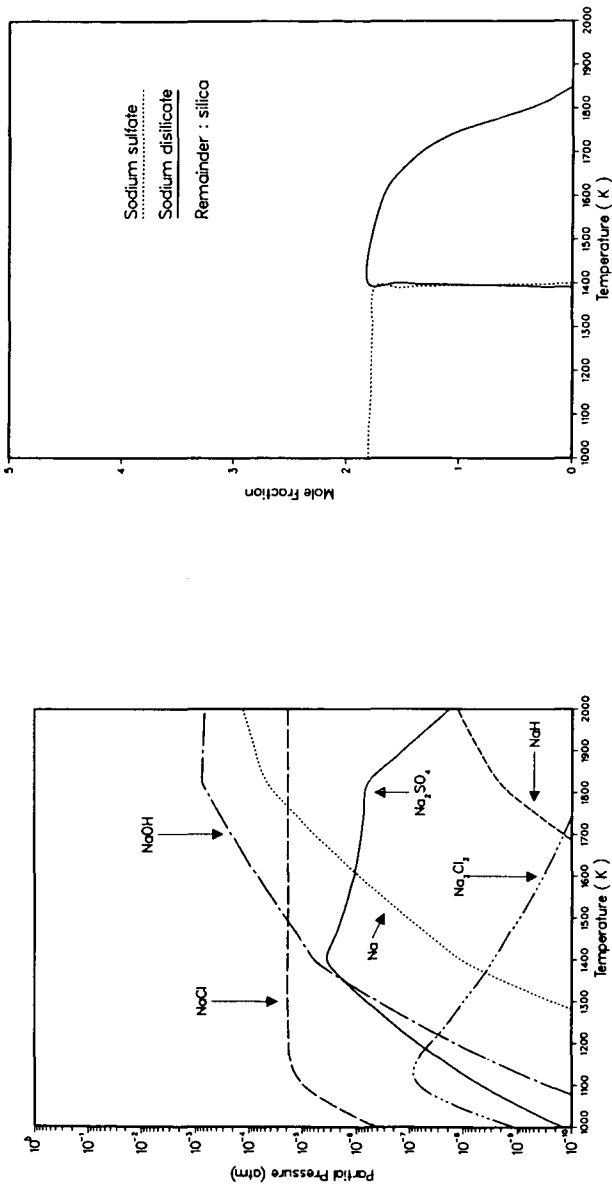


Figure 1. Sodium containing gas species predicted to form upon combustion of semianthracite Pennsylvania Seam #2 coal (PSOC #627) in 20% excess oxygen at various combustion temperatures. Chemical species considered in the calculation are given in Table I.

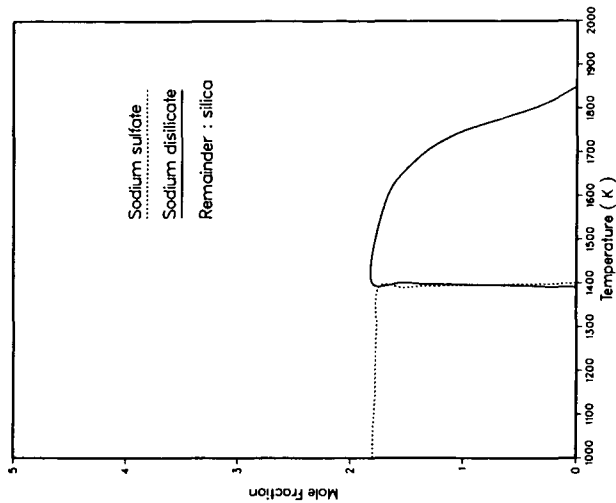


Figure 2. Condensed phases predicted to form upon the combustion of semianthracite Pennsylvania Seam #2 coal (PSOC #627) in 20% excess oxygen at various combustion temperatures.



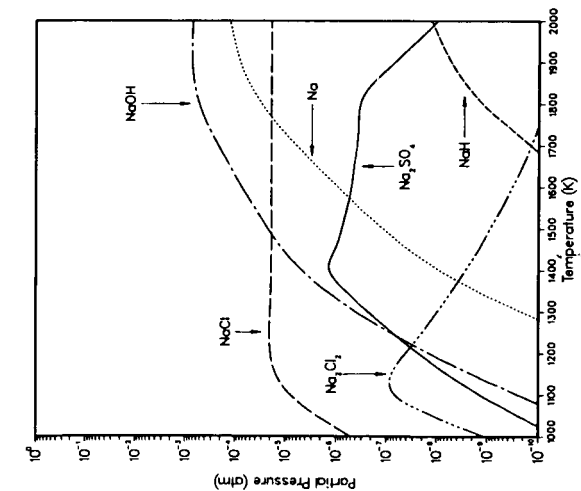


Figure 3. The effect of reducing the free energy of  $\text{Na}_2\text{SO}_4$  by 1 percent. This distribution of gas species is to be compared with Figure 1.

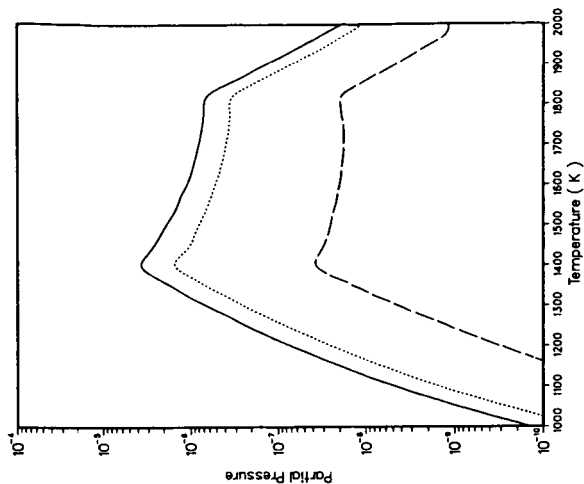


Figure 4. The effect of varying the free energy of  $\text{Na}_2\text{SO}_4$ ; solid line - JANAF data, dotted line - less stable by 1 percent, dashed line - less stable by 5 percent.

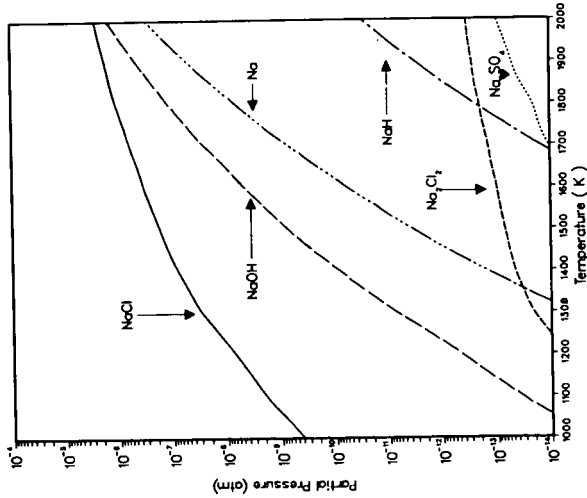


Figure 5. The effect of considering aluminum containing species in the calculations. This distribution is to be compared with that shown on Figure 1.

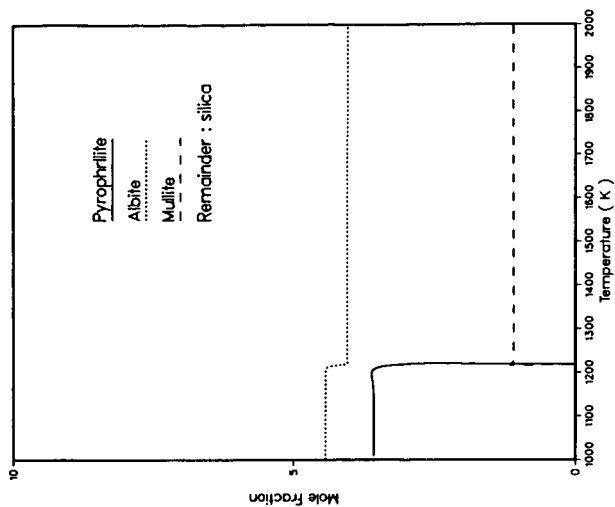


Figure 6. The effect of considering aluminum containing species in the calculations on the condensed phase distribution. This figure is to be contrasted with Figure 2.

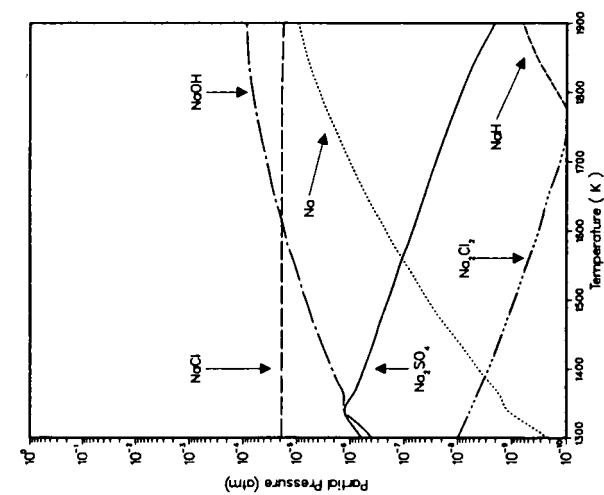


Figure 7. The effects of liquid solution formation between silica and sodium disilicate. This figure is to be compared with Figure 1.

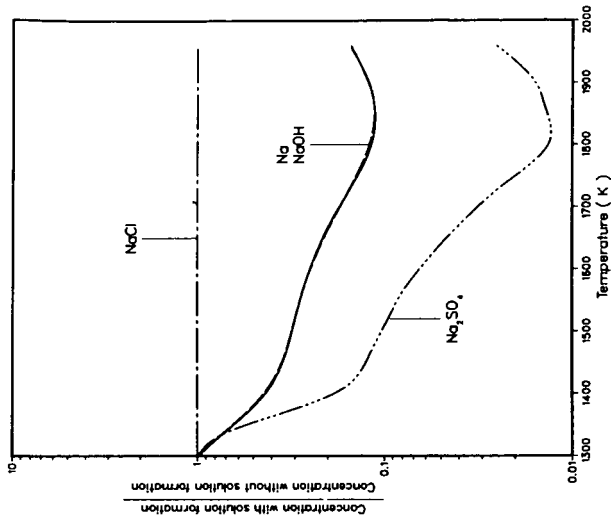


Figure 8. The effect of liquid solution formation between silica and sodium disilicate on the concentrations of species in the gas phase.

## COMPARISON OF INORGANICS IN THREE LOW-RANK COALS

S. A. Benson

Grand Forks Energy Technology Center  
U.S. Department of Energy  
Grand Forks, N.D. 58202

P. L. Holm

University of Minnesota  
Crookston, MN 56716

### INTRODUCTION

In the use of low-rank coals it has been found that inorganic materials present in these coals can have adverse effects on process performance. During combustion processes some inorganics are liberated and react with other inorganics causing combustor fouling problems (1). The unique characteristics of the flyash produced upon combustion, frequently, if concentrations of sodium and sulfur are low, produces a high resistivity ash making it difficult to collect in an electrostatic precipitator (2). In fluidized bed combustion, the inorganics of some low-rank coals can be used for sulfur retention (3) but bed agglomeration is a problem with high concentrations of sodium (4). In coal conversion processes the inorganic material can serve either as catalysts or catalyst poisons.

The occurrence of inorganic materials in low-rank coals is very complex. They are present as discrete mineral phases, as ions held by ion pair bonding with carboxyl groups or clays, and as coordinated metal ions. Knowledge of the distribution of inorganics within the coal could be used to predict effects in a given process.

We have chosen to compare the way in which inorganic material is found in three coals. These coals are two lignites from the Beulah mine, North Dakota, and the Bryan Mine, Texas and one subbituminous coal from the Rosebud mine, Montana.

1

### EXPERIMENTAL

The coals were treated using a method modified from the procedure reported by Miller and Given (5). Figure 1 shows a flow sheet of the procedure used to examine the various coals. Each coal was ground to approximately 400 mesh in an alumina grinding apparatus. The ground coal was dried using a freeze drier. Analysis of the dried coal was performed using x-ray fluorescence (XRF) and neutron activation analysis (NAA). Duplicate samples were run by placing 15-20 g of coal in a plastic beaker with 100 ml of 1M ammonium acetate. This was heated to about 70°C and stirred for 20 hours. The sample was filtered, the residue washed and dried. The solution was transferred to a 500 ml volumetric flask and made up to volume.

The solution was analyzed by inductively coupled argon plasma spectroscopy (ICAP). Samples of the residue were analyzed by XRF and NAA. The residue was treated a second time with ammonium acetate followed by two 1M hydrochloric acid extractions using the same procedure as ammonium acetate extraction.

XRF analyses were performed using the energy-dispersive Kevex\* 0700 subsystem. ICAP analysis were obtained using a Jarrell-Ash Mark I Model 975\* multi-element analyzer. Analysis is controlled by a computer using a program for 22 elements. Neutron activation analysis used in this study was performed at North Carolina State University. The system and procedures have been described elsewhere (6).

## RESULTS:

The table following shows the initial analysis of the three coals under consideration.

TABLE I  
INITIAL ANALYSIS OF COALS, PARTS PER MILLION

Analysis	Beulah N.D. Lignite	Bryan Texas Lignite	Rosebud Montana Sub-bituminous
Al	3940	12360	3370
Ba	630	190	190
Ca	12800	7130	3520
Cr	3	21	4
Cu	22	24	30
Fe	5000	20950	8450
K	930	1970	120
Mg	2490	2000	920
Mn	58	300	35
Na	4340	310	87
Ni	22	40	52
Sr	485	80	90
Ti	185	1410	280
Ash	9.5%	24.5%	4.9%

These are followed by the analyses obtained after the samples had been extracted twice with ammonium acetate. Table II shows the amount extracted from the original coal and the percent of the original.

Table III contains the results of the samples which have been extracted twice by hydrochloric acid. The amount extracted and the percent of the original coal are given.

## DISCUSSION

Examination of the initial analysis reveals the dramatic differences in the amounts of inorganic material between the three coals. Aluminum, iron, potassium, and titanium are very high in the Bryan coal compared to the values for the Beulah and Rosebud coals. In general, the Bryan has a much high inorganic content which

\*Reference to specific brand names does not imply endorsement by the U.S. Department of Energy.

TABLE II  
ANALYSIS OF COALS AFTER EXTRACTION WITH AMMONIUM ACETATE

Analysis	Beulah		Bryan		Rosebud	
	PPM Extracted	% Extracted	PPM Extracted	% Extracted	PPM Extracted	% Extracted
Al						< 1
Ba	239	38	53	28	57	30
Ca	9728	76	442	62	2003	56
Cr			3	14		
Cu						
Fe						< 1
K	186	20	177	9	2	2
Mg	2241	90	1880	94	598	65
Mn	17	30	129	43	7	20
Na	3645	84	232	75	70	81
Ni						
Sr	422	87	65	81	22	90
Ti						
Ash remaining		4.9		23.8		3.8

TABLE III  
ANALYSIS OF COALS AFTER EXTRACTION WITH HYDROCHLORIC ACID

Analysis	Beulah		Bryan		Rosebud	
	PPM Extracted	% Extracted	PPM Extracted	% Extracted	PPM Extracted	% Extracted
Al	2750	70	2719	22	1213	36
Ba	378	60	104	55	116	61
Ca	2688	21	1283	18	1408	40
Cr	1.5	51	9	41	1.5	37
Cu	21	90	10	76	5	18
Fe	1950	39	14246	68	5154	61
K			157	8	24	20
Mg	100	4	120	6	257	28
Mn	40	70	153	51	24	70
Na	43	1	9	3	10	12
Ni	6	27	21	52	3	5
Sr	63	13	15	19	56	63
Ti	22	12	409	29	154	55
Ash remaining		1.2		22.6		2.8

can also be seen by referring to the ash content listed in Table I. Further note should be taken of the high sodium content for the Beulah coal and related combustion problems (1).

The ammonium acetate extraction removes those inorganics associated as ions held by ion pair bonds to the carboxyl groups or to the clay minerals. The result of this extraction procedure is summarized in Table 2. For Beulah lignite most of the Ca, Na, Mg and Sr are bound to the carboxyl groups or possibly with the clays. The Bryan and Rosebud coals show similar trends for Ca, Na, and Sr. On the other hand, the Mg in Rosebud indicates a different association in the coal.

The hydrochloric acid extractions remove those species present in the coals as oxides, carbonate minerals, and coordinated metal ions. Larger discrepancies were noted between the coals extracted with HCl than ammonium acetate extracted. The fact that 70% of the Al is removed from Beulah is possibly explained by it being removed from the clay materials (7) but this is not well understood. Of particular interest is the removal of Ca, Mg and Sr in the Rosebud, which suggest that these elements were present as carbonate minerals. This relationship has also been suggested by Finkelman (8). The Fe is present in the coals as possibly a carbonate (siderite), oxide, and pyrite.

The changes in percent ash determined in the coal, after the ammonium acetate and HCl extractions reveal large changes in the amount of ash in Beulah and Rosebud. The total amount of inorganics removed by the ammonium acetate of the Beulah is approximately 48%. The percentage of ash removed for Rosebud was approximately 22% with ammonium acetate. The Bryan lignite has only 3% of its ash associated with the ion exchangeable fraction. The major inorganic constituents remaining in the coals after both extractions consist of quartz, clays and pyrite.

## CONCLUSIONS

The alkaline and alkaline earth metals in all three coals are partially or totally removed with ammonium acetate extraction. The major differences between the coals are:

1. 48% of the total inorganics of the Beulah are removed with ammonium acetate by far the highest of 3 coals.
2. Bryan Texas lignite consists of mostly extraneous mineral matter including clays and quartz minerals (9).
3. The Rosebud subbituminous has higher percentages of Mg, Ca, and Sr associated as carbonates, revealed in the HCl extractions.

## REFERENCES

1. D.K. Rindt, M.L. Jones, and H.H. Schobert. Investigations of the mechanism of ash fouling in low-rank coal combustion, Preceeding of the Engineering Foundation Conference, Henniker, NH, July 12-17, 1981
2. S.J. Selle, L.L. Hess, and E.A. Sondreal. Western fly ash composition as an indicator of resistivity and pilot ESP removal efficiency. Paper No. 75-02.5. Presented at 1975 Meeting, Air Pollution Control Association, Boston, MA, June 15-20, 1975.

3. G.M. Goblirsch, and E.A. Sondreal. Low-rank coal atmospheric fluidized-bed combustion technology. Proceedings, Technology and Use of Lignite, BuMines-Univ. of N. Dak. Symposium, Grand Forks, N. Dak., May 30-31, 1979, GFETC/IC-79/1, pp. 75-107.
4. S.A. Benson, F.R. Karner, G.M. Goblirsch, D.W. Brekke. Bed agglomerates formed by atmospheric fluidized bed combustion of a North Dakota lignite. ACS, Div. of Fuel Chem. Preprints, 27, No. 1, 174(1982).
5. R.N. Miller, and P.H. Given. Variations in inorganic constituents of some low-rank coals. in R.W. Bryers. Ash deposits and corrosion due to impurities in combustion gases. Hemisphere Publishing Corp., Washington, D.C. 1977. pp 39-50.
6. J.N. Weaver in Analytical Methods for Coal and Coal products, Vol I p. 377-401. Ed. Academic Press, Inc. N.Y. (1978).
7. R.N. Miller and P.H. Given. A geochemical study of the inorganic constituents in some low-rank coals. U.S. DOE report FE-2494-TR-1 (1979)
8. R.B. Finkelman in Atomic and Nuclear Methods in Fossil Energy Research p. 146-150 141, Plenum Press, New York and London, 1982
9. Energy Resources Co. Inc., Walnut Creek, CA 94596. Low-rank Coal Study, National Needs for Resource Development-Resource Characterization. DOE/FC/10066-T1 (Vol. 2) Nov. 1980, p 95-109



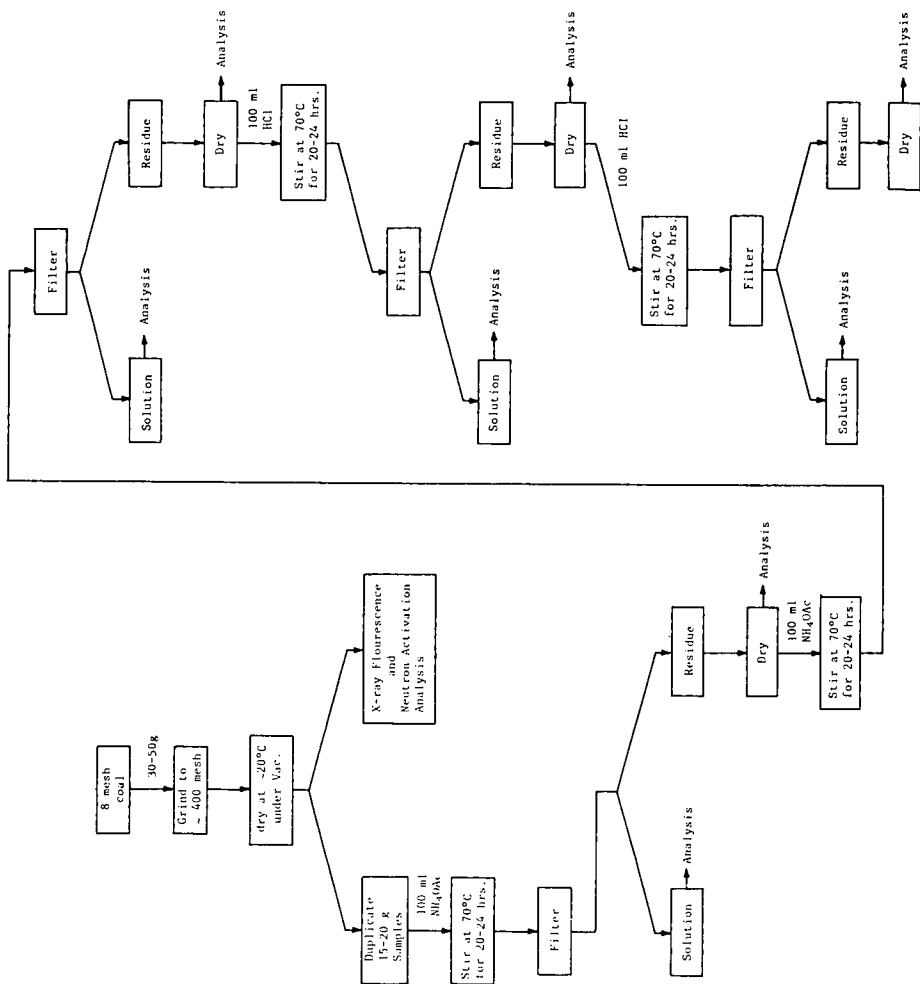


FIGURE 1. Flow diagram of extraction procedure.

# Thermodynamics of Coal Chars; Correlation of Heat Capacity with Composition and Pyrolysis Conditions

Leslie L. Isaacs  
Elliot Fisher

Department of Chemical Engineering  
The City College of CUNY  
140th Street and Convent Avenue  
New York, NY 10031

## Introduction

Heat capacity data for a char can be used to calculate the variation of the thermodynamic properties, H, S, G, etc. with temperature. Factors which affect the heat capacity are:

- o the rank and inorganic matter content of the parent coal;
- o the gaseous atmosphere present during pyrolysis;
- o the thermal history of the char.

Thermal history for a char is determined by:

- o the pyrolysis temperature;
- o the rate at which the coal temperature is raised from the ambient to the pyrolysis temperature;
- o the residence time of the char at the pyrolysis temperature.

The thermodynamic literature (1-5) for chars usually covers only limited temperature ranges and the thermal histories and compositions of the char samples are ill-defined or unavailable. The additivity approach (6,7) is usually employed to correlate the heat capacities in terms of char constituents; organic matter, ash and moisture.

In the thesis work of Wang (8) the effect and relative importance of the factors listed was assessed using a selected set of chars. Experimental data was collected between 80°K and 300°K. It was found that the heat capacities could be correlated with compositions and pyrolysis temperatures using a modified form of the Debye model for heat capacities (9). The correlation is in the form of an expression for an effective Debye temperature,  $\theta(\text{Tr})$ :

$$\theta(\text{Tr}) = \theta_0(\text{Tr}) \exp[I(\text{Tr})/x(1-x)] \quad 1)$$

where Tr is a reduced temperature defined as:

$$\text{Tr} = T(\text{K})/T_{\text{pyrolysis}}(\text{K})$$

1-x = the atomic fraction of carbon in the ash free dry char.

$\theta_o(Tr)$  = a Debye temperature at  $Tr$  for a hypothetical char containing carbon atoms only.

$I(Tr)$  = an interaction parameter between the carbon atoms and the "other" atoms in the char.

$\theta_o$  and  $I$  were found by empirical fitting of the data for each family of chars. A char family consists of all the chars prepared from the same coal with one hour residence time.

Our present objective is to:

- o Test the limits of applicability of Equation 1 as an extrapolating function to calculate heat capacities of chars;
- o To refine the correlation model;
- o To factor into the correlating the effect of residence time at pyrolysis temperature.

### Experimental Technique

The suite of samples from Wang's work was used for heat capacity measurements between 300°K and 900°K. The data were obtained using the differential scanning calorimetry (DSC) technique. Instrumentation consisted of a Dupont model 910 scanning calorimeter and a Dupont model 1090 thermal analyzer system. Sample heat capacities were calculated using the measured heat capacity of Sapphire as a standard for comparison.

### Results

Typical experimental information obtained is illustrated in the following figures.

#### Effect of Pyrolysis Temperature

In Figure 1 we show DSC scans for two chars prepared from demineralized Virginia Coal (PSOC-265). The results show that the heat capacity of the chars increase with temperature between 300K and 900K. Also the char prepared at 1100°C has a higher heat capacity at any given temperature (over the range) than the 700°C char. For quantitative comparison the heat capacities need to be normalized. The normalizing procedure is arbitrary. We have elected to normalize all our data to the number of atoms in the ash free char.

#### Effect of Residence Time

In Figure 2 we show DSC scans for chars prepared from demineralized Virginia coal at 1100°C pyrolysis temperature.

The chars differ in their thermal history by the length of their residence time at pyrolysis temperature. The normalized heat capacities at a given temperature vary in magnitude with the residence time.

A minimum in heat capacity is seen to occur if the data is replotted as heat capacity versus residence time. From the present data the minimum is around two hours residence time. Our interpretation of this phenomenon is that two separate events are being observed. One is the equilibration of the chemical composition at 1100°C by breakage of C-H bonds. The smaller the number of such bonds in the char the smaller is its heat capacity. The second is the approach of the char to structural equilibrium by solid state diffusion. The char is graphitizing with an apparent increase in heat capacity.

#### Effect of Retained Inorganic Matter

In Figure 3 the DSC scans of chars prepared at 700°C with one hour residence time are compared. Both of these chars were prepared from Virginia coal. However, in one case the coal was demineralized using the acid wash procedure prior to pyrolysis. On a per gram sample basis the heat capacity of the mineral matter containing char is about 40 to 80% higher than the demineralized char. The inorganic matter heat capacity is additive to the organic matter heat capacity.

#### Conclusions

At the time of preparation of this preliminary paper (December 1982) the calculation for testing and refining the correlation model have not been completed. We expect to be able to present them at the meeting.

#### References

1. Delhaes, P., and Y. Hishiyama. Carbon 8:31 (1970).
2. Kamiya, K., S. Mrosowski and A.S. Vagh. Carbon 10:267 (1972).
3. "Thermal Data on Gasifier from Synthane Test," Internal Report, Thermodynamics Research Group, Department of Energy, Bartlesville Energy Research Center (1973).
4. Kasatochkin, V.I., K. Usenbaev, V.M. Zhadanov, K. Sabyraliev, M. Rasalhaev and E. Zhumalieva. Dokl. Akad. Nauk (USSR), 216:93 (1974).
5. Tye, R.P., Desjarlais, A.O., Singer, J.M., High Temper - High Pressures, 13:57 (1981).
6. Kirov, N.Y. Brit. Coal Util. Res. Assoc. Mon. Bull. 29 (1965), p. 33.

References (cont.)

7. Eisermann, W., P. Johnson and W.L. Conger. Fuel Proc. Technol. 3:39 (1980).
8. Isaacs, L.L. and Wang, W.Y. in "Chemical Engineering Thermodynamics." S.A. Newman, Ed. (Ann Arbor Science 1982) pps. 451-459.
9. Maradudin, A.A. in "Solid State Physics" (Academic Press, 1966) 18: p. 274.

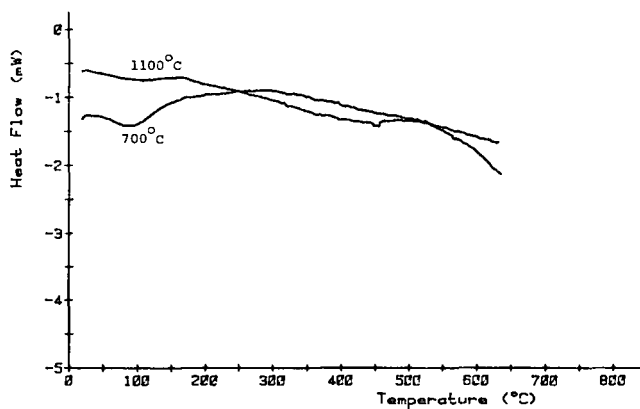


Figure 1. DSC Scans on Virginia Chars. (One hr. residence time - demineralized).

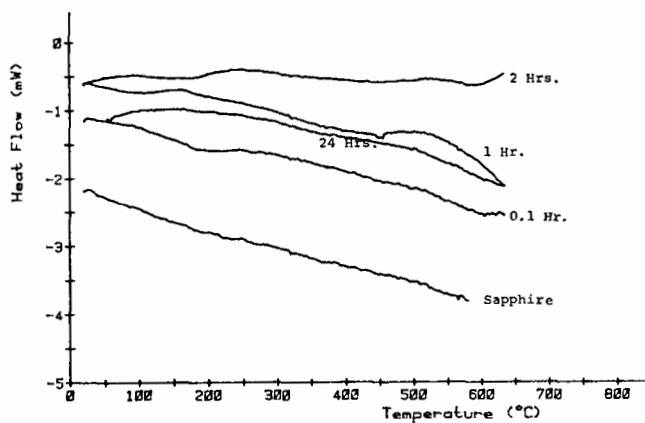


Figure 2. DSC Scans on Virginia chars. (1100°C Demineralized)

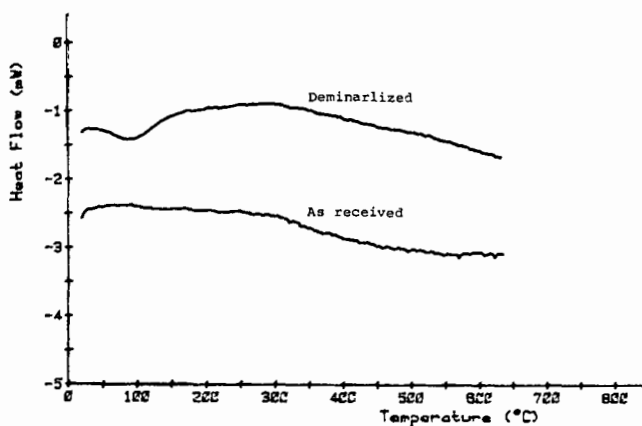


Figure 3. DSC Scans on Virginia chars. (700°C - One hour residence time)

GAS CRACKING CHARACTERISTICS IN THE COMMERCIAL RANGE OF OPERATIONS. R. Orriss, G. B. Nowowiejski and A. P. Moore. The M.W. Kellogg Company, 3 Greenway Plaza East, Houston, Texas 77046.

The cracking of gases for ethylene production has undergone a resurgence in recent times in the U.S.A. Prices for ethane have truly made it the feedstock of opportunity. Ethane continues to be of great interest as a feedstock in areas which have large gas reserves, among these being Canada, Indonesia, Nigeria, etc. Cracking conditions for ethane and propane require some interesting evaluations evolving from the unique situation with gases whereby unconverted feedstock is recovered as a pure product and can be recycled. The recycling of unconverted feed impacts the recovery section capacity and the ultimate yield of products obtained. This paper will show how the selection of severity is influenced by the values placed on feed, capital and by-products, for pure feeds and mixtures of ethane and propane. In designing new plants, the designer must also consider the effects of contact time and partial pressure. This paper will also look at the basic variations which affect capacity and ultimate yields as partial pressure and contact time are varied over the practical ranges achievable in commercial operations.

IMPLICATIONS OF FEEDSTOCK FLEXIBILITY IN THE DESIGN OF OLEFINS PLANTS. Stephen DeHaan. C-E Lummus, Combustion Engineering, Inc., 1515 Broad Street, Bloomfield, New Jersey 07003.

Currently operational olefins plants crack feeds ranging from ethane to vacuum gas oil. Until recently, most individual plants were designed to utilize a single feed. Even plants with some feedstock flexibility were usually based on either natural gas derived feedstocks or crude oil based feedstocks. Current and predicted future market forces dictate that new plants have considerably more flexibility. To assess the impact of feedstock flexibility on overall plant energy consumption and capital costs, a selection of case studies are analyzed.

OPTIMAL CONTROL OF AN OLEFINS PLANT. M. D. Weiss, Bechtel Petroleum, Inc., Houston, Texas 77001-2166

Within the past five years improvement in microprocessor computer control of Olefins Plants have enabled realization of numerous benefits in economy and energy savings in these facilities. The use of advanced control facilitated by microprocessor distributed control made optimization and control of pyrolysis furnaces, distillation columns, dryers, and other unit operation readily available to the ordinary control engineer, using environmental variable control, material balance control, heat balance control, energy minimization, and pollution control. Details will be supplied of control techniques used in the pyrolysis furnace, demethanizer system, acetylene removal and methyl acetylene/propadiene removal reactors, depropanizer, various driers and distillation columns, resulting in cost and energy savings, and in better control when the plant is operated at reduced capacity.

REACTOR SURFACE EFFECTS DURING STEAM PYROLYSIS OF A WHOLE CRUDE. C. W. Chang and B. L. Crynes. School of Chemical Engineering, Oklahoma State University, 423 Engineering North, Stillwater, OK 74078.

The thermal decomposition of an Alaskan crude oil in the presence of steam was studied in unpacked, downflow reactors. The experiments were conducted at essentially atmospheric pressure over a temperature range of 650-800 C with a mass ratio of oil-to-steam of 2.5. Four different reactors; 304 ss, alonized 304 ss, Vycor and Inconel 600, were chosen to study wall effects. The products from the pyrolysis reactions were lumped into three distinct entities: (i) a heavy liquid fraction boiling in the range of 210-550 C, (ii) a light liquid fraction from  $C_4$  to boiling point of 210 C, and (iii) gas plus coke.

A model of reversible series reactions was postulated to fit the experimental data, and successfully predicted the trends of conversion and yields. The different surfaces showed varying effects on product distributions and coke formation.

FLASH PYROLYSIS PROCESS FOR THE PRODUCTION OF CHEMICALS AND FUELS FROM BIOMASS. Muthu S. Sundaram, Meyer Steinberg, and Peter Fallon, Process Sciences Division, Department of Energy and Environment, Brookhaven National Laboratory, Upton, NY 11973.

The objective of the work is to produce transportation fuels and chemical feedstocks from Biomass via Flash Pyrolysis. Experiments were conducted with oven-dried, saw-dust of Douglas Fir wood in a downdraft, continuous flow, bench scale reactor. The pyrolysis-gasification of wood particles was done in one step with no use of catalysts. The influence of various gaseous environments - which include hydrogen, helium and methane - on the reactivity of wood was investigated. The combined effects of high heat-up rate ( $10^4 - 10^5$  °C/sec) of the wood particles and short residence times (0.5 - 4 sec) of the devolatilization products resulted in an almost complete gasification of carbon (99% C) in the feed wood at 850°C and 50 psi hydrogen pressure. Pyrolysis in methane was characterized by high yields of ethylene (up to 21% C) and BTX (up to 12% C). The effects of various pyrolysis atmospheres and major process variables on the yield and distribution of products were studied in detail. The composition of pyrolysis tars and basic kinetic data were also obtained. Preliminary economic analyses for the production of pipeline gas and methanol and chemical feedstocks have been made.

GAS EVOLUTION DURING PYROLYSIS OF CHATTANOOGA OIL SHALE R. J. Feng and M. D. McKinley. Chemical and Metallurgical Engineering Department, The University of Alabama, P. O. Box G, University, Alabama 35486.

A composite sample of Chattanooga oil shales from several counties in the states of Alabama and Tennessee was pyrolyzed in a nitrogen atmosphere to 990°C at three heating rates; 2, 5, and 12°C/min. The nonisothermal pyrolysis processes were carried out either without temperature soaking or with 10 hours isothermal soaking at 230°C. The oil shale particle sizes examined were -3+4 mesh and -8+16 mesh. A first order kinetic rate equation was used as the nonisothermal kinetic model in this study. Two kinetic parameters, frequency factor and activation energy, were evaluated by fitting the model kinetic equation to the gas evolution data using a nonlinear least squares program. The major gases identified in the pyrolysis gas include hydrogen, carbon monoxide, methane, carbon dioxide, ethene, ethane, and propane. The oil yield increased from 31.88 % to 54.79 % of the modified Fischer Assay as the heating rate changed from 2 to 12°C/min. The total volumes of gaseous products decreases from 85.68 cm<sup>3</sup>/g raw shale to 36.23 cm<sup>3</sup>/g raw shale when the heating rate increased from 2 to 12°C/min. Generally, lower heating rates tended to shift the maximum gas evolution rate to lower temperatures. Soaking the oil shale particles isothermally at 230°C for 10 hours did not improve the oil yield in this study. The nonisothermal kinetic model used gave a good representation of the thermogravimetric experimental data measured.



COAL ANALYSIS USING THERMOGRAVIMETRY. M. A. Serageldin and Wei-Ping Pan.

Thermogravimetric, TG, analysis is increasingly being used today to obtain kinetic data related to coal decomposition. However, this method is open to criticism on the basis that the meaning of the activation energy of solid state reactions obtained from TG experiments is not clear. In this study a linear relationship between procedural activation energy and enthalpy of reaction was found. This is typical of elementary reactions of atoms and small radicals. The effects of alkali metal salts on the decomposition of coal under three gas atmospheres ( $N_2$ ,  $CO_2$ , and air) were investigated. Several features were reported such as the effect of the catalysts on coal conversion and  $CH_4$ ,  $CO$  and  $CO_2$  emission. These were related to observed changes in activation energy.

KINETIC INVESTIGATION OF LIGNITE PYROLYSIS. Jefferson Jih and Uzi Mann, Department of Chemical Engineering, Texas Tech University, Lubbock, Texas 79409.

In this paper we describe an experimental method for determining the individual kinetic parameters (frequency factors and activation energies) for the formation of gaseous, liquid and solid products during lignite pyrolysis. The system constructed facilitates the collection of the gas and tar formed and measurement of the solid weight loss as a function of time. In addition, the technique facilitates monitoring the solid temperature with time. The latter enables one to account for the solid "heating-up" effect in determining the kinetic parameters.

The pyrolysis of San Miguel (Texas) lignite between 600 and 950°C was investigated. It was found at these temperatures the sum of all lignite decomposition reactions is exothermic. This is probably due to partial simultaneous oxidation of the lignite with structure oxygen. An attempt is described for estimating the pyrolysis rates constant by subtracting of the originated gaseous carbon products from the total gas generated. Experimental kinetic data of Texas lignite are analyzed and the theoretical basis and computation procedures of estimating the kinetic parameters are discussed.

LIGNITE DEVOLATILIZATION IN A FIXED BED REACTOR. A. J. Gokhale and R. Mahalingam, Department of Chemical Engineering, Washington State University, Pullman, WA 99164.

Devolatilization of lignite coal with a steam/oxygen mixture in a fixed-bed, atmospheric pressure reactor, in the temperature range 300 C to 550 C, with the objective of studying the tars. The particle sizes were (-2+1), (-3+2) and (-4+3) mm. The tar yield was observed to increase and then decrease with temperature, due to secondary cracking reactions. The melting point, viscosity and specific gravity of the tar samples increased with increase in devolatilization temperature. A first order single reaction model, when fitted to the experimental data, yielded an energy of activation in the range 15 to 18 kCal/mol, irrespective of particle size. A series-parallel reaction model indicated that the cracking of tar to char kinetically represented the most difficult step.

PYROLYSIS OF WESTERN CANADIAN COALS IN A SPOUTED BED REACTOR. A. Jarallah and A. P. Watkinson. Department of Chemical Engineering, The University of British Columbia, Vancouver, B.C. Canada V6T 1W5.

Coal pyrolysis has been studied in a 12.8 cm dia. continuous spouted bed reactor with the aim of determining conditions for maximum liquid yields from Western Canadian coals. Nitrogen and nitrogen/carbon dioxide mixtures and coal of size -  $3.36 + 1.12$  mm are fed at atmospheric pressure to an electrically heated reactor containing sand. The tar yield is determined by sampling the outlet gas through a series of cooled impingers. The spouted bed pyrolyzer behaves in a manner similar to a fluidized bed unit, and shows a maximum tar yield with temperature at a fixed feed rate. At a given pyrolyzer temperature, the tar yield was inversely proportional to the coal feed rate over the range 0.4 to 7.6 kg/h. Coal type strongly influenced the liquid yields as expected. A bituminous coal (Sukunka) from the Peace River coal field gave a maximum tar yield at  $600^{\circ}\text{C}$  of 31% wt/wt MAF coal at a feed rate of  $116 \text{ kg/hr-m}^2$ . The corresponding gas yield was 2.8%, and the char yield (uncorrected) was 64%. At about the same throughput, a maximum tar yield of 19.4% wt/wt MAF coal at  $580^{\circ}\text{C}$  was found for Balmer coal - a bituminous coal from the Crowsnest coal field. A sub-bituminous coal, Forestburg, from the Edmonton Formation produced significantly higher gas yields of 20% versus 6% for the bituminous coals due to higher  $\text{CO}_2$  production and a tar yield of 21% at  $530^{\circ}\text{C}$ . With Sukunka coal, a steady increase in tar yield from 20.4 to 22.4 to 26.7% wt/wt MAF coal was found as the average coal particle size was reduced from 2.28 to 0.95 mm to 0.65 mm. No significant effects on tar yield were found for variations in bed depth, or vapour residence time.

FAST FLAMES AND DETONATIONS. John H.S. Lee, McGill University, 817 Sherbrooke St.W. Montreal, Quebec H3A 2K6.

Turbulence and adiabatic heating by shock waves are two important physical mechanisms whereby the combustion rate of a given fuel-air mixture can be increased dramatically. Apart from enhancing the energy and mass transport rates, turbulence also increases the area of the burning surface significantly. Adiabatic compression of the unburned mixture by shock waves provides an effective mechanism due to the strong exponential temperature of chemical reaction rates. The present paper describes some recent investigations of very fast turbulence flames and detonations in homogeneous fuel-air mixtures. Unlike most studies on turbulence flames where the flame is stabilized in a steady turbulent flow of unburned mixture, the present study deals with freely propagating flames where turbulence in the unburned flow ahead of the flame is induced by obstacles. Very fast flames can be generated in this manner and permits a closer look at the turbulent quenching mechanism which eventually places the upper bound on the maximum turbulent burning rate of a given system. The detonation mode of combustion exploits the shock heating mechanism to achieve the required burning rate associated with a supersonic combustion wave. The structure of detonation waves is one consisting of multiple shock intersections giving its universal cellular structure. Significant advances have been made in recent years in achieving a direct linkage between the microscopic cellular structure of the detonation front and the various macroscopic dynamic detonation properties of the mixture itself (i.e., detonability limits, initiation energy, characteristic chemical times, critical diameter, etc.).

CHEMICAL KINETIC - FLUID DYNAMIC INTERACTIONS IN DETONATIONS, E. S. Oran, Naval Research Laboratory, Code 4040, Washington D. C., 20375.

In this review we summarize the work done at the Naval Research Laboratory aimed at deciphering some of the important basic interactions occurring in detonations in gaseous mixtures. The tools for these studies have been one- and two-dimensional numerical models which couple a description of the fluid dynamics to descriptions of the detailed chemical kinetics and physical diffusion processes. Four topics will be discussed; i) the sensitivity of ignition times to perturbations in pressure or temperature [1]; ii) the structure of ignition behind shock waves and the transition to detonation [2]; iii) detailed simulations of the propagation of detonations and the structure of detonation cells [3]; iv) power-energy relations for detonation initiation [4]. We will emphasize the common factors in these topics, all of which involve a close coupling between fluid dynamics and chemical kinetics. This coupling is especially apparent in cases of weak ignition or marginal detonations.

- (1) E.S. Oran and J.P. Boris Weak and Strong Ignition, II, in Combust. Flame, Nov., 1982
- (2) K. Kailasanath and E. Oran, to appear Combust. Sci. Tech., 1983.
- (3) E.S. Oran, T. R. Young, J.P. Boris, M.J. Picone, and D. H. Edwards, Proceedings of the 19th Symposium on Combustion, to appear 1983.
- (4) K. Kailasanath, in preparation.

CHEMICAL KINETIC FACTORS IN GASEOUS DETONATIONS. C. K. Westbrook, Lawrence Livermore National Laboratory, P. O. Box 808, Livermore, California 94550.

Computer modeling techniques have been applied to study hydrogen and hydrocarbon oxidation in gaseous detonation waves. Characteristic reaction times and lengths are computed for combustible gas mixtures which have been compressed and heated by a shock wave traveling at the Chapman-Jouguet detonation velocity. These characteristic times and lengths correlate well with observed detonation parameters, including critical tube diameters for transition to spherical detonation, detonation cell sizes, critical initiation energies, and lean and rich limits for detonation in a linear tube. Detailed kinetic analysis of the structure of the induction zone in these models has been carried out and provides a great deal of new insight and information. In particular, these results show how kinetic modification of detonation parameters can occur. Inhibition or extinction of a detonation is shown to occur from increases in the ignition delay time, and increased detonability or kinetic sensitization results from decreased ignition delay times. Both processes are explained by their influence on details in the reaction mechanisms used by the numerical model.

PERTURBED OSCILLATORY REACTIONS AND EFFICIENCY OF ENGINES. John Ross, Stanford University, Department of Chemistry, Stanford, California 94305

The combustion of certain reactants ( $\text{CH}_3\text{CHO}$ ,  $\text{C}_2\text{H}_6$ , isobutane) run in a well stirred continuous reactor show a variety of nonlinear properties including multiple stationary states, and simple and complex temporal oscillations of concentrations of chemical intermediates. External periodic perturbations of oscillatory reactions lead to entrainment, quasi-periodic variations, resonance responses in amplitudes, phase locking, and the possibility of a degree of control of dissipation and hence efficiency of the combustion process. We conclude with a new example of an engine which uses  $\Delta G$ , not  $\Delta H$ , of a reaction.

A REVIEW OF PLASMA JET IGNITION. R. M. Clements, Department of Physics, University of Victoria, Victoria, British Columbia, Canada, V8W 2Y2.

During the last decade or so there has been considerable interest in lean burn internal combustion engines. The motivating reasons for this are the reduction of pollutants and increased fuel economy. However such mixtures are difficult to ignite and have longer burn times by comparison to stoichiometric mixtures. One way of alleviating these problems is with plasma jet ignition. The mechanical construction of the igniter as well as the associated electrical circuitry required to power the igniter will be discussed. The igniter produces a "puff" of gas which is the ignition kernel. How this "puff" behaves will be examined when it is either in the presence or the absence of a combustible mixture. This will be done in the light of the relative roles of fluid mechanical turbulence and chemical effects. Finally the practical aspects of using these igniters in internal combustion engines and the associated problems will be reviewed.

EXPERIMENTAL AND COMPUTATIONAL STUDIES OF THE CHEMISTRY OF IGNITION PROCESSES.  
Thompson M. Sloane and John W. Ratcliffe, Physical Chemistry Department, General Motors Research Laboratories, Warren, Michigan 48090

In order to explore the detailed chemistry of ignition by electric spark, plasma jet, and photochemical methods, a molecular beam mass spectrometer system for making time-resolved measurements of transient combustion phenomena has been constructed. Radicals as well as stable components of a propagating flame and of an ignition kernel have been detected. Simultaneous schlieren photographs characterize the physical processes involved in the ignition as well as the nature of the interaction of the flame with the sampling cone. These experimental results are supplemented with computational studies of idealized ignition processes. Such computations, which employ a one-dimensional model that includes detailed chemical kinetics and fluid mechanics, are helpful in understanding the chemistry of ignition processes. Our most recent experimental and computational results will be presented.

NITROGEN CHEMISTRY IN FLAMES: OBSERVATIONS AND DETAILED KINETIC MODELING. A. M. Dean, M. S. Chou and D. Stern. Exxon Research and Engineering Company, Corporate Research-Science Laboratories, P.O. Box 45, Linden, New Jersey 07036.

Spatially resolved concentration profiles of  $\text{NH}_3$ ,  $\text{NH}_2$ ,  $\text{NH}$ ,  $\text{NO}$ , and  $\text{OH}$  have been measured in rich ( $\phi = 1.28$ - $1.81$ ) atmospheric pressure  $\text{NH}_3/\text{O}_2/\text{N}_2$  flames. All species other than  $\text{NO}$  were observed via laser absorption.  $\text{NO}$  data were obtained via laser induced fluorescence and calibrated by absorption measurements in lean ammonia flames. These measurements formed the basis for an extensive series of mechanistic calculations to better define the high temperature kinetic behavior in ammonia flames. The measured  $\text{NO}$  concentrations were an order of magnitude lower at 3-4 mm above the burner than one would predict from a conventional measurement of ammonia oxidation. Furthermore, the  $\text{NH}$ ,  $\text{NH}_2$ , and  $\text{NH}_3$  concentrations were much lower than predicted. These comparisons strongly suggest that "new" reactions such as  $\text{NH}_2 + \text{NH}_2$  to ultimately yield  $\text{N}_2$  are important in these flames. Inclusion of these reactions yielded results in good agreement with the observations.  $\text{NO}$  profiles have also been measured in rich ( $\phi = 1.7$ - $1.8$ ) atmospheric pressure  $\text{CH}_4/\text{O}_2/\text{air}$  flames. These  $\text{NO}$  measurements are the first to delineate the spatially resolved formation of "prompt  $\text{NO}$ ". The rise and subsequent decay of the  $\text{NO}$  signal within the flame front is discussed in terms of an expanded prompt  $\text{NO}$  mechanism. The above examples illustrate the wealth of kinetic information that can be obtained by coupling laser diagnostic techniques to detailed kinetic calculations in flames. The recent advances in computational techniques and the ability to directly monitor reactive intermediates have presented kineticists with new opportunities to probe complex flame systems.

THE FORMATION OF NO AND  $N_2$  FROM  $NH_3$  IN FLAMES. R. J. Blint and C. J. Dasch.  
Physics Department, General Motors Research Laboratories, Warren, Michigan 48090.

Ammonia oxidation at high temperatures is an interesting kinetic system of significant technological importance for NO formation and destruction. Recent work has largely been devoted to the moderate temperature (1300 K) region in which  $NH_3$  can quantitatively destroy NO. This paper will describe flame studies (1800- 2800 K) of  $NH_3$  oxidation in which  $NH_3$  is a model compound for the conversion of fuel-bound nitrogen to NO and  $N_2$ . A detailed (42 reactions) reaction scheme has been constructed from literature rate constants which predicts our measured flame speeds, major specie profiles, and NO levels in ammonia-oxygen-diluent flames. These predictions require that the radical pool size and the  $N_2$ /NO branching be correctly described. This mechanism has been further tested against our measurements of NO emissions from  $CH_4$ -air flames doped with  $NH_3$  and NO. This Fenimore-type "loading" experiment indicates that  $NH_3$  is pivotal, but that many reaction partners (OH, O,  $O_2$ ,  $NH_2$ , as well as NO) are important.

CHEMICAL KINETIC EFFECTS IN SOOT FORMATION. Irvin Glassman, Kenneth Brezinsky, Alessandro Gomez and Fumiaki Takahashi. Department of Mechanical and Aerospace Engineering, Room D-329 Engineering Quadrangle, Princeton University, Princeton, New Jersey 08544.

Evidence indicates that the fuel pyrolysis rate is the controlling factor in soot formation. Under pre-mixed flame conditions, the rate of increase with temperature of fuel pyrolysis to form the soot precursors is slower than the rate of increase of oxidation. Thus increasing the flame temperature decreases the tendency to soot. Sooting equivalence ratio data and chemical kinetic flow reactor results support this postulate and show that previous lists categorizing the tendency of fuels to soot are misleading. Recent kinetic results on the oxidation of aromatics gives great insight with regard to the aromatics propensity to soot. Since there is no oxidative attack of the fuel in a diffusion flame, sooting tendency increases with increasing flame temperature. Smoke point data as a function of temperature reveals the importance of fuel pyrolysis kinetics and initial fuel structure. Flow reactor pyrolysis kinetic results indicate that not only is the pyrolysis rate important, but also the pyrolysis intermediates formed.

SURFACE GROWTH OF SOOT PARTICLES IN PREMIXED ETHYLENE FLAMES  
Stephen J. Harris and Anita M. Weiner. General Motors Research Laboratories  
Warren, Michigan 48090.

Most of the mass of soot particles is provided by a heterogeneous process called surface growth, in which gas phase hydrocarbon molecules (growth species) react chemically with and become incorporated into the soot particles. We have found that the greatly increased surface growth found in richer flames is accounted for primarily by the increased surface area available for growth in those flames, rather than by a higher concentration of growth species. Thus, richer flames are sootier because they have a higher nucleation rate. Depletion of the growth species does not occur in our flames. Therefore, the final mass reached by the soot particles, when surface growth has virtually ceased, is determined by a decrease in the reactivity of the soot. Our data and our analysis are consistent with surface growth being due primarily to a first order reaction of acetylene with the soot particles, diacetylene playing a minor role.

ION CONCENTRATIONS IN PREMIXED ACETYLENE FLAMES.\* D.G. Keil, R.J. Gill, and D.B. Olson

A large variety of ionic species have been observed in premixed  $C_2H_2/O_2$  flames. In nonsooting flames, the major ionic species are of low mass (19 or 39 amu) while in fuel rich, sooting flames, much higher ion masses are observed, in support of an ionic soot precursor mechanism. In order to evaluate the role of flame chemi-ions in the soot initiation process, we have used the electrostatic Langmuir probe technique to measure absolute total ion concentration profiles as functions of height above the burner in low pressure, laminar premixed  $C_2H_2/O_2$  and  $C_2H_2/O_2/M$  ( $M$  = diluent) flames with equivalence ratios,  $\phi$ , from considerably less than to significantly greater than the threshold equivalence ratio,  $\phi_c$ , where soot is first observed. The maximum flame ion concentration decreases with increasing equivalence ratio in both nonsooting and sooting flames. However, in very fuel rich sooting flames the maximum ion concentration eventually begins to increase with further flame enrichment. This phenomenon and the observed temperature effects on the ion profiles, ion concentrations, and soot threshold will be described. The implications of the observations on the ionic theory of soot formation will be discussed.

\*Work supported by DOE-Pittsburgh Energy Technology Center under Contract No. DE-AC22-80PC30304 and Air Force Office of Scientific Research under Contract No. F49620-81-C-0030.

REACTIVITIES AND STRUCTURES OF  $C_5H_5^+$  IONS AND THEIR RELATIONSHIP TO SOOT FORMATION. F. W. Brill, T. J. Buckley, and J. R. Eyler, Department of Chemistry, University of Florida, Gainesville, Florida 32611 and S. G. Lias and P. J. Ausloos, National Bureau of Standards, Washington, D.C. 20234.

Ion-molecule reactions have been proposed as important in the process of soot nucleation in fuel-rich flames (1). We have begun (2,3) a program of measuring the rates of ion-molecule reactions involving known flame ions and neutrals, and of using a variety of mass spectrometric techniques to determine the structures of the various isomeric ions which may be involved in these reactions. Early work concentrated on  $C_2H_2^+$  ions, but studies have now been extended to  $C_5H_5^+$ . Several isomeric  $C_5H_5^+$  ions can be formed by electron impact on neutral precursors, and we have determined their ion-molecule reaction rate constants with a number of neutrals found in flames, and have carried out both experimental and theoretical studies to help determine which of many possible structures should be assigned to each isomer. Structure and reactivity results will be presented and their relevance to ionic soot formation mechanisms discussed.

1. H.F. Calcote, Combustion and Flame 42, 215 (1981).
2. P.J. Ausloos and S.G. Lias, J. Amer. Chem. Soc. 103, 6505 (1981).
3. F.W. Brill and J.R. Eyler, J. Phys. Chem. 85, 1091 (1981).

THE DEPENDENCE OF SOOT YIELD ON FLAME CONDITIONS -- A UNIFYING PICTURE.  
Howard S. Homan, Exxon Research and Engineering Company, P. O. Box 51, Linden,  
NJ 07036.

A plot is presented which summarizes the trends of soot yield as a function of flame temperature and equivalence ratio for both premixed flames and diffusion flames. Schematic contours of soot yield are drawn to represent trends induced from published data. For underventilated diffusion flames, the increase in soot yield with increasing flame temperature and with addition of small amounts of oxygen to the fuel side are represented. For premixed flames, the increase in soot yield with increasing equivalence ratio and the decrease in soot yield with increasing flame temperature are represented. For overventilated diffusion flames, the soot yield is a function of heterogeneous post-flame oxidation which is discussed separately from the plot. For reference, calculated values of adiabatic flame temperature versus equivalence ratio are included. A hypothetical laboratory burner experiment -- a consolidation of experiments cited in the literature -- is presented to show how the plot unifies much phenomenological data on soot formation. Armed with this summary, a researcher should be better able to interpret the complex changes of soot yield with operating conditions of practical devices.

KINETICS OF COAL PARTICLE GASIFICATION.\* T.G. DiGiuseppe, S. Madronich, and W. Felder, AeroChem Research Laboratories, Inc., P.O. Box 12, Princeton, NJ 08540

An understanding of the chemical and physical processes of coal gasification may be obtained through a detailed study of the kinetics of volatile reaction products released during pyrolysis of coal particles. We have recently begun a systematic investigation of the chemical transformations occurring during the gasification of coal particles, using AeroChem's High Temperature Fast Flow Reactor (HTFFR). Freshly prepared sized coal particles are entrained into the HTFFR through a fluidized bed and are pyrolyzed under controlled conditions of temperature, pressure, and gas flow velocity. Kinetic and mechanistic information is obtained by real time detection of the primary products of the pyrolyzing coal. In our initial experiments, gas chromatography has been used for the detection of carbon monoxide, methane, water, and carbon dioxide. Quantitative measurements of the concentrations of these species have been obtained for 100  $\mu\text{m}$  diam coal particles pyrolyzing at temperatures from 1000 K to 1300 K at pressures to 50 Torr, and residence times from 0.5 to 1.5 s. Gas chromatographic and mass spectrometric techniques are currently being used for the quantitative detection of hydrocarbon products. These results will be applied to the development of basic quantitative models of the coal gasification process.

\*Work supported by the Gas Research Institute under Contract No. 5081-360-0531.



THEORETICAL INVESTIGATIONS OF REACTION PATHWAYS FOR THE OXIDATION OF NH AND NH<sub>2</sub> RADICALS\* C. F. Melius and J. S. Binkley. Sandia National Laboratories, Livermore California 94550.

Reaction intermediates and possible products for the reactions of the NH and NH<sub>2</sub> radicals with O, O<sub>2</sub> and NO have been investigated using the recently developed BAC-MP4 method (bond-additivity corrections applied to fourth-order Møller-Plesset perturbation theory). Stationary-point geometries have been calculated for stable minima and selected transition structure species using a split-valence polarized basis at the Hartree-Fock level. Using these geometries zero-point vibrational corrections and fourth-order perturbation theory total energies are combined with the bond-additivity corrections to obtain final total energies. In those cases where transition structure calculations have not been performed, estimates of the barriers are made. These results are used to predict likely pathways for reactions of these species occurring under various temperature and pressure conditions. Our results are compared with available experimental data and with various chemical kinetics models used in combustion.

\*This work was supported by the U.S. Dept. of Energy.

LASER PHOTOLYSIS/LASER-INDUCED FLUORESCENCE KINETIC STUDIES OF ELEMENTARY COMBUSTION REACTIONS.\* Frank P. Tully, Applied Physics Division, Sandia National Laboratories, Livermore, CA 94550.

A new, laser-based, chemical kinetics technique has been demonstrated in studies of the reactions of the hydroxyl radical with prototype hydrocarbon fuel molecules. Following reaction initiation by excimer laser photolysis, time-resolved OH concentration profiles were measured with a highly sensitive, quasi-cw, laser-induced fluorescence method. The visible output of a synchronously pumped dye laser, a train of pulses of 3-6 nJ energy and 8-10 ps duration at a repetition rate of 246 MHz, has been frequency-doubled using temperature- and angle-tuned SHG crystals. More than 50 mW of quasi-cw, tunable ultraviolet, laser radiation has been generated. OH fluorescence was excited at 308.16 nm, and OH decay profiles, characterized by at least one order of magnitude improvement in S/B over those obtainable with resonance lamp detection, were collected as functions of gas mixture composition. Absolute reaction rate coefficients were measured over the temperature and pressure ranges 291-1000 K and 50-600 Torr, respectively. Mechanistic information was obtained directly from the OH decays and as a result of deuterium substitution in reactants. For example, in the reaction between hydroxyl radicals and ethylene, the mechanism is dominated at low temperatures by electrophilic addition of OH to the double bond, and, as the temperature is raised, by increasingly rapid decomposition of the thermalized adduct HOC<sub>2</sub>H<sub>4</sub> back to reactants. The current status of experiments utilizing this powerful technique will be discussed.

\*This work was supported by the U.S. Department of Energy.

LASER PYROLYSIS/LASER FLUORESCENCE MEASUREMENT OF THE OH + C<sub>2</sub>H<sub>2</sub> REACTION RATE NEAR 1200 K\*. Paul W. Fairchild, Gregory P. Smith, and David R. Crönsley. SRI International, Menlo Park, California 94025.

A laser pyrolysis/laser fluorescence apparatus has been used to measure the rate constant for the reaction of hydroxyl radicals with acetylene at temperatures near 1200 K. A mixture of SF<sub>6</sub>, N<sub>2</sub> and H<sub>2</sub>O<sub>2</sub> was irradiated with a pulsed CO<sub>2</sub> laser, causing rapid heating and pyrolyzing the peroxide to form OH radicals. The OH concentration is then measured using fluorescence from electronically excited OH. This is produced by a

frequency doubled dye laser, fired after a variable time delay following the  $\text{CO}_2$  laser. Addition of  $\text{C}_2\text{H}_2$  causes a decrease in the OH signal with time, permitting a measurement of the rate constant. Experiments were performed at a total pressure of 40 torr and a temperature of  $1160 \pm 50$  K as determined by rotational excitation scans in the OH. A value of  $4 \times 10^{-13} \text{ cm}^3/\text{sec}$  was determined for these conditions; measurements extending the range of temperature and pressure are in progress.

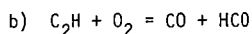
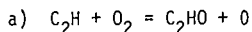
\*Supported by the Department of Energy under Contract DE-AC03-81ER10906.

MEASUREMENT OF THE  $\text{C}_2$  ( $a^3\Pi_u$ ) DISAPPEARANCE RATES WITH  $\text{O}_2$  IN THE 298 - 1300 K TEMPERATURE RANGE. Steven L. Baughcum and Richard C. Oldenberg, University of California, Los Alamos National Laboratory, Chemistry Division, Los Alamos, New Mexico, 87545.

The disappearance rates of  $\text{C}_2$  ( $a^3\Pi_u$ ) ( $v=0$ ,  $v=1$ , and  $v=2$ ) in the presence of  $\text{O}_2$  have been measured over the 298-1300 K temperature range. The  $\text{C}_2$  is produced by 2-photon dissociation of  $\text{CF}_3\text{CCCF}_3$  at 193 nm and probed by laser-induced fluorescence tuned to the  $d(^3\Pi_u) + a(^3\Pi_u)$  transition. The disappearance rate of  $\text{C}_2$  ( $a^3\Pi_u$ ) ( $v=0$ ) as a function of temperature is fit extremely well by the Arrhenius expression ( $k(T) = A \exp(-E/RT)$ ) with a barrier of 0.97 kcal/mole. The quality of the fit over such a large temperature range provides a test of previously proposed models of the  $\text{C}_2 + \text{O}_2$  system, which do not predict simple Arrhenius behavior. Our results are consistent with a model in which the equilibration rate between  $\text{C}_2$  ( $a^3\Pi_u$ ) and  $\text{C}_2$  ( $X^1\Sigma_g^+$ ) in the presence of  $\text{O}_2$  is the rate limiting step, rather than the reaction rate. The measured barrier height of 0.97 kcal/mole is then the barrier for intersystem crossing in the  $^3\text{C}_2 + \text{O}_2 \rightarrow ^1\text{C}_2 + \text{O}_2$  reaction. Additional experiments on  $\text{C}_2$  ( $X^1\Sigma_g^+$ ) kinetics will be presented.

REACTION OF  $\text{C}_2\text{H}$  WITH  $\text{O}_2$ : RATE CONSTANT FOR CO FORMATION. A. H. LAUFER and R. LECHLEIDER, National Bureau of Standards, Chemical Kinetics Division, Center for Chemical Physics, Washington, DC 20234.

The rate constant for CO production from the reaction of  $\text{C}_2\text{H}$  with  $\text{O}_2$  has been investigated using flash photolysis of a suitable  $\text{C}_2\text{H}$  precursor in conjunction with analysis of CO by absorption in the vacuum ultraviolet.  $\text{C}_2\text{H}$  concentrations were determined by titration with added alkanes followed by gas chromatographic analysis of product  $\text{C}_2\text{H}_2$ . The rate constant was determined to be  $4.0 \pm 0.5 \times 10^{-12} \text{ cm}^3 \text{ molec}^{-1} \text{ s}^{-1}$ . The CO increase is best explained as originating from two primary reaction channels



The best fit to the data suggests that (a) represents 20% of the total process. The relationship of the  $\text{C}_2\text{H} + \text{O}_2$  rate constant to those for reaction of  $\text{C}_2\text{H}$  with hydrocarbons will be discussed.

REACTION OF CARBON MONOXIDE WITH OXYGEN ATOMS PRODUCED IN THE THERMAL DECOMPOSITION OF OZONE, S. Toby, S. Sheth, F.S. Toby, Dept. of Chemistry, Rutgers University, Piscataway, NJ 08854

The reaction of CO with  $O_3$  has been reinvestigated in the range 80-160°C and it was shown that the previously reported<sup>1</sup> complex rate law occurs as the result of a chain reaction initiated by trace impurities in the CO. This conclusion was also in accord with a computer simulation of the system. When the CO was rigorously purified<sup>2</sup> the reaction reduced to the sequence  $O_3 + CO \xrightarrow{1} O(^3P) + O_2 + CO$ ,  $O(^3P) + O_3 \xrightarrow{2} 2O_2$  followed by reactions of  $O(^3P)$  with CO. These reactions lead to chemiluminescence and by measuring the emitted intensity we measured  $k_4/k_2$  for  $O(^3P) + CO \xrightarrow{4} CO_2(^3B_2)$ . The rates of reactions 4 and 2 were found to have the same temperature dependence in the range studied. There was no third body effect on reaction 4 which is in agreement with the mechanism postulated by Pravilov and Smirnova<sup>3</sup>.

1. S. Toby and E. Ullrich, Int. J. Chem. Kins., 12, 535 (1980).
2. D.H. Stedman, D.K. Branch and R. Pearson, Anal. Chem., 51, 2340 (1979).
3. A.M. Pravilov and L.G. Smirnova, Kinetika i Kataliz, 22, 832 (1981).